

NASA Technical Memorandum 81371

PRELIMINARY ANALYSIS OF STS-2 ENTRY FLIGHT DATA

April 1982

LIBRARY COPY

APR 22 1982

LANGLEY RESEARCH CENTER
LIBRARY, NASA
HAMPTON, VIRGINIA

NASA



NASA Technical Memorandum 81371

PRELIMINARY ANALYSIS OF STS-2 ENTRY FLIGHT DATA

NASA Ames Research Center
Dryden Flight Research Facility
Edwards, California

NASA
1982

N82-22304 #



NOMENCLATURE

Acronyms

ACIP	aerodynamic coefficient identification package
ADB	aero data book
ASI	aero stick input
C.G.	center of gravity
CSS	control stick steering
DFRF	Dryden Flight Research Facility
FS	fuselage station
GPC	general purpose computer
GMT	Greenwich mean time
IMU	inertial measurement unit
JSC	Johnson Space Center
MMLE	modified maximum likelihood estimation
OI	operational instrumentation
PIO	pilot-induced oscillation
PKQ	suppression factor
PSF	pounds per square foot
PTI	programmed test input
RCS	reaction control system
RHC	rotational hand controller
SEADS	Shuttle Entry Air Data System
STS	space transportation system
TAEM	terminal area energy management
VEAS	velocity equivalent airspeed, knots
WS	wing station

Symbols

a_x		longitudinal acceleration, g
a_n		normal acceleration, g
a_x		longitudinal acceleration, g
a_y		lateral acceleration, g
BF		body flap, deg
b		span, ft
C_L		lift coefficient
C_D		drag coefficient
C_l		rolling moment/ $\bar{q}Sb$
$C_{l\delta_a}$	$= \frac{\partial C_l}{\partial \delta_a}$	
$C_{l\beta}$	$= \frac{\partial C_l}{\partial \beta}$	
$C_{l\delta_r}$	$= \frac{\partial C_l}{\partial \delta_r}$	
C_m		pitching moment/ $\bar{q}S\bar{c}$
C_{mq}	$= \frac{\partial C_m}{\partial q}$	
C_{mSB}	$= \frac{\partial C_m}{\partial SB}$	
$C_{m\dot{\gamma}}$	$= \frac{\partial C_m}{\partial \dot{\gamma}}$	
$C_{m\alpha}$	$= \frac{\partial C_m}{\partial \alpha}$	
$C_{m\delta_e}$	$= \frac{\partial C_m}{\partial \delta_e}$	
C_{mBF}	$= \frac{\partial C_m}{\partial BF}$	
C_n		yawing moment/ $\bar{q}Sb$
$C_{n\beta}$	$= \frac{\partial C_n}{\partial \beta}$	
$C_{n\delta_a}$	$= \frac{\partial C_n}{\partial \delta_a}$	

$C_{n\delta_r}$	$= \frac{\partial C_n}{\partial \delta_r}$
C_y	yawing moment/ $\bar{q}S$
$C_{y\delta_a}$	$= \frac{\partial C_y}{\partial \delta_a}$
$C_{y\beta}$	$= \frac{\partial C_y}{\partial \beta}$
$C_{y\delta_r}$	$= \frac{\partial C_y}{\partial \delta_r}$
\bar{c}	mean aerodynamic chord, ft
D	drag, lb
h	altitude
L/D	lift to drag ratio
L_{RJ}	rolling moment due to roll jet
L_{YJ}	rolling moment due to yaw jet
M	Mach number
M_{YJ}	pitching moment due to yaw jet
N_{RJ}	yawing moment due to roll jet
N_{YJ}	yawing moment due to yaw jet
p	roll velocity, deg/sec
q	pitch velocity, deg/sec
\bar{q}	dynamic pressure, psf
S	wing area, ft ²
SB	speed brake
t_0	plot start time (Greenwich mean time)
V	velocity
x	body axis longitudinal coordinate
Y_{RJ}	yawing force due to roll jet
Y_{YJ}	yawing force due to yaw jets

y	body axis spanwise coordinate
z	body axis vertical coordinate
α	angle of attack, deg
β	angle of sideslip, deg
δ_a	aileron deflection, deg
δ_e	elevator position, deg
$\delta \dot{e}$	$= \frac{\partial \delta_e}{\partial t}$
δ_r	rudder position
Δ	increment
θ	pitch angle
ϕ	roll angle

INTRODUCTION

Dryden has completed a preliminary analysis of the data obtained during entry of the STS-2 flight. There were two significant changes from the first to second flight as far as data analysis is concerned. First, the inclusion of numerous planned performance and stability and control maneuvers, increased the flight data base considerably, but second, the failure of the ACIP recorder decreased the quality of analysis obtained from those maneuvers.

In this report, results from performance and stability and control analysis are compared with that from STS-1 and pre-flight predictions. The effects of the missing ACIP data are discussed as well as the benefits derived from the planned maneuvers.

Section two of this report presents the results of Dryden's aerothermal analysis for the flight. STS-2 data is added to STS-1 data for fuselage station 877 and wing station 240. Structural temperature comparisons are shown for wing stations 328 and 134. Surface temperature comparisons are presented for these wing and fuselage stations.

Some concluding remarks and Dryden's recommendations are presented in the third section and a list of references is included as section four.

PERFORMANCE, STABILITY, AND CONTROL

Introduction

One of the objectives during the STS-2 entry was to obtain aerodynamic data for performance, stability, and control analysis. Data were obtained from specialized inputs such as pitch, roll, and yaw pulses and a push over/pull up maneuver as well as from the operational maneuvers. A summary of the flight conditions available for analysis is shown in table 1. Unfortunately, the analysis of these data has been hampered by the loss of the ACIP recorder. This data recording package contained the high resolution measurements of the angular rates and linear accelerations as well as the high sample rate data for many of the other aerodynamic parameters. As a result, the ACIP parameters had to be replaced by lower quality GPC data from the OI recorder. This provided adequate data for the extraction of stability and control derivative information and these results and their accuracy will be discussed in a subsequent section. The GPC data was not adequate for the determination of lift and drag characteristics. As a result, longitudinal acceleration data was extracted from the IMU data and this data in conjunction with optical tracking data was used to calculate the performance characteristics. All predicted data shown were calculated using the onboard recording of the conditions prior to each maneuver. The weight, cg, and inertia values used are shown in table 2.

Stability and Control Derivative Extraction Results

The STS-2 flight data includes intentional stability and control maneuvers in addition to the planned bank reversals similar to those on STS-1.

All of the stability and control maneuvers were excellent and performed as planned. All of the intentional stability and control maneuvers as well as the bank reversals were analyzed and stability and control derivatives were obtained.

The mathematical formulation of the technique used in the following analysis is contained in references 1-3. Some of the practical implications of applying the MMLE-3 program to flight data are contained in references 4 and 5. The preliminary results for STS-1 are contained in references 6 and 7.

In general the analysis of STS-2 closely followed that of STS-1 described in references 6 and 7. There were two major factors that affected the analysis of STS-2. Specially designed maneuvers for stability and control analysis were performed however no high quality rate gyro and accelerometer data were available from the ACIP systems. The special maneuvers enhanced the quality of the stability and control estimates but the loss of the ACIP data degraded the estimates, especially in particular flight regimes. The net result was data comparable in quality to that of STS-1.

STS-2 Longitudinal Analysis

Intentional maneuvers for obtaining longitudinal stability and control characteristics were performed only during the early portion of the entry. Data were analyzed throughout the rest of the entry using any available small motions. The analysis of extremely small maneuvers was limited by the loss of the high resolution ACIP data. As in STS-1, analysis of several of the small incidental maneuvers was degraded by motion of the body flap, which

was instrumented at only 1 sample per second. Generally reasonable estimates were obtained throughout the entry, but the scatter of the estimates was considerable in some areas because of the marginal quality maneuvers used. No axial force derivatives have been obtained, since most of this data was analyzed prior to receipt of the IMU data, which contains the only useable a_x measurement.

Estimates of the pitch jet derivatives are presented in figure 1 as a function of dynamic pressure. The jet derivatives show similar trends to those observed on STS-1. The pitching moment from the up-jets (pitch nose up) is consistently 8 to 12 percent lower than predicted. The pitching moment from the down-jets (pitch nose down) agrees well with predictions at zero dynamic pressure, but does not show any sign of the large change predicted above 0 psf.

The jet derivatives presented in this figure were obtained with a model assuming that the total jet effectiveness is proportional to the number of jets firing. The predictions indicate that the jet interference effect should be modeled as independent of the number of jets firing. In order to evaluate these competing models, the four Aero Stick Inputs (ASI) were re-analyzed allowing different derivative estimates for two down-jets firing and four down-jets firing. The ASI's all had significant periods when two down-jets were firing and when four down-jets were firing, making this analysis possible. None of the maneuvers from STS-1 or the incidental maneuvers from STS-2 contained sufficient information for the analysis. Figure 2 presents the results of the non-linear down-jet analysis. The results are not definitive, but do tend to indicate different per-jet effectiveness when four jets are firing opposed to two. It is interesting that this difference is not observed in

the $\bar{q}=0.6$ psf ASI, where it might be postulated that the interference effect is not yet significant.

There were no maneuvers in either flight allowing analysis of the variation in up-jet effectiveness as a function of the number of jets firing. Since the predicted interference effect from the up-jets is much smaller than for the down-jets, the exact form of the up-jet interference is probably not a significant issue.

Figure 3 shows the static aerodynamic derivatives plotted as functions of Mach number. In general the normal force derivatives show significantly more scatter than the pitching moment; the normal force derivatives are generally more difficult to estimate and this problem was exacerbated by the resolution of the OI a_N accelerometer. $C_{m\alpha}$ agrees well with predictions above Mach 10. The scatter above Mach 23 is due to the difficulty of estimating aerodynamic derivatives at very low dynamic pressures, this also applies to the other aerodynamic derivative. Between Mach 1 and 10, there is a lot of scatter in $C_{m\alpha}$ due to the marginal quality of the maneuvers used. The points with smaller uncertainty levels tend to be less stable than predictions, but a definitive statement about $C_{m\alpha}$ in this region must await better maneuvers. The one subsonic data point with small uncertainty level agrees well with predictions. $C_{m\delta_e}$ shows trends similar to $C_{m\alpha}$. Above Mach 4, the data generally agrees well with predictions. Below Mach 4, there is significant scatter, with the better data points indicating the same or slightly less effectiveness than predicted.

$C_{m\delta_f}$ appears to be lower than predicted below Mach 12 and slightly higher than predicted above Mach 12. The body flap derivative estimates, however, are suspect because of the 1 sample-per-second instrumentation of

the body flap and the consequent uncertainty of the precise timing of the body flap motion compared to the vehicle response.

There is a significant amount of scatter in the estimates of M_{YJ} , due to the difficulty of estimating this fairly small term. The flight estimates are strong enough, however, to indicate that the true value is considerably less than predicted above Mach 8. It should be noted that this derivative applies to the absolute value of the yaw jet signal. It is independent of which side the yaw jets fire on.

None of the normal force derivative estimates give sufficient information to suggest changes from the predicted values. For the most part, the scatter and uncertainty levels are as large as the estimates.

Cm_q was estimated for the maneuvers below Mach 3; above Mach 3 it was held fixed at predictions. The Cm_q estimates are shown in figure 4. Even when the two points with largest uncertainty levels are eliminated, the scatter is too large to regard the estimates as useful. Accurate estimation of Cm_q will require much better maneuvers than the incidental motions used for this analysis.

Lateral-Directional Analysis

The rotary or rate derivatives were held fixed for all of the results presented here. Attempts were made to determine the rotary derivatives below Mach 3 but an in-depth assessment showed there was insufficient information to get meaningful estimates. It is not felt that fixing the rotary derivatives has had an adverse effect on the results presented herein.

A study also showed that reliable information on the sideslip and aileron

(differential elevon) derivative could not be obtained below a dynamic pressure of 10 psf. Therefore all data are presented here for dynamic pressure below 10 psf is for the sideslip and elevon derivatives fixed at the flight determined value near a dynamic pressure of 10 psf.

In general the effect of the yaw jets below a Mach number of 3 was found to be weak. Thus for most of the cases in this regime the yaw jets were fixed at the Aero Data Book (ADB) values. The modeling of the reaction control jets was done in the same manner as described in reference 6. The force is in pounds per jet and the moments are in foot pounds per jet. A pair of one up-firing jet and one down-firing jet is defined as two roll jets firing. The derivative determined by this definition is the average effect of these two jets. The reason the total forces and moments are used is that it is easier to assess differences between the flight and ADB values. That is, in the dimensionless form used in the ADB (where interference or interaction effects are usually small compared to the primary jet effect) a small error in mass or inertia will have a large effect on the interaction effect. Assuming no error in the vacuum thrust of the jets, a 5% error in the inertias could look like a 100% error in the interaction effect if the interactions effect were 5% of the primary thrust value. This makes the error in the jet derivatives difficult to assess. Therefore in this report the total forces and moments are used to give a better feel as to the magnitude of differences between the flight and ADB values. In order to update the ADB and simulator results, the analysis will have to be redone with the same model as the ADB uses. This will only be meaningful if the differences in the total force and moments from flight and ADB are actual errors in the ADB predictions rather than errors in mass, or inertia.

All of the maneuvers from the flight were used in this analysis. These maneuvers include programmed test inputs (PTI's), bank reversals, and any maneuvers resulting from an independent pilot input. Although the derivatives are adversely affected everywhere by the loss of the ACIP data some of the small maneuvers, particularly at low \bar{q} , were totally useless.

The GPC air data (angle of attack, angle of sideslip, dynamic pressure, velocity, Mach number and altitude) were used throughout the analysis. These GPC data were used for their dynamic characteristics as well as for nondimensionalizing the derivatives. $V/1000$ was used for Mach number above $M=4$.

Below a Mach number of 3 the angle-of-sideslip calculated from the sideprobes was studied. The data were certainly representative of the expected angle-of-sideslip response, that is the effect of wind shear was essentially eliminated. The sideprobe sideslip was used in the derivative extractions and no marked improvement was found in the results. This was due to the potentially tremendous unknown transport lags in the sideprobe system at very low static pressure. Some theoretical lags were calculated to be up to several seconds. In addition to the lag there is an effect of attenuation of the dynamic response. Also the sideprobes were not intended as primary source of sideslip measurement, so the data used for the calculation may not be sufficient for the purpose of stability and control derivative measurement. The problem is still being studied, therefore the GPC data for sideslip was used for all of the analysis in this report. It should be noted that the transport lags need to be kept to a minimum and fully documented in the SEADS system if useful dynamic information is to be obtained for angle-of-attack and angle-of-sideslip.

Derivative Results

The derivative estimates obtained to date are shown in figures 5 thru 13. The derivative estimates are plotted as a function of Mach number or \bar{q} . The symbol is the derivative estimate and the vertical bars are the uncertainty bounds (refs. 4 and 5). The poorer the estimate, the larger the uncertainty bounds. The dashed line is a fairing of the flight-determined derivative estimates, and the solid line is the ADB value for the derivative at the same flight conditions as the flight maneuvers were obtained. The solid ticked lines are a ± 1 variation applied to the ADB values. The flight data is faired with a dotted line where the fairing is very uncertain. All data is referenced to 65% of the body length. The squares are for STS-1 and the circles for STS-2.

The lateral-directional stability and control derivatives are plotted as a function of Mach numbers for all cases where \bar{q} from GPC is greater than 10 psf in figures 5 through 10. The RCS jet derivatives are plotted versus \bar{q} in figures 11 through 13 for \bar{q} between 0 and 20 psf. The jet derivatives are plotted versus \bar{q} at low \bar{q} as the effect is due more to \bar{q} than Mach number at low \bar{q} .

C_{l_B} (figure 5) from flight is less negative than ADB values above $M=10$. It is somewhat more negative below $M=10$. It is within the variation, throughout the Mach range. A less certain fairing is shown below $M=3$ as the values in this region are very sensitive to analysis technique. The fairing is in agreement with the STS-1 fairing (ref. 6) above $M=4$.

The C_{n_B} (fig. 5) fairing for flight is within the plus or minus variation from the ADB. There is fair agreement between flight and data book for

most Mach numbers with a tendency to differ between M=8-12 and near M=20. A dotted fairing is once again used below M=3. The fairing is in good agreement with that shown in ref. 6 except between M=4-8 and near M=10.

The $C_{l_{\delta a}}$ (fig.6) fairing from flight is within the ADB variations everywhere except below M=3 and between M=18-21. The region between Mach 18 and 21 shows all of the flight values higher than predicted but the scatter in the data and the size of the uncertainties indicate that the derivatives obtained so far are not strongly defined. More PTI's in this region and availability of the higher resolution ACIP data should resolve this issue. The derivative is better defined in figure 6 than it was for STS-1 in ref. 6.

The fairing for $C_{n_{\delta a}}$ (fig. 6) is within the ADB variations. The fairing agrees with the ADB throughout. A weakly determined $C_{n_{\delta a}}$ between M=18-21 is indicated. PTI's and the ACIP data should help here also. The fairing shown here and in the fairing shown in reference 6 are in fair agreement for $M < 20$. The trend in figure 6 is well defined above M=23; a trend that differs from STS-1 is probably due to the large number of high quality test maneuvers obtained on STS-2.

Figure 7 shows the flight determined $C_{l_{\delta r}}$ and $C_{n_{\delta r}}$. The fairing agrees with the ADB. The data from STS-2 PTI's indicates the high value of $C_{l_{\delta r}}$ from STS-1 (ref. 7) is not realistic.

The fairing of L_{y_j} (fig. 8) is within the ADB variations. There is very poor agreement above M=8 where the flight data is very well defined. This indicates important difference between the vehicle and the prediction. This strong indication was also evident on STS-1 (ref. 6).

The flight data and ADB values are very good for N_{y_j} (fig. 8) as they were for STS-1.

The Y_{YJ} (fig. 9) is in good agreement with the ADB. There is an indication of less interaction than predicted at the higher Mach numbers.

The $C_{Y\beta}$ (fig. 9) fairing from flight is within the variations throughout the Mach range. There is good agreement below $M=12$. A less negative value is indicated above $M=12$. The data from STS-2 agrees with that of STS-1 (ref. 6) above $M=4$. Below $M=4$ STS-2 data is more in agreement with the ADB. $C_{Y\delta_a}$ and $C_{Y\delta_r}$ (fig. 10) are in agreement with ADB predictions.

Figure 11 shows L_{YJ} as a function of \bar{q} for STS-1 and STS-2. There is good agreement between ADB and flight at \bar{q} near zero but the ADB shows a much greater interaction effect than the flight data. The fairing of the flight data is outside the variations below a \bar{q} of 16 psf. The lower interaction effect for L_{YJ} was noted above $M=8$ previously. Since the vacuum thrust value is in good agreement with the ADB it indicates that the ADB interaction effects value should be changed.

Figure 11 shows N_{YJ} as a function of \bar{q} . There is good agreement between STS-2 data and ADB throughout the \bar{q} range. The values for STS-1 indicate a lower value. This could be due to a difference between the moment of inertia (I_z) from STS-1 to STS-2, although the predicted values of I_z are nearly the same. The discrepancy could also be due to the difference between ACIP data on STS-1 and OI data on STS-2. This issue is currently unresolved, but does point out the desirability of on orbit maneuvers to check the moments of inertia.

Figure 12 shows L_{RJ} as a function of \bar{q} . There is poor agreement between flight and ADB. The values of flight and ADB near a \bar{q} of zero differ significantly. It could indicate a greater impingement effect than is predicted. The interaction effect is less than predicted. This is strongly

indicated by the flight data and the ADB should be changed.

Figure 12 also shows N_{RJ} versus \bar{q} . The vacuum thrust values are in good agreement with prediction but the interaction effect is predicted to be greater than that found in flight. STS-2 data shows an indication that of a difference between flight and ADB and in the same direction as STS-1. Once again this could be due to the inertia or the data quality.

Figure 13 shows Y_{YJ} as a function of \bar{q} . There is excellent agreement between flight and ADB.

The Y_{RJ} versus \bar{q} is shown in figure 13. There is poor agreement for the low \bar{q} below 6 psf. This may indicate that the interaction effect is about right, but that the impingement value is incorrect. This discrepancy has not been resolved. It is interesting to note how consistent the flight determined vacuum thrust values are.

Most of the data given in figures 11-13 were obtained from STS-1. This is because the ACIP data is of much better quality so the smaller maneuvers can be analyzed. The OI data were not found adequate to analyze these small maneuvers.

In general the flight estimates are good above $M=3$. There is a significant amount of scatter indicated at some of the flight conditions. If the PTI maneuvers are separated from the other maneuvers the trends are somewhat more consistent. Therefore the scatter could be due to the PTI maneuvers being superior maneuvers or due to the amount of motion in the response and control variables and therefore the scatter being an indication of nonlinearities with respect to the response and control variables.

Comparison of Flight and Predicted Response

The linear lateral-directional derivatives from the previous section have been used to calculate the response to a bank angle command at $M=1.6$. The response is shown in figure 14 along with the values of the linear derivatives. A small neutrally damped oscillation is seen throughout the maneuver. To examine this further, another run was made with no yaw jets and is shown in figure 15. The residual oscillation is much larger in this case ($P = \pm 2$ deg/sec) and is slightly divergent. The frequency of the oscillation does not correspond exactly to that seen in flight (.15 HZ compared to .2 HZ) which would suggest possible non-linear aerodynamics. The derivatives were obtained from the PTI maneuvers which are significantly larger than the flight oscillations. Because of the extremely low rate of divergence and the well behaved response to large inputs, this oscillation should be of no consequence even with the loss of the yaw jets.

Control Use and Trim

The amount of control used during the entry is shown in figure 16. The data indicates the maximum used during each 20 second interval. There was more control use during the STS-2 entry than during the STS-1 entry due to the large number of stability and control tests. Even with these tests, aileron and rudder shows only small use compared to their total authority.

The body flap and elevator positions are shown in figure 17 as a function of velocity. At several speeds, manual bodyflap settings were made from which the elevator/body flap relationship can be obtained. These are shown in figure 18 for $M=12$, 18, and 21. The flight and predicted trends

are about the same except for a bias. Since the flight and predicted value of elevator effectiveness are nearly the same figure 3b, the larger body flap deflections required for trim in flight are most likely the result of a C_{m0} difference between flight and predictions.

Subsonic Performance

The lift and drag characteristics have been determined from about 20,000 feet to touchdown. The data were analyzed using a linear regression technique to determine the difference between the flight and predicted values of C_L and C_D . The form of the equations used in the regression analysis is shown in figure 19. The increments ΔC_L and ΔC_D represent the values that must be added to the predictions to obtain the results observed in flight and include the effects of angle of attack, elevator, speedbrake, body flap, landing gear, and ground effects. The ground effect function was chosen to be similar in shape to the predicted ground effect increment.

Since the data available are limited, the data of STS-1 were combined with that of STS-2 for analysis and a time history of this data set is shown in figure 20. A comparison of the C_L and C_D with the predictions is shown in figure 21. The results of the regression analysis are shown in figure 22. Comparisons of the flight and modified predictions are shown in figure 23. The results of this analysis provide a reasonable estimate of the lift and drag characteristics along the nominal approach and landing profile. The applicable range of these results is $\alpha = 0-15$ and $\delta_e = 0-10$ and extrapolation beyond these values is questionable. This is especially true of the drag increment due to δ_e for negative values of δ_e . This can be seen in figure 24 where the increments have been added to the ADB for nominal approach

conditions.

As previously discussed, the apparent lag in the angle-of-attack system complicates the analysis of the stability and control parameters. Similarly, the analysis of the performance data is complicated because of this apparent lag problem. In order to reduce the uncertainties in the flight derived performance parameters, a lag correction and/or calibration term needs to be determined for the angle-of-attack measurement.

Final Approach and Landing

A time history of the landing is shown in figure 25. The surface winds were approximately 20 knots down the runway. A speedbrake effectiveness test was performed at an altitude of 12-15,000 feet which put the aircraft below the nominal trajectory. At the conclusion of this test, the auto system was engaged resulting in several oscillations of $\pm 0.5g$ in the process of acquiring the desired trajectory. Once the desired trajectory was acquired, the system tracked in a smooth manner although at a lower than nominal speed. Manual control was used from preflare to landing.

The engagement of the auto system when significantly off trajectory (3-5,000 ft) would not generally occur in routine operation. However, the observed oscillations do indicate that the auto system is not configured to handle these situations gracefully. For the low energy situation, such as was the case in this flight; the use of the auto system could result in a dangerously low airspeed approach while attempting to hit the nominal touch-down point.

The final flare and landing were made manually. The pilot inputs were small and very little PIO suppressor activity (PKQ) was observed. An

interesting comparison of the control system activity for the TAEM and Auto-land modes and the CSS manual mode can be seen in the elevator rate time history. In the TAEM mode, the elevator rates are low (2-3 deg/sec). The elevator rates in the autoland and CSS modes are higher and quite similar with rates around 10 deg/sec. A smooth touchdown was made at about 175 knots.

Table 1. STS-2 Entry Maneuvers

Event	GMT (Day 318)	Velocity, Fps.	Altitude, Feet	Maneuver Trim Conditions				
				Elevon	Body Flap	Speed Brake	Angle of Attack	Bank Angle
Pitch ASI-1 ($\bar{q}=0.3$)	20:53:03	24600	328000	1.0	6.8	0	41.0	1
Pitch ASI-2 ($\bar{q}=3$)	20:54:42	24604	282000	-2.0	12.6	0	39.5	-2
Roll ASI-1 ($\bar{q}=4$)	20:55:06	24584	274000	-2.0	15.8	0	39.5	2
Roll ASI-2 ($\bar{q}=8$)	20:55:37	24530	262000	4.0	14.0	0	41.0	14
Pitch ASI-3 ($\bar{q}=10$)	20:55:54	24475	257500	-2.0	17.2	0	39.0	-2
First Turn	20:56:08	24430	254000	-	-	-	-	-
Pitch ASI-4 ($\bar{q}=16$)	20:56:49	24220	248500	1.0	15.5	0	40.0	69
Roll ASI-3 ($\bar{q}=18$)	20:58:07	23720	244900	1.5	15.0	0	39.7	82
PTI-1	20:59:38	23100	239050	1.1	15.0	0	40.0	69
Body Flap Pulse/PTI-1	21:02:24	21560	230000	0.8	15.0	0	40.0	61
Pitch ASI-5	21:03:41	20680	224500	0.5	15.7	0	38.0	58
POPU-1	21:03:52	20500	223400	0	15.7	0	39.2	58
First Bank Reversal	21:04:31	19960	219100	-	-	-	-	-
PTI-1	21:06:22	17935	205400	1.4	13.5	0	40.6	-58
Body Flap Pulse	21:06:33	17750	203600	1.3	13.5	0	40.1	-51
Body Flap Pulse/ PTI-1	21:08:50	13850	179600	0.3	13.0	0	39.7	-62
Second Bank Reversal	21:11:10	9350	153750	-	-	-	-	-

Table 1. Continued

Event	GMT (Day 318)	Velocity, Fps.	Altitude, Feet	Maneuver Trim Conditions				
				Elevon	Body Flap	Speed Brake	Angle of Attack	Bank Angle
PTI-1	21:12:02	7910	14500	2.5	10.3	87.2	31.2	51
PTI-2	21:13:32	5750	122250	4.0	8.5	87.2	22.9	46
Third Bank Reversal	21:14:18	4900	112600	-	-	-	-	-
PTI-3	21:14:50	4150	106400	9.5	8.5	87.2	19.6	-41
PTI-4	21:15:47	3120	93600	8.5	2.1	69.0	17.7	-36
Fourth Bank Reversal	21:16:23	2520	83600	-	-	-	-	-
PTI-5	21:16:52	2140	77750	1.2	-2.8	55.6	12.8	25
PTI-6	21:17:42	1480	65000	0.5	-10.6	55.6	8.3	0
PTI-7	21:18:30	980	50800	6.0	-9.6	55.6	7.0	4
PTI-8	21:18:47	880	45000	7.5	-7.5	47.0	9.2	2
Speedbrake Sweep	21:20:33	560	14400	-	-	-	-	-

Table 2

STS-2

WEIGHT, CG, INERTIAS

Weight	204774	Lbs.
IX	938368.1	Slug-ft. ²
IY	6888342.3	Slug-ft. ²
IZ	7200872.3	Slug-ft. ²
IXZ	157082.3	Slug-ft. ²
IXY	7367.1	Slug-ft. ²
IYZ	1386.8	Slug-ft. ²

XCG = 1097.3 ZCG = 372.3 YCG = -.3 inches

These were used as constants for the entire entry.

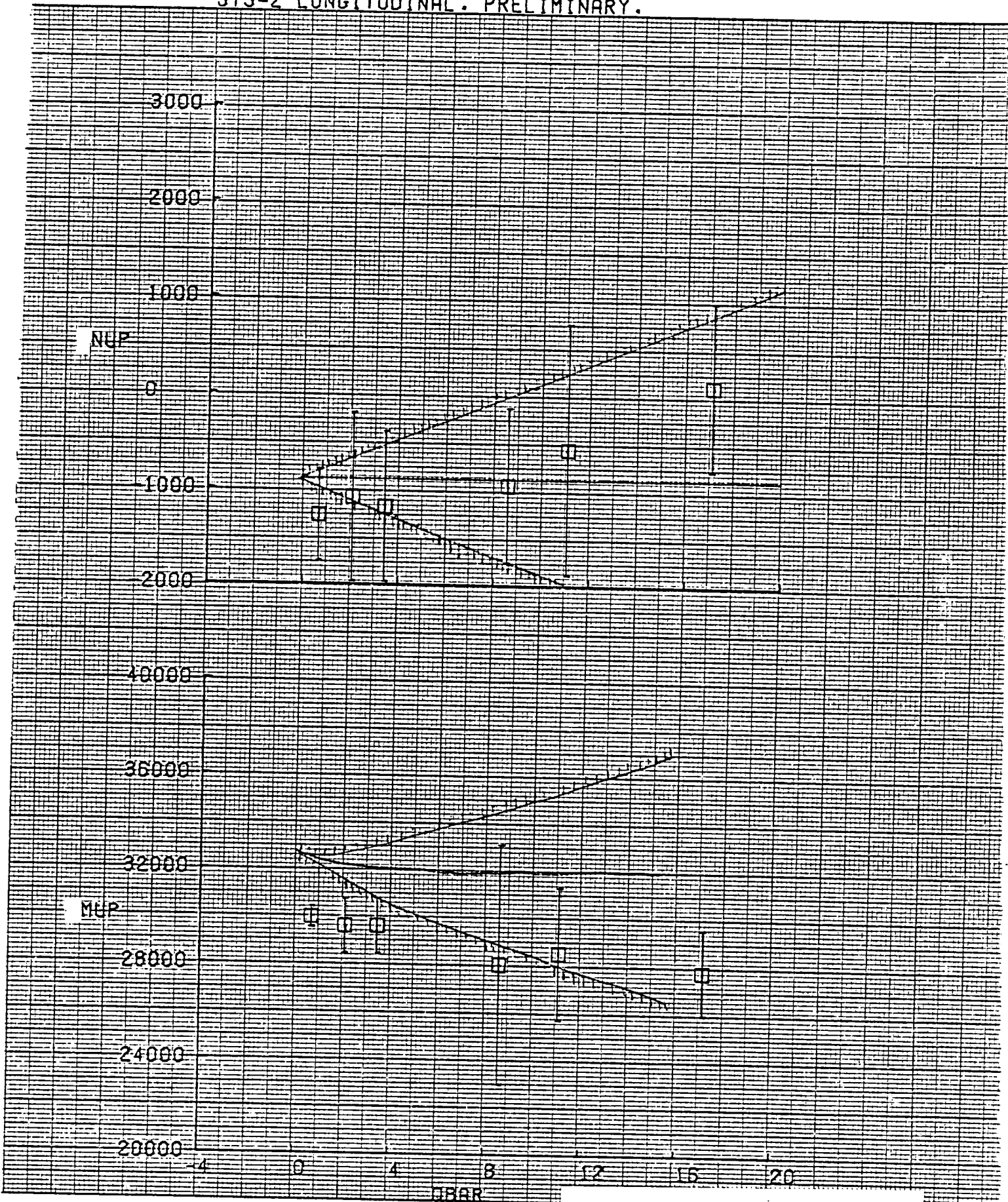


Fig. 1a Correlation of Flight and Predicted Values of Pitch-up jets C_N and C_M vs \bar{q}

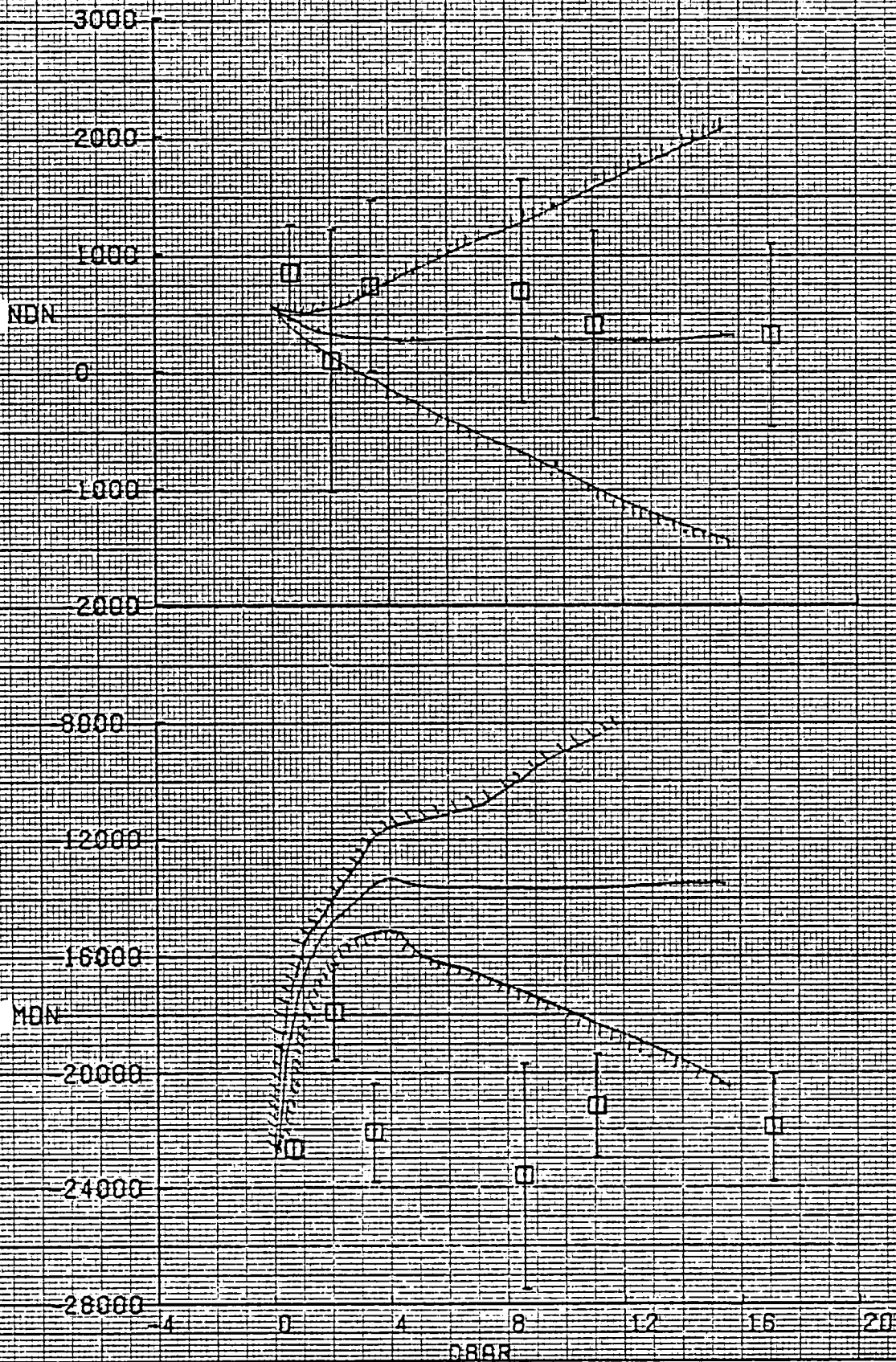


Fig. 1b (concluded) Pitch-Down
 Jets - C_N and C_M vs \bar{q}

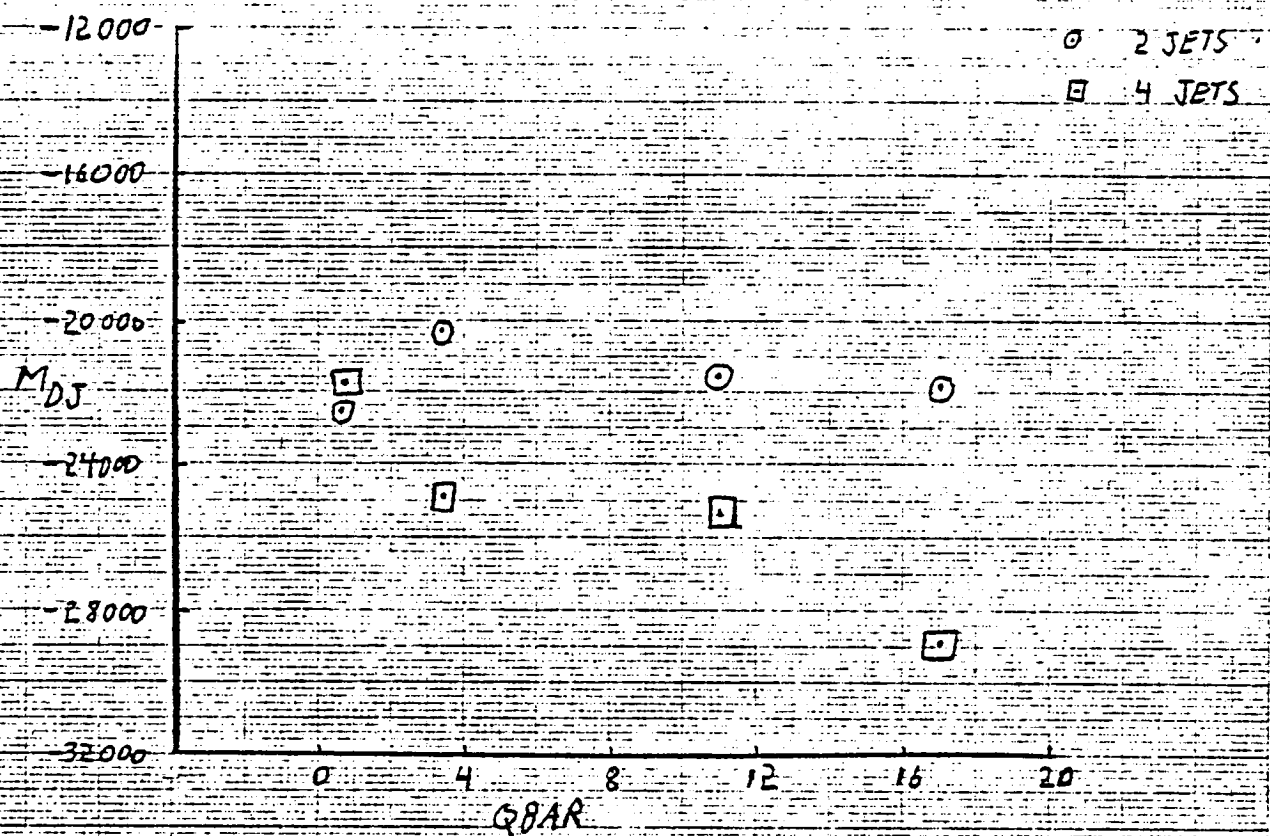


Fig. 2 Non-linear Down-Jet Analysis Results

STS-2 LONGITUDINAL. PRELIMINARY.

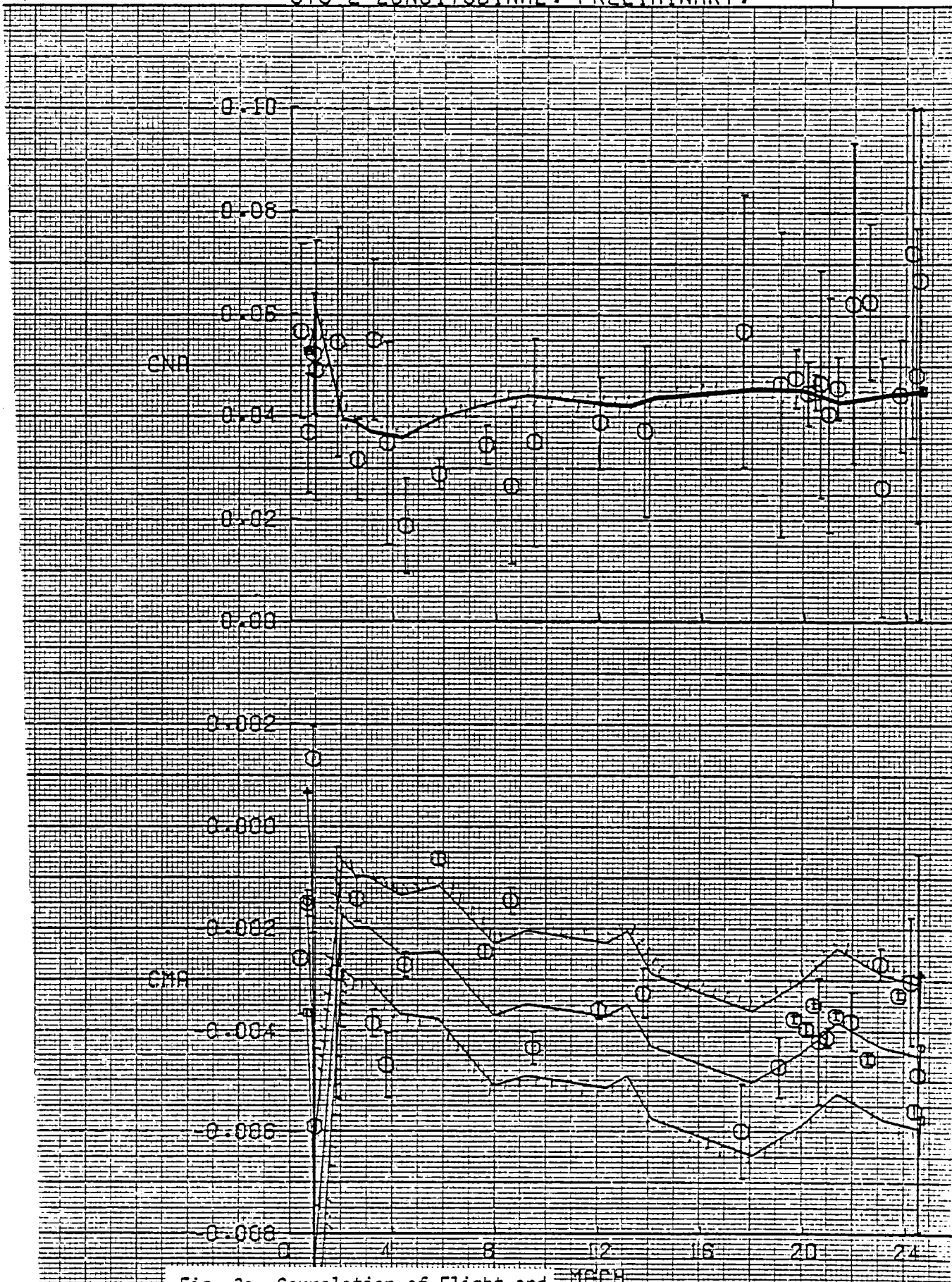


Fig. 3a Correlation of Flight and Predicted Values of a Longitudinal Derivatives - $C_{N\alpha}$ and $C_{M\alpha}$ vs M

STS-2 LONGITUDINAL. PRELIMINARY.

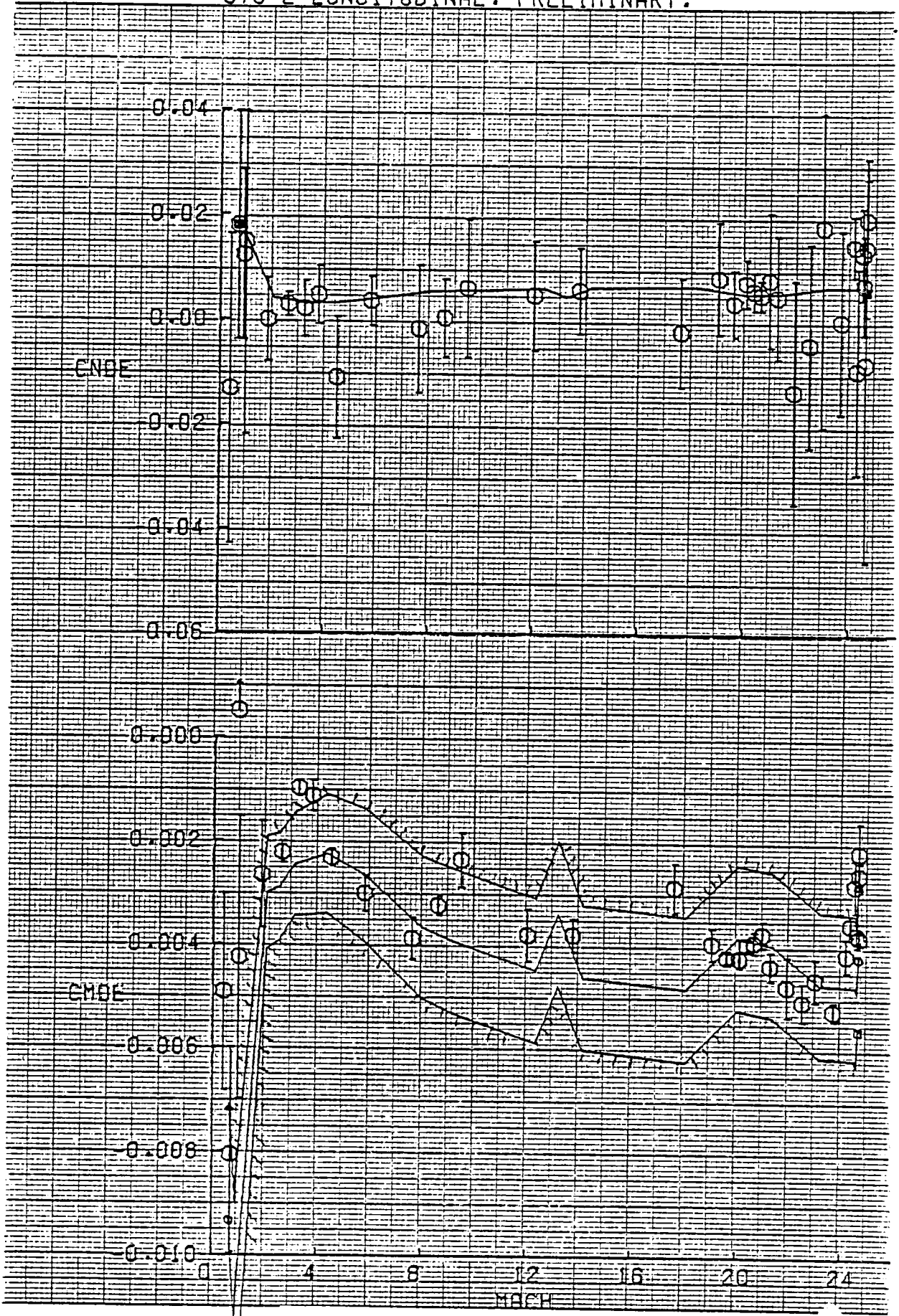


Fig. 3b (cont) $C_{N_{S_e}}$ and $C_{M_{S_e}}$ vs M

STS-2 LONGITUDINAL. PRELIMINARY.

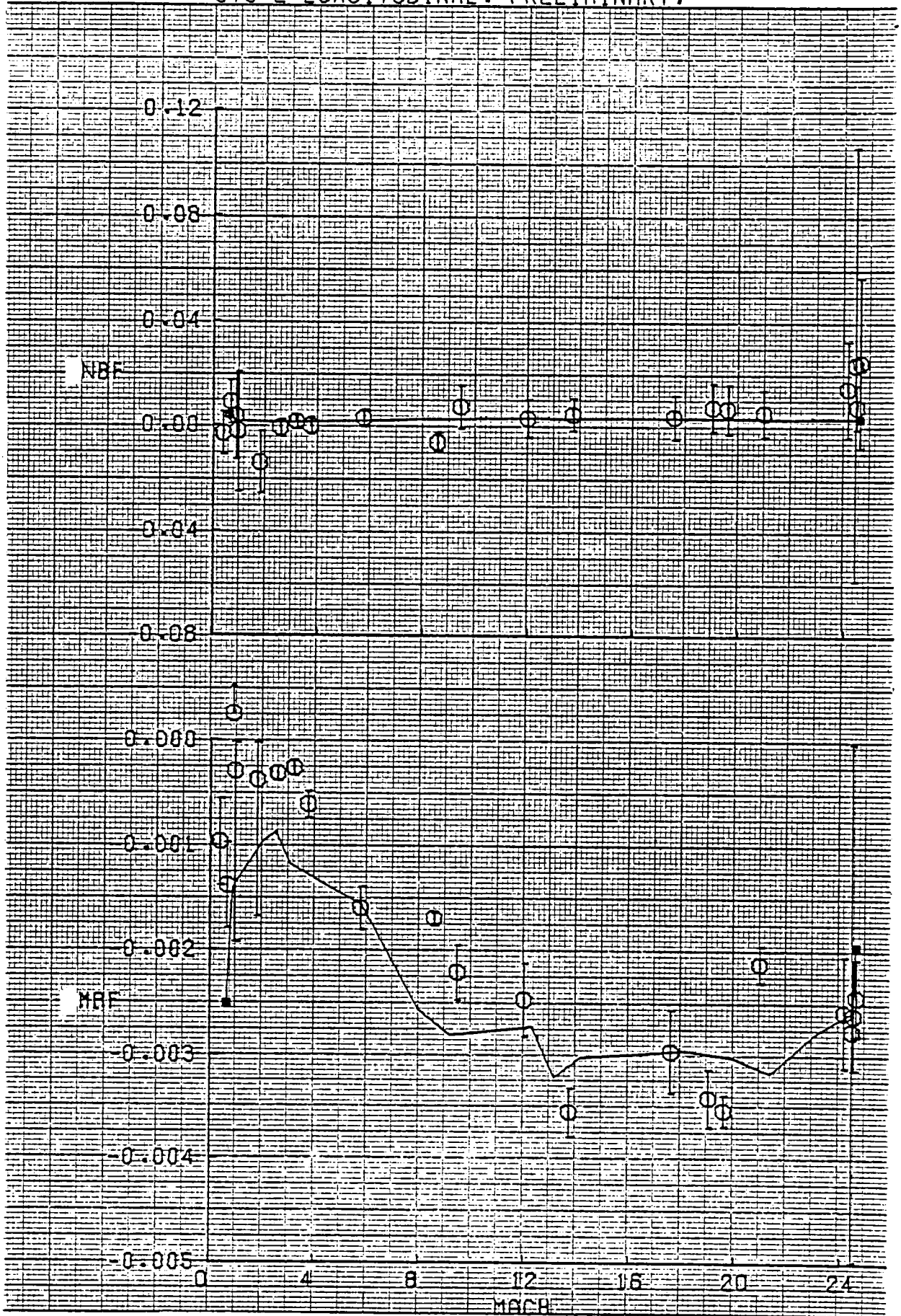


Fig. 3c (cont) $C_{n_{BF}}$ and $C_{m_{BF}}$ vs M

1 STS-2 LONGITUDINAL. PRELIMINARY.

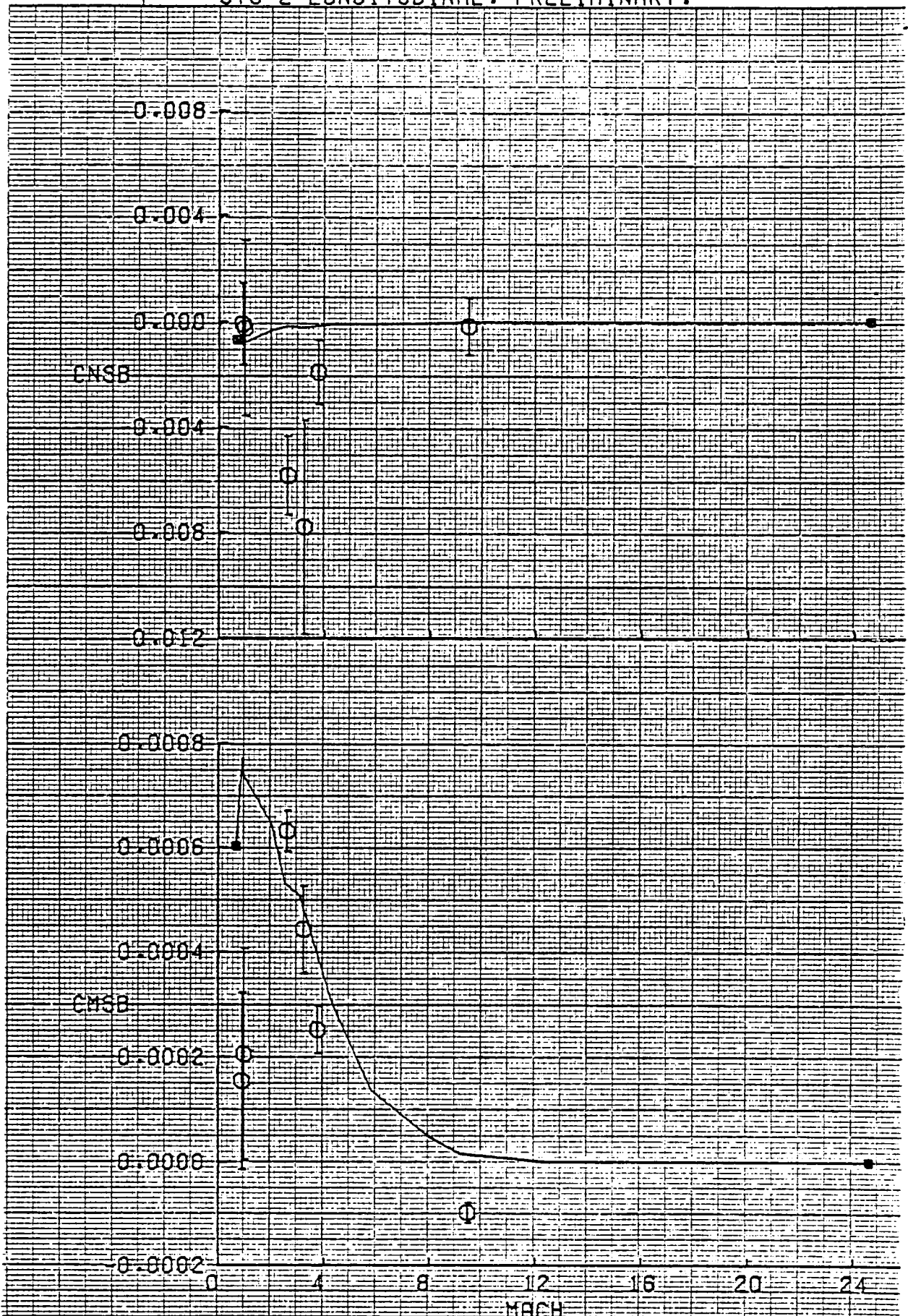


Fig. 3d (cont) $C_{n_{SB}}$ and $C_{m_{SB}}$ vs M

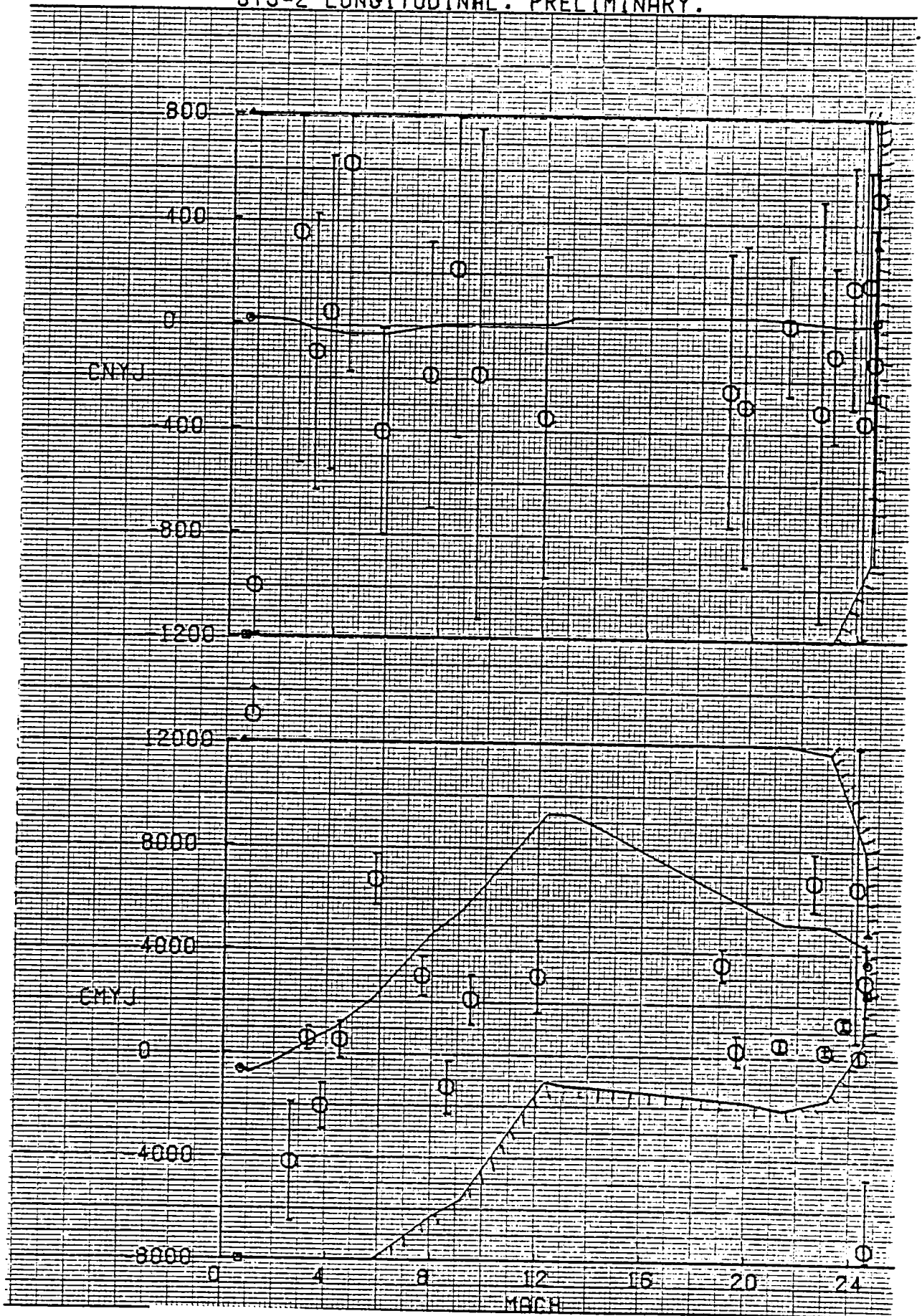


Fig. 3e (concluded) $C_{M_{yT}}$ and $C_{M_{yT}}$
 vs M

82/01/21. 13.42.08.
STS-2 LONGITUDINAL. PRELIMINARY.

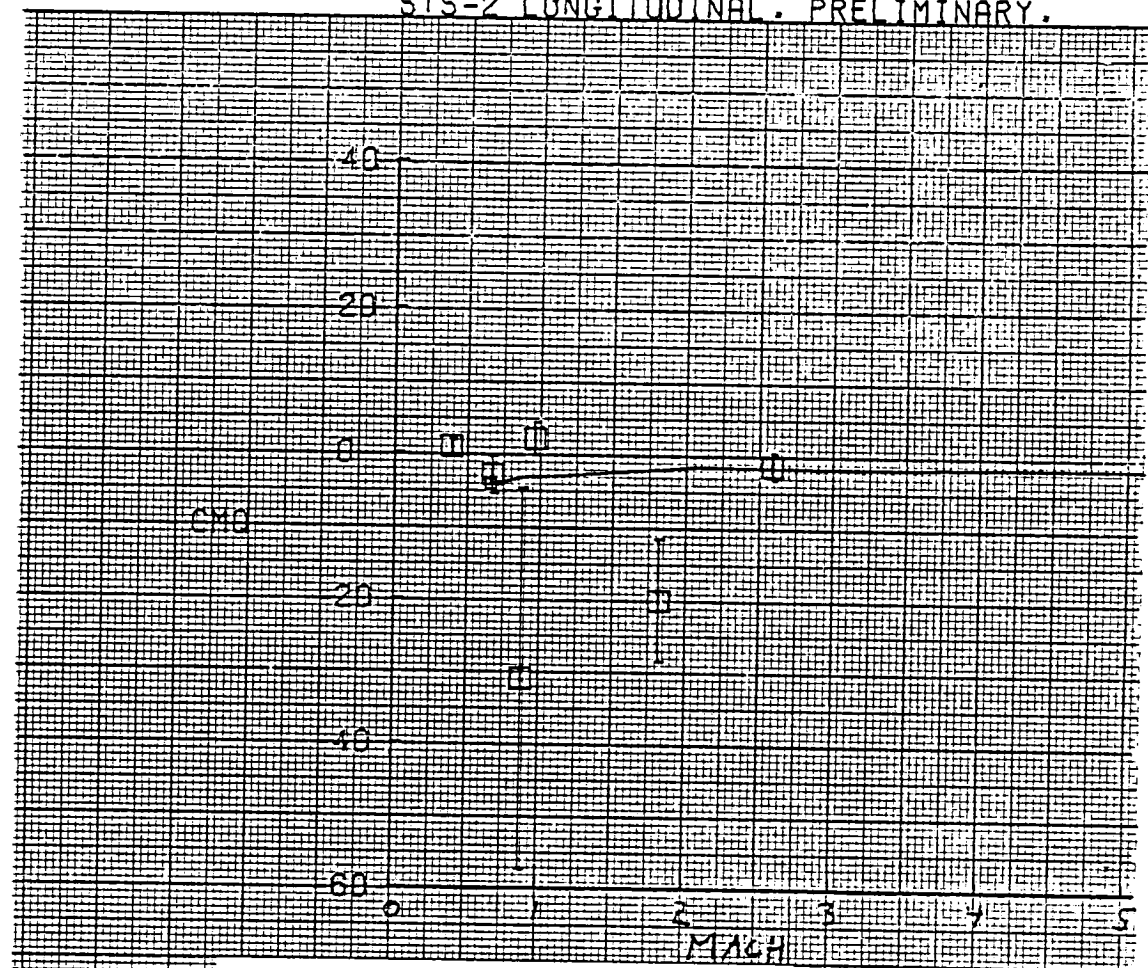


Fig. 4 Correlation of Flight and Predicted Values of C_{M_g} vs M

SHUTTLE STS-1 AND 2 PRELIMINARY

FLIGHT:	SYMBOL:
STS-1	□
STS-2	○

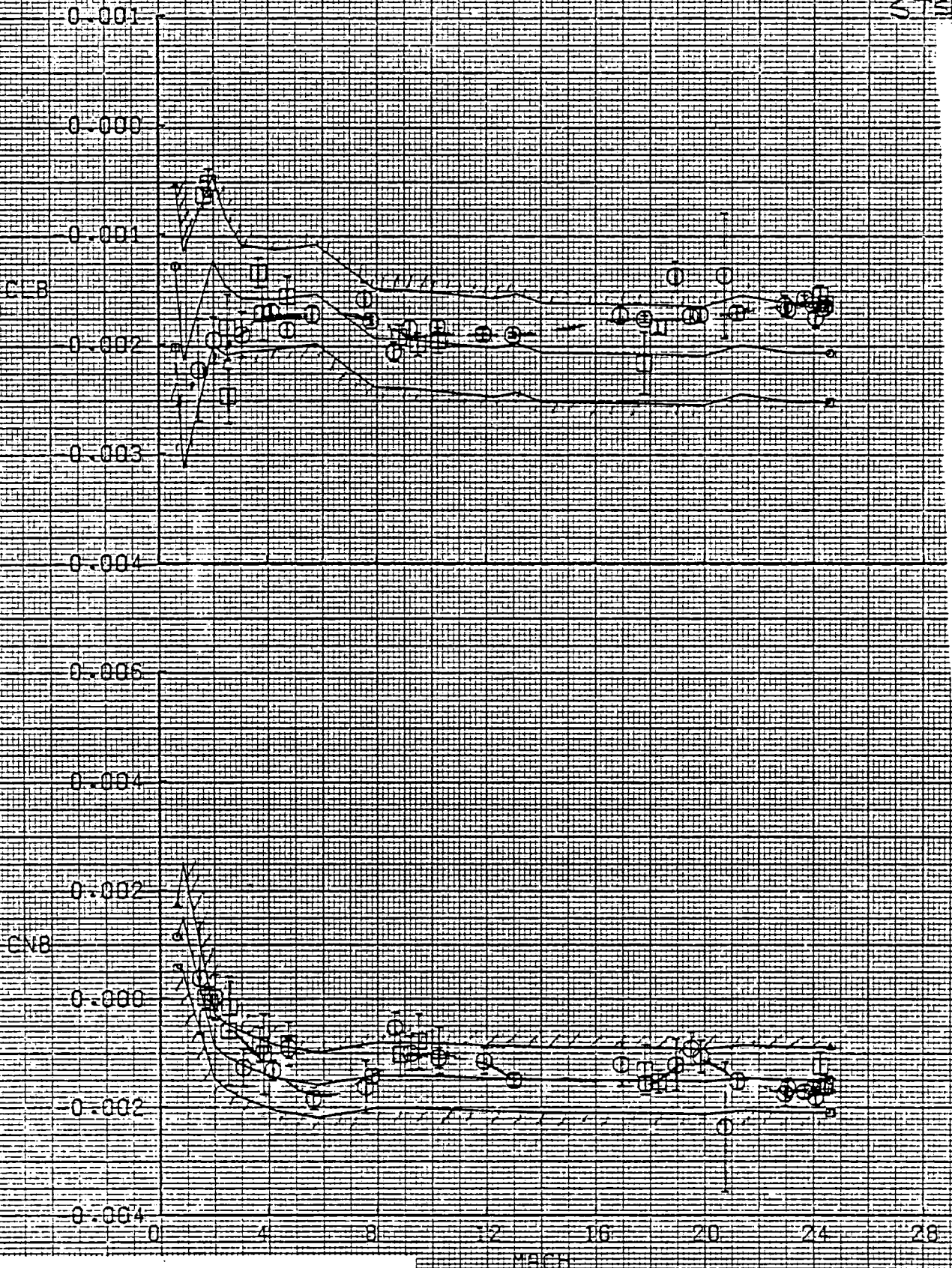


Fig. 5 Correlation of Flight and Predicted Values of $C_{x/B}$ and $C_{x/B}$ vs M

SHUTTLE STS-1 AND 2 PRELIMINARY

FLIGHT
SYMBOL

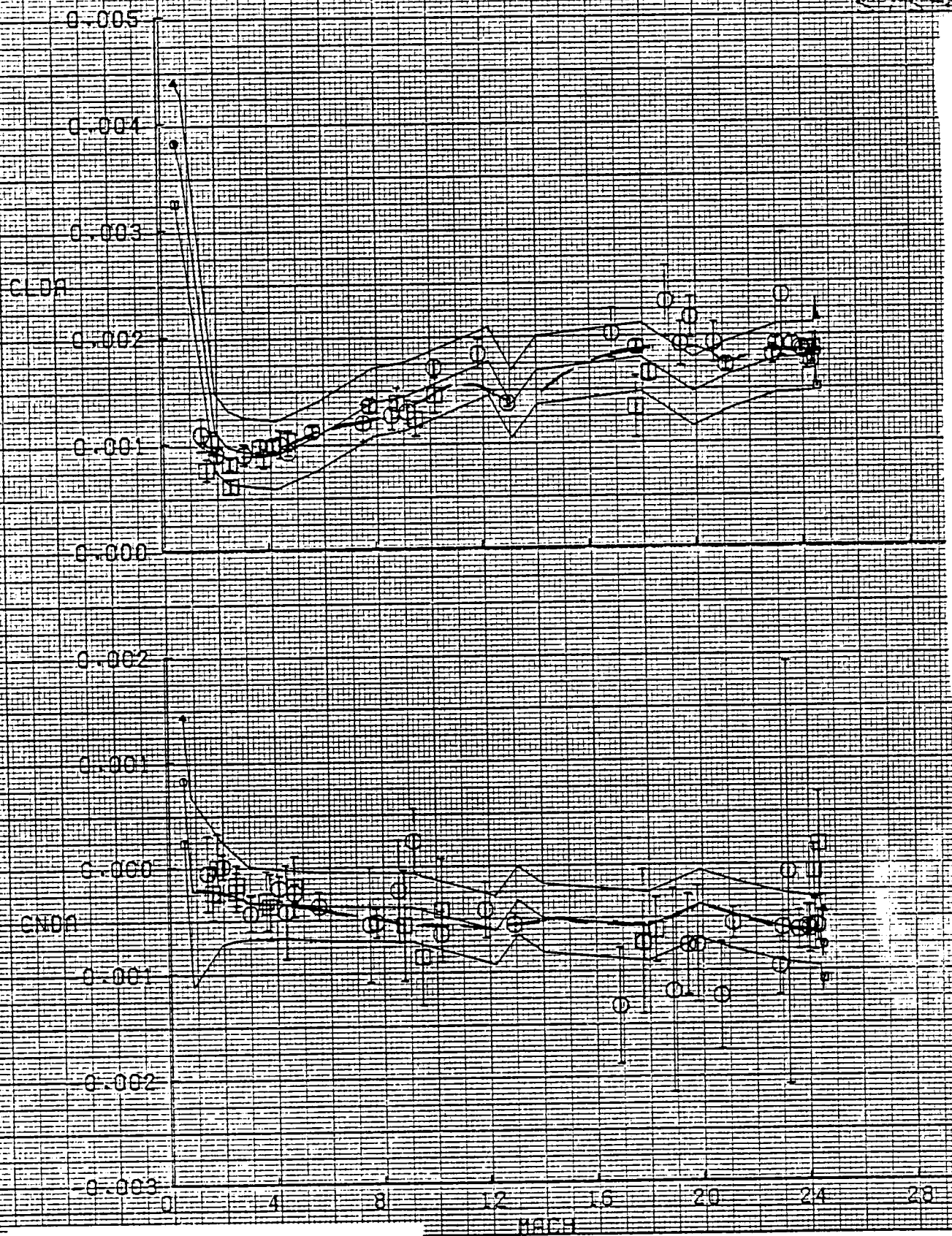


Fig. 6 Correlation of Flight and Predicted Values of C_{2sa} and C_{nsa} vs M

SHUTTLE STS-1 AND 2 PRELIMINARY

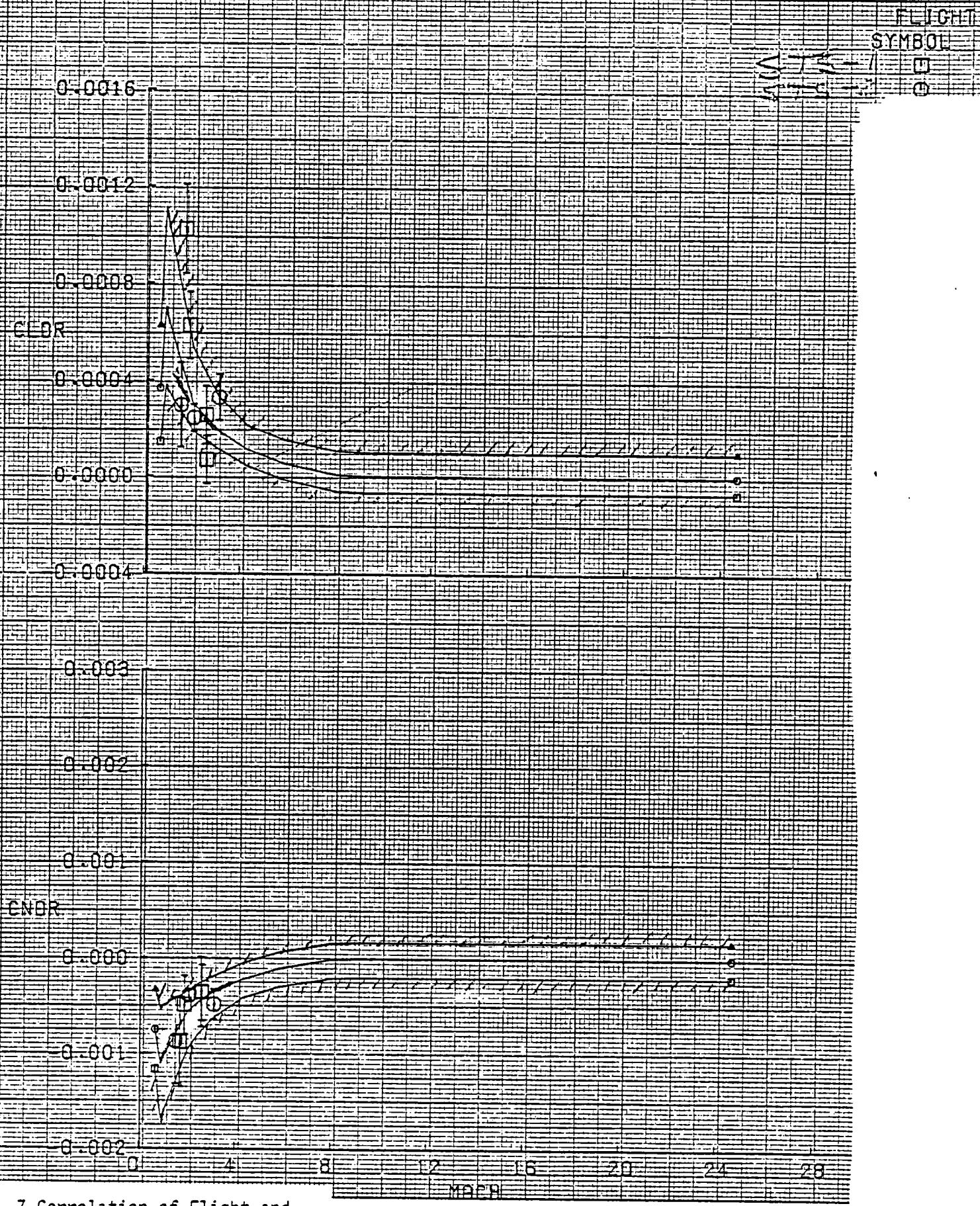


Fig. 7 Correlation of Flight and Predicted Values of $C_{L_{SR}}$ and $C_{N_{SR}}$ vs M

SHUTTLE STS-1 AND 2 PRELIMINARY

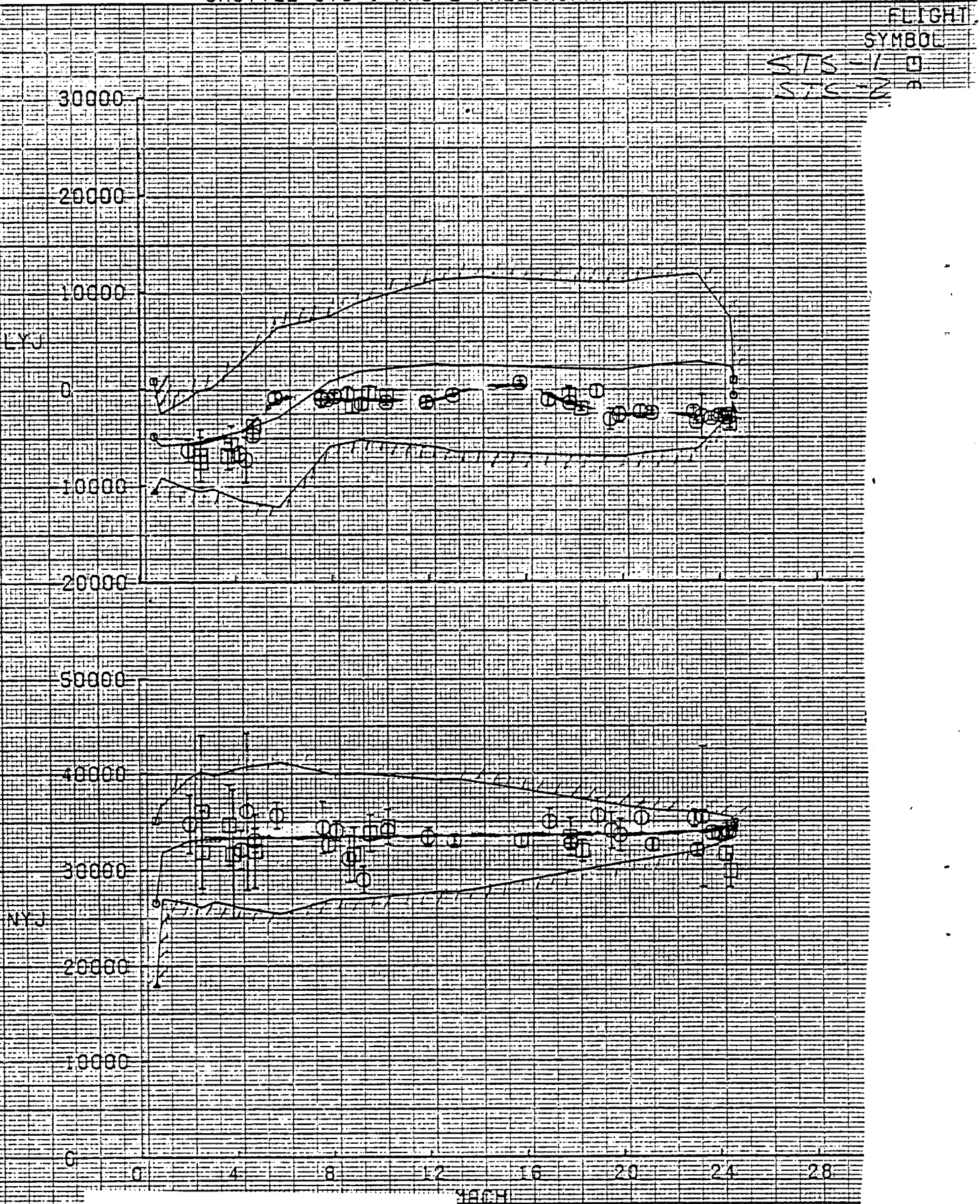


Fig. 8 Correlation of Flight and Predicted Values of L_{y_j} and N_{y_j} vs M

SHUTTLE STS-1 AND 2 PRELIMINARY

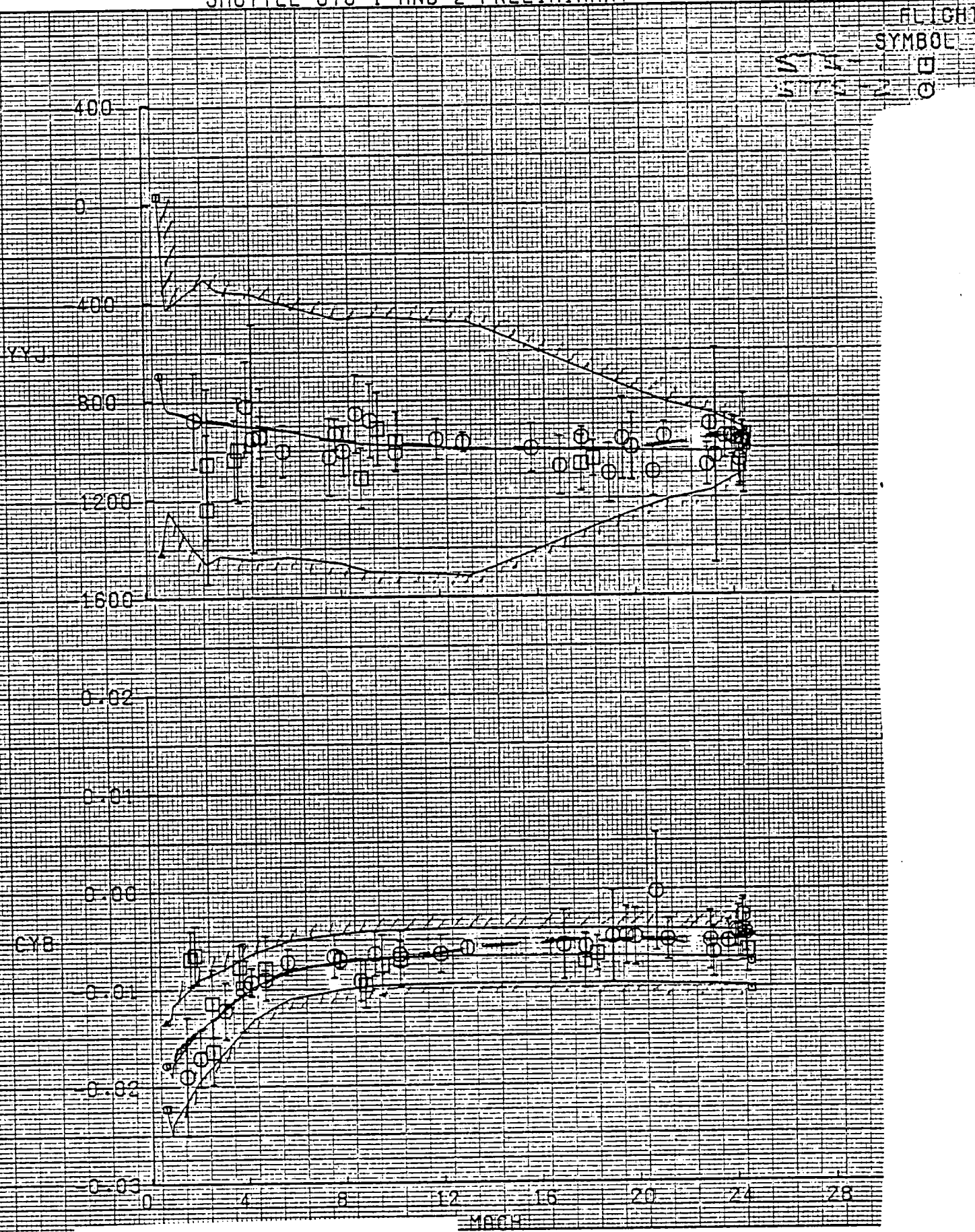


Fig. 9 Correlation of Flight and Predicted Values of Y_{y3} and C_{yB} vs M

SHUTTLE STS-1 AND 2 PRELIMINARY

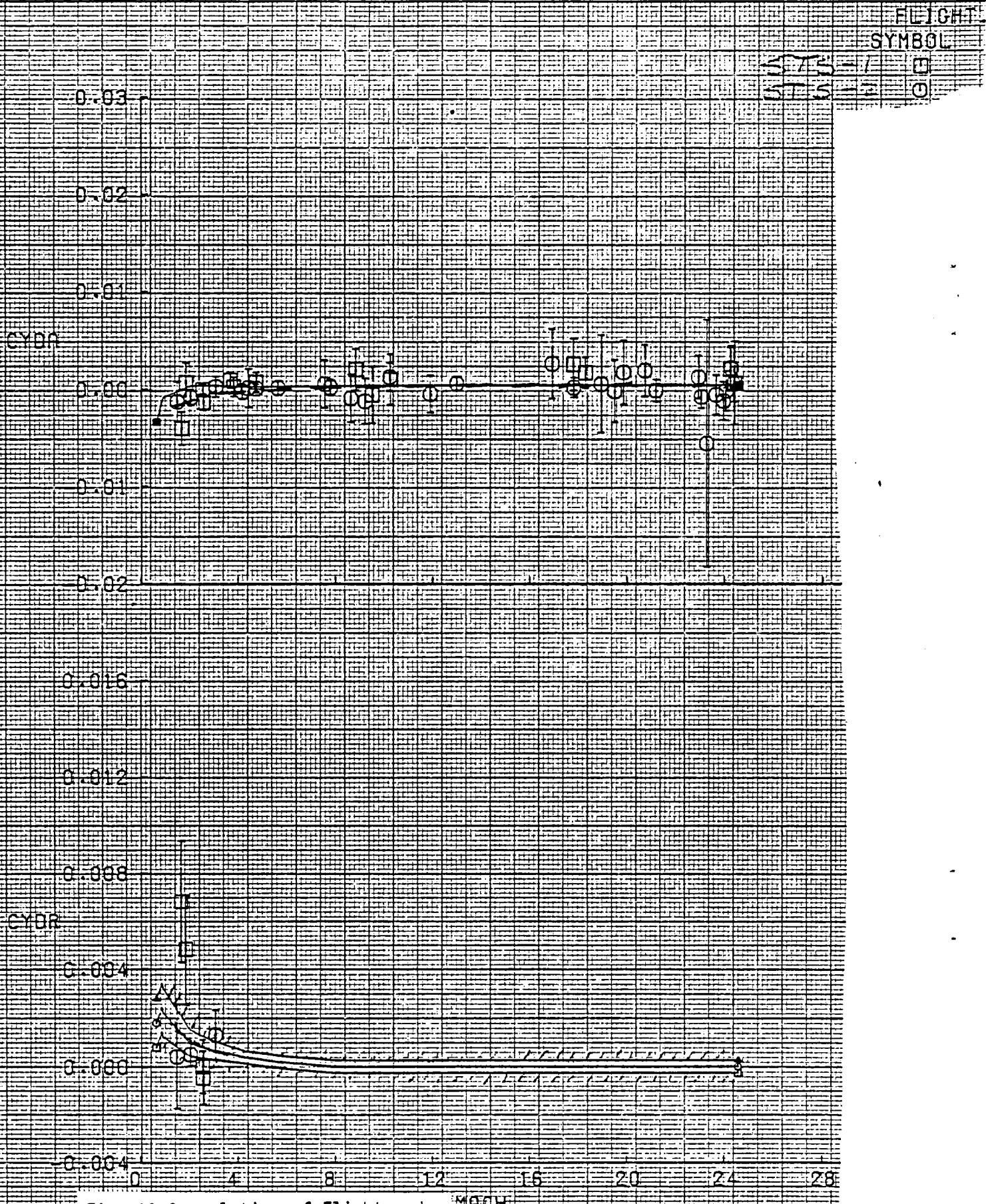


Fig. 10 Correlation of Flight and Predicted Values of C_{y_s} and C_{y_r} vs M

STS-2 LAT-OIR QBAR VARIATION PRELIMINARY

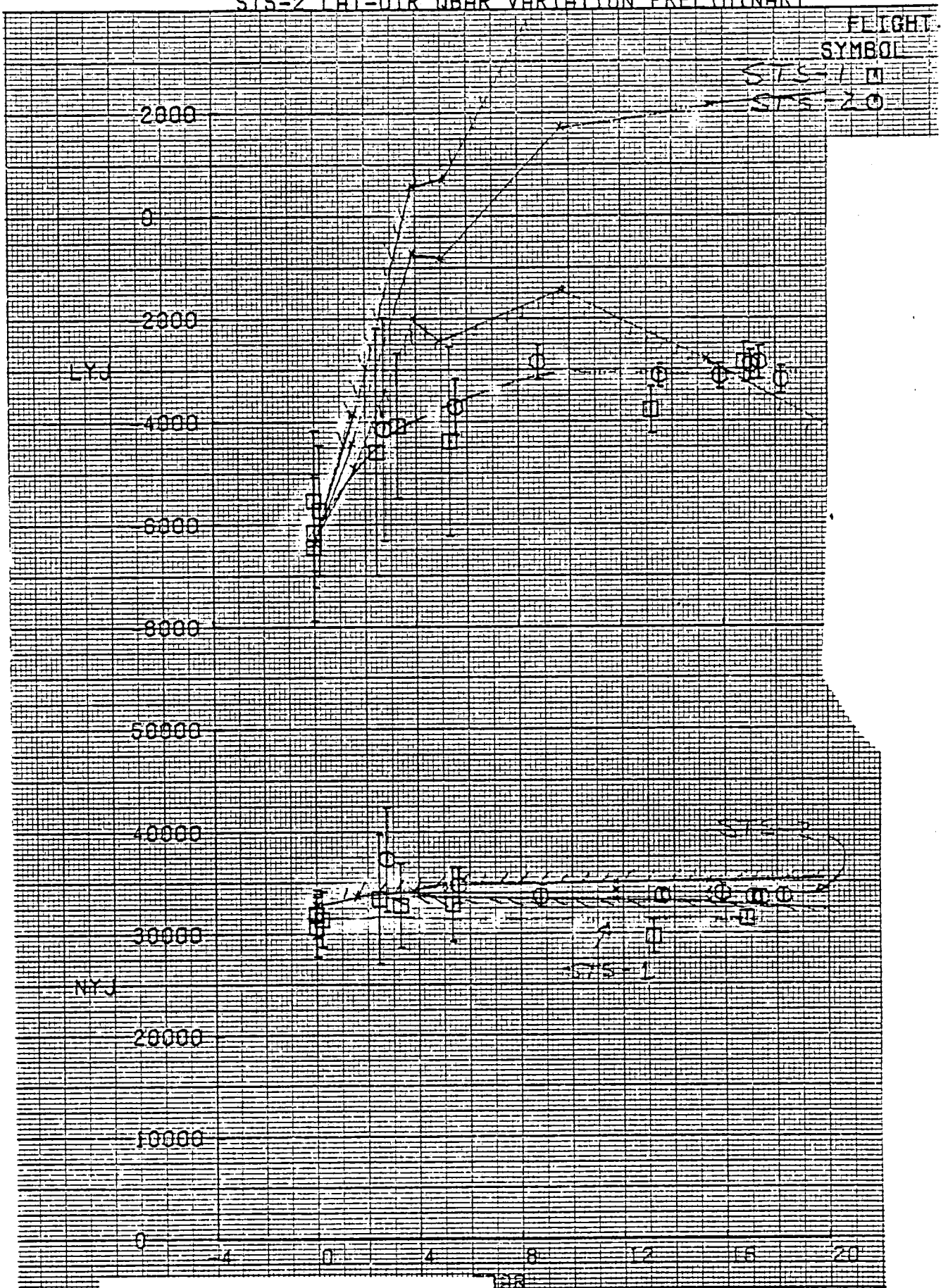


Fig. 11 Correlation of Flight and Predicted Values of L_{y_j} and N_{y_j} vs \bar{q}

STS-2 LAT-DIR QBAR VARIATION PRELIMINARY

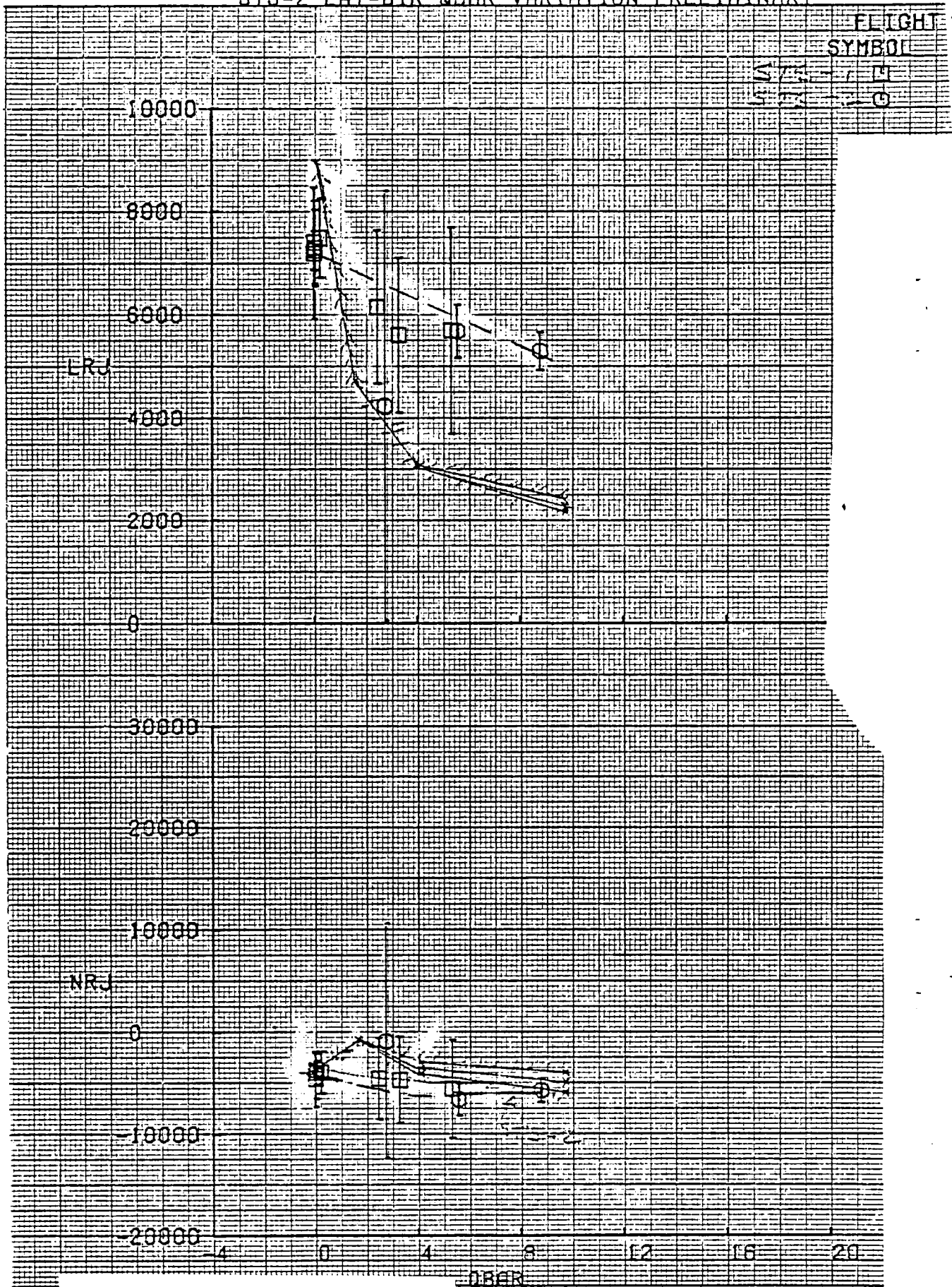


Fig. 12 Correlation of Flight and Predicted Values of L_{RT} and N_{RT} vs \bar{q}

STS-2 LAT-DIR OBAR VARIATION PRELIMINARY

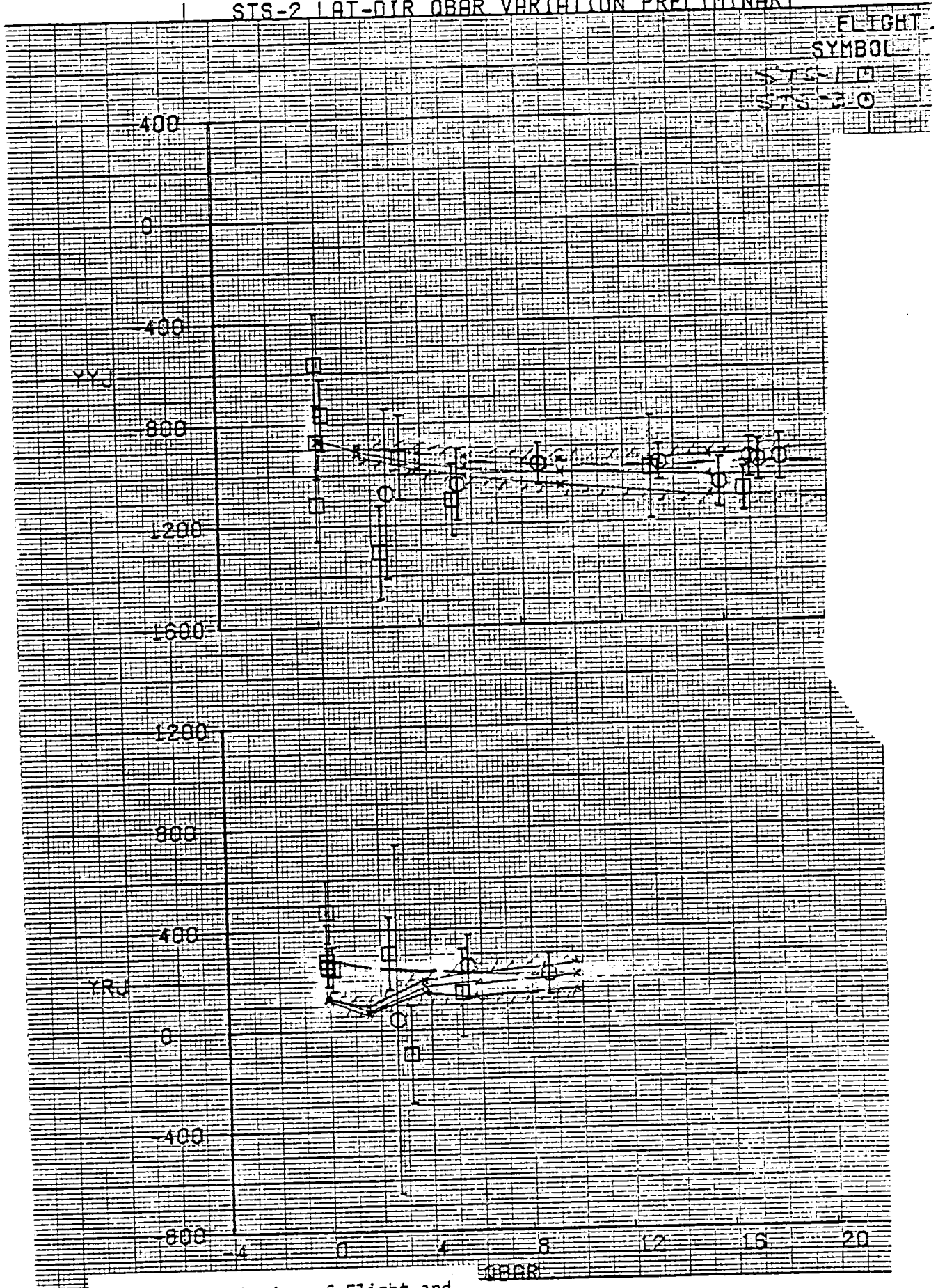
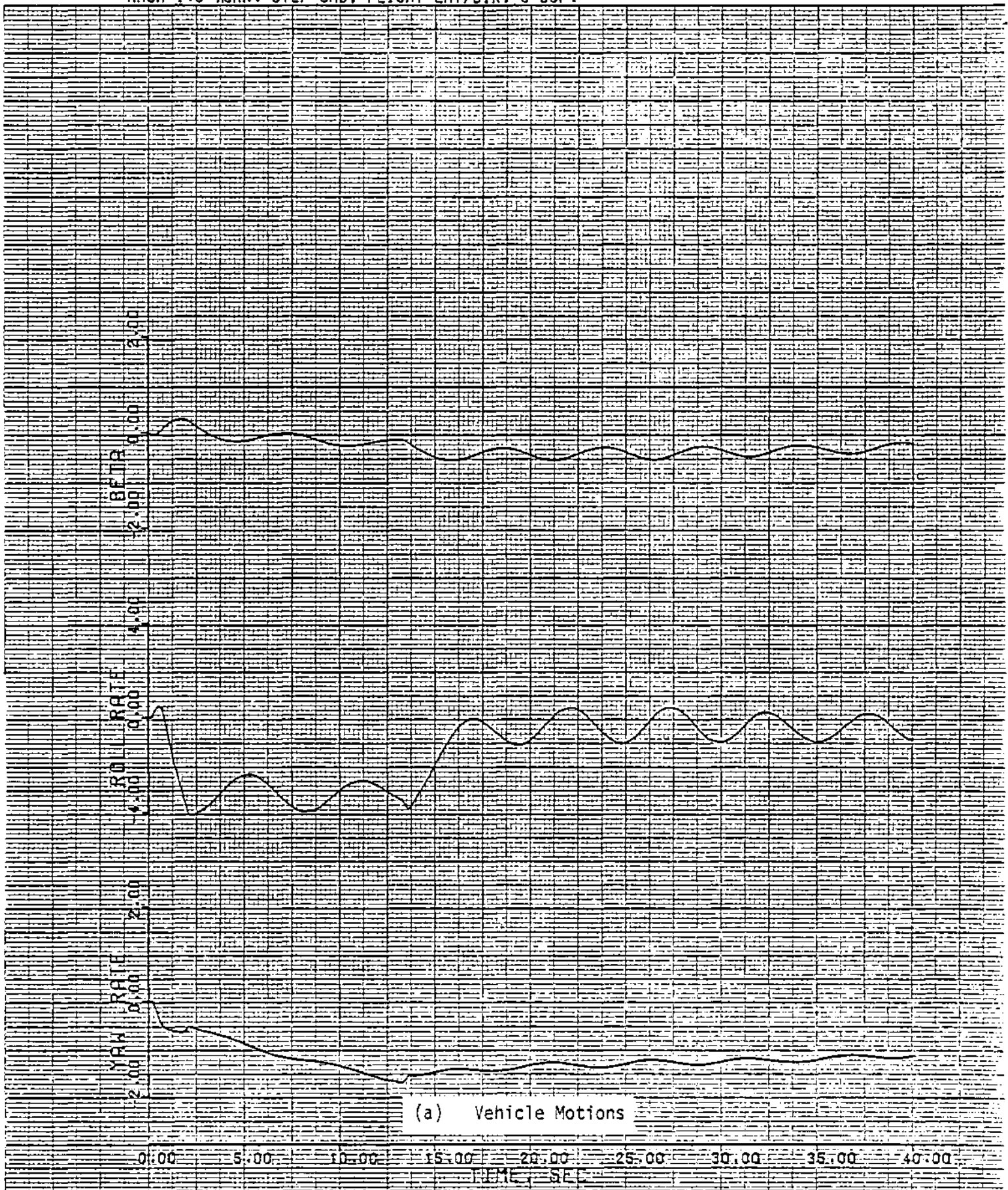


Fig. 13 Correlation of Flight and Predicted Values of Y_{YJ} and Y_{RJ} vs \bar{q}



(a) Vehicle Motions

Figure 14 - Simulated Turn at M = 1.6. Yaw Jets on Linear Derivatives, 5 degrees of Freedom

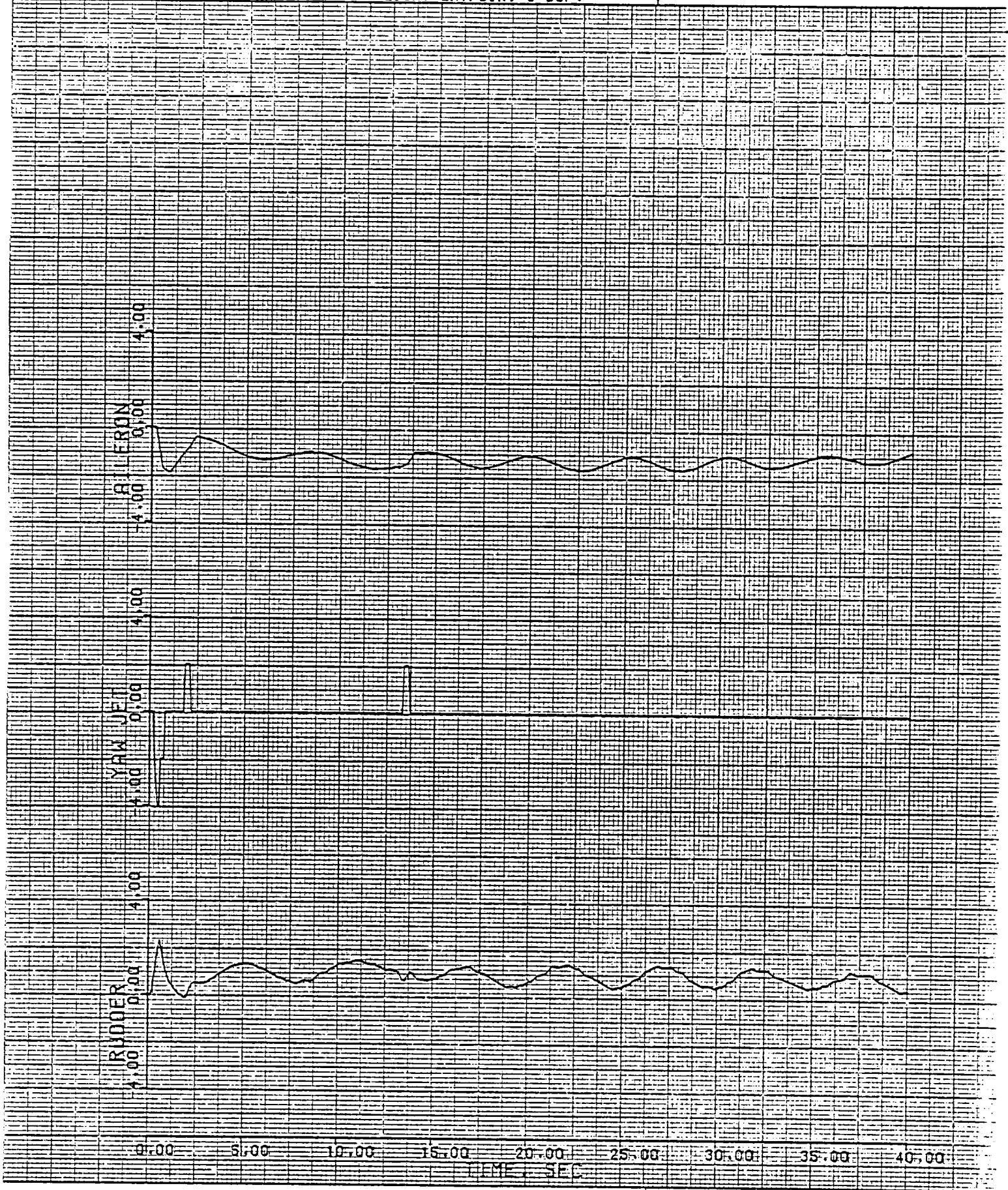


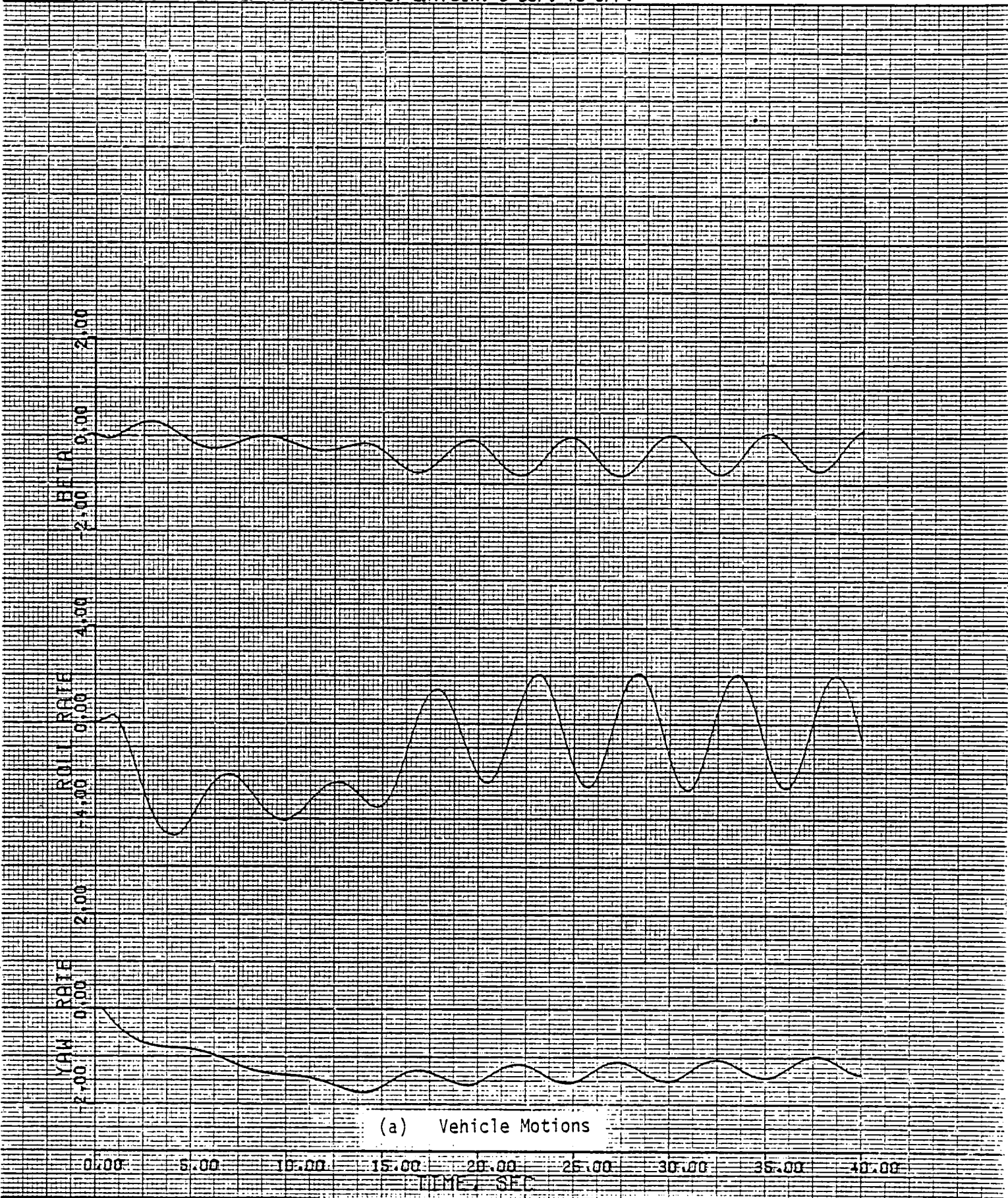
Figure 14 Continued (b) Control Responses

M = 1.6 STS-2 Lateral-Directional Derivatives

C_l	β	-0.0022
	ξ_a	0.00095
	ξ_r	0.00030
	L_{YJ}	-7500.
C_n	β	0.0
	ξ_a	0.0
	ξ_r	-0.0005
	N_{YJ}	33000.
C_y	β	-0.020
	ξ_a	0.0005
	ξ_r	0.0007
	Y_{YJ}	-900.

Figure 14 (concluded) (C) Linear Derivative Values

MACH 1.6 TURN. STEP CMD. STS-2 FLT LAT/DIR. 5 DOF. YJ OFF.



(a) Vehicle Motions

Figure 15 - Simulated Turn at M = 1.6. Yaw Jets Off Linear Derivatives, 5 degrees of Freedom

MACH 1.6 TURN. STEP CMD. STS-2 FLT LAT/DIR. 5 DOF. YJ OFF.

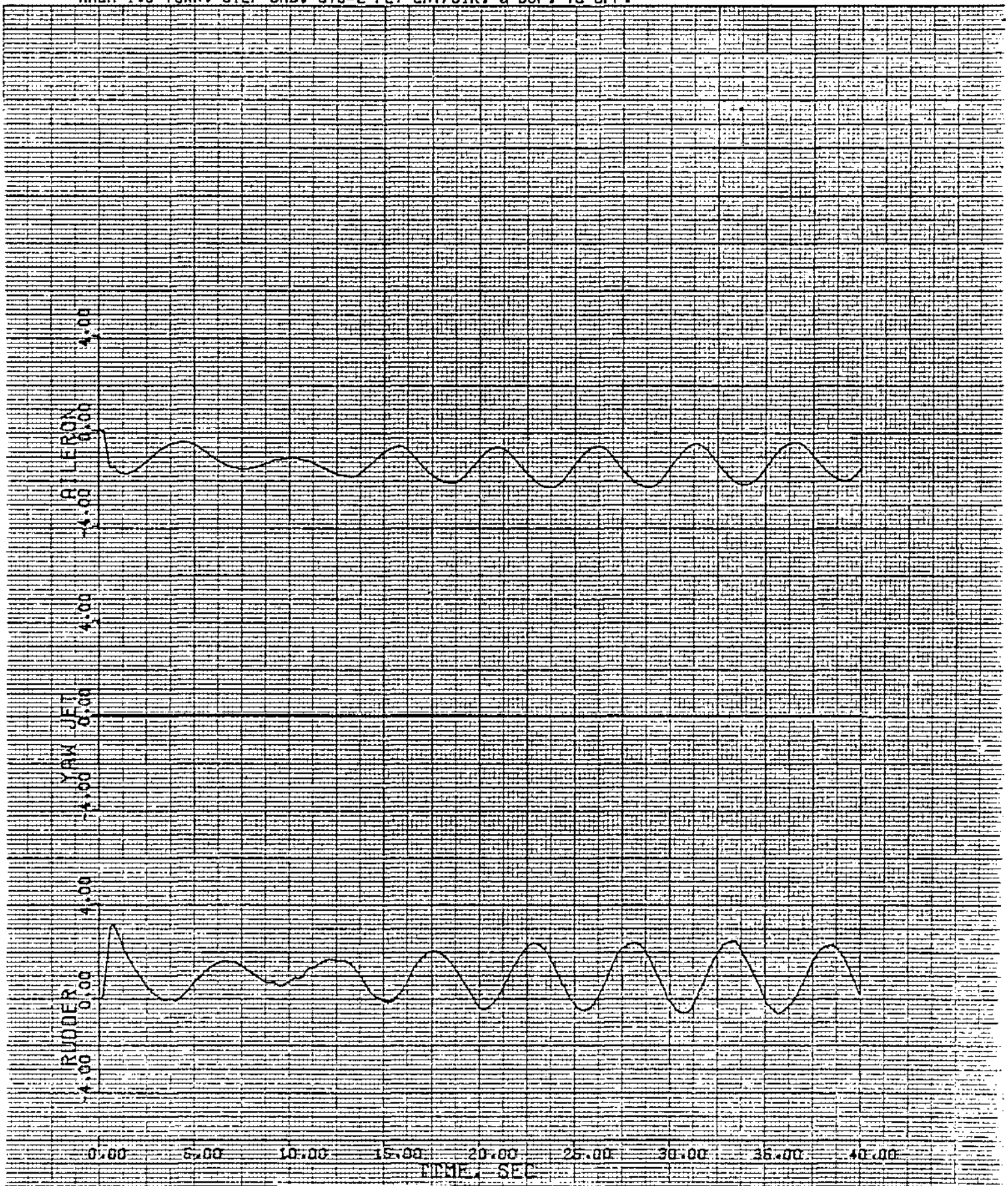


Figure 15 Concluded (b) Control Responses

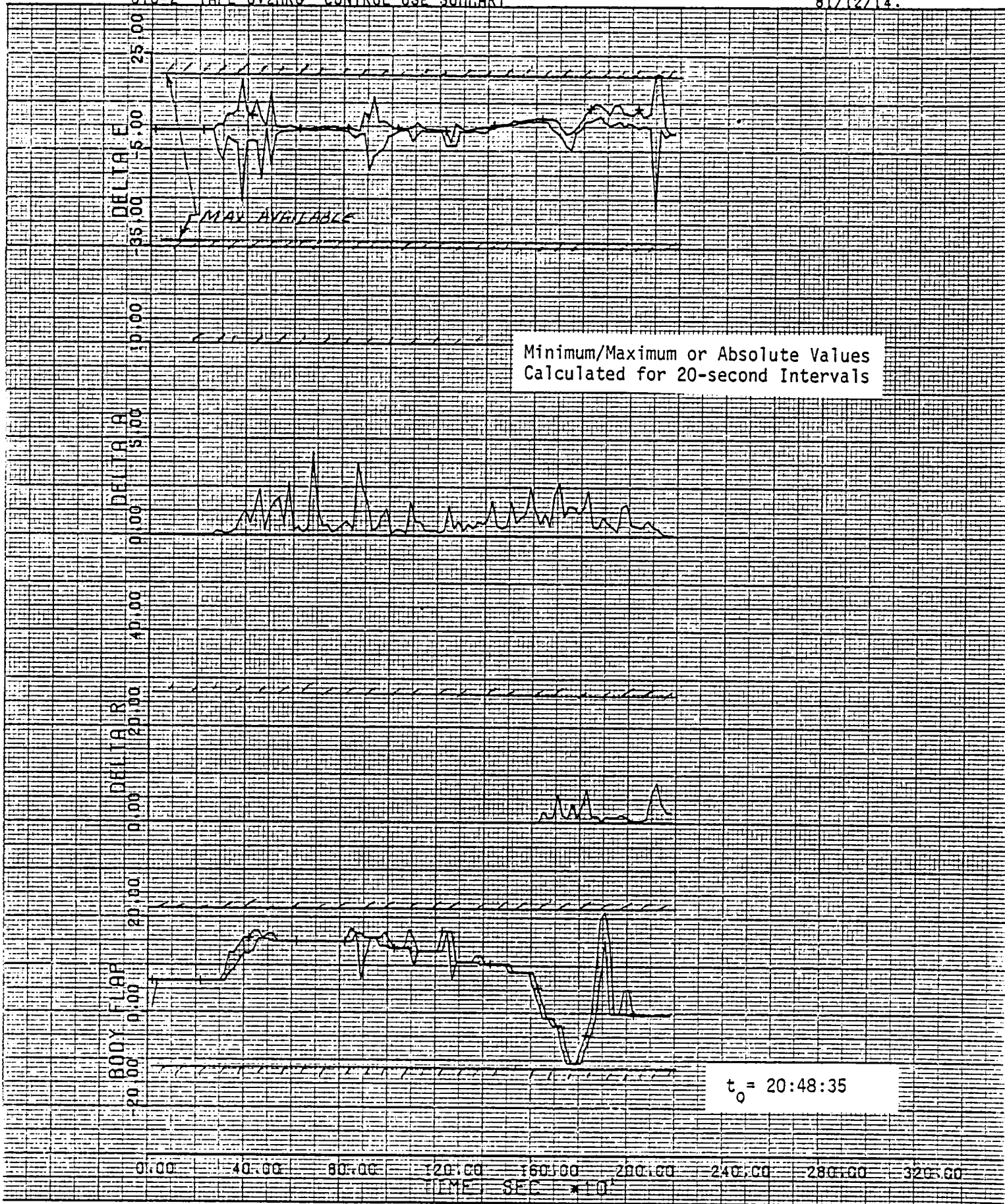


Figure 16 (a) Control use During Entry

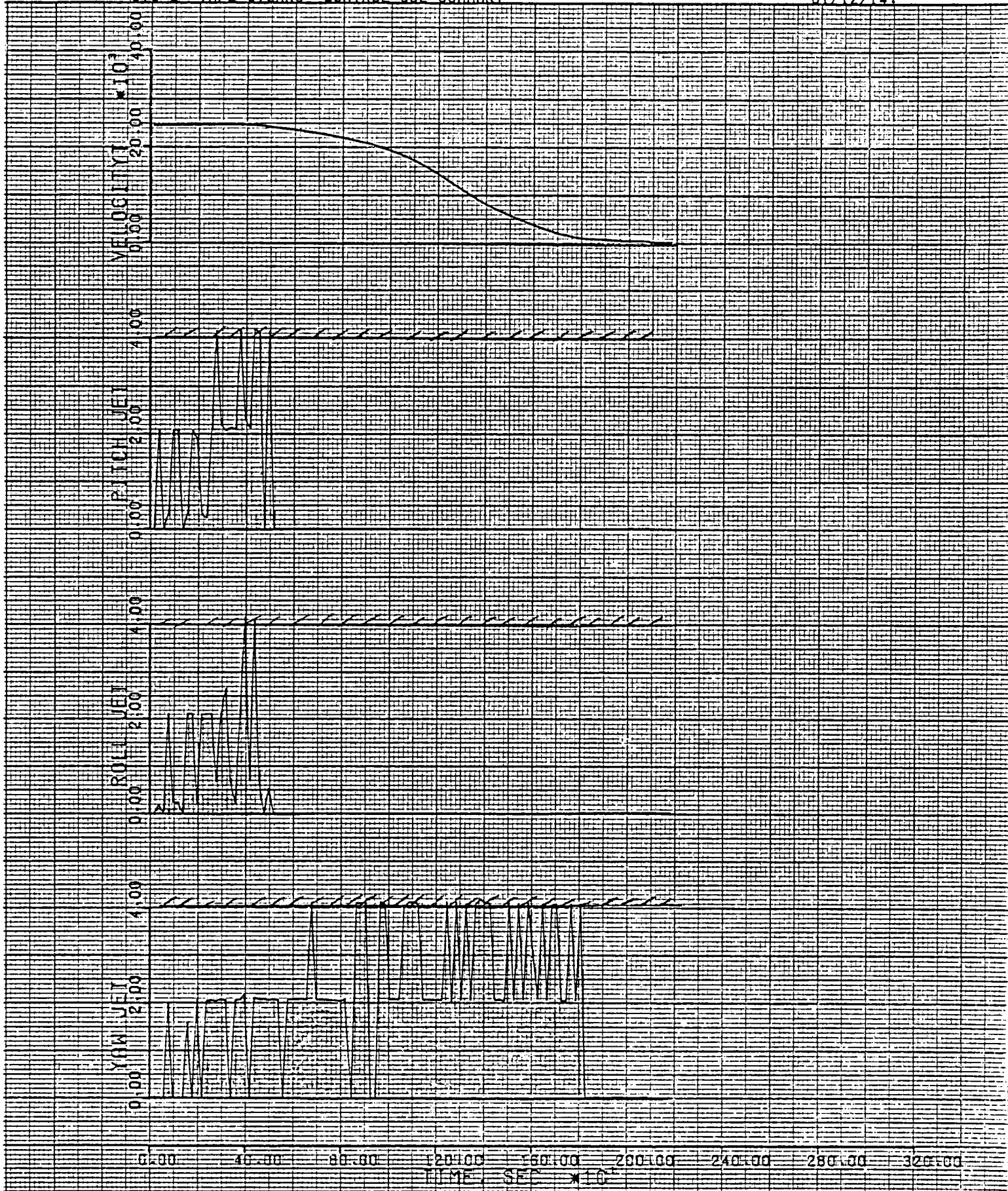
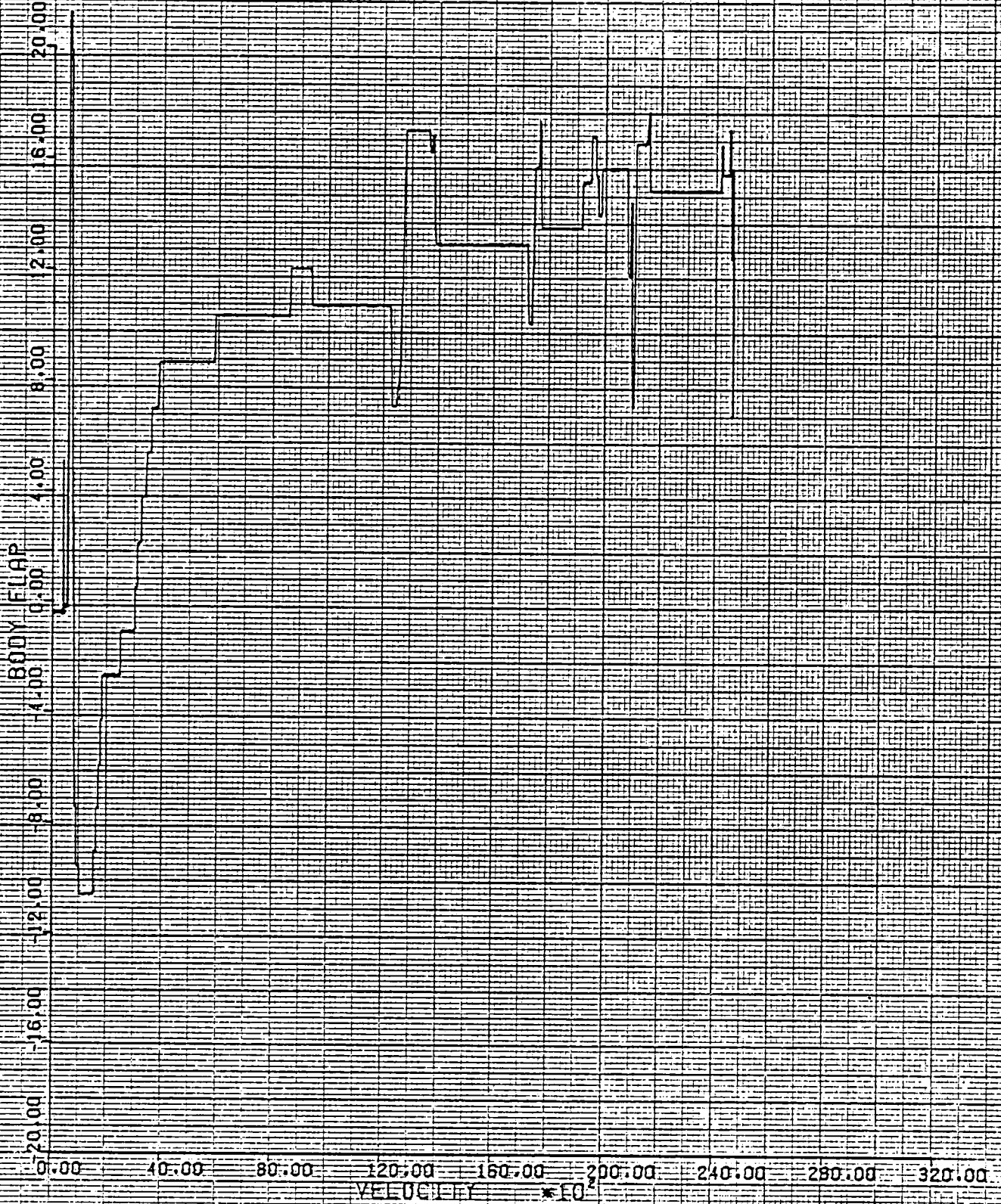


Figure 16 (b) Concluded

STS-2 ENTIRE FLIGHT TAPE 0V2MRC



(a) Body Flap

Figure 17 - Longitudinal Trim Characteristics

STS-2 ENTIRE FLIGHT TAPE OV2MRO



(b) Elevator

Figure 17 Concluded

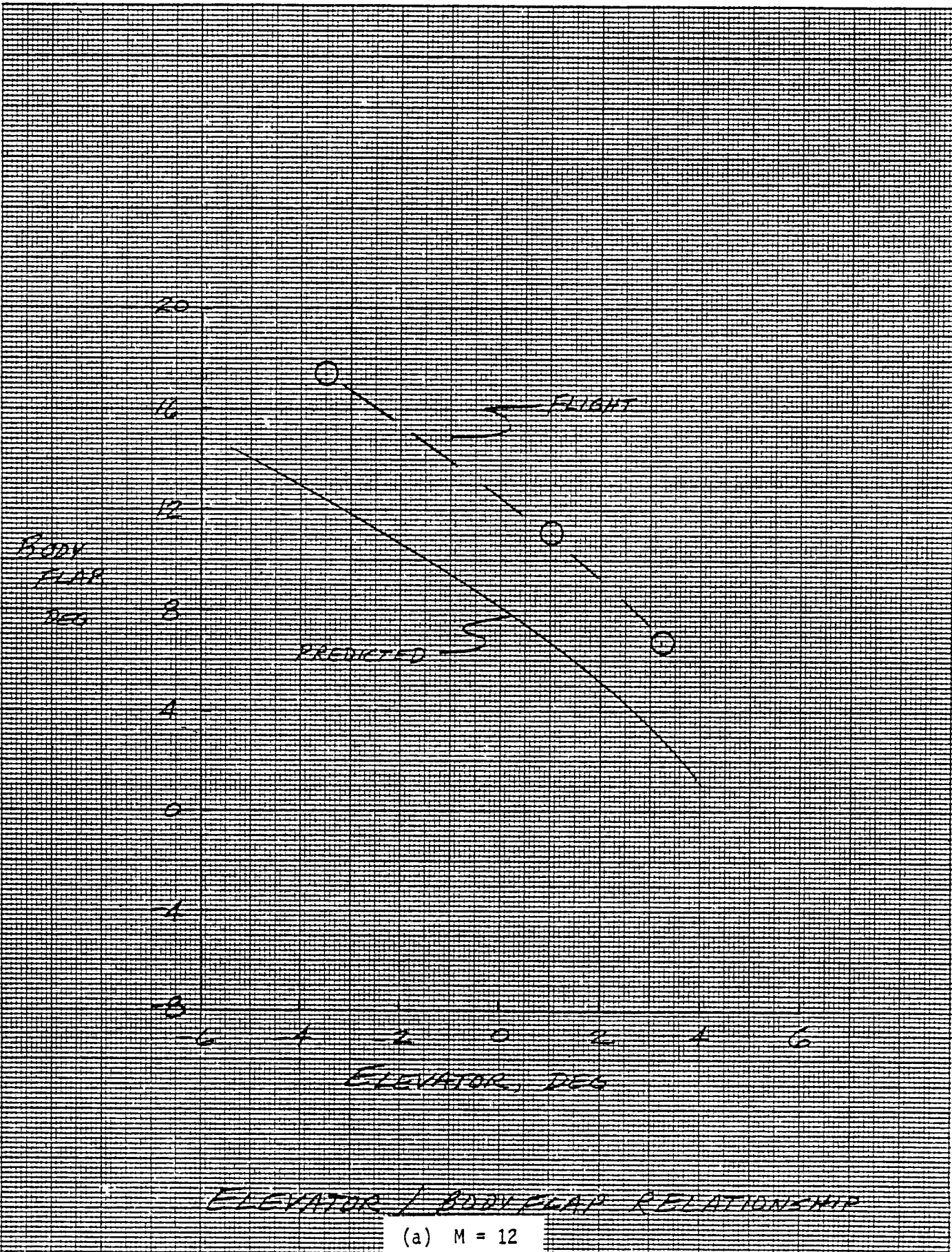
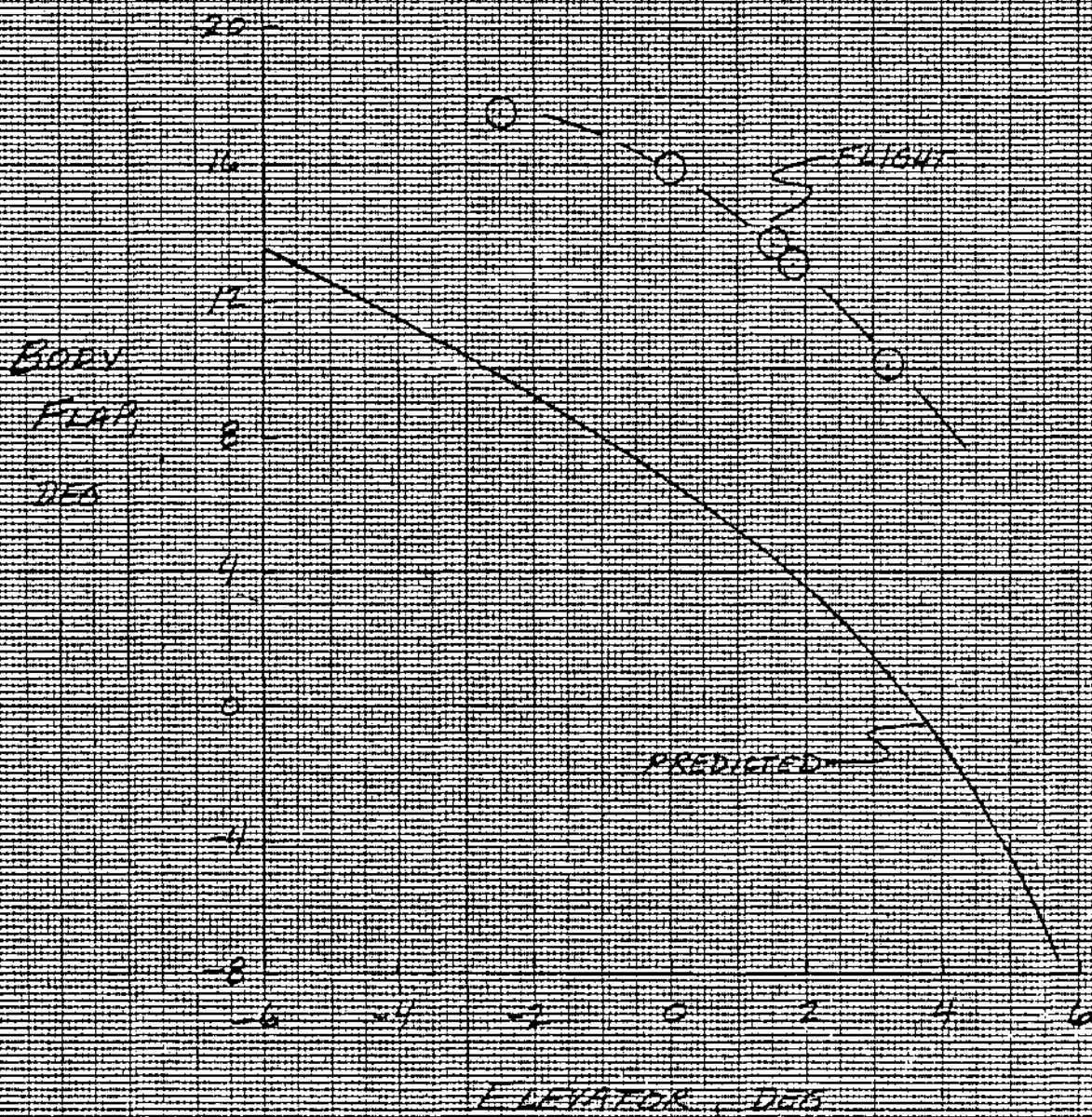


Figure 18 - Comparison of Flight and Predicted Body Flap as a Function of Elevator Position



ELEVATOR / BODY FLAP RELATIONSHIP

Figure 18 Continued (b) M = 18

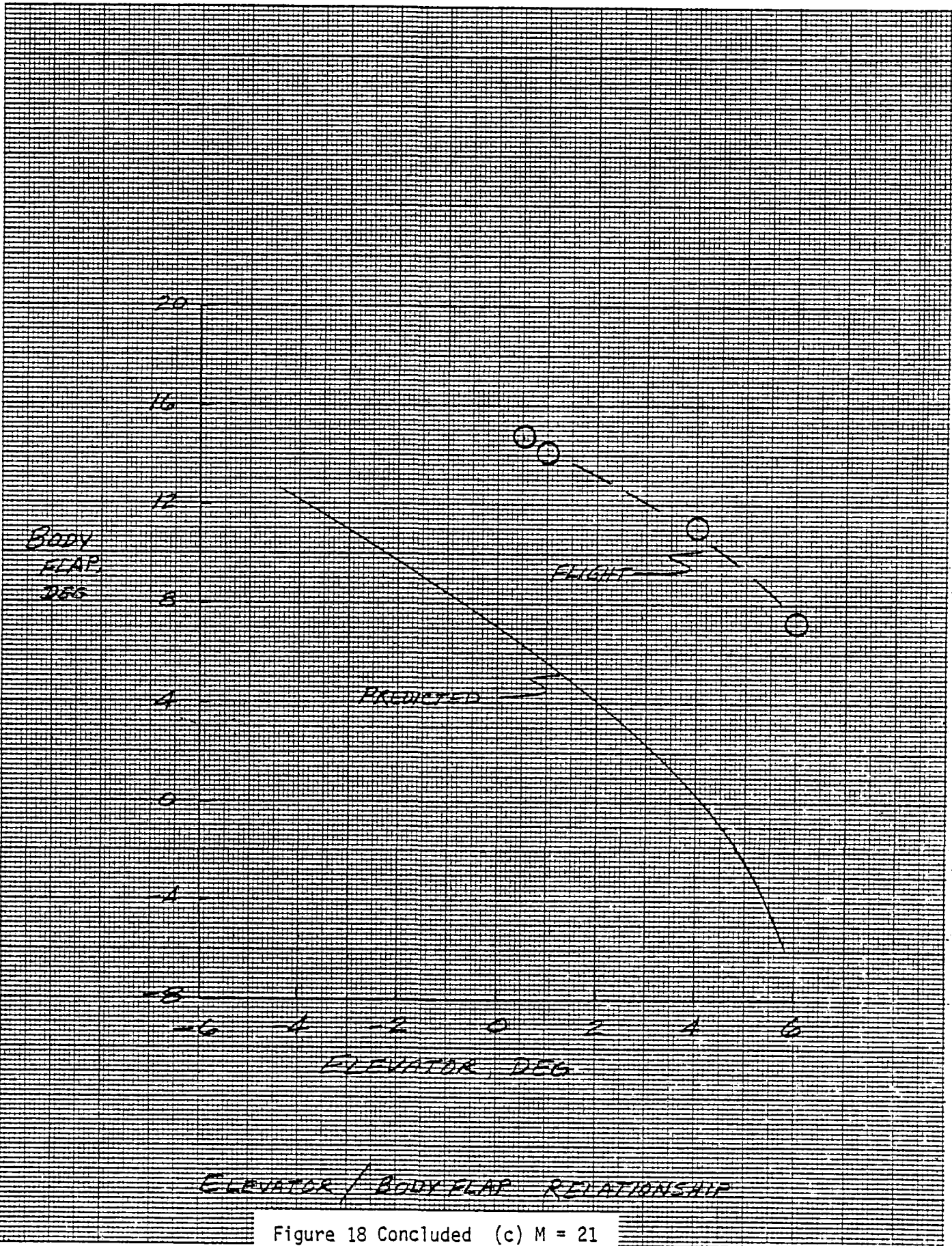


Figure 18 Concluded (c) M = 21

REGRESSION ANALYSIS

$$\Delta C_L = C_{L \text{ FLIGHT}} - C_{L \text{ PREDICTED}}$$

$$\Delta C_D = C_{D \text{ FLIGHT}} - C_{D \text{ PREDICTED}}$$

$$\Delta C_L = a_1 \alpha + a_2 DE + a_3 SB + a_4 FHB + a_5 BF + a_6 GR + a_7 \alpha^2 + a_8$$

$$\Delta C_D = b_1 \alpha + b_2 DE + b_3 SB + b_4 FHB + b_5 BF + b_6 GR + b_7 \alpha^2 + b_8$$

Where α = angle of attack

DE = elevator

SB = speed brake

BF = body flap

GR = 0.0 gear up, GR = 1.0 gear down

FHB = function of altitude

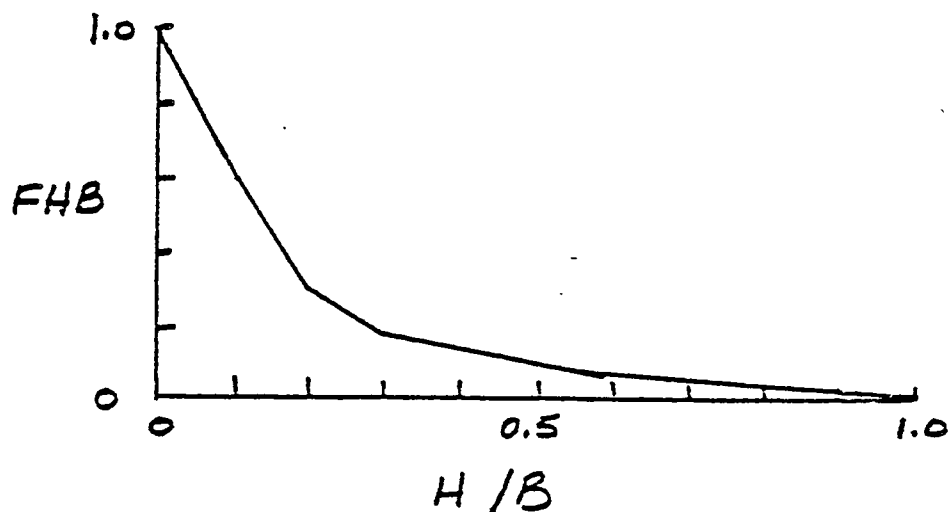


Figure 19 - Equations used for the Regression Analysis

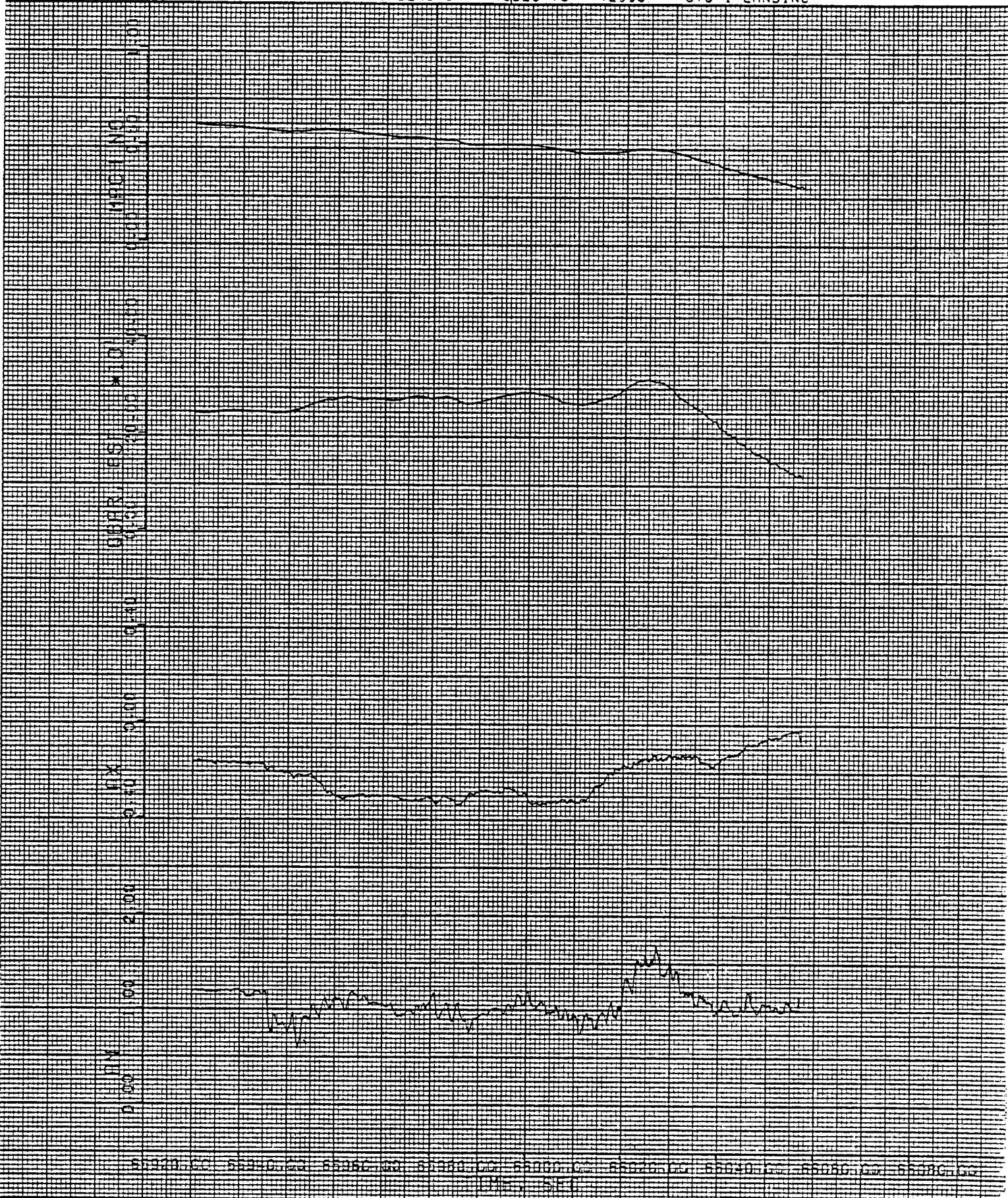


Figure 20 - Input Data to Regression Analysis

(a) STS-1



Figure 20 Continued (b) STS-1

4-PT AVG DATA FROM MACH NUMBERS OF .6472 TO .3044 STS-2 LANDING

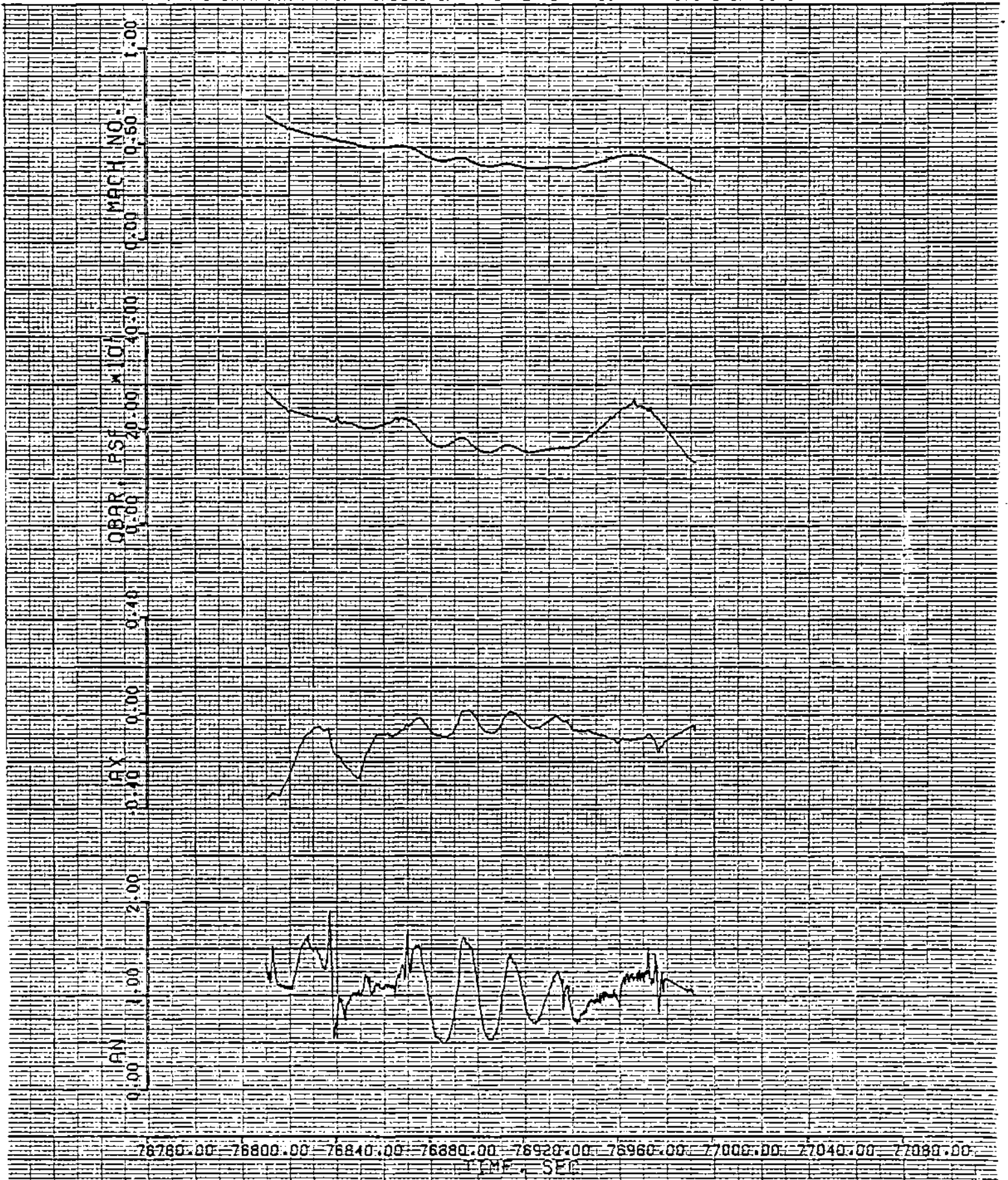


Figure 20 Continued (c) STS-2

4-PT AVG DATA FROM MACH NUMBERS OF .6472 TO .3044 STS-2 LANDING

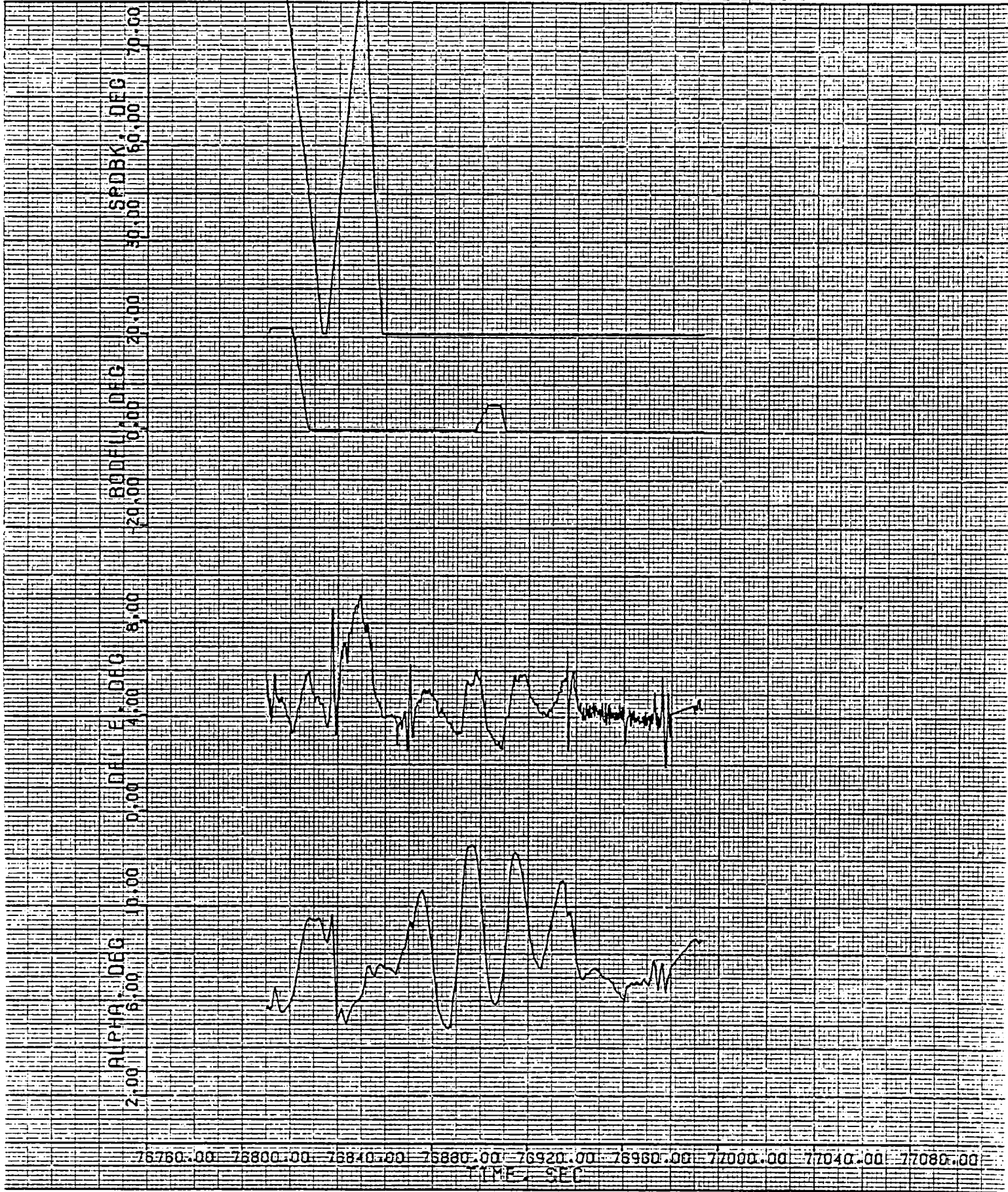


Figure 20 Concluded (d) STS-2

DELTA CL = 0.0000 ALPHA 0.0000 DELTAE 0.0000 SPDBK 0.0000 FMB
 0.0000 RODFLP 0.0000 SEAR 0.0000 ALF2 0.0000 CONST

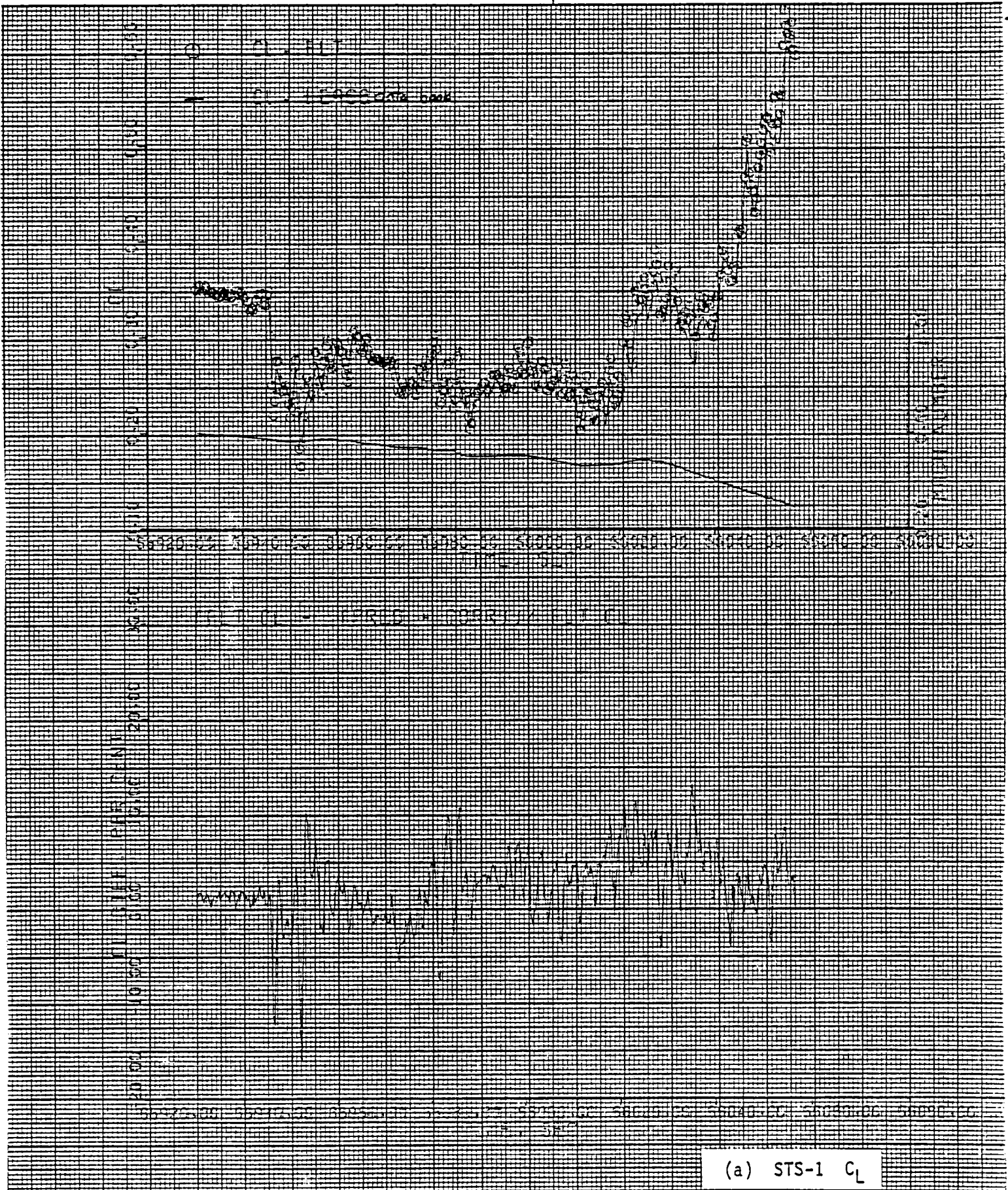


Figure 21 - Comparison of Flight C_L and C_D vs Predictions

DELTA CL = 0.0000 ALPHA 0.00000 DELTAE 0.00000 SPOBK 0.00000 FHB
 0.00000 BODFLP 0.00000 GEAR 0.00000 ALF2 0.00000 CONST

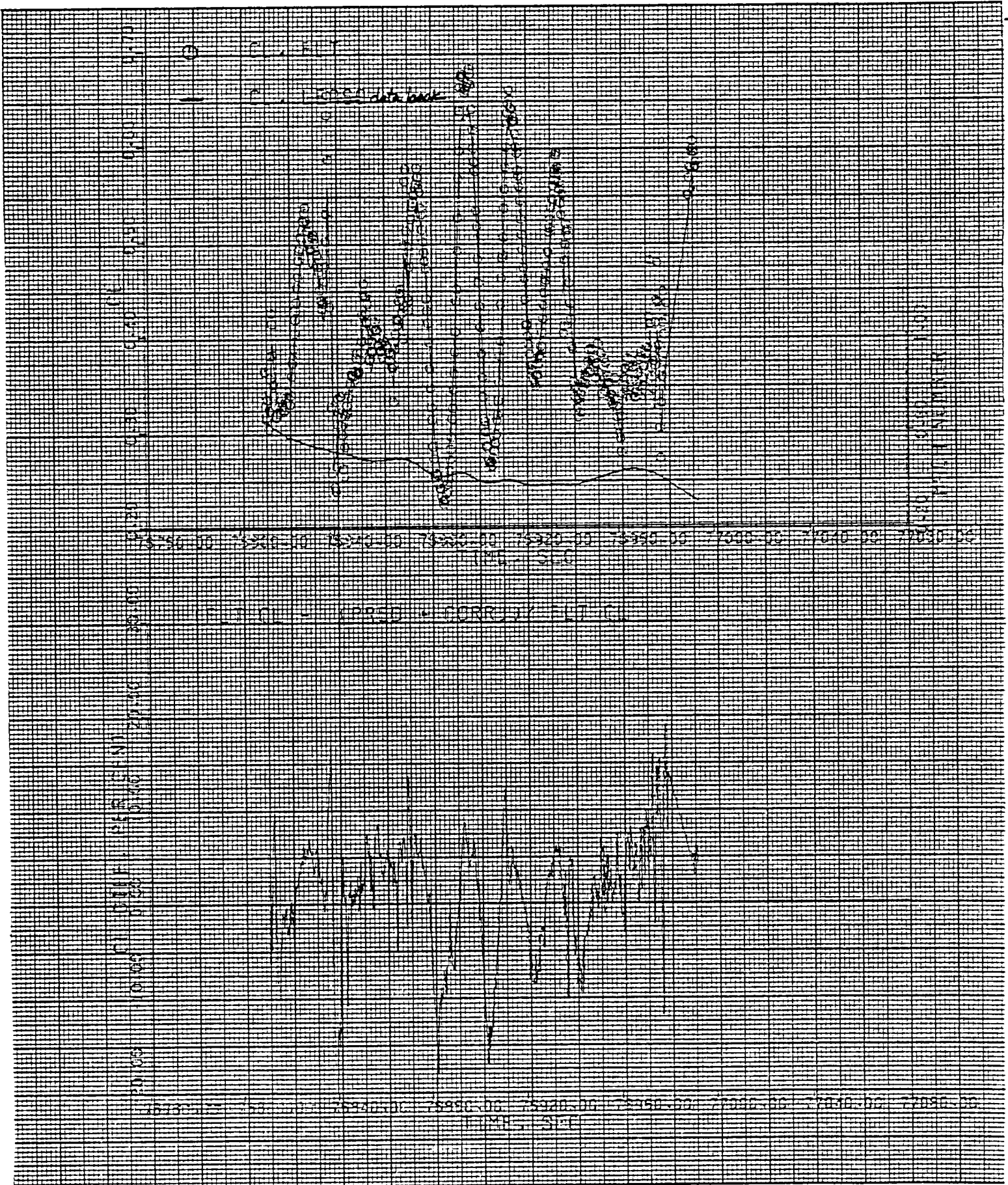


Figure 21 Continued (b) STS-2 C_L

DELTA CD = 0.0000 ALPHA 0.0000 DELTAE 0.0000 SPDBK 0.0000 FMS
 0.0000 RODFLP 0.0000 GEAR 0.0000 ALF2 0.50000 CONST

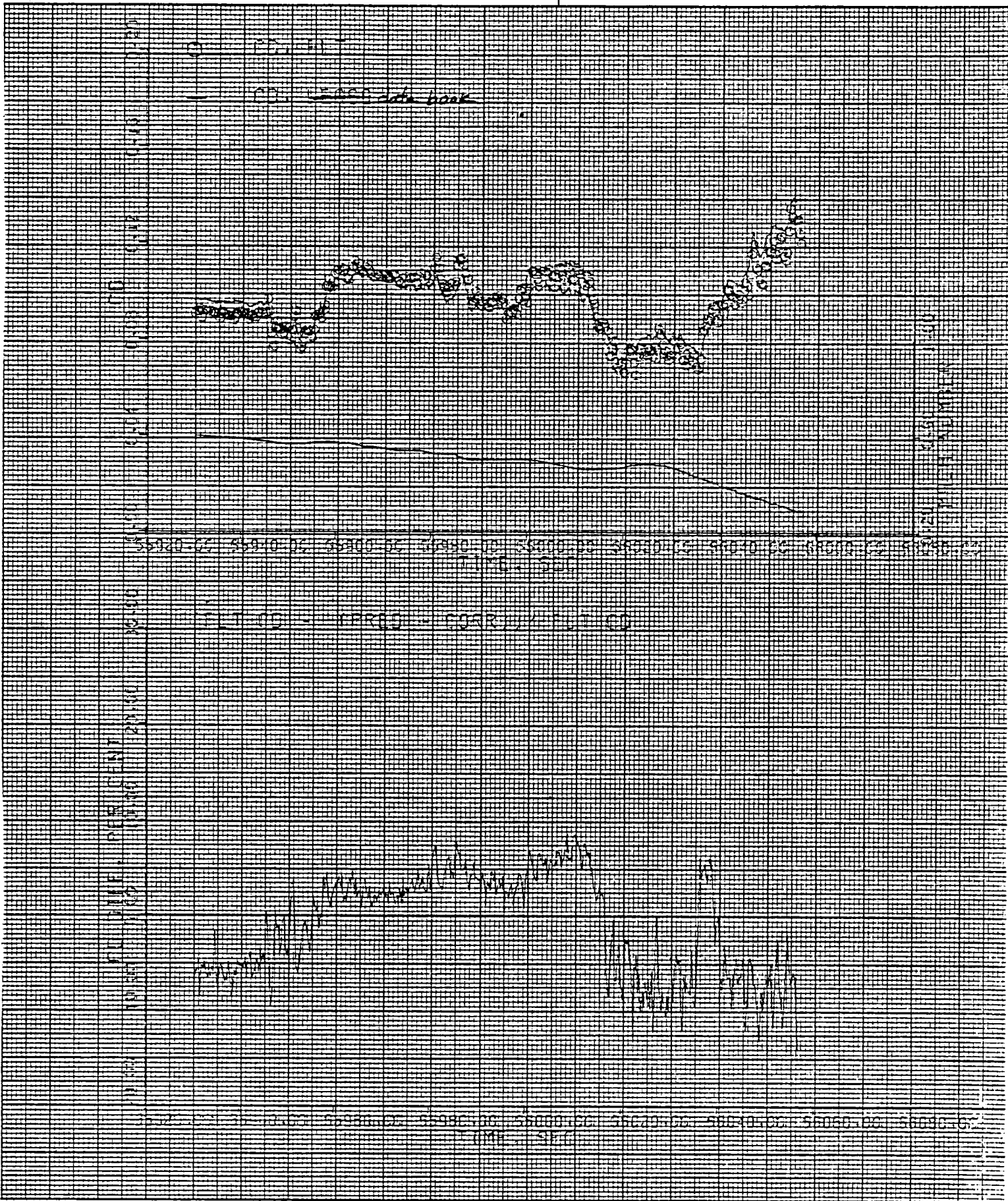


Figure 21 Continued (c) STS-1 C_D

DELTA CD = 0.0000 ALPHA 0.0000 DELTAE 0.0000 SPDBK 0.0000 FMS
 0.0000 BODFLP 0.0000 GEAR 0.0000 ALF2 0.0000 CONST

0 CD - CD
 CD - LEISSO data book

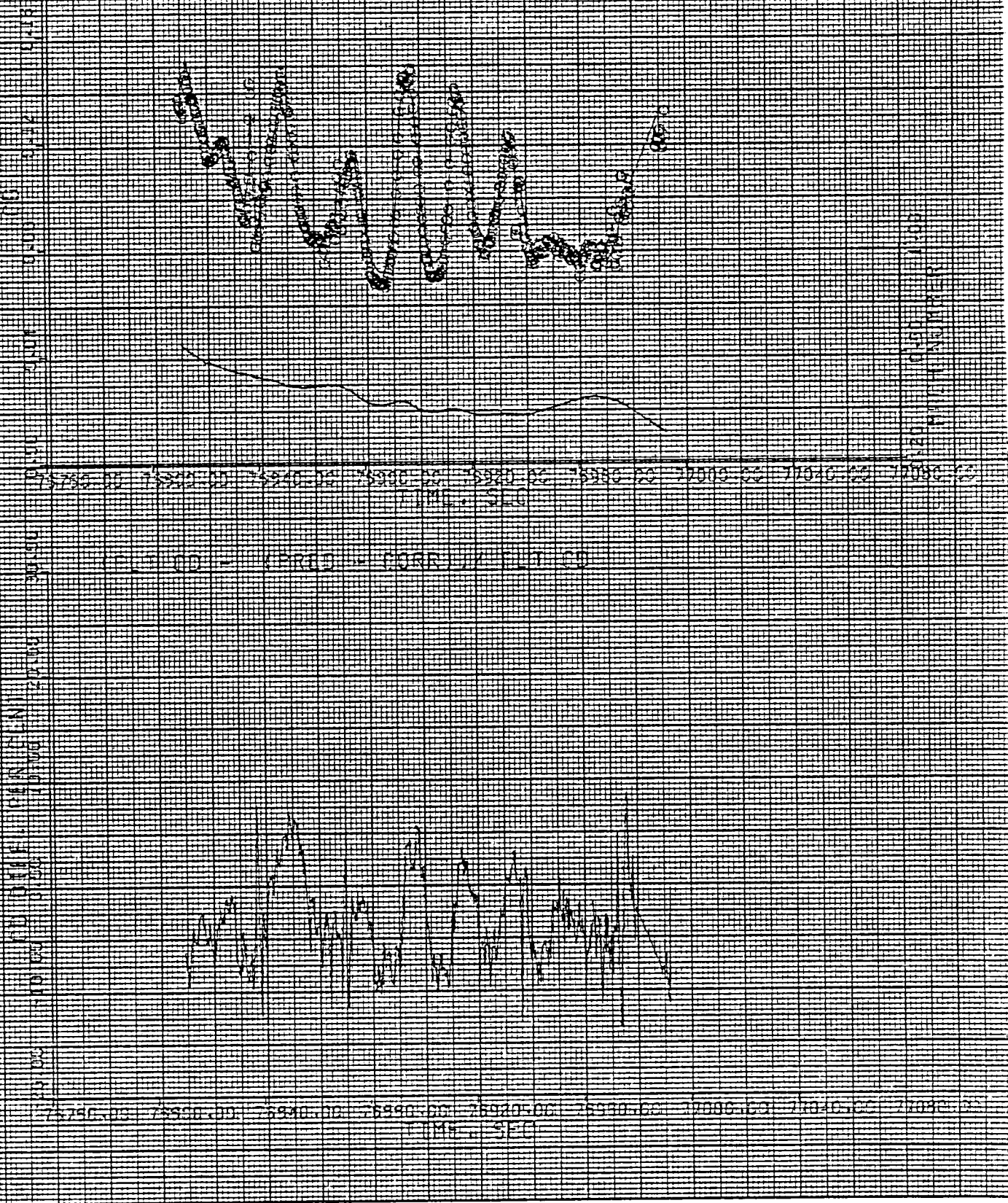


Figure 21 Continued (d) STS-2 C_D

DELTA L/D = 0.0000 ALPHA 0.0000 DELTAE 0.0000 SPDBK 0.0000 FHB
 0.0000 BODFLP 0.0000 GEAR 0.0000 ALF2 0.0000 CONST

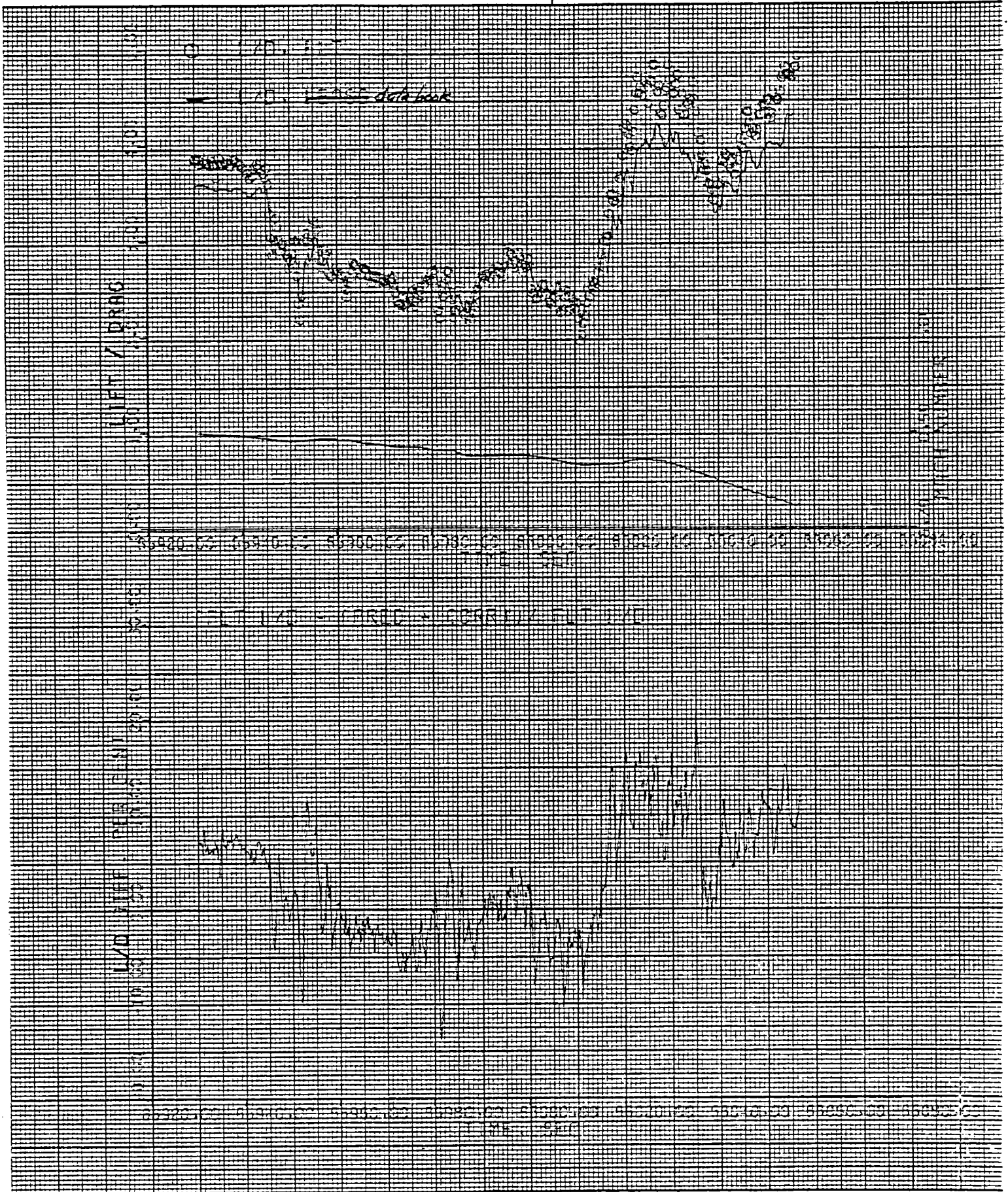


Figure 21 Continued (e) STS-1 L/D

DELTA L/D = 0.0000 ALPHA 0.0000 DELTAE 0.0000 SPDBK 0.0000 FHB
 0.0000 BODFLP 0.0000 GEAR 0.0000 ALF2 0.0000 CONST

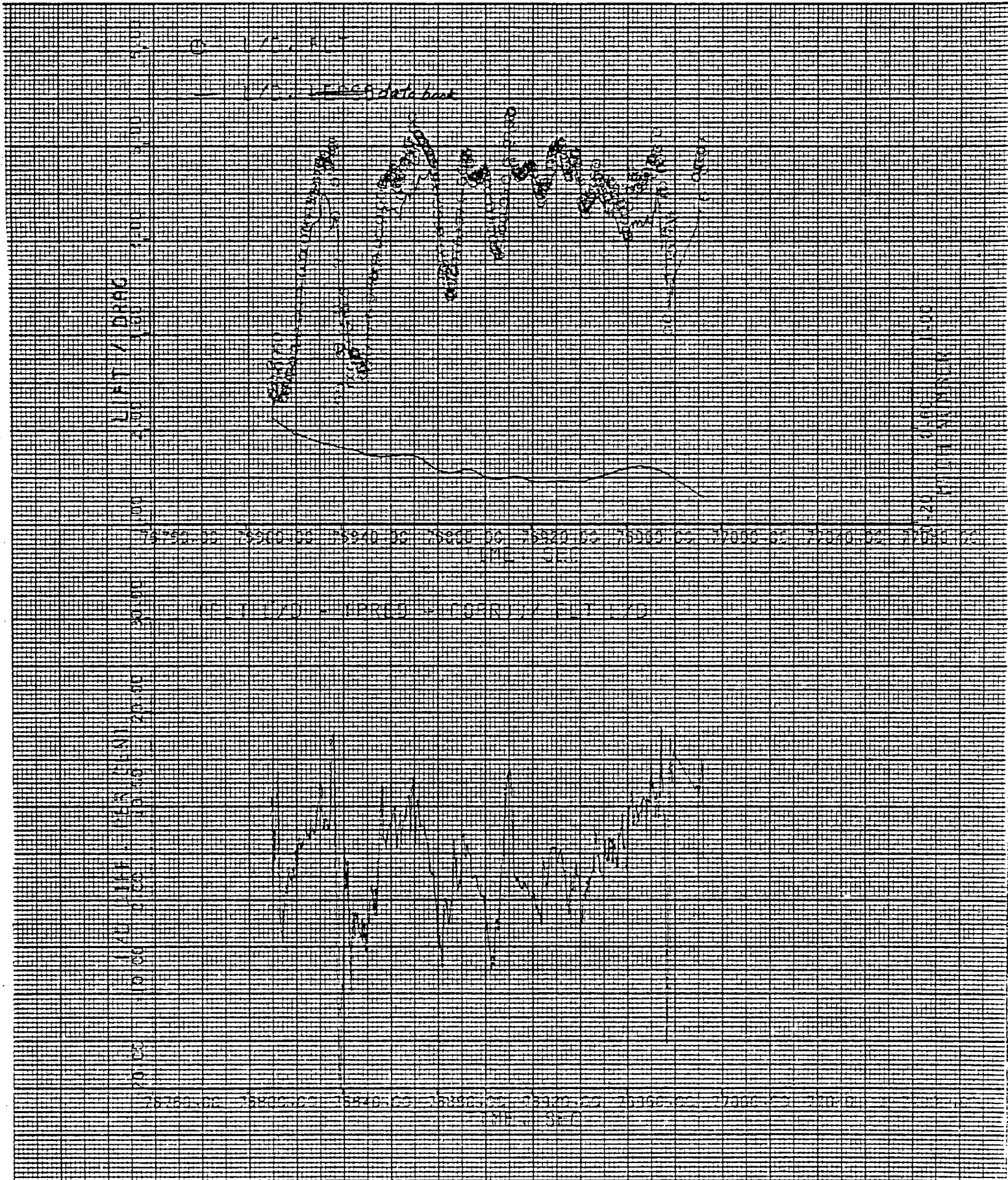


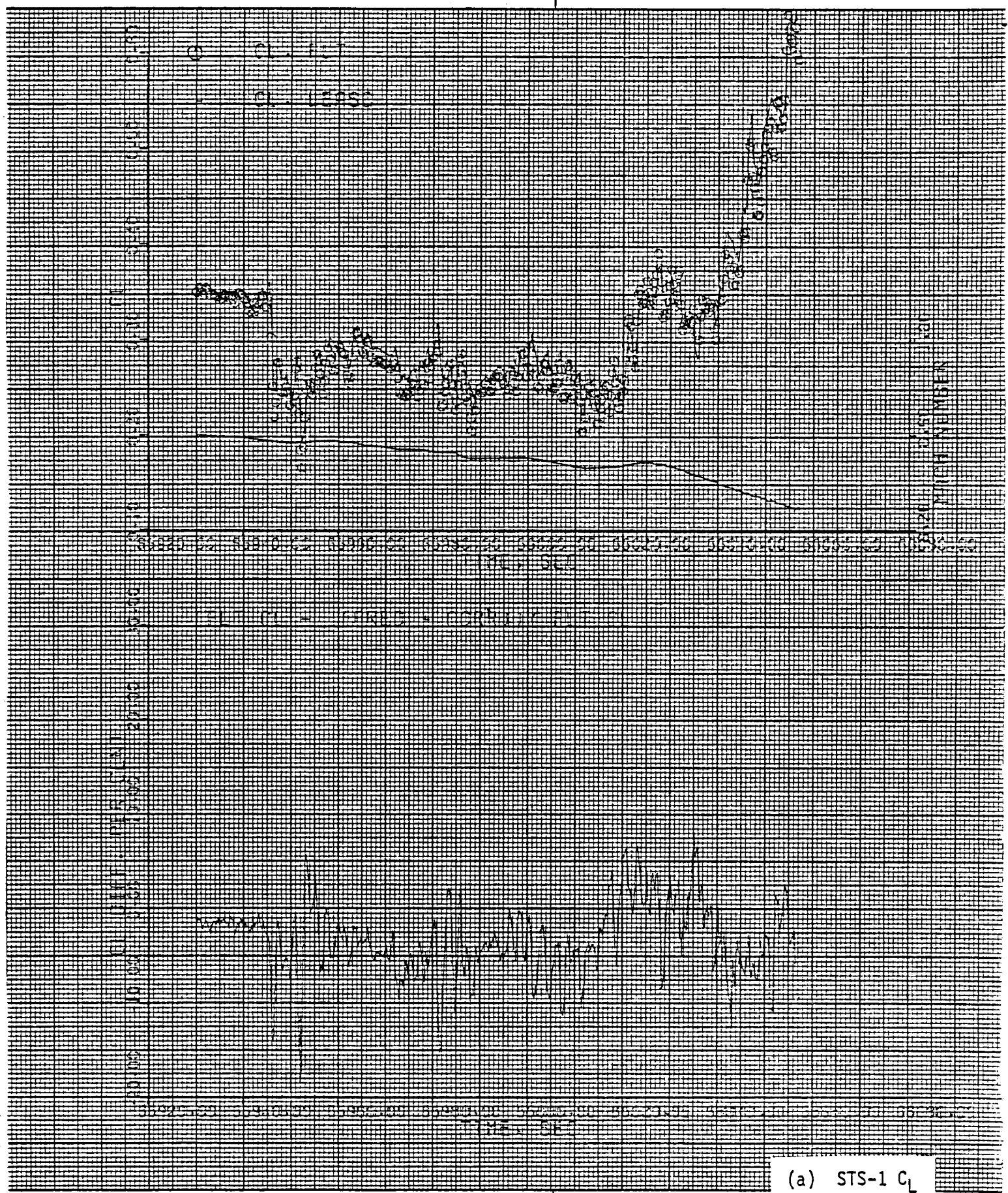
Figure 21 Concluded (f) STS-2 L/D

$$\begin{aligned}
\Delta C_L = & - 0.00827 \\
& - 0.00237 \alpha + 0.00028 \alpha^2 \\
& + 0.00451 \text{ DE} \\
& - 0.00017 \text{ SB} \\
& + 0.00004 \text{ BF} \\
& + 0.01186 \text{ GR} \\
& - 0.00310 \text{ FHB}
\end{aligned}$$

$$\begin{aligned}
\Delta C_D = & + 0.00454 \\
& - 0.00456 \alpha + 0.00027 \alpha^2 \\
& + 0.00270 \text{ DE} \\
& - 0.00006 \text{ SB} \\
& + 0.00009 \text{ BF} \\
& + 0.00031 \text{ GR} \\
& - 0.01186 \text{ FHB}
\end{aligned}$$

Figure 22 - Results of the Regression Analysis

DELTA CL = -.00237 ALPHA .00451 DELTAE -.00017 SPDBK -.00310 FHB
 .00004 BODFLP .01195 GEAR .00029 ALF2 -.00927 CONST



(a) STS-1 C_L

Figure 23 - Comparison of C_L and C_D vs Modified Predictions

DELTA CL = -.00237 ALPHA .00451 DELTAE -.00017 SPDBK -.00310 FHB
 .00004 BODFLP .01195 GEAR .00029 ALF2 -.00927 CONST

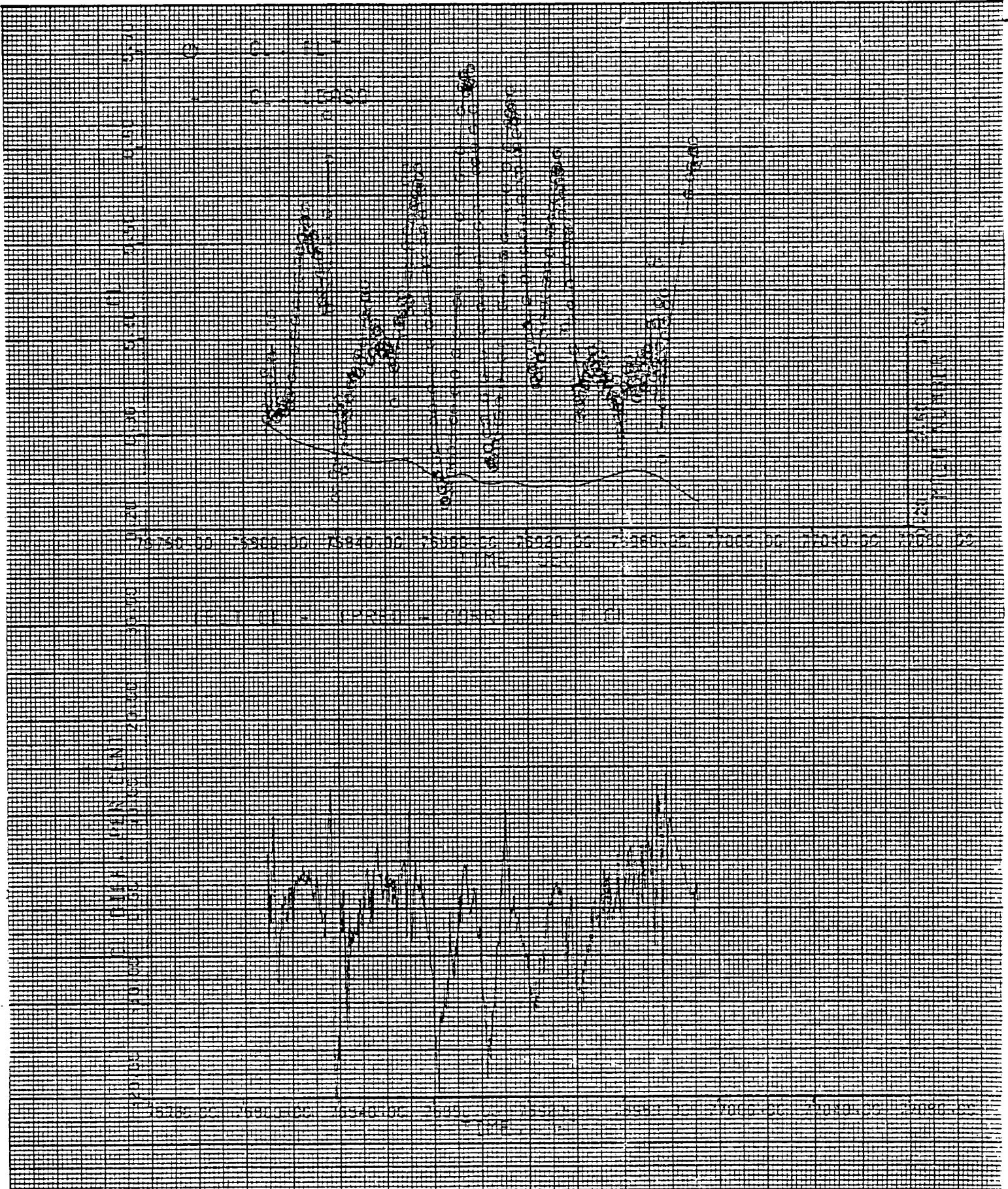


Figure 23 Continued (b) STS-2 C_L

DELTA CD = -.00455 ALPHA .00270 DELTAE -.00006 SPDBK -.01196 FHB
 .00009 BOFLP .00031 GEAR .00027 ALF2 .00454 CONST

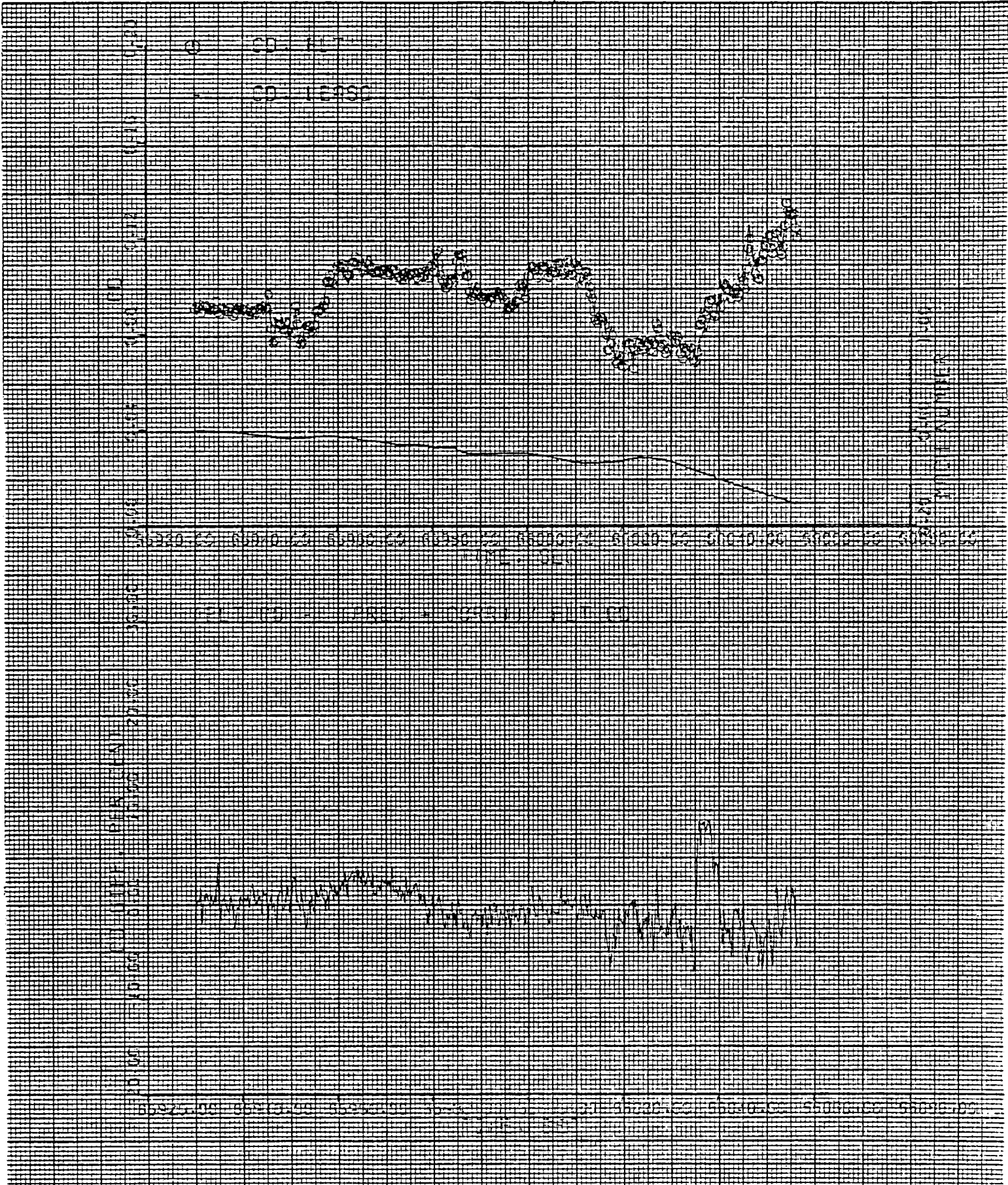


Figure 23 Continued (c) STS-1 C_D

DELTA C_D = -.00453 ALPHA .00270 DELTAE -.00009 SPOBK -.01196 FHB
 .00009 RODFLP .00031 GEAR .00027 ALF2 .00454 CONST

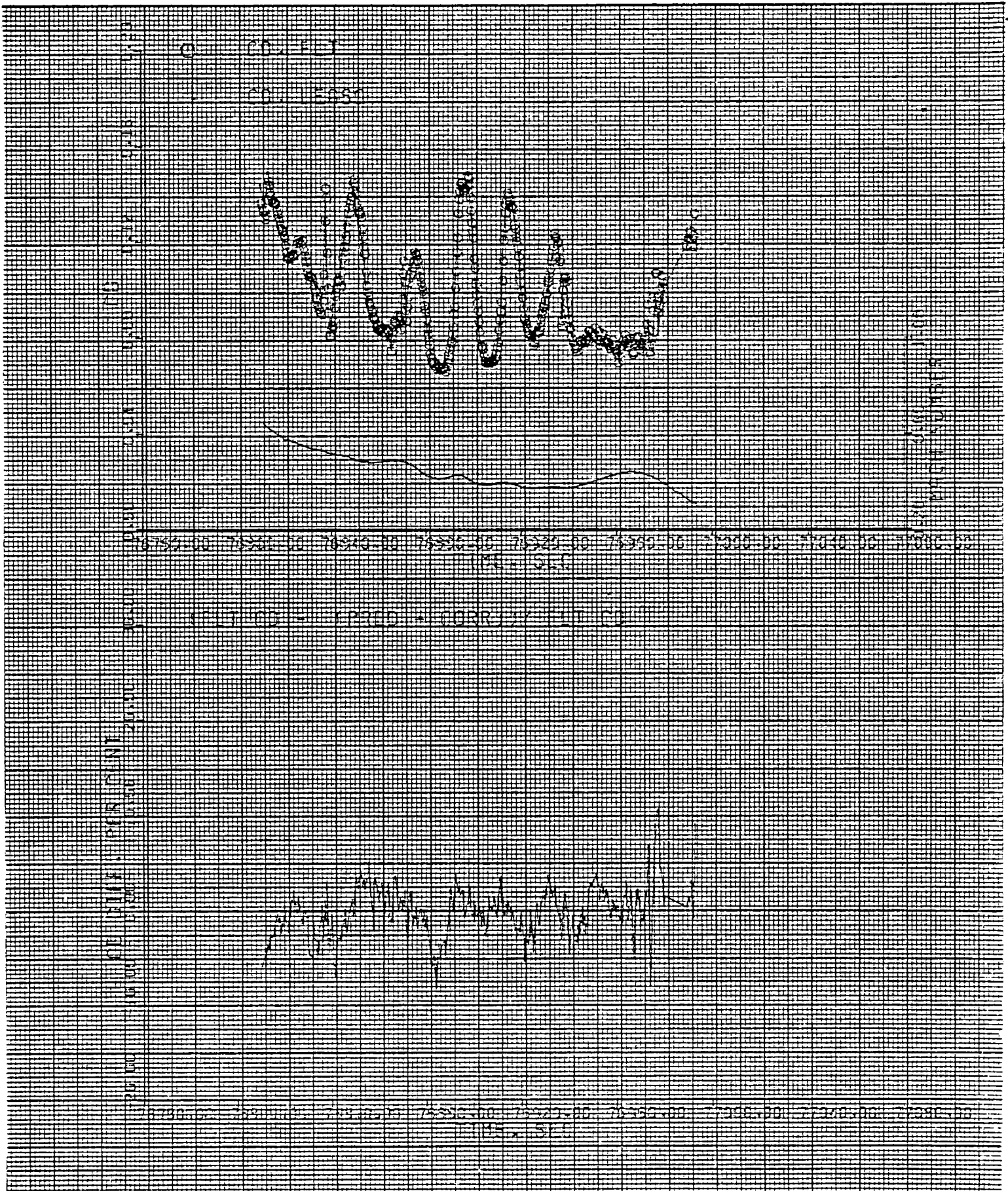


Figure 23 Continued (d) STS-2 C_D

STS-1 FLT L/D COMPARED WITH PREDICTED L/D WHERE
 PRED L/D = CL.CORR / CD.CORR USING LEAST SQUARE FIT FOR CL AND CD

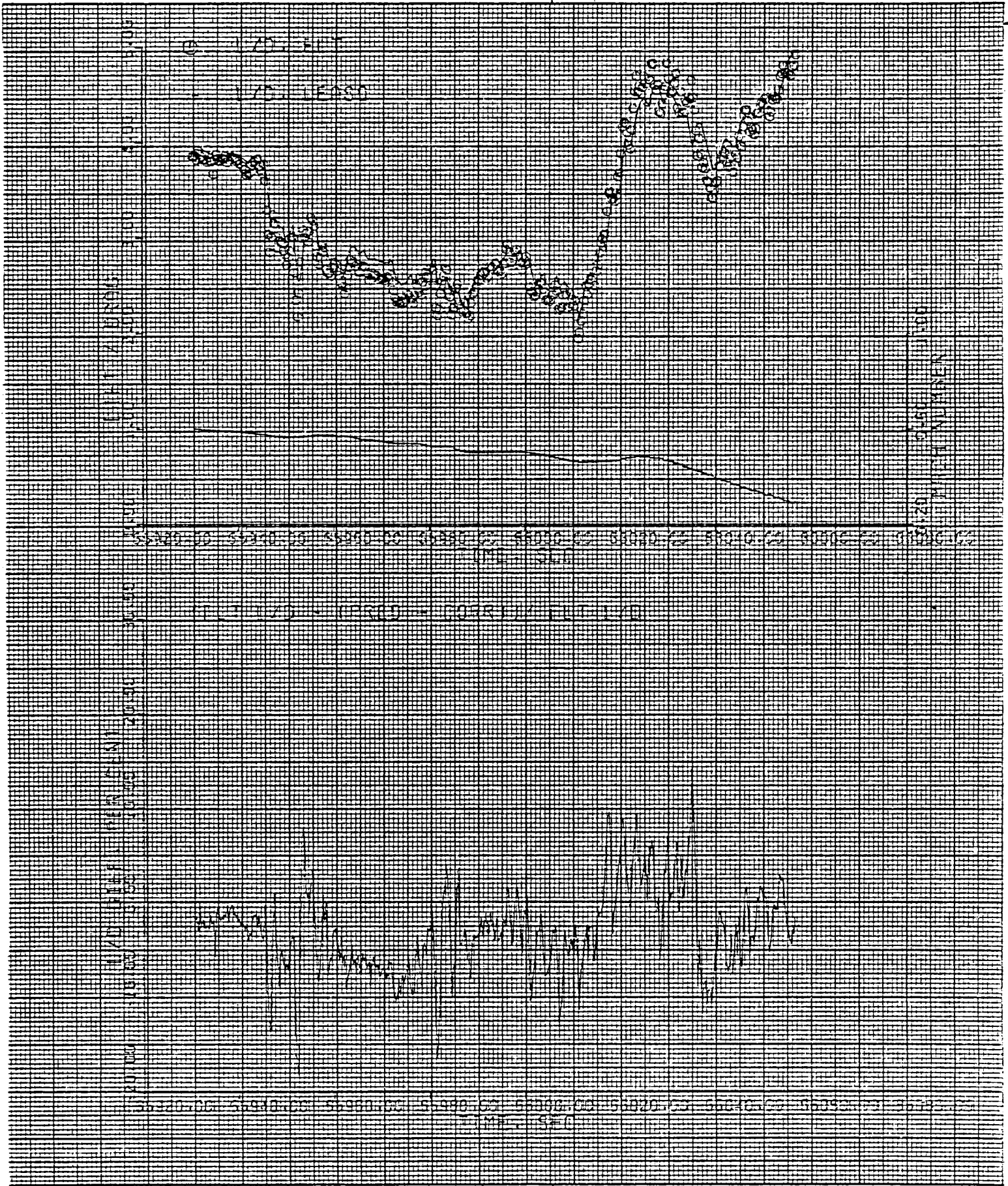


Figure 23 Continued (e) STS-1 L/D

STS-2 FLT L/D COMPARED WITH PREDICTED L/D WHERE
 PRED L/D = CL.CORR / CD.CORR USING LEAST SQUARE FIT FOR CL AND CD

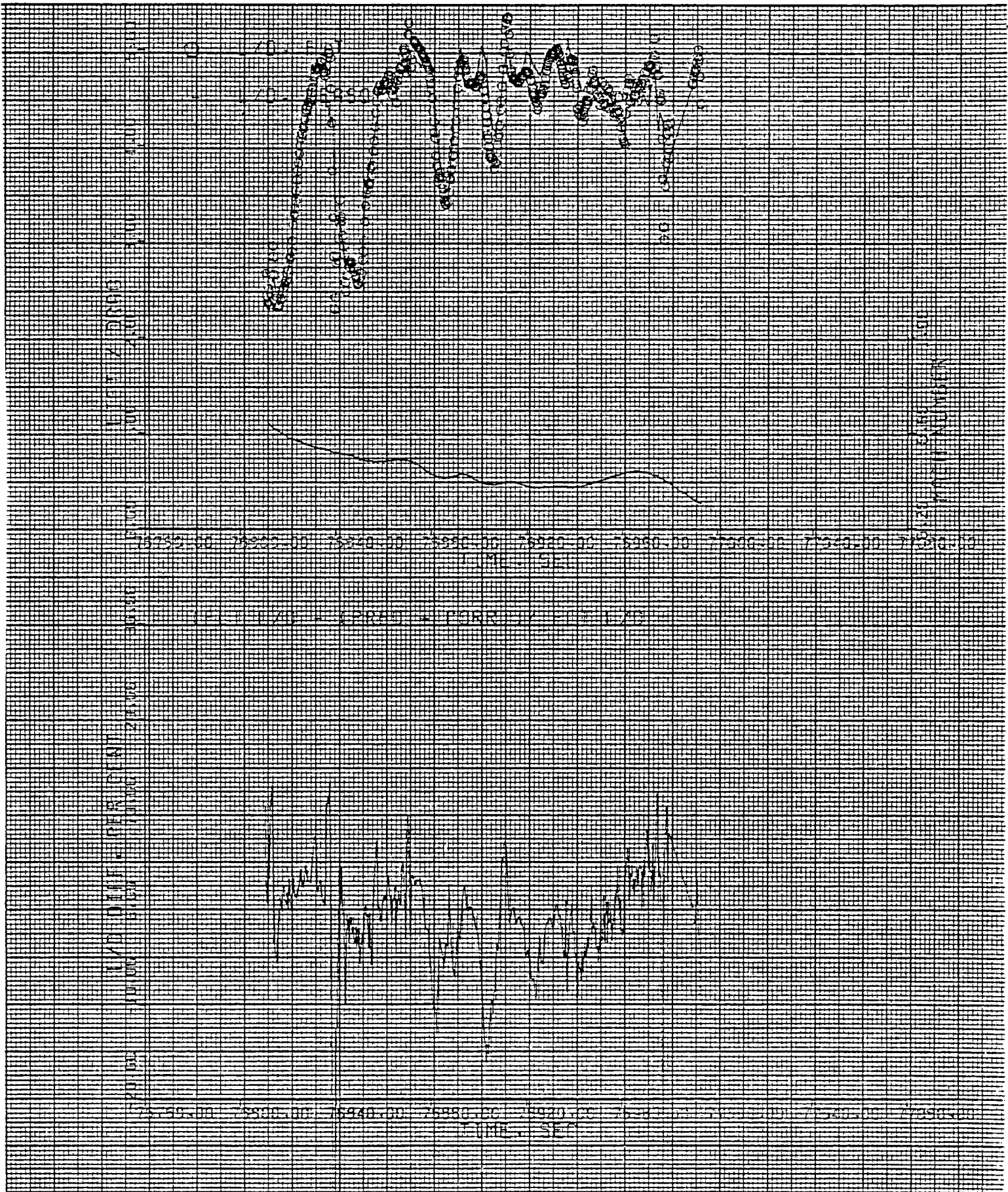


Figure 23 Concluded (f) STS-2 L/D

CORRECTIONS APPLIED TO DATA BOOK

$M = 0.6$

— ORIG PRED
 - - - MOD PRED

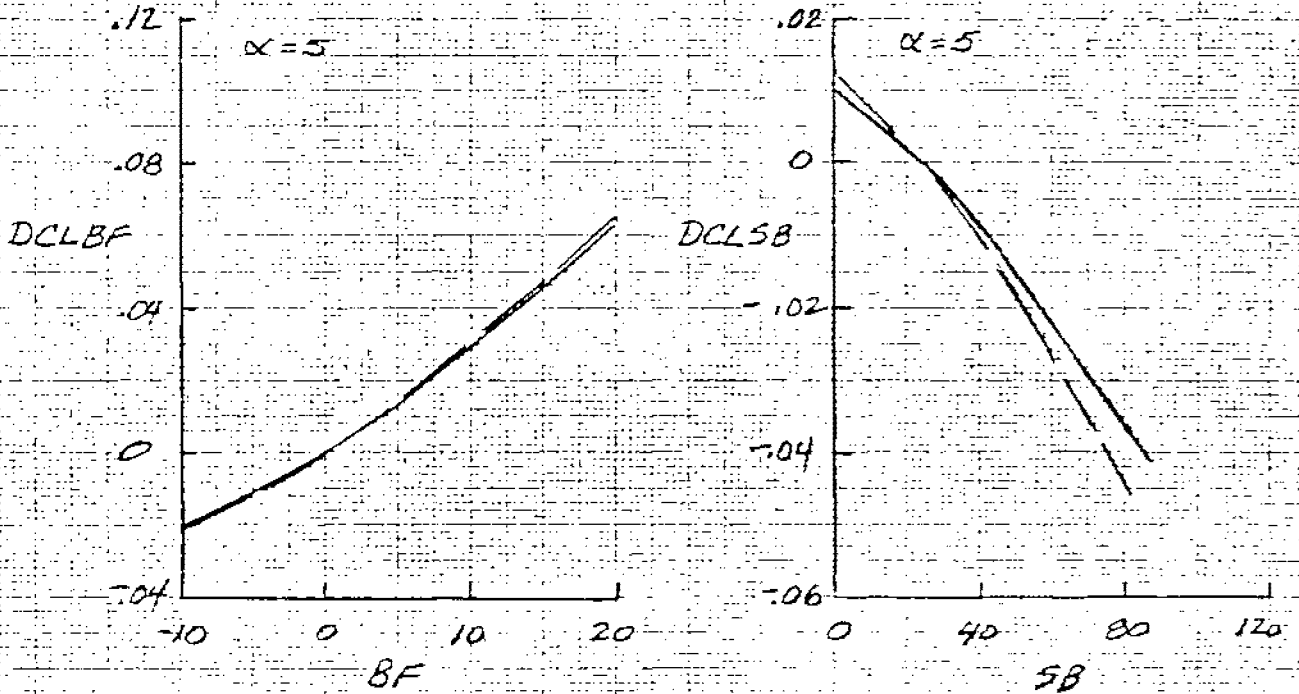
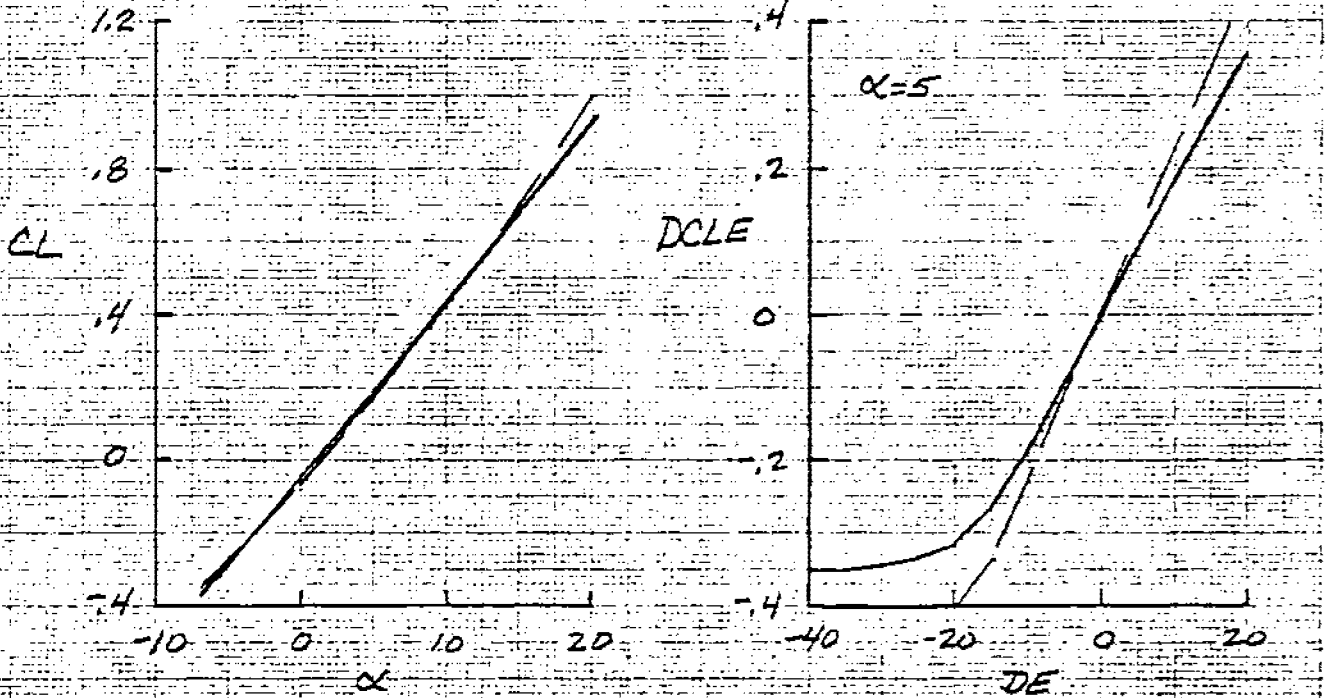


Figure 24 - Comparison of Modified vs Original Predictions

CORRECTIONS APPLIED TO DATA BOOK

$M = 0.6$

——— ORIG PRED
 ——— MUD PRED

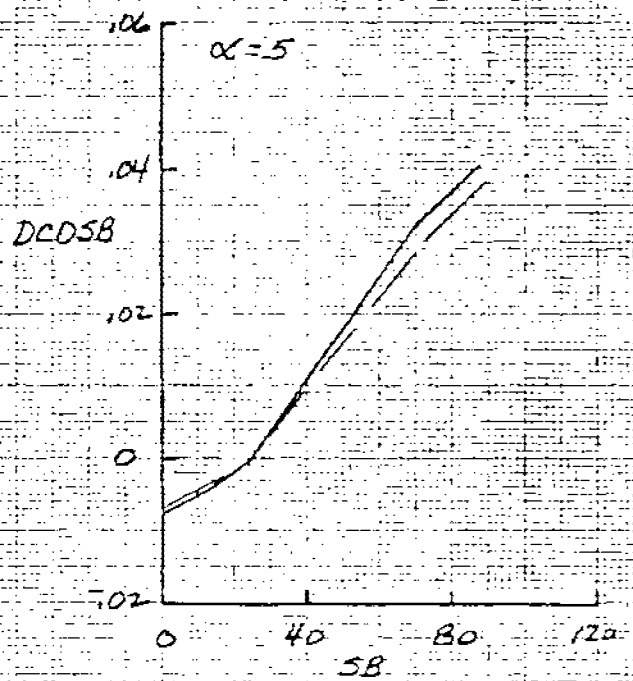
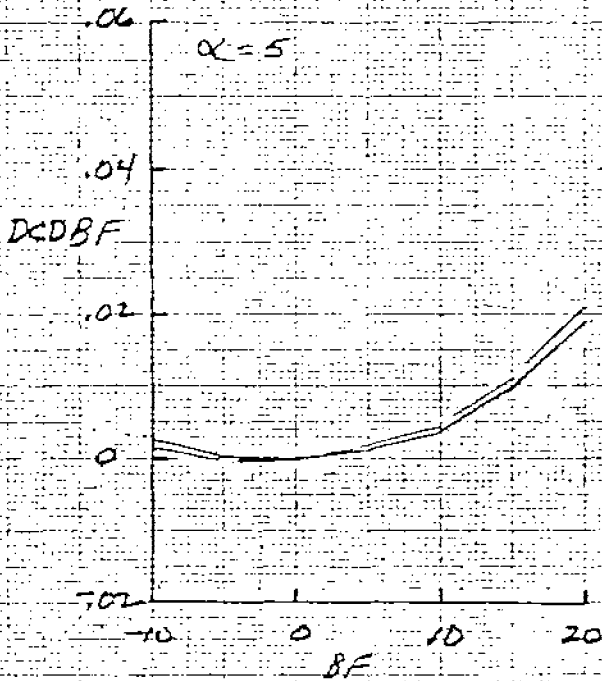
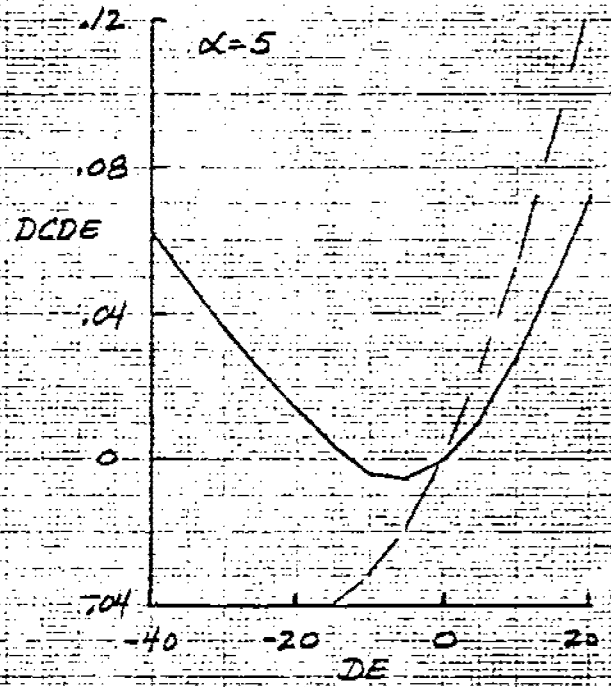
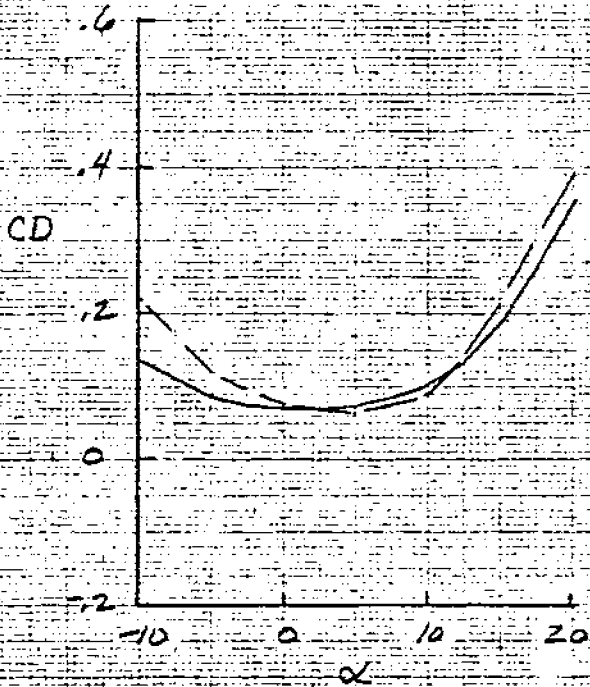


Figure 24 Continued (b) C_D

CORRECTIONS APPLIED TO DATA BOOK

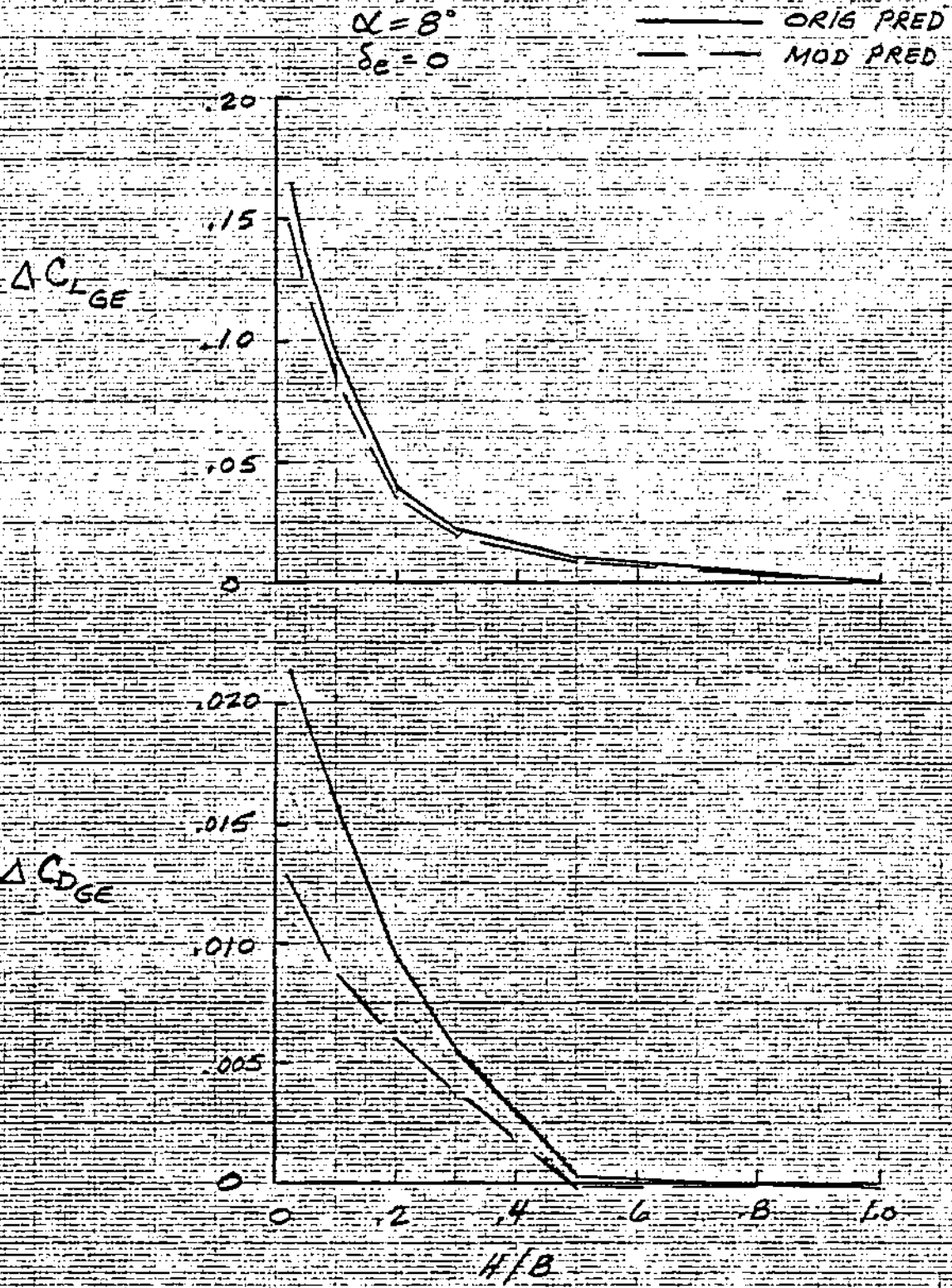


Figure 24 Concluded (c) Ground Effects

STS-2 TAPE 0V2MRG LANDING



Figure 25 (a) Time History of Approach and Landing

STS-2 TAPE 0V2MRG LANDING

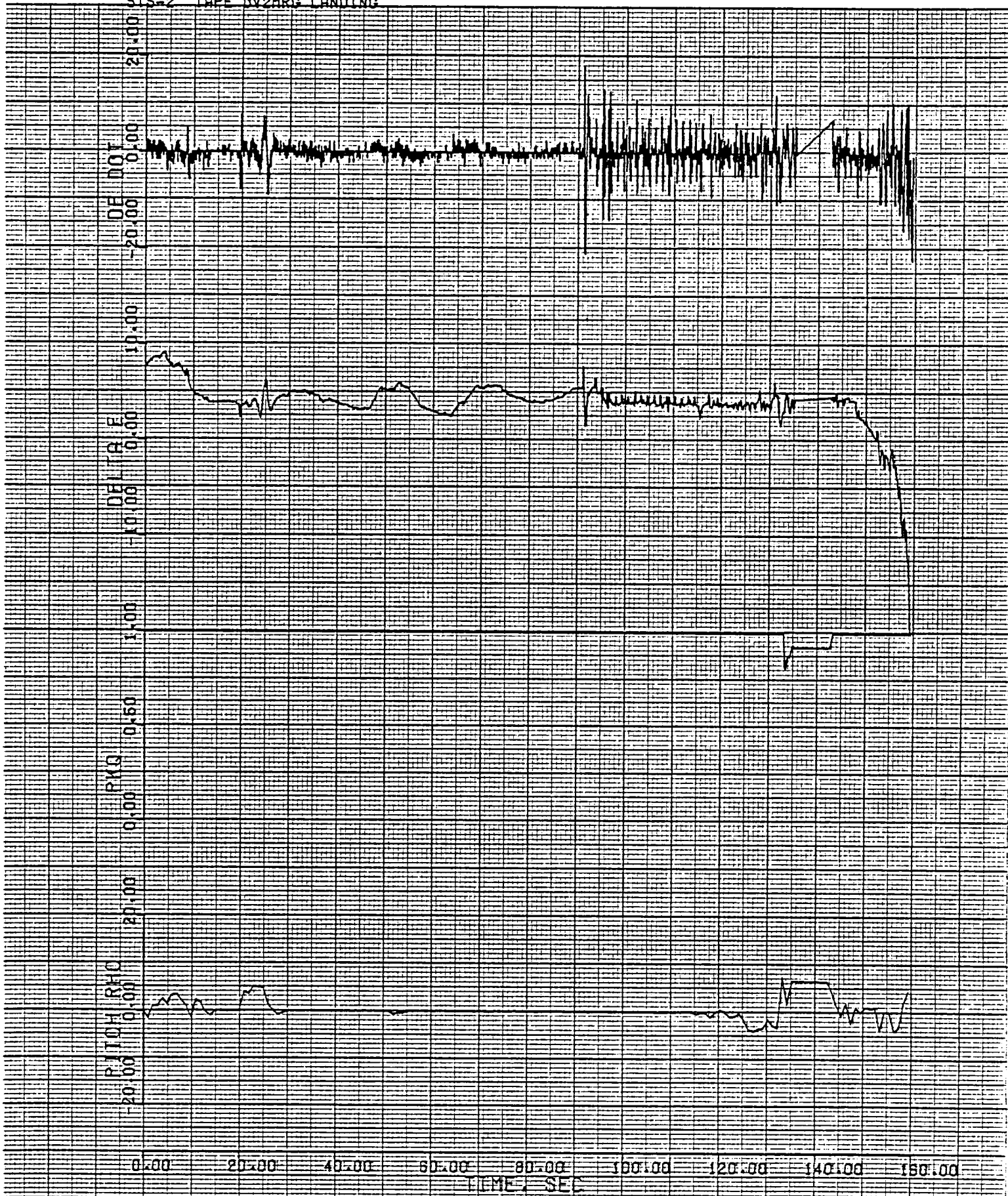


Figure 25 (b) Continued

STS-2 TAPE 0V2HR3 LANDING

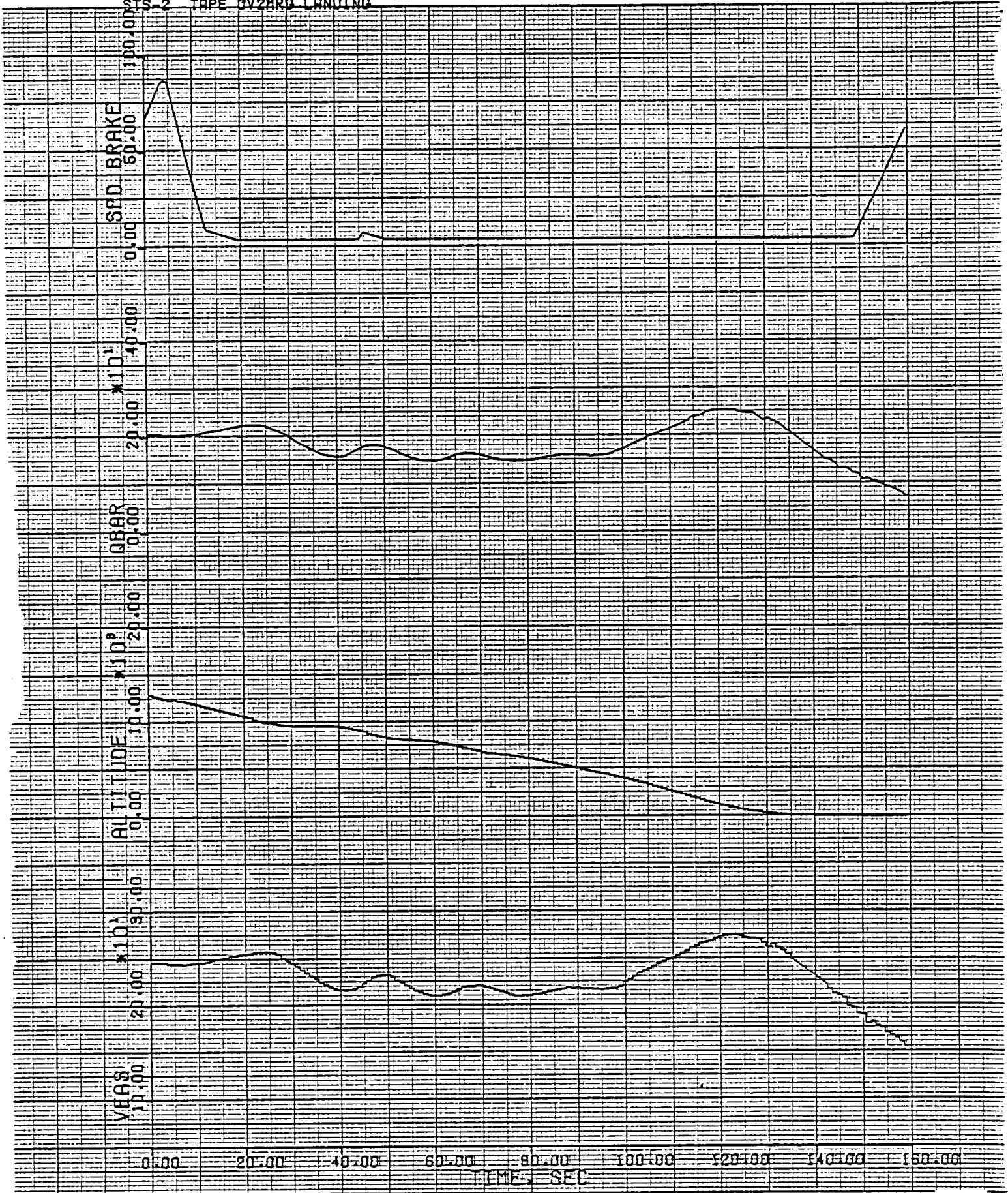


Figure 25 (c) Continued

STS-2 TAPE RV2MRG LANDING

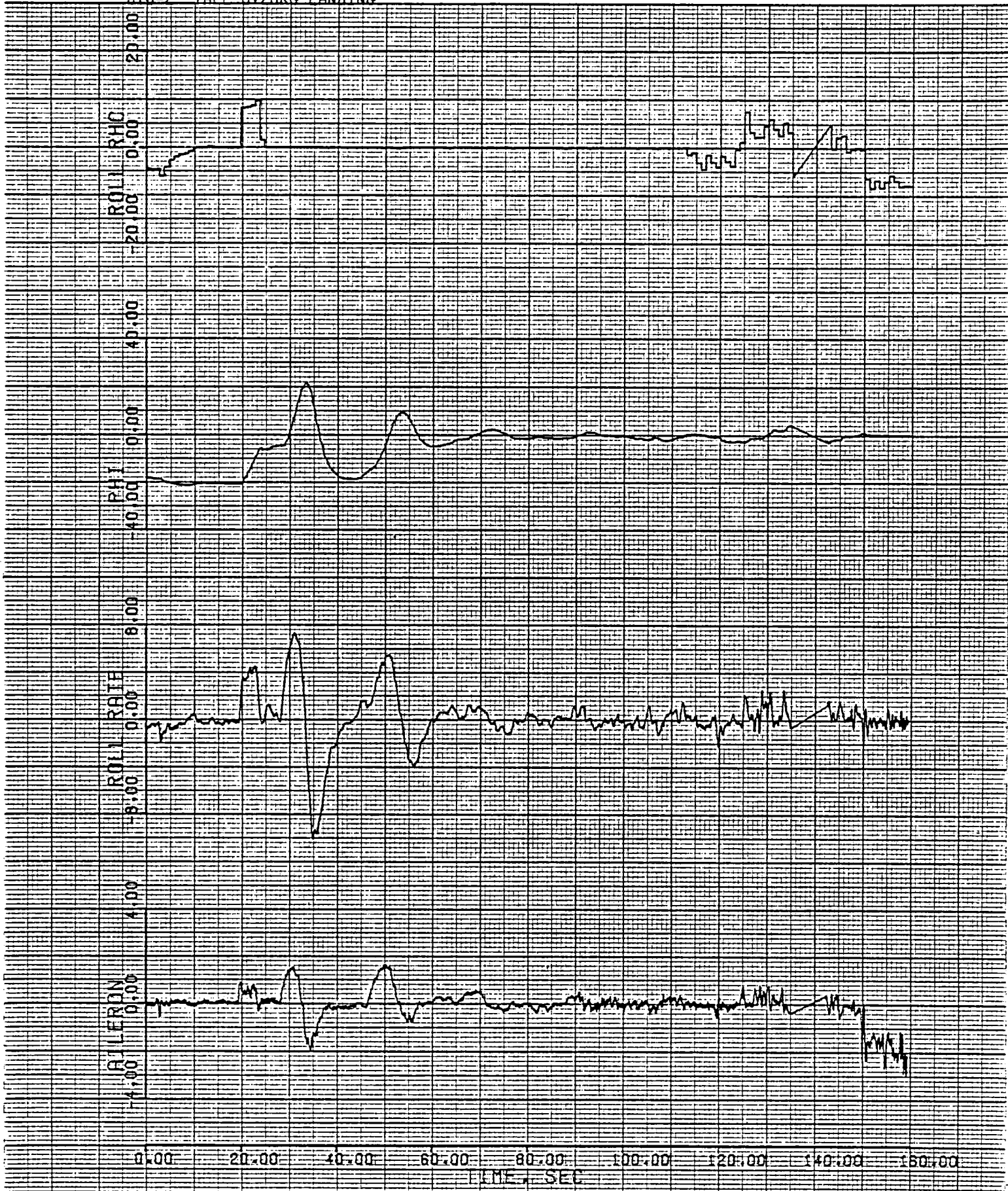




Figure 25 (e) Continued

STS-2 TAPE 0V2MRG LANDING

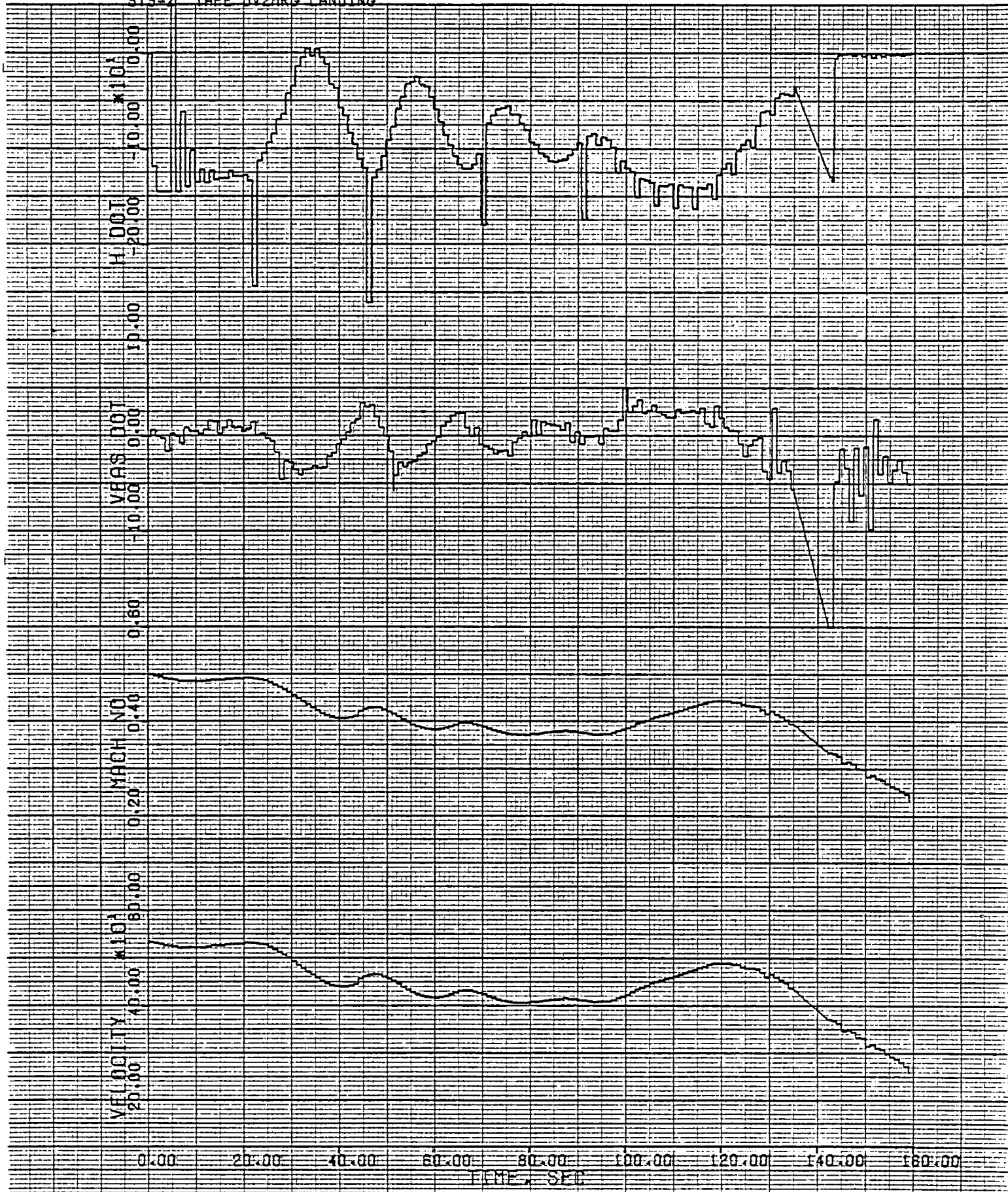


Figure 25 (f) Concluded

Aerothermal Analysis

Dryden Structures Section is performing surface heating and heat transfer analysis of selected Orbiter cross sections to support strain gage load measurement. Orbiter flight temperature measurements were obtained at Dryden and are compared with predicted results in the following section.

Trajectory - Comparison of the nominal STS-1 time history with measured results for STS-1 and STS-2 are shown in figure 26. Due to trajectory differences, STS-2 heating was about 7% greater than STS-1.

FS 877 Structural Temperatures - Figure 27 shows the analysis mode, figure 28 indicates locations of structural temperatures and figures 29 thru 32 compare measured and predicted values. The STS-2 values are slightly greater than STS-1 consistent with the general level indicated by the trajectory. Note that for STS-2, data were recovered from entry to landing. The comparisons with predictions were similar for STS-1, with the glove lower surface STS-2 measured temperature significantly lower than predicted. The STS-2 measured value for the longeron agreed more closely than the STS-1 measured value.

WS 240 Structural Temperatures - Figure 33 shows the temperature measurement locations and figures 34 thru 47 compare predicted and measured values. Again agreement between STS-1 and STS-2 measured values was excellent except for V09T9147 on the lower skin (fig. 34). No explanation for this difference has yet been found.

WS 328 Structural Temperatures - Figure 48 shows the analytical model and figure 49 shows the three structural temperature measurement locations. Figures 50 thru 52 compare predicted and measured values. The measured data were slightly higher than predicted.

WS 134 Structural Temperatures - Figure 53 shows the structural temperature measurement locations and figures 54 thru 59 compare predicted vs measured values. It should be noted that no measurements were available at WS 134. They were either at WS 158 or WS 114. The lower cover measurements were significantly higher than predictions and those on the upper cover surface were slightly higher.

FS 877 Surface Temperatures - Figure 60 shows the locations of surface temperature measurements and figures 61 thru 65 compare measured and predicted values. The transition from laminar to turbulent flow is clearly apparent. The lower surface measured values are slightly higher than predicted, while somewhat lower at the top centerline.

Wing Surface Temperatures - Figure 66 shows the locations of wing surface measurements and figures 67 thru 72 compare measured and predicted values for WS 134 lower surface. Measured values were somewhat higher than predicted. Note that in general the measurements were located somewhat outboard of WS 134. Figures 73 and 74 compare measured and predicted values for the upper surface at WS 134. Agreement was good in the glove area (V0779608) but measured values were higher than predicted further aft (V0979163).

Figures 75 thru 82 compare measured and predicted lower surface temperatures at WS 240. The measured values fell between turbulent and laminar predictions and show a clearly defined transition. Figures 83 and 84 compare measured and predicted upper surface temperatures at WS 240. The measured values agreed well with laminar predictions.

Figures 85 thru 87 compare measured and predicted lower surface temperature at WS 328. The measured values are somewhat higher than prediction, especially at mid chord. Figures 88 thru 90 compare measured and predicted upper surface temperatures at WS 328. The measured values are generally slightly lower than predicted.

Wing Leading Edge Temperatures

For STS-2 a high radiometer reading of 2900° F was obtained on the inside face of the carbon - carbon wing leading edge at 53% span.

A one-dimensional heating analysis at the stagnation point of the wing leading edge at the 55% wing span location was made. The maximum calculated surface temperature was 2614° F. It should be noted that this temperature (2614° F) is the maximum temperature expected at the leading edge. The average leading edge temperature will be about 200° F less than the maximum value. The stagnation point calculation was made for the STS-2 profile.

Figure 91 shows the predicted temperature time histories for outer and inner surfaces of the leading edge at the stagnation point.

FLIGHT TRAJECTORIES (80701.14 STS-1)

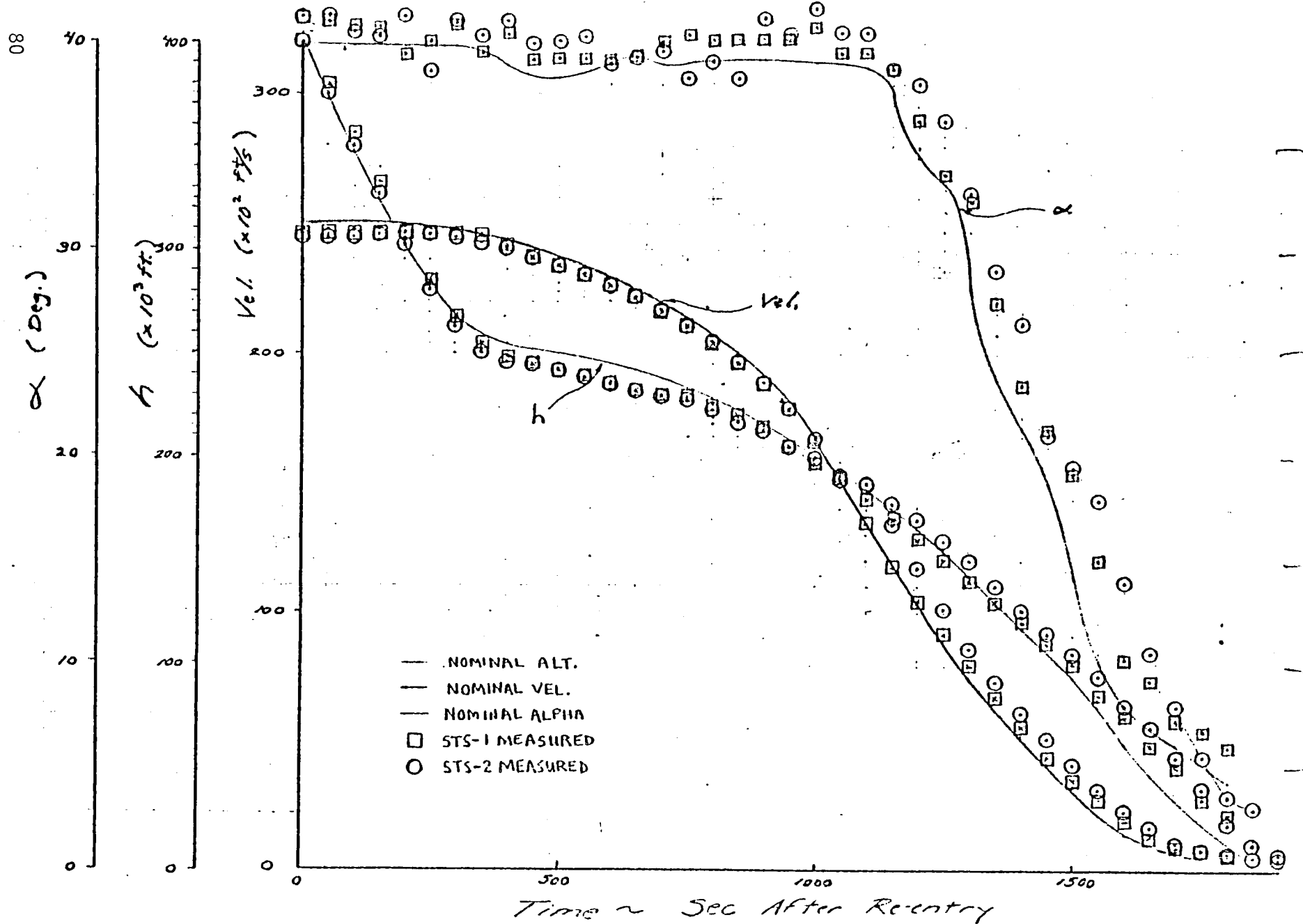


Figure 26 Comparison of the nominal STS-1 trajectory time history with measured results for STS-1 and STS-2.

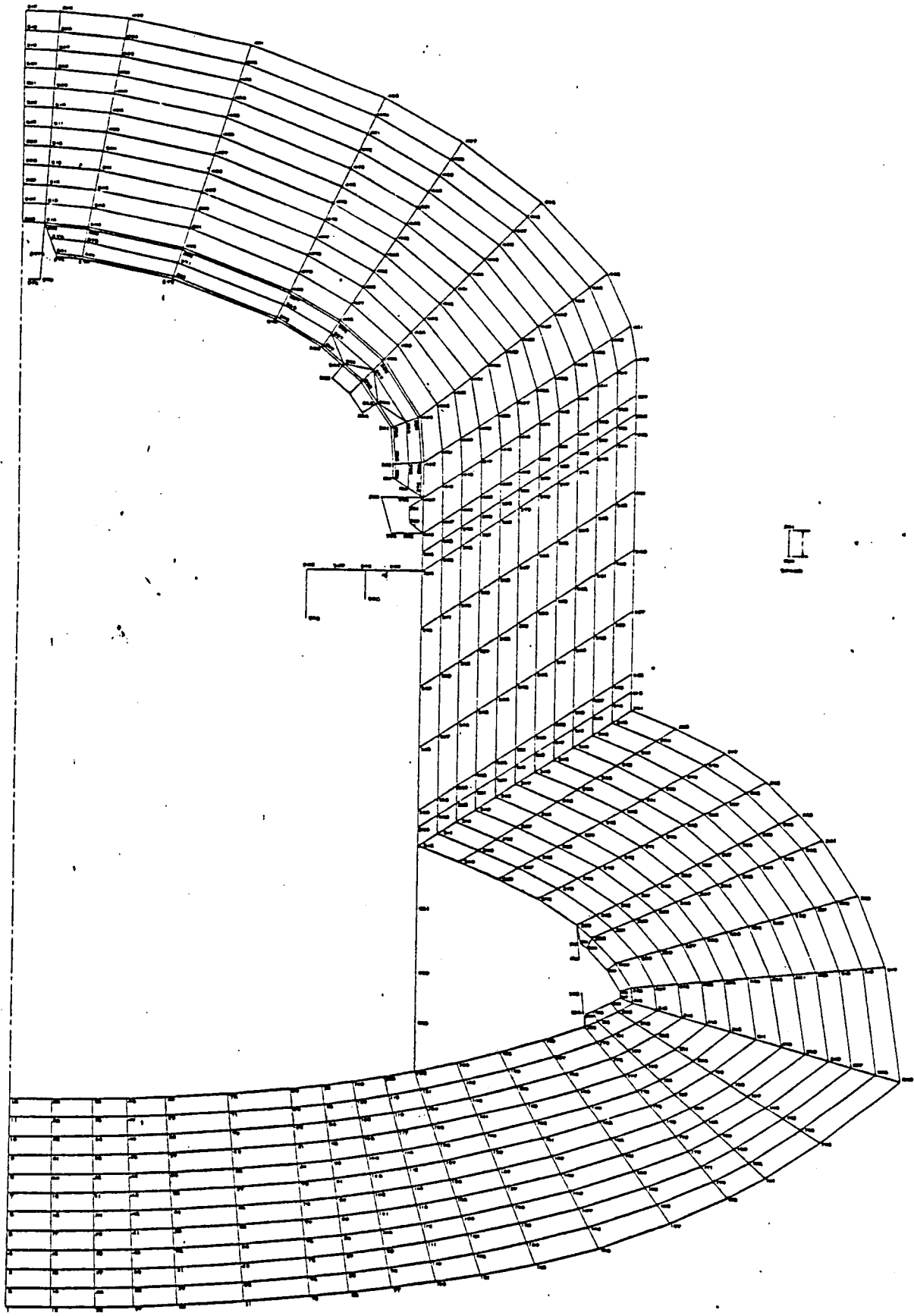


Figure 27 Analytical Model of FS 877.

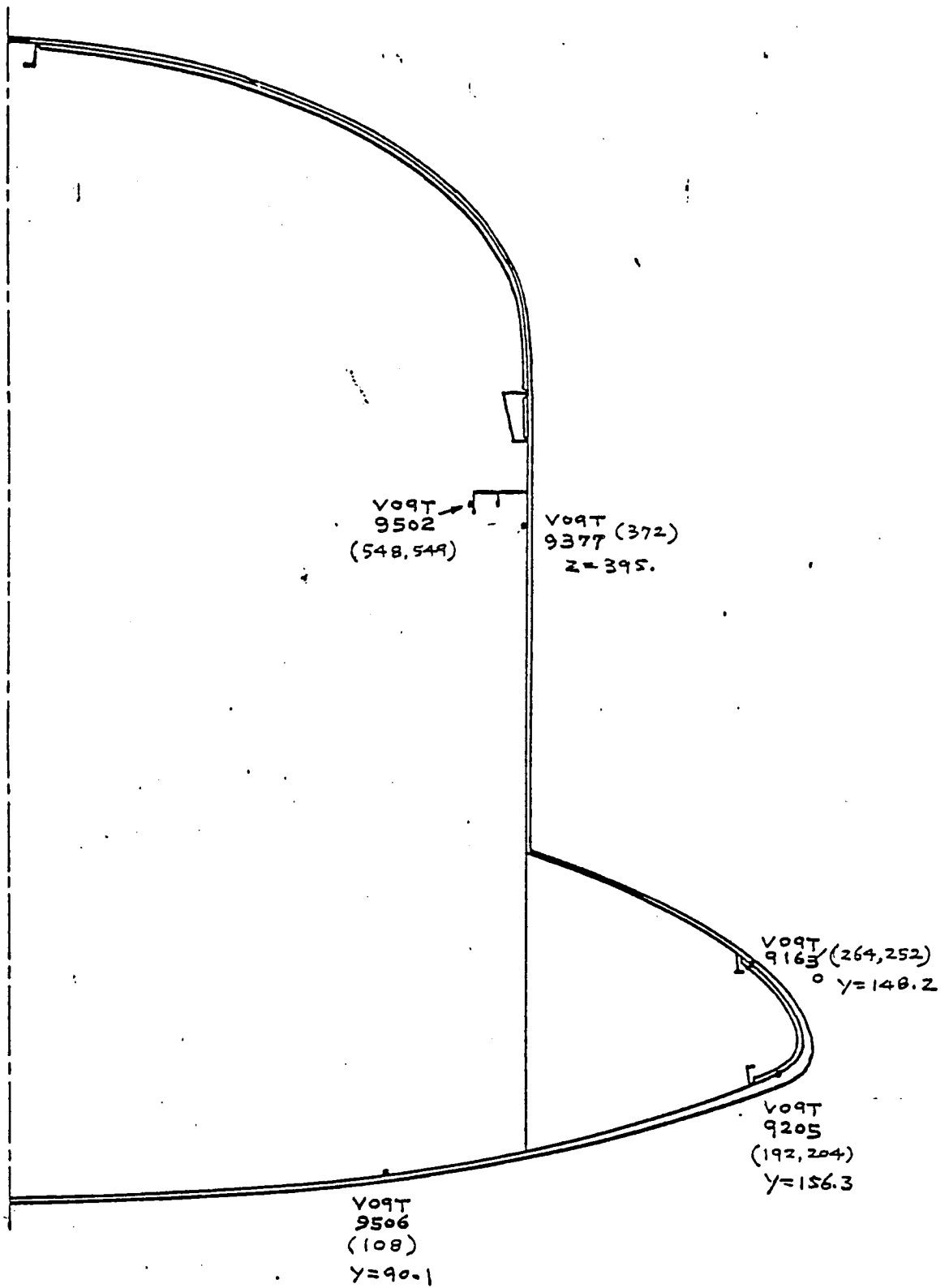


Figure 28 Locations of structural temperatures at FS 877.

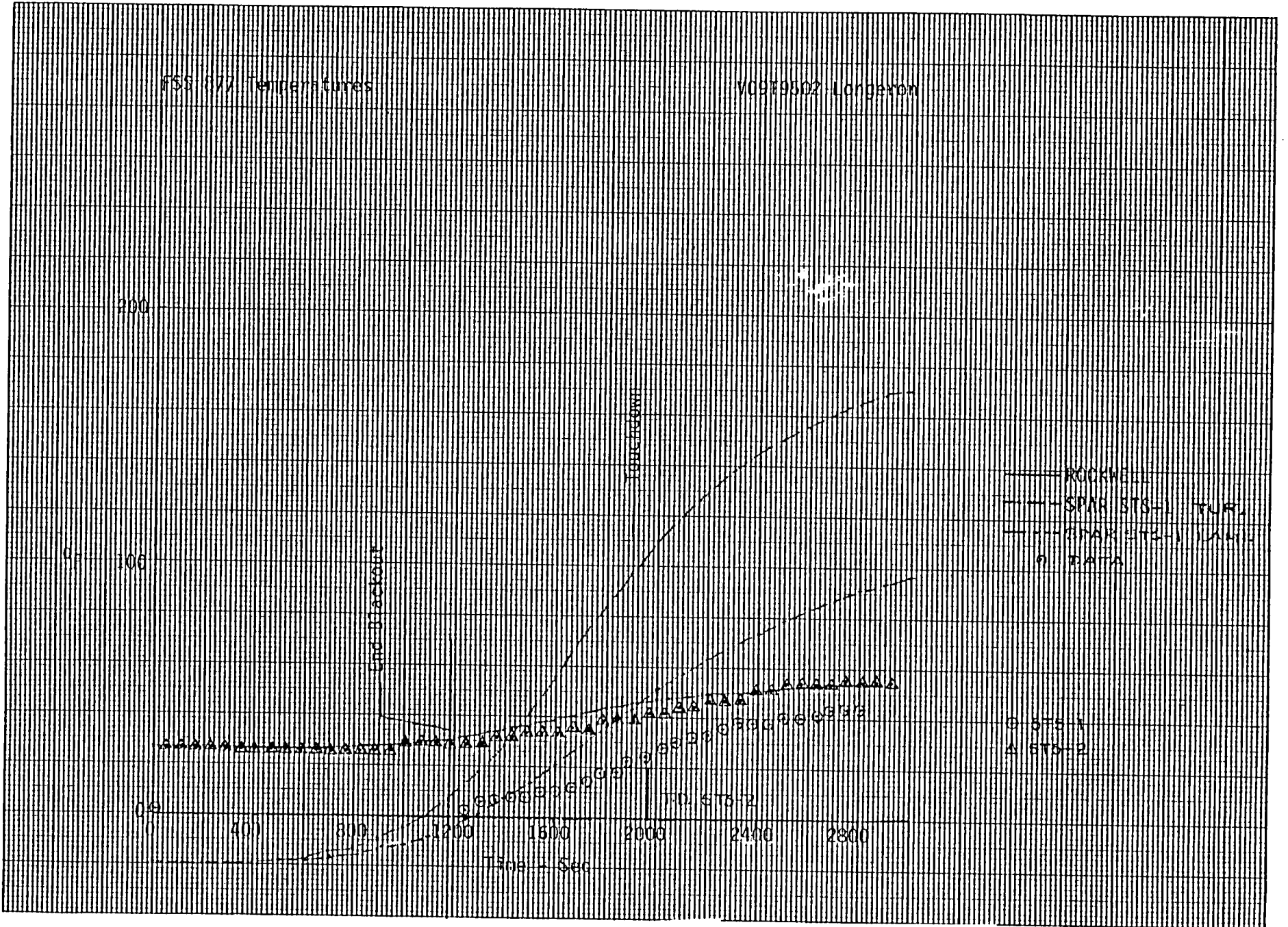


Figure 29 - Flight Temperatures Compared to Predictions - Fuselage

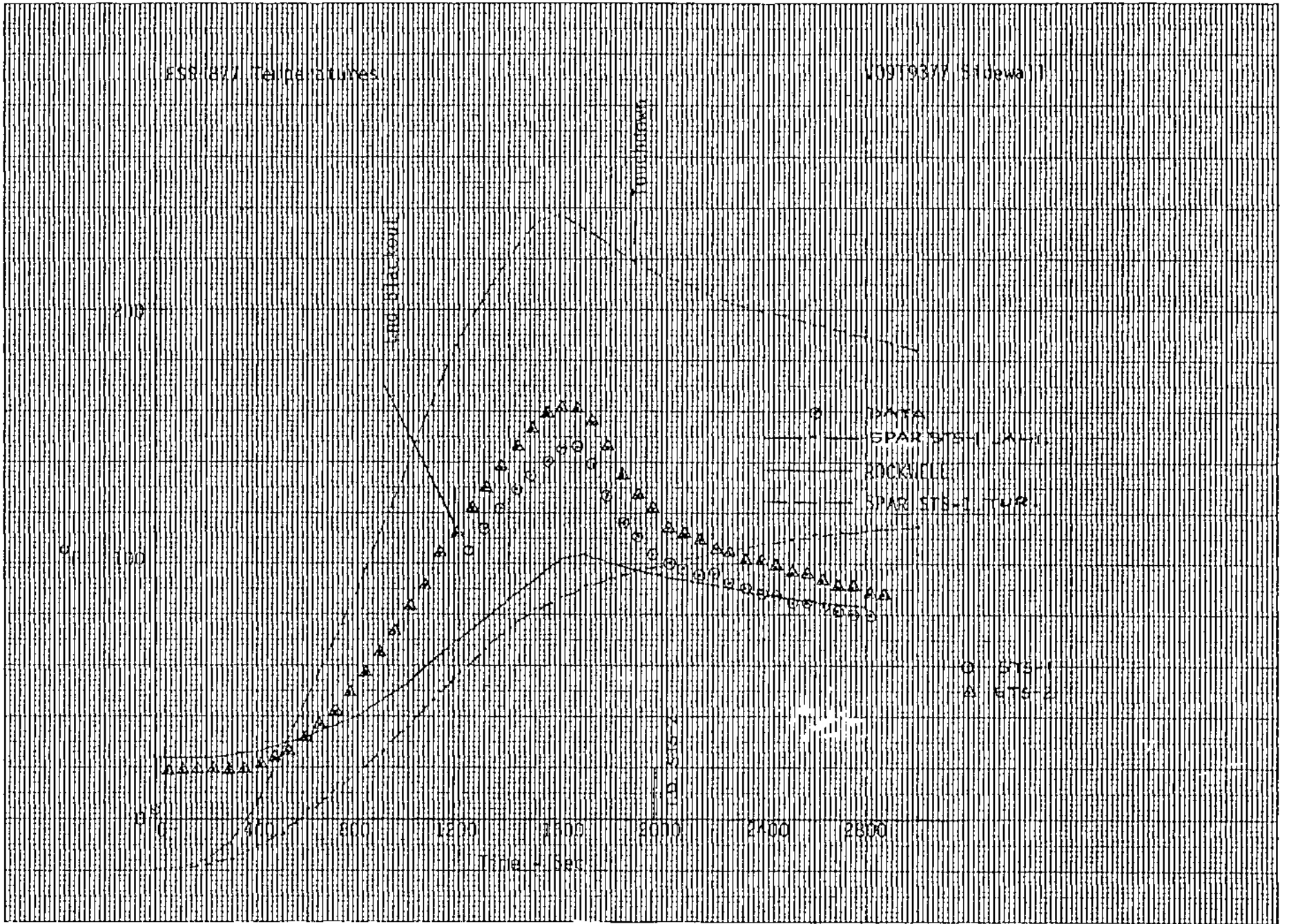


Figure 30 - Flight Temperatures Compared to Predictions - Fuselage

11/16/77

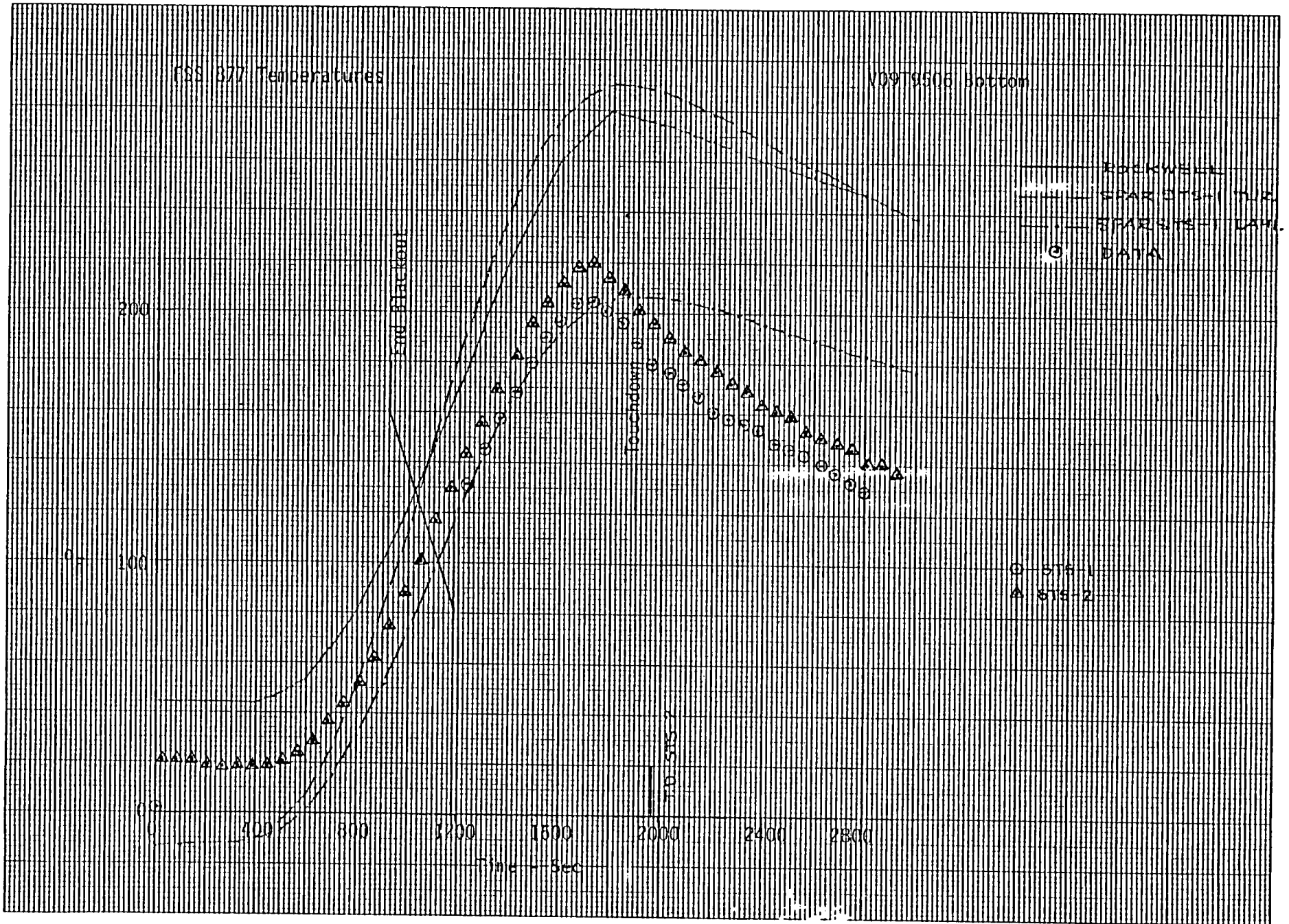


Figure 31 - Flight Temperatures Compared to Predictions - Fuselage

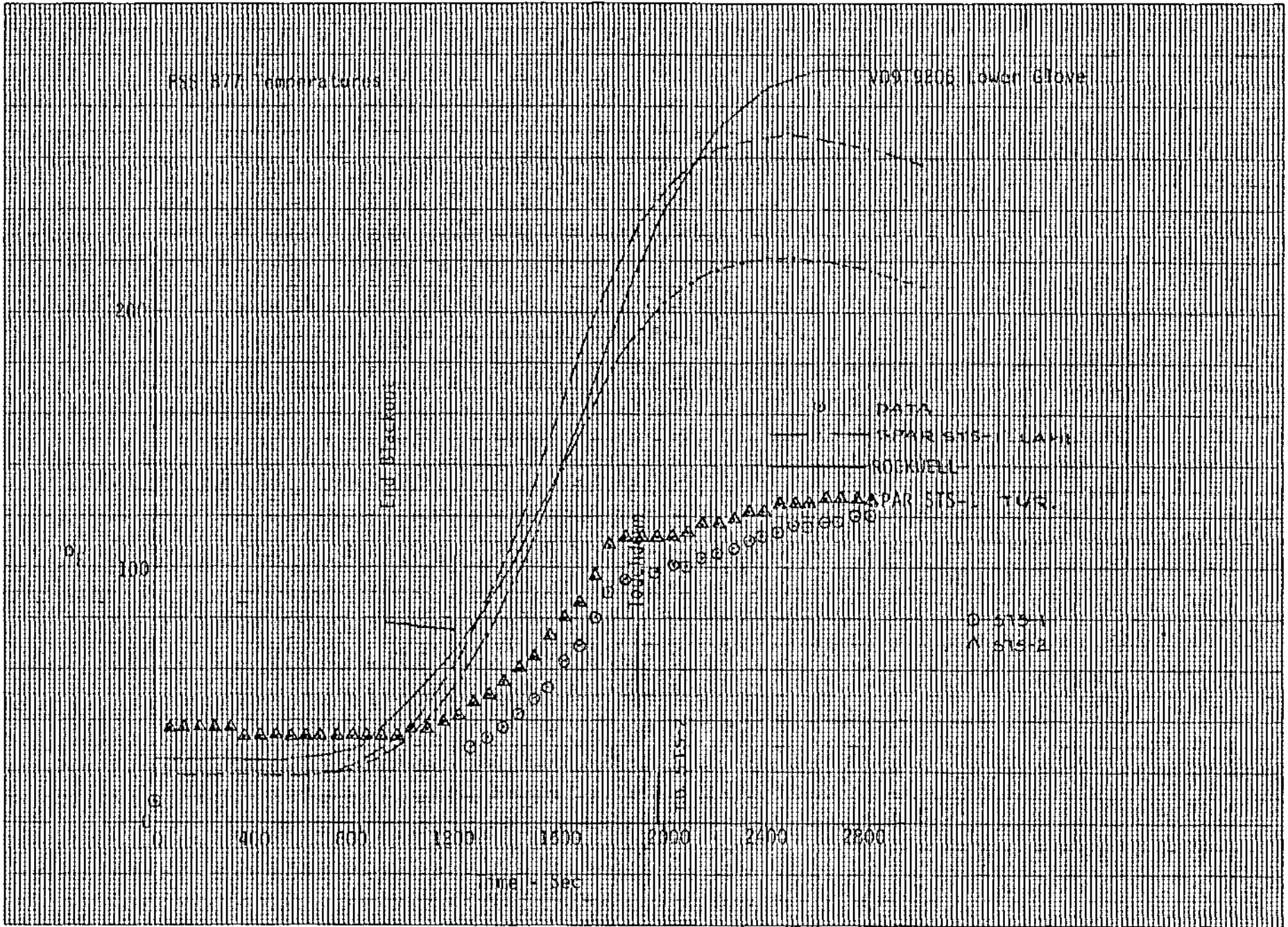


Figure 32 - Flight Temperatures Compared to Predictions - Fuselage

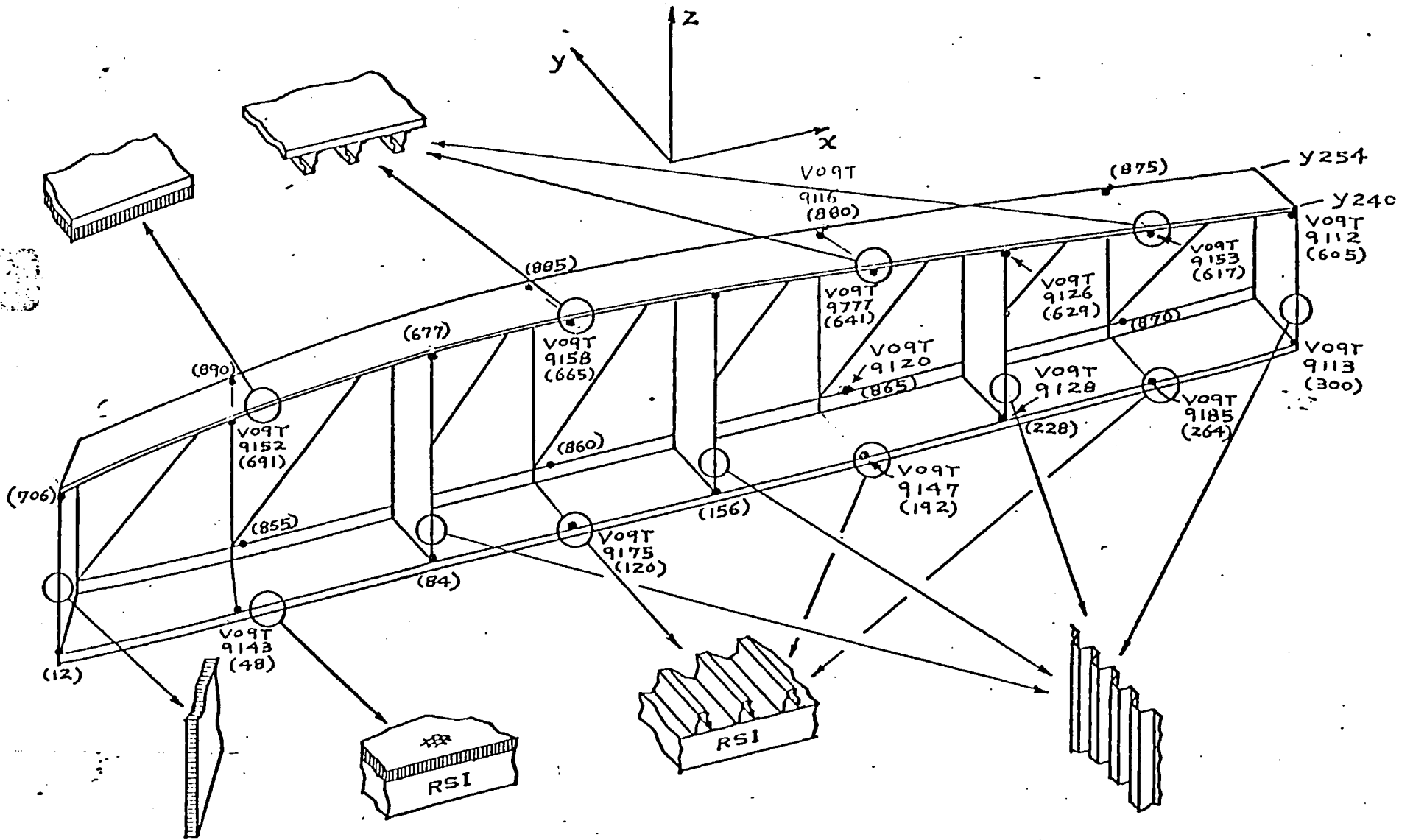


FIGURE 8 . GEOMETRY OF WING SEGMENT BETWEEN W/S 240 AND W/S 254.

Figure 33 W.S. 240 Thermocouple Location

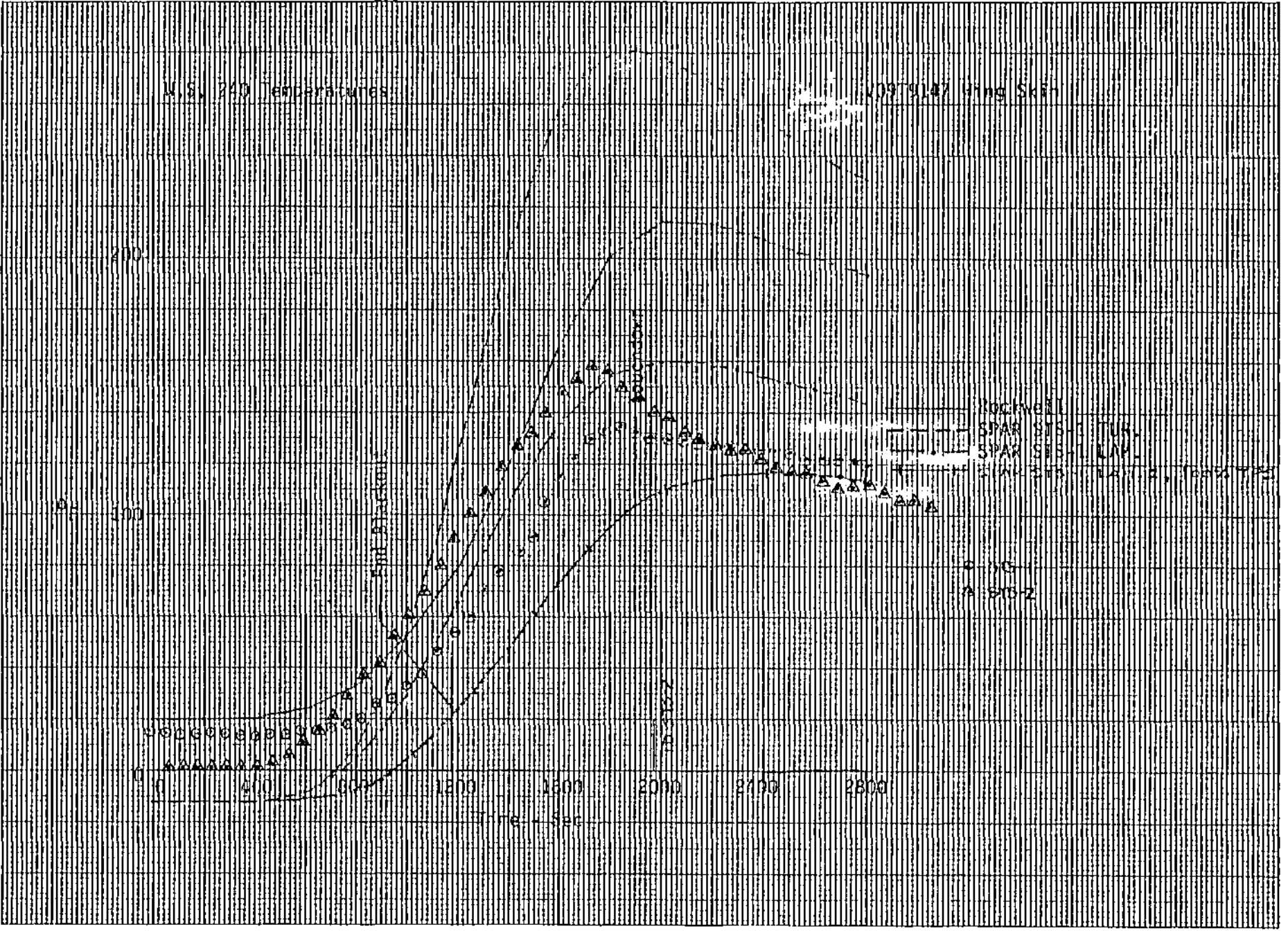


Figure 34 - Flight Temperatures Compared to Predictions - Wing

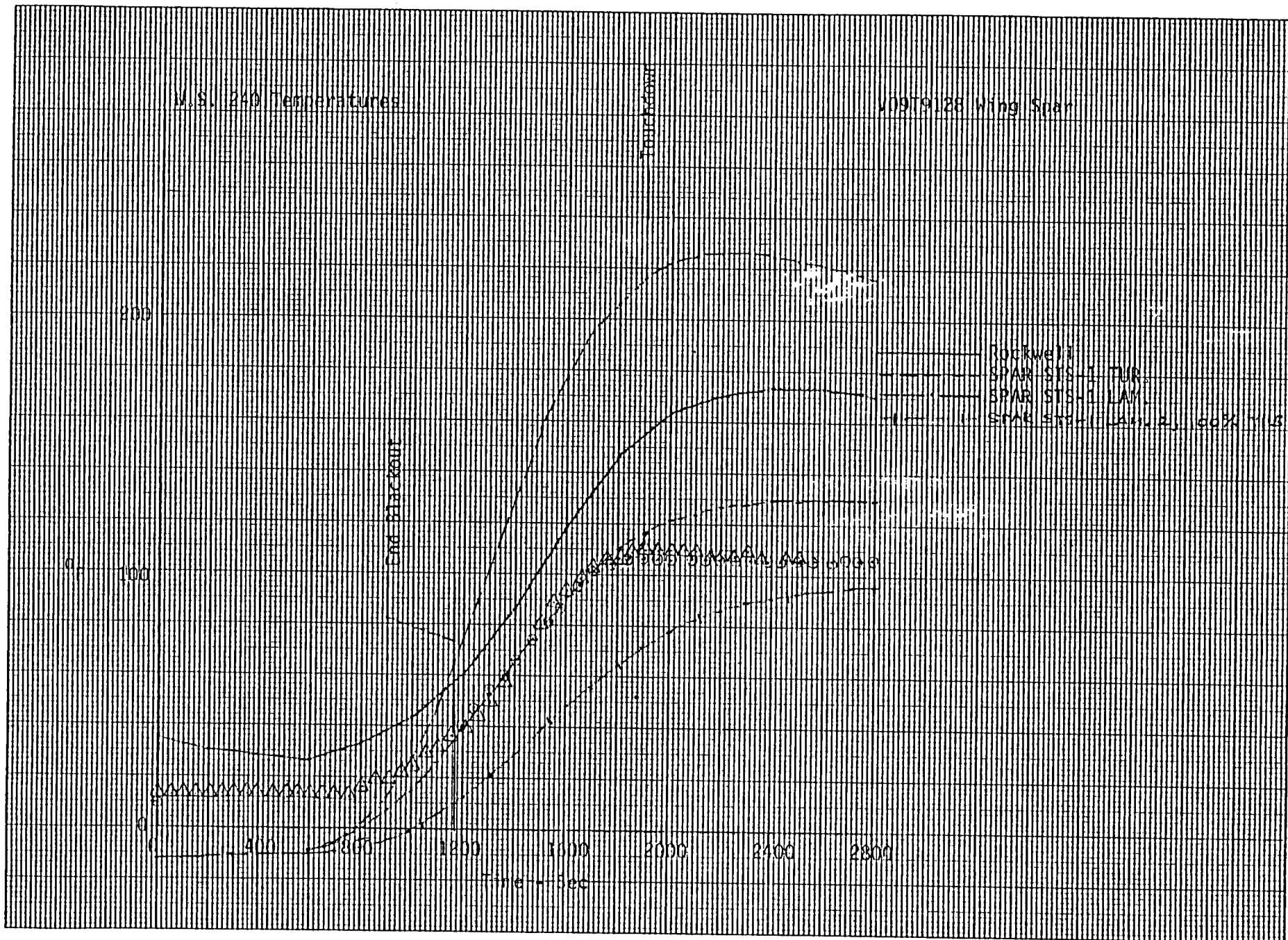


Figure 35 - Flight Temperatures Compared to Predictions - Wing

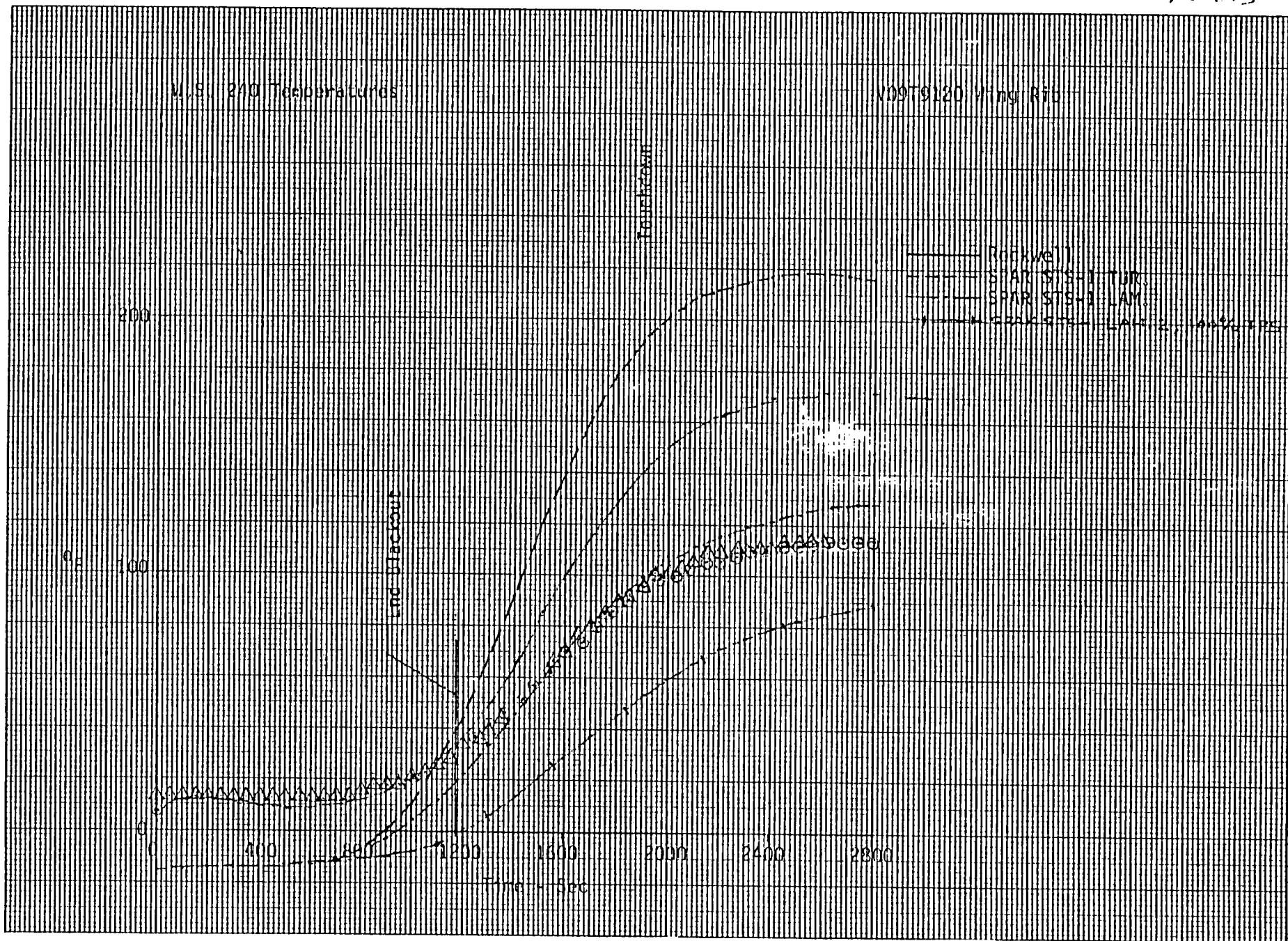


Figure 36 - Flight Temperatures Compared to Predictions - Wing

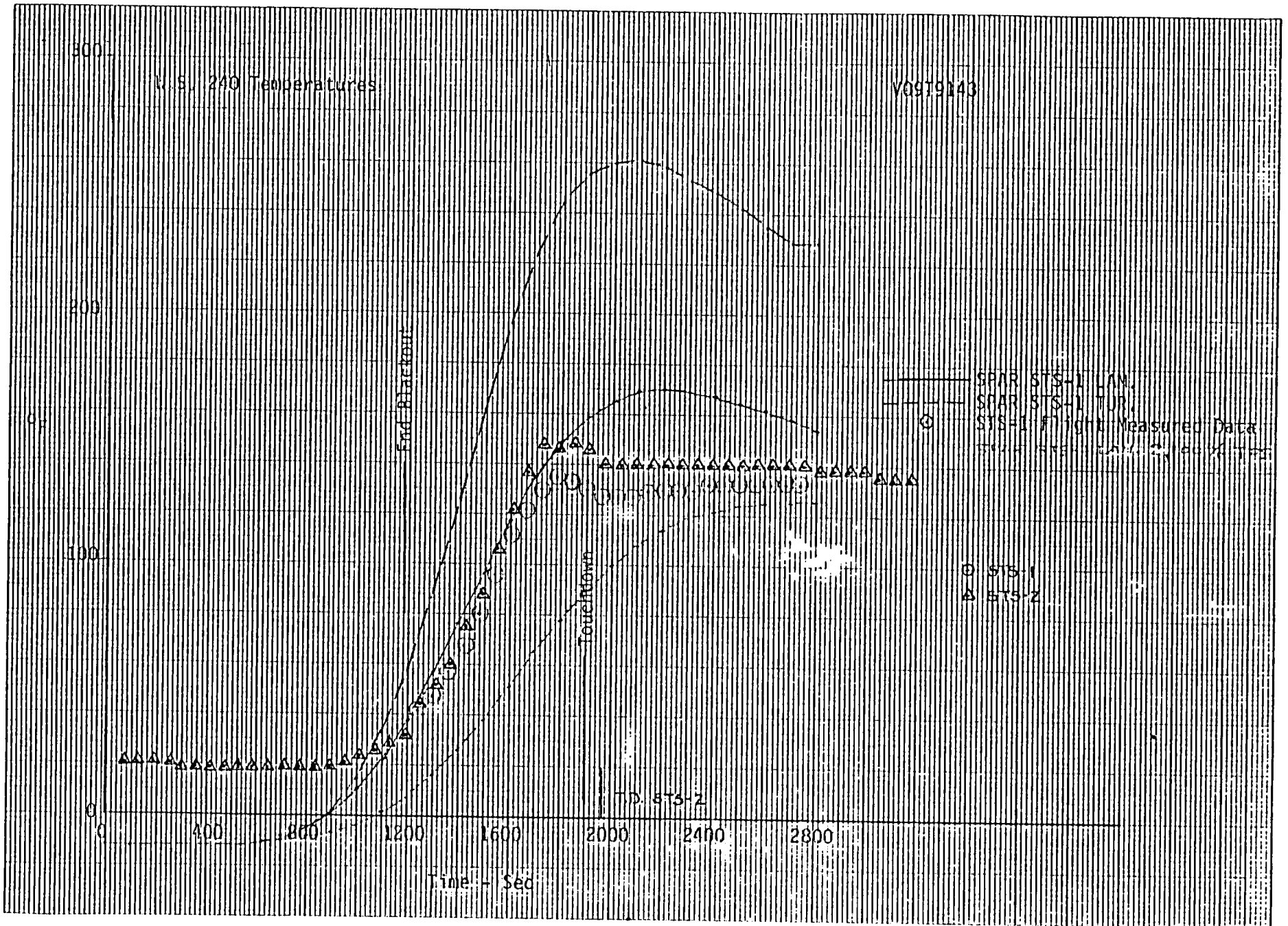


Figure 37 - Flight Temperatures Compared to Predictions - Wing

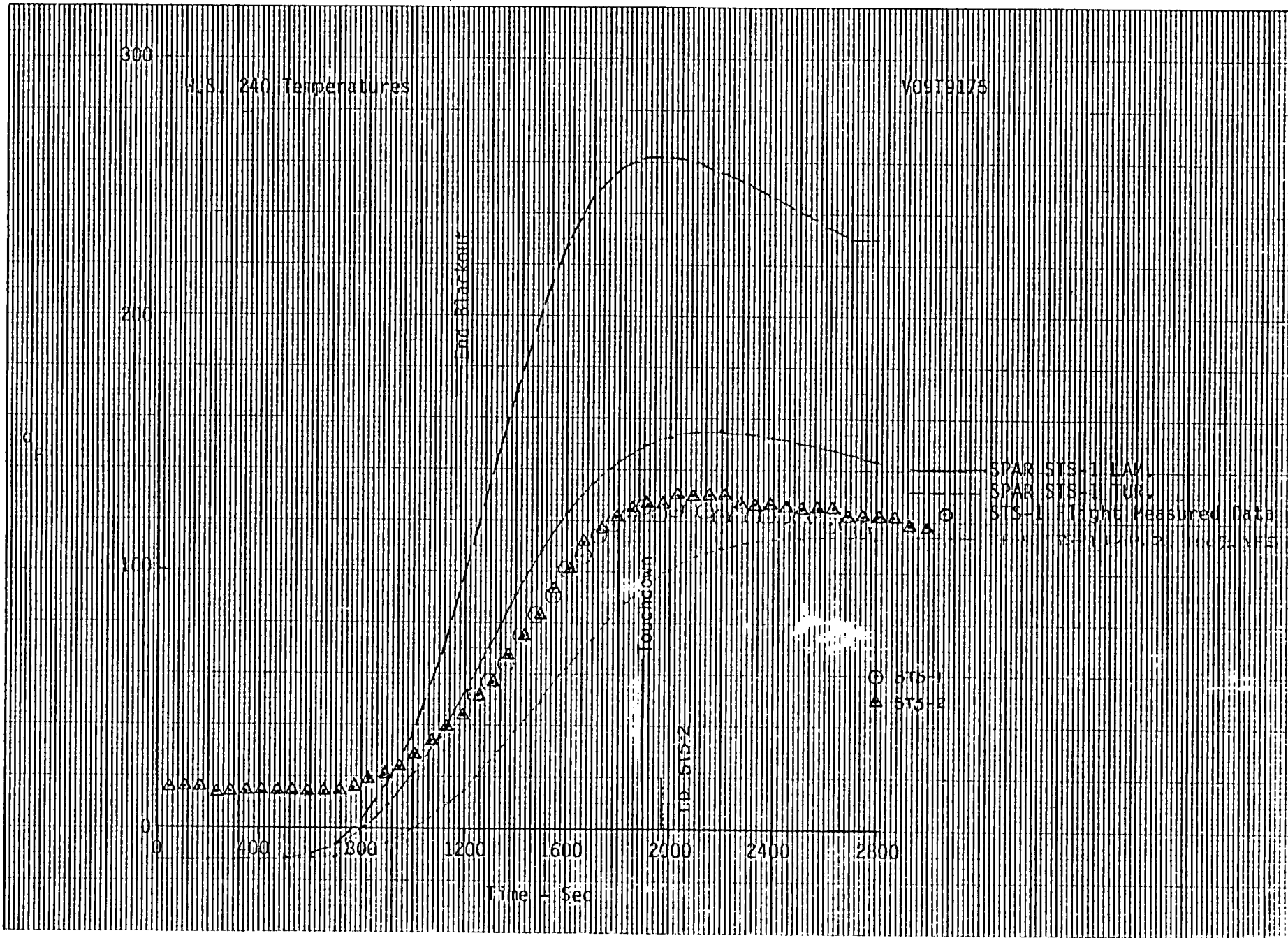


Figure 38 - Flight Temperatures Compared to Predictions - Wing ¹²⁰ 175

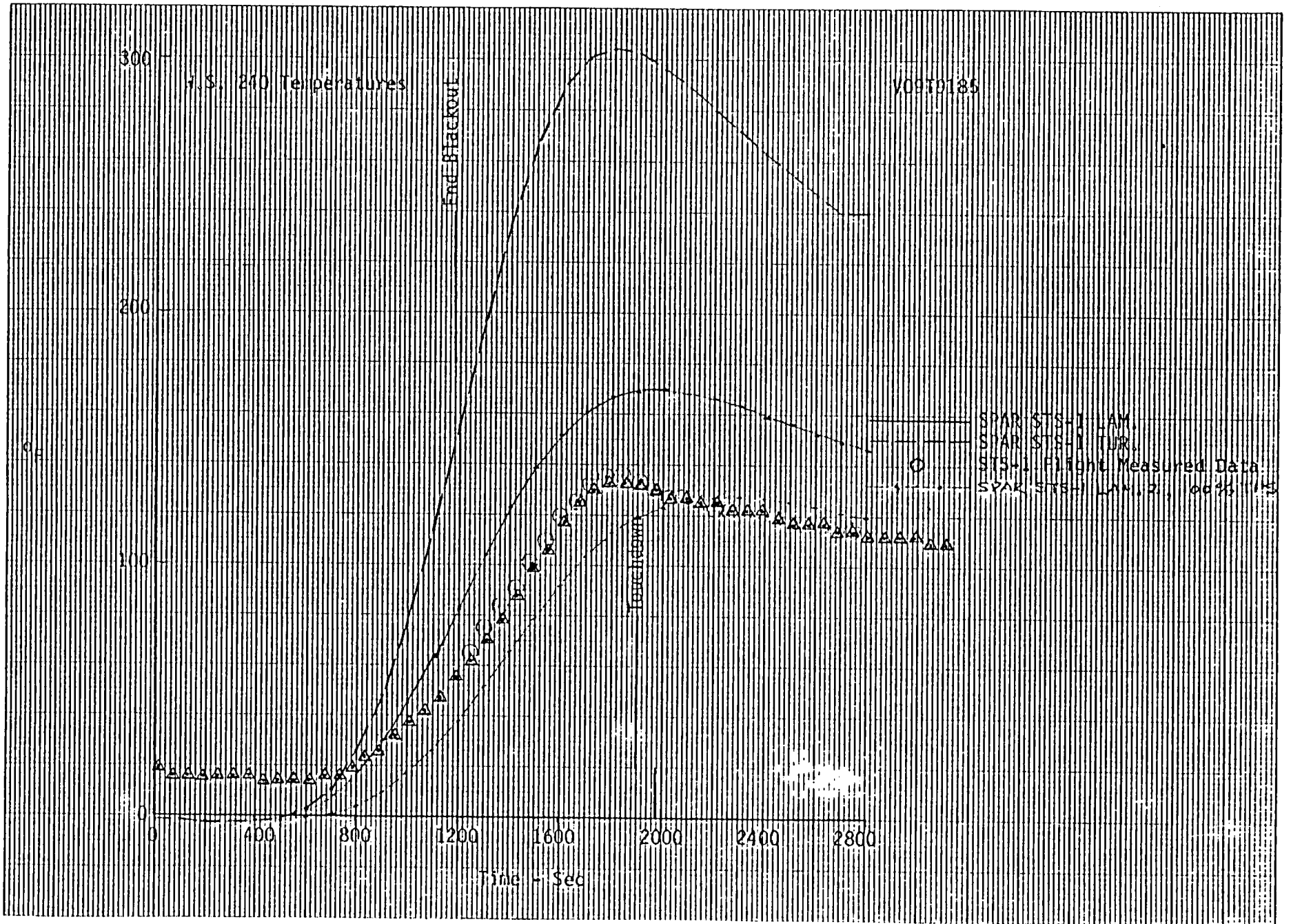


Figure 39 - Flight Temperatures Compared to Predictions - Wing

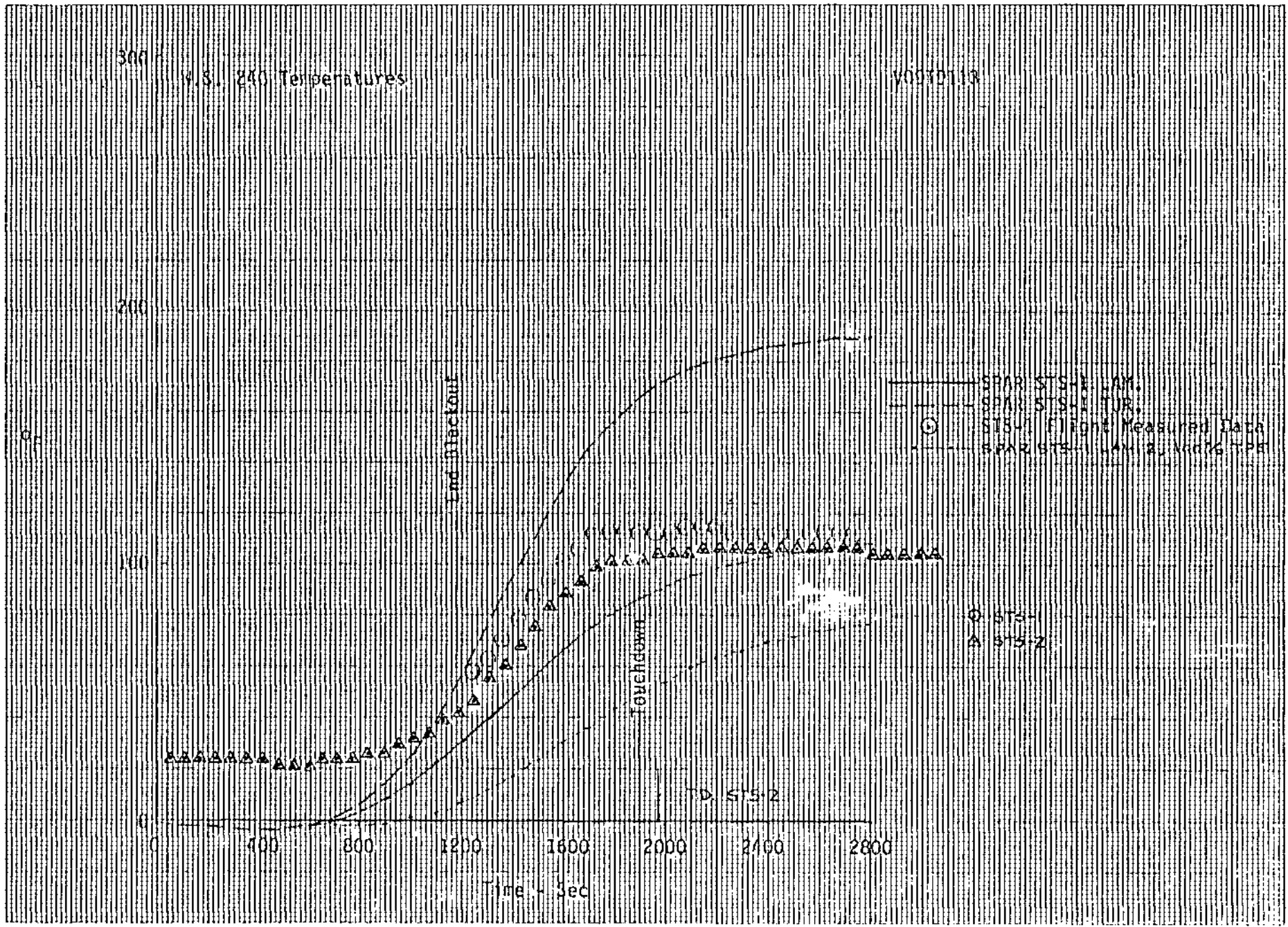


Figure 40 - Flight Temperatures Compared to Predictions - Wing

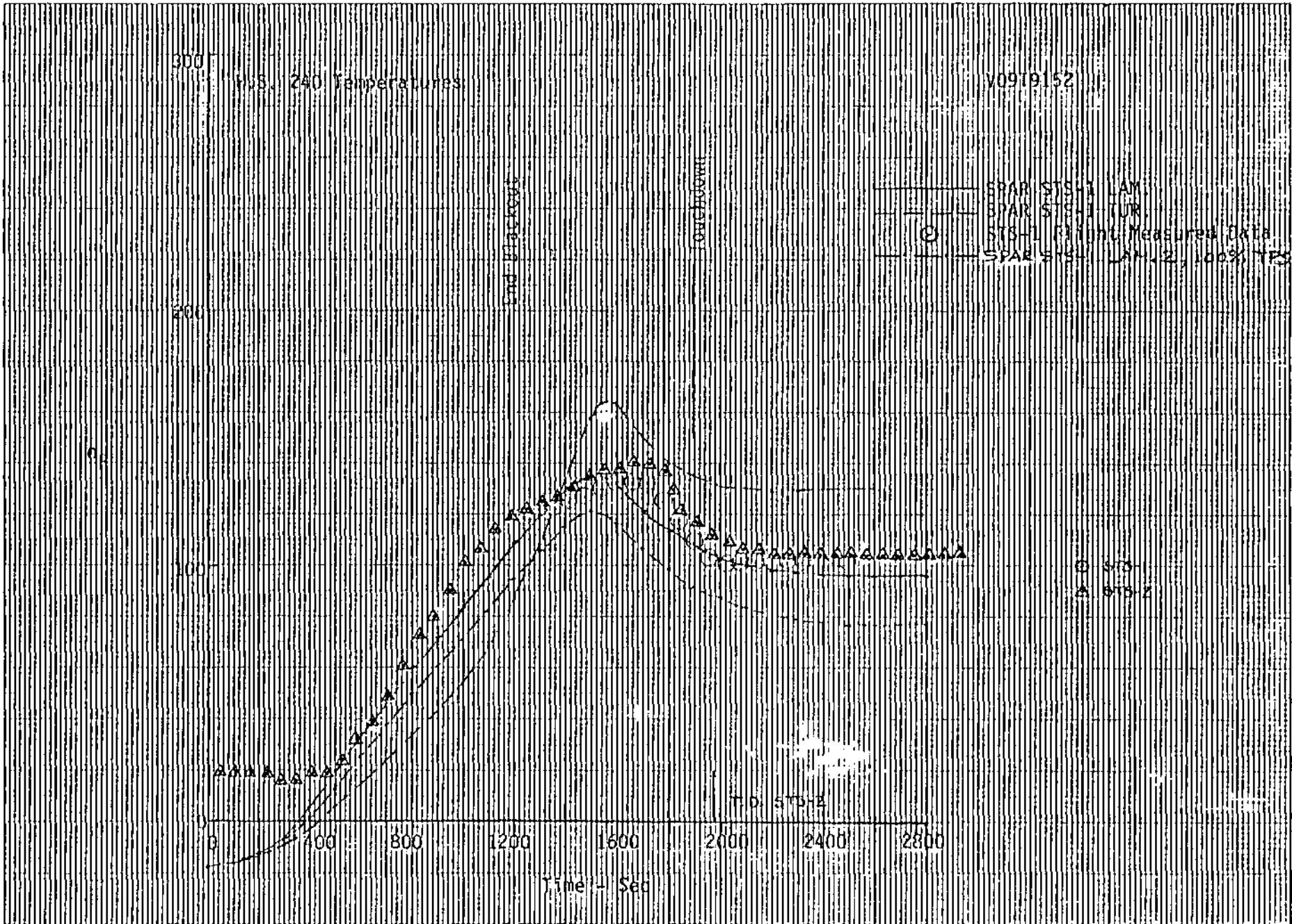


Figure 41 - Flight Temperatures Compared to Predictions - Wing de 691
 910

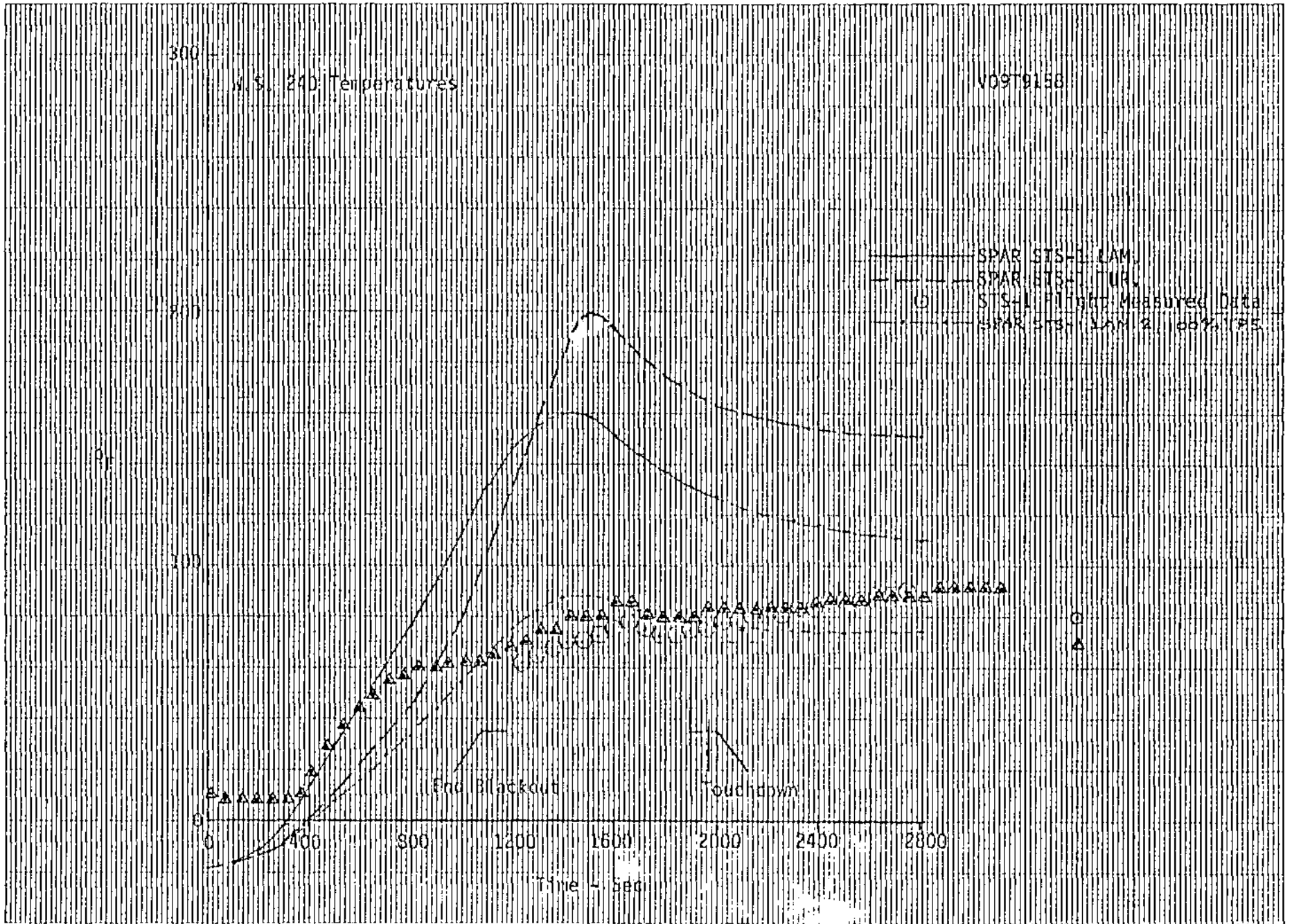


Figure 42 - Flight Temperatures Compared to Predictions - Wing *10/16/85*

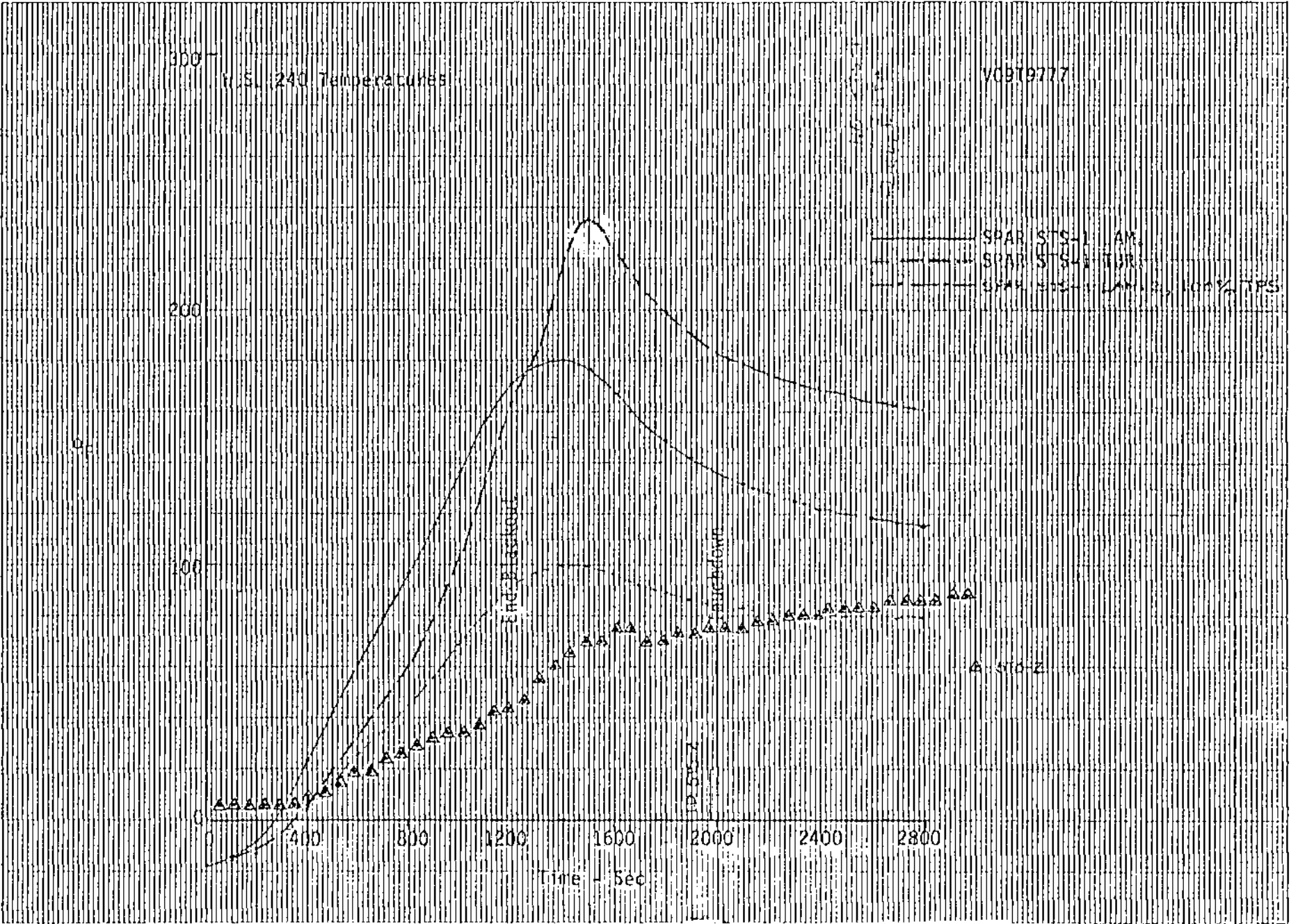


Figure 43 - Flight Temperatures Compared to Predictions - Wing

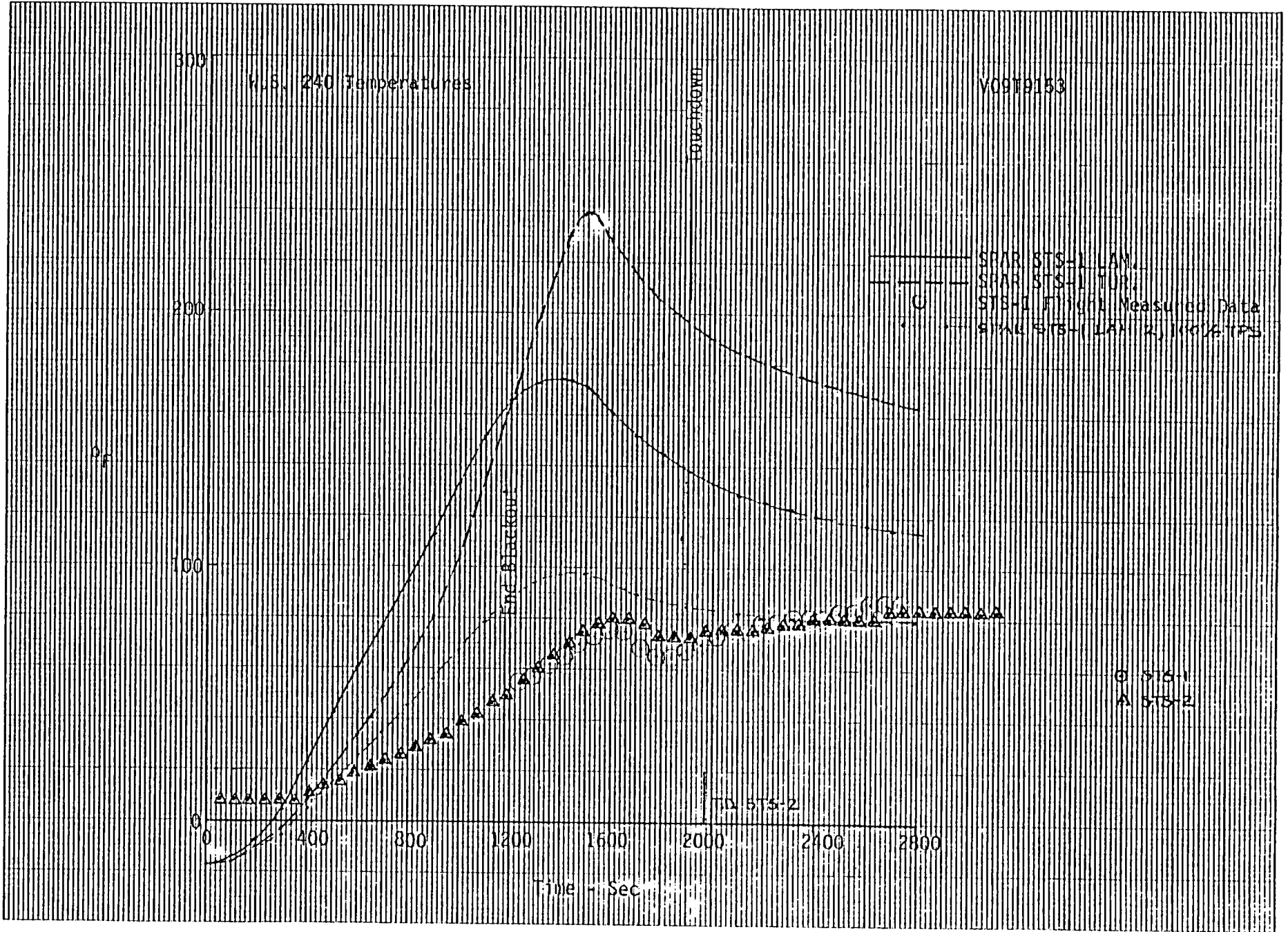


Figure 44 - Flight Temperatures Compared to Predictions - Wing

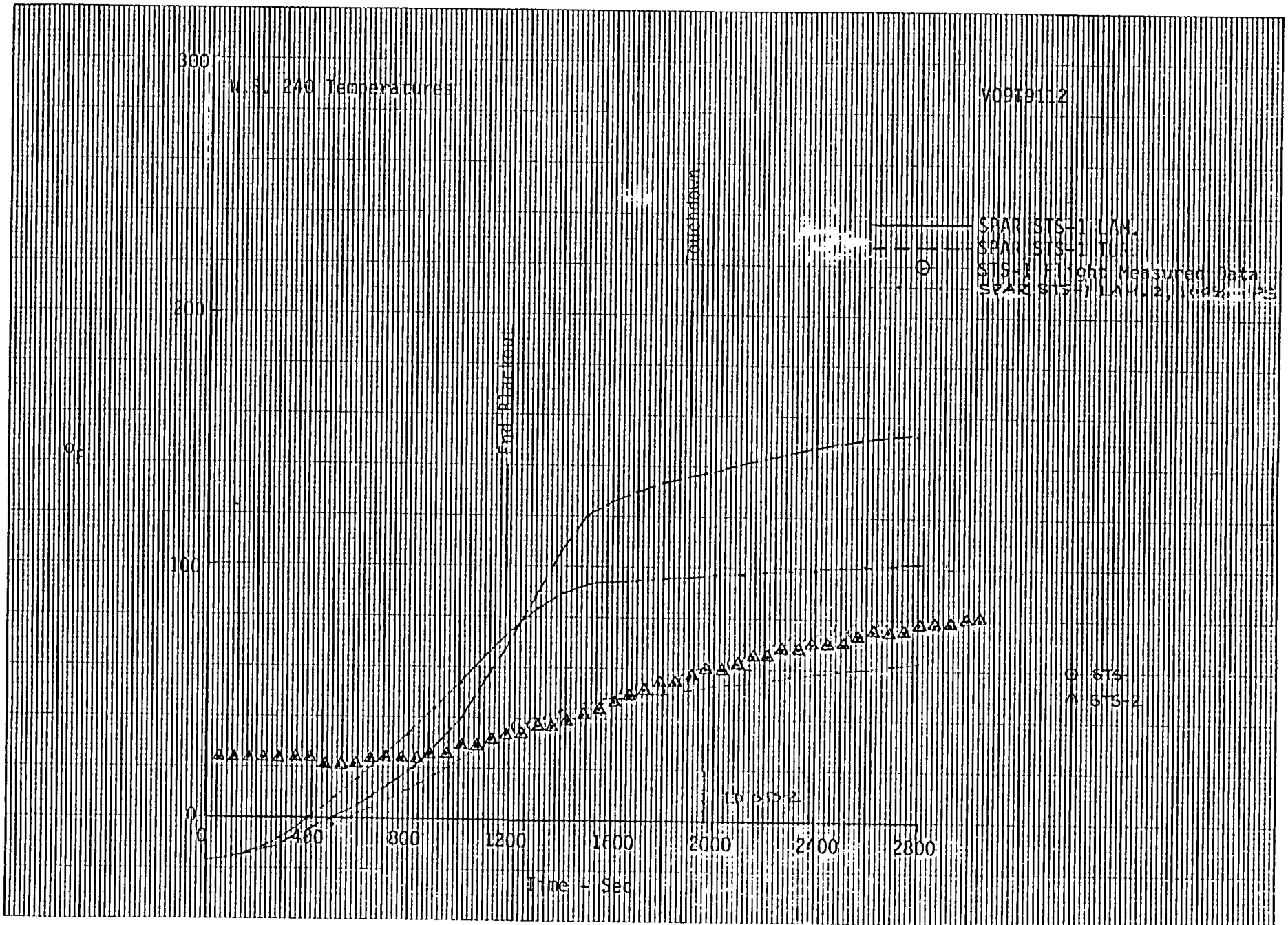


Figure 45 - Flight Temperatures Compared to Predictions - Wing 605

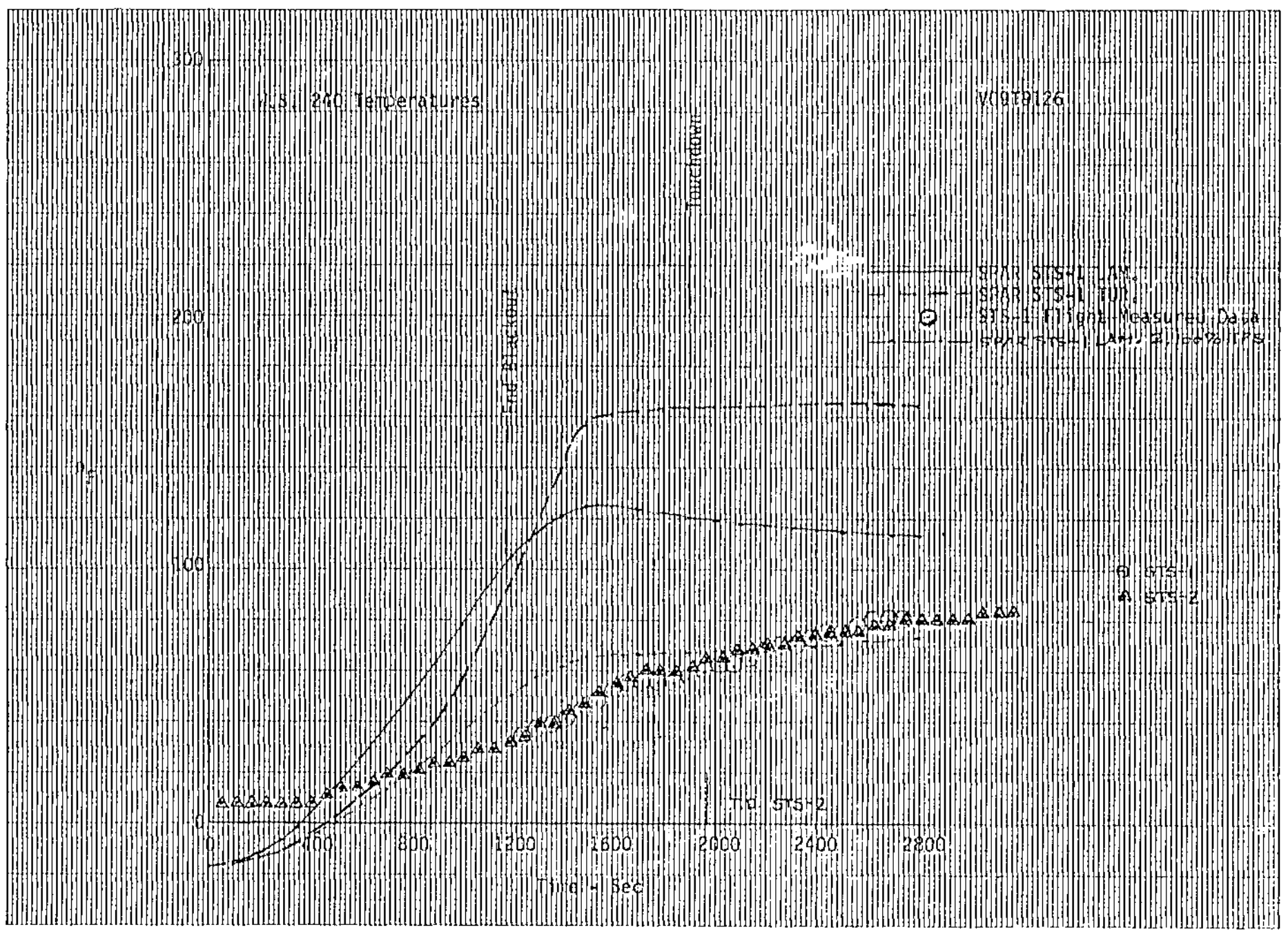


Figure 46 - Flight Temperatures Compared to Predictions - Wing

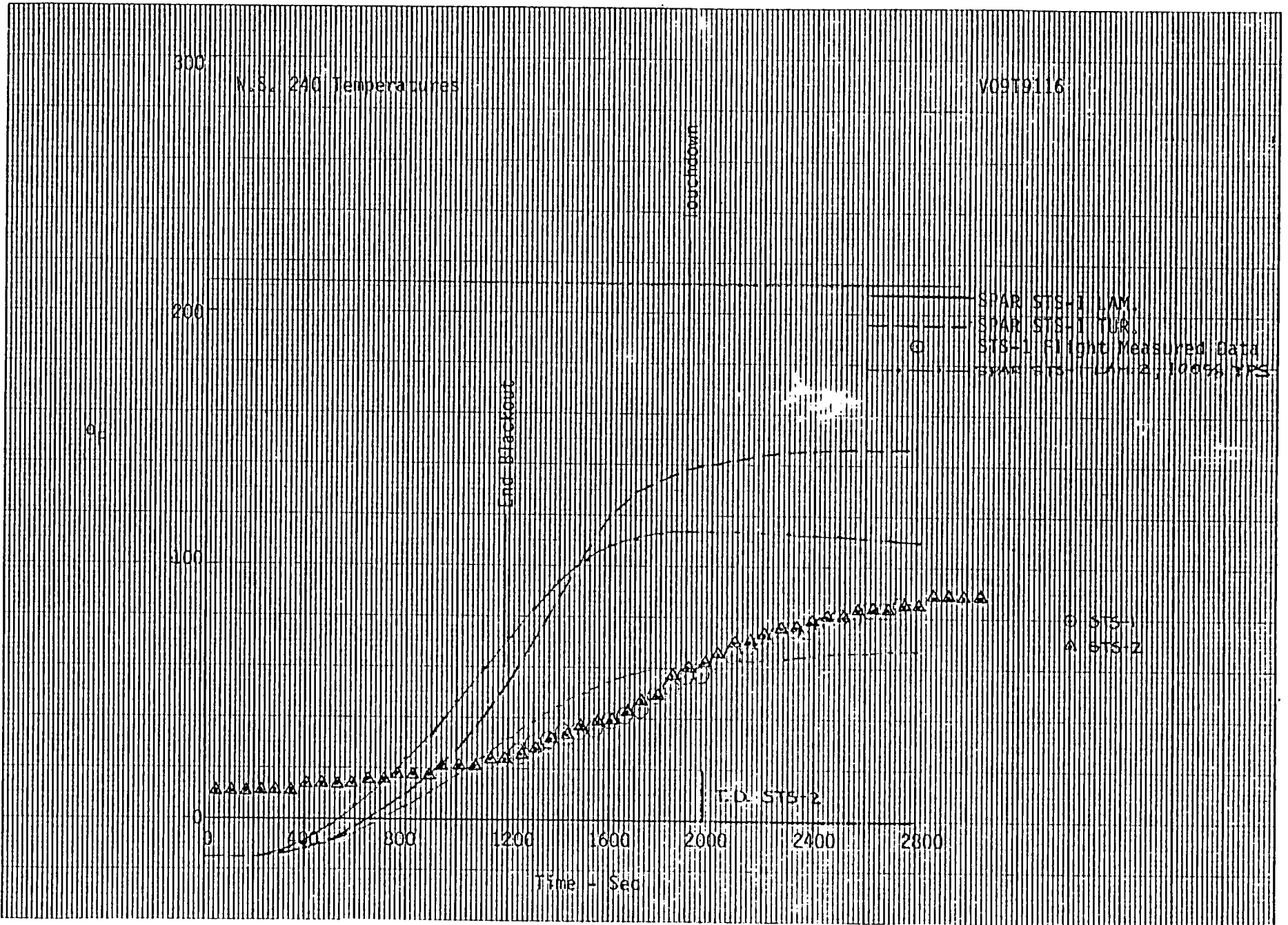


Figure 47 - Flight Temperatures Compared to Predictions - Wing

Page 40
700

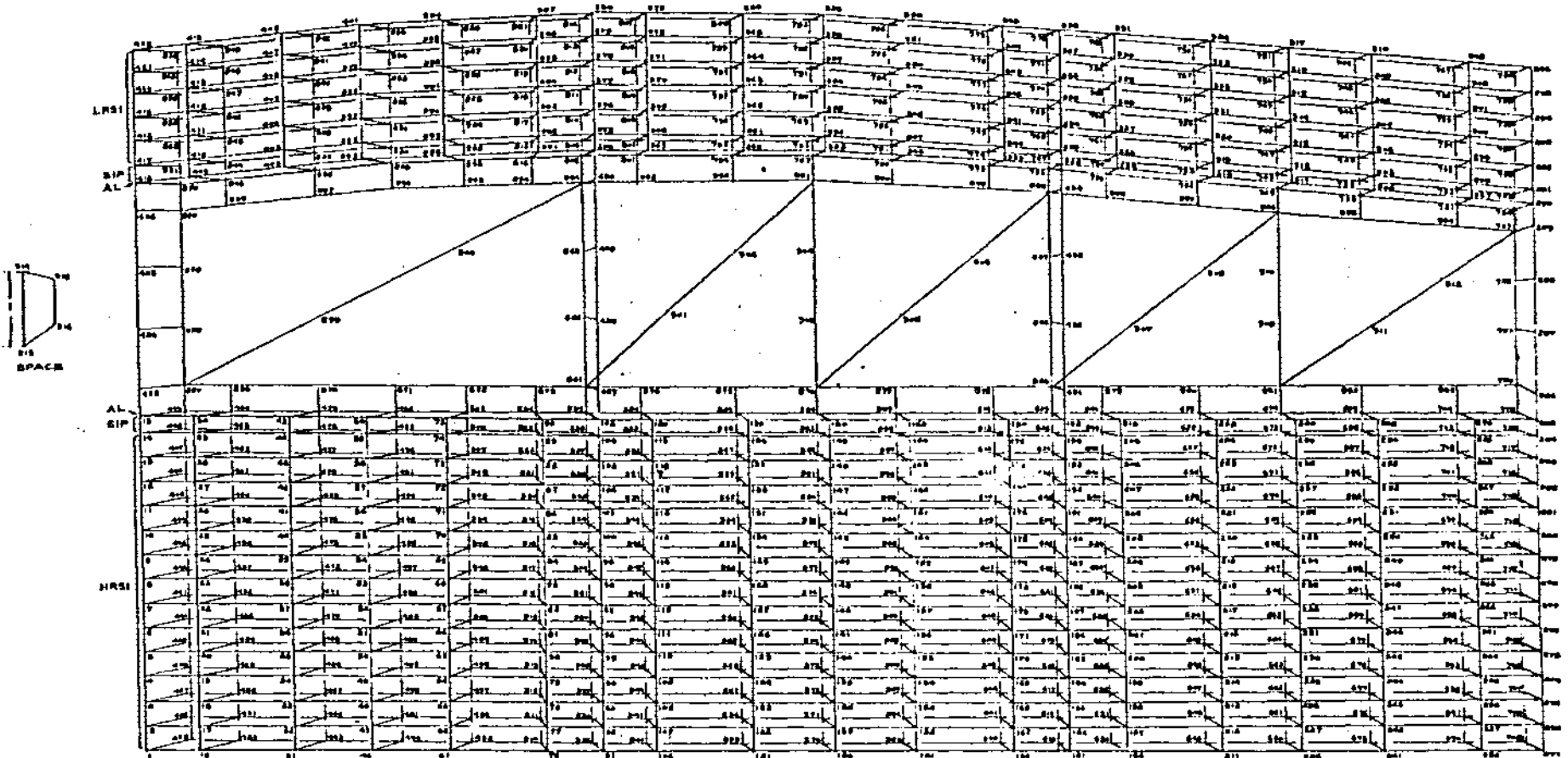


Figure 48 Analytical model of WS 328.

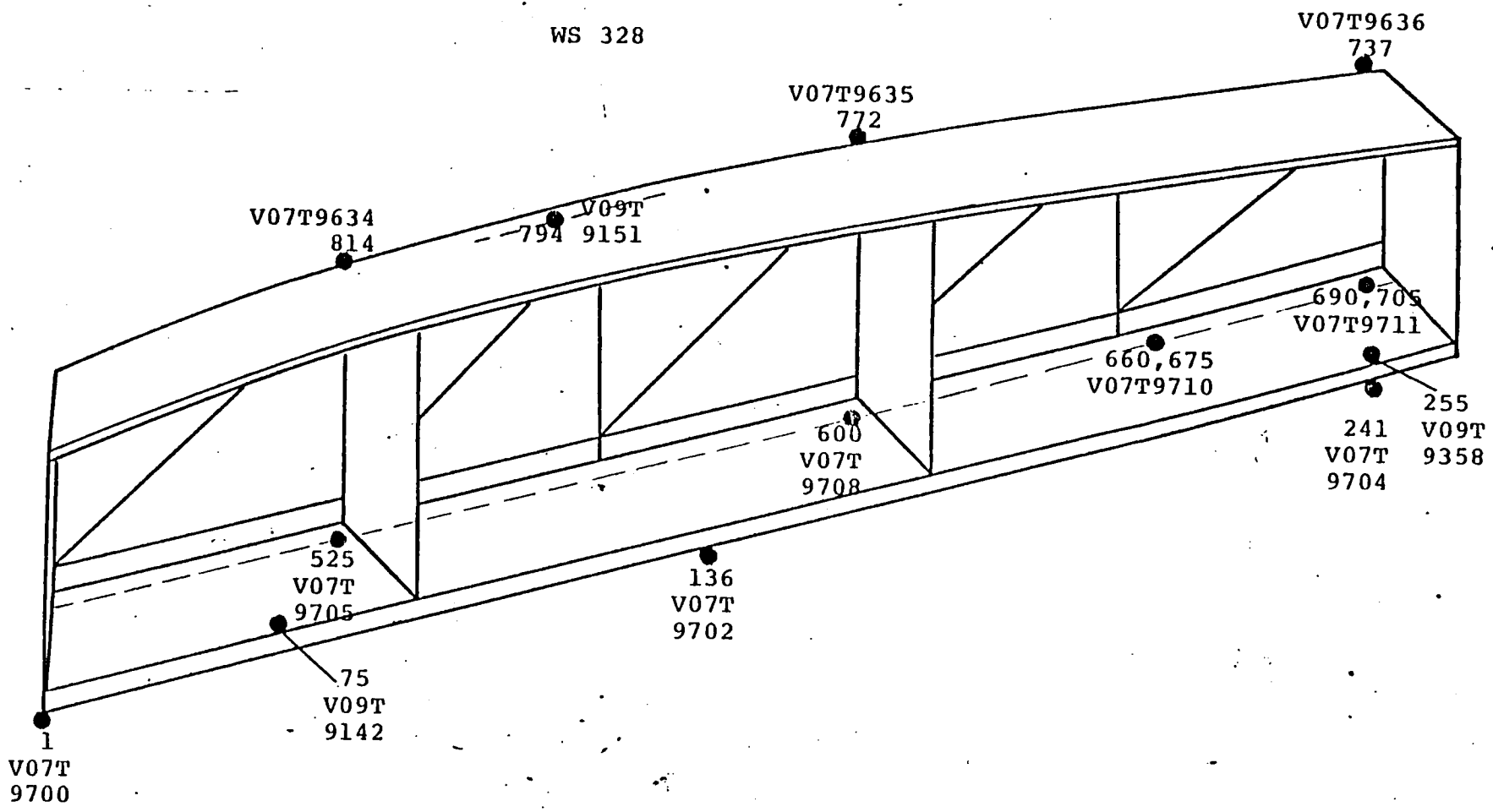


Figure 49 Structural measurement locations at WS 328.

JL0C 75

104

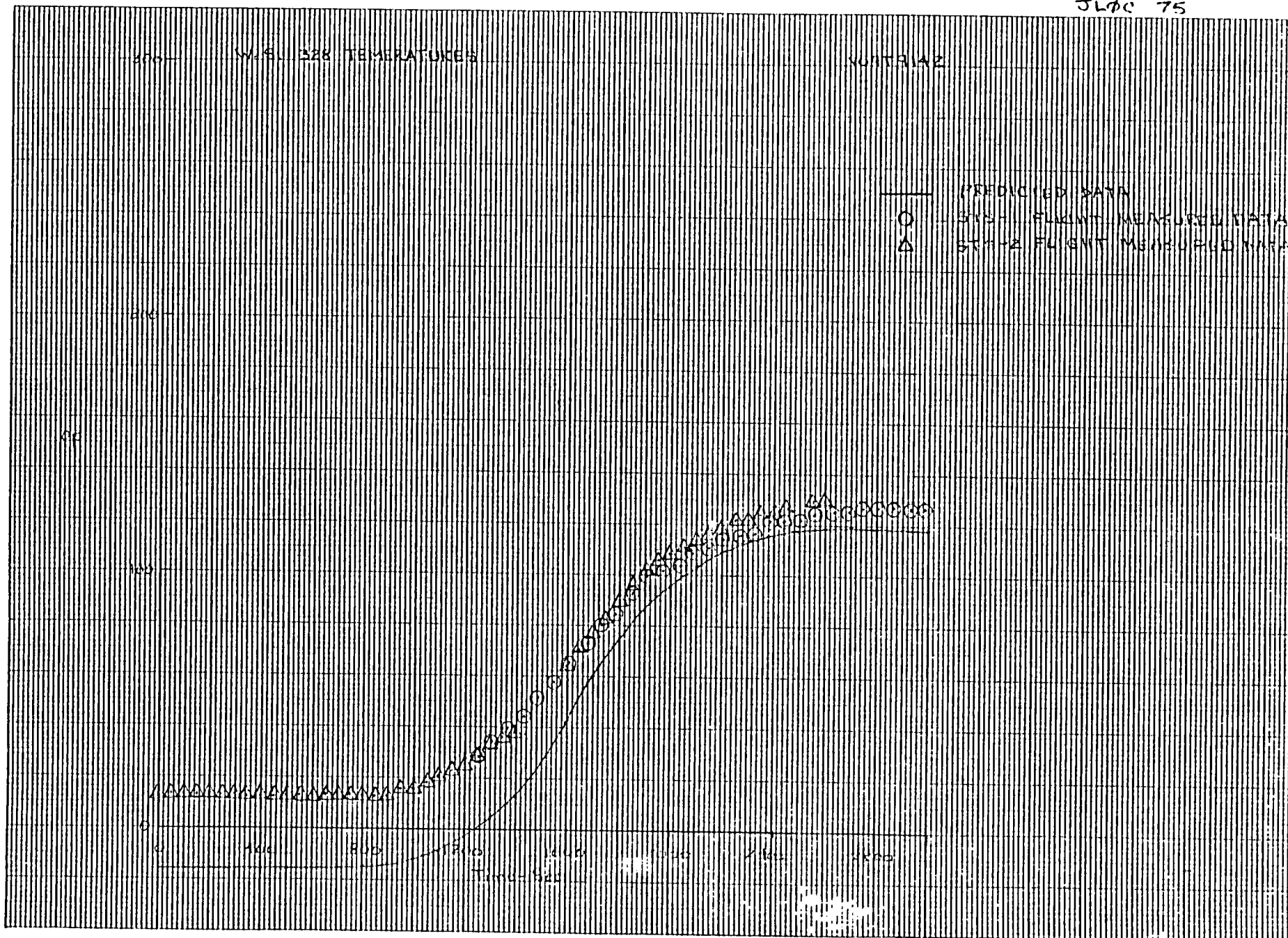


Figure 50 - Flight Temperatures Compared to Predictions - Wing

JL0C 260

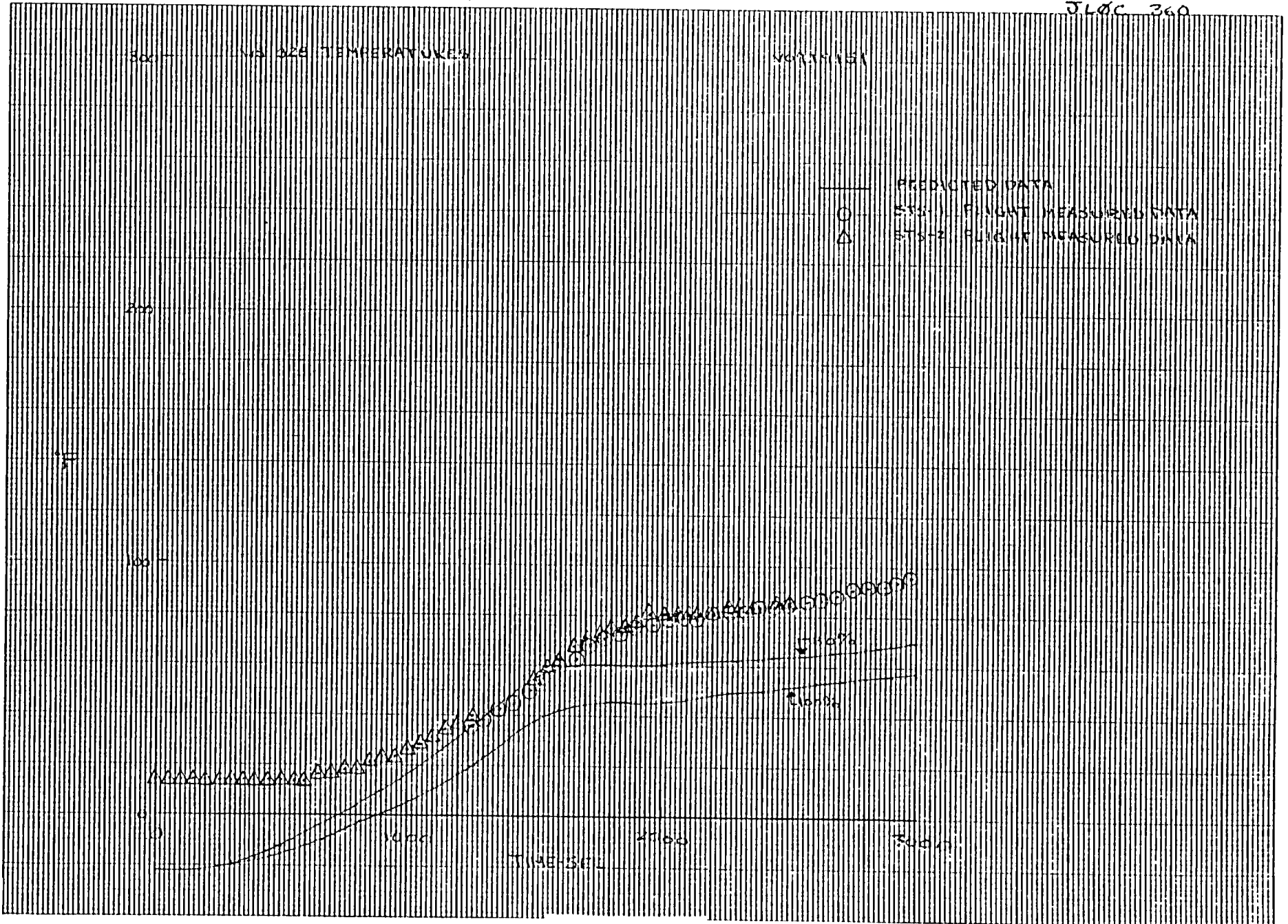


Figure 51 - Flight Temperatures Compared to Predictions - Wing

DLAC 255

106

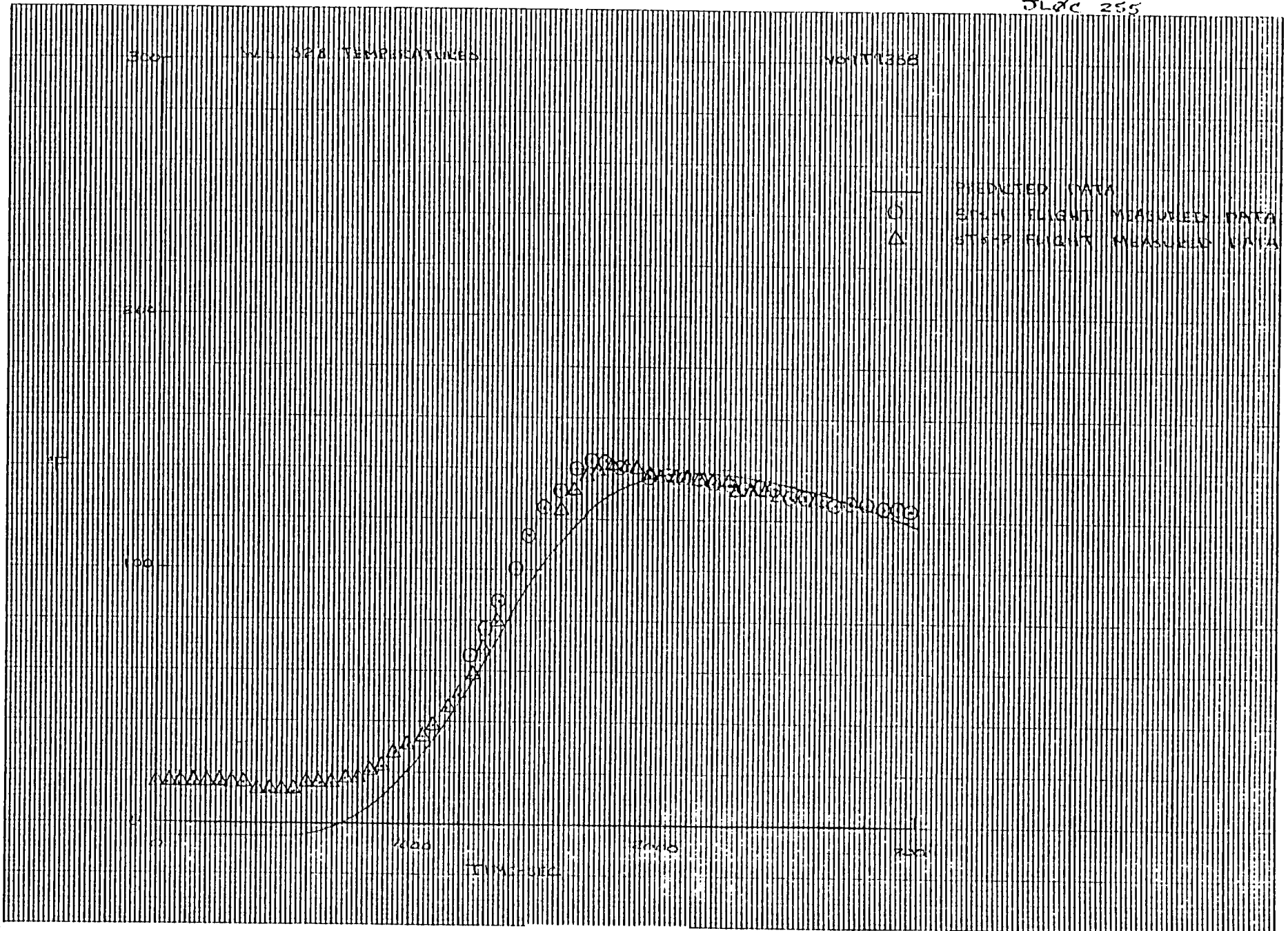


Figure 52 - Flight Temperatures Compared to Predictions - Wing

STRUCTURE TC

TOUCHDOWN 10:20:58 1916 sec.

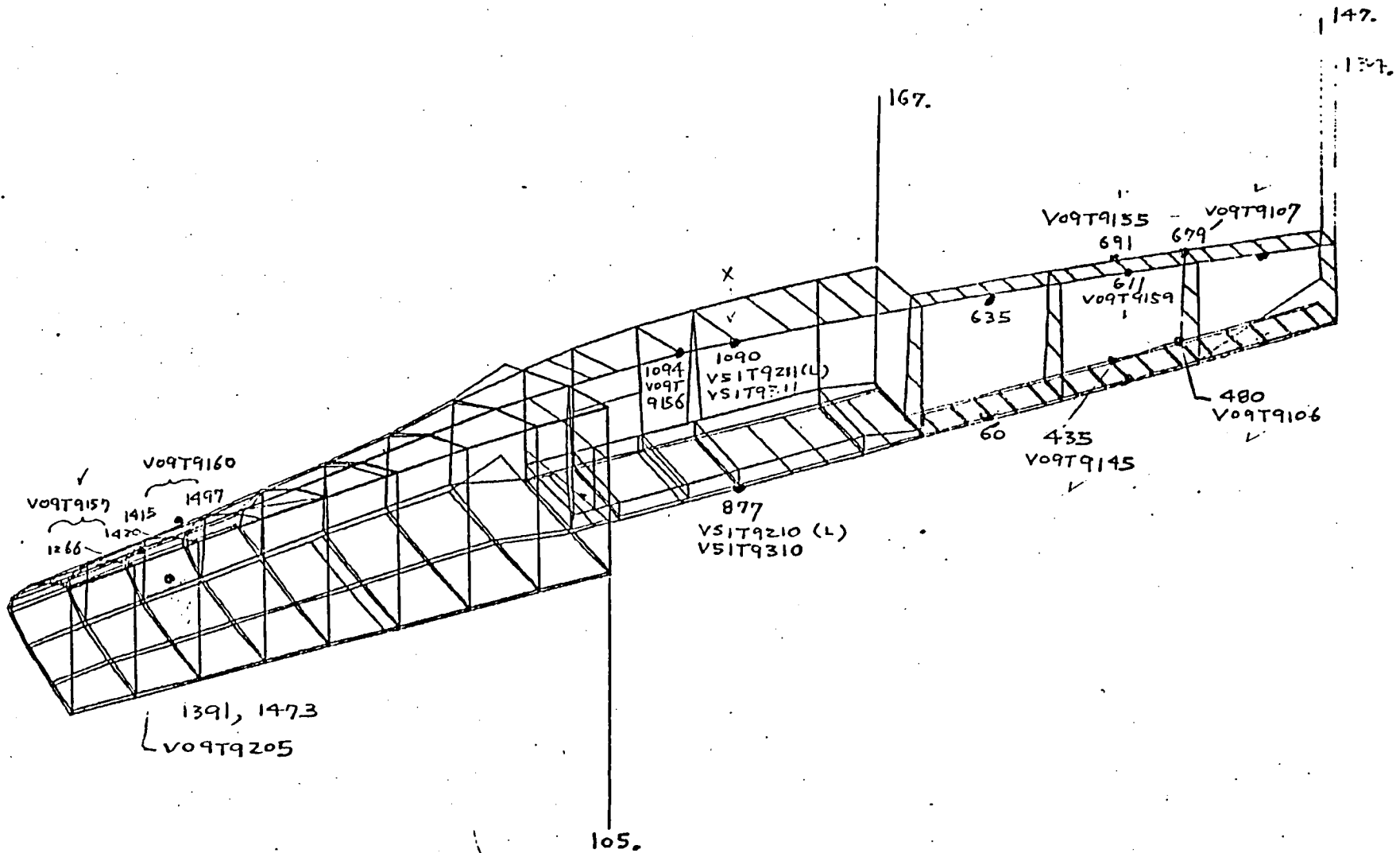


Figure 53. Structural temperature measurement locations at WS 134.

JL0C 435 (V09T9145) LWR

V09T9145

X 1

.

Y

-158

TRIP 1.117"

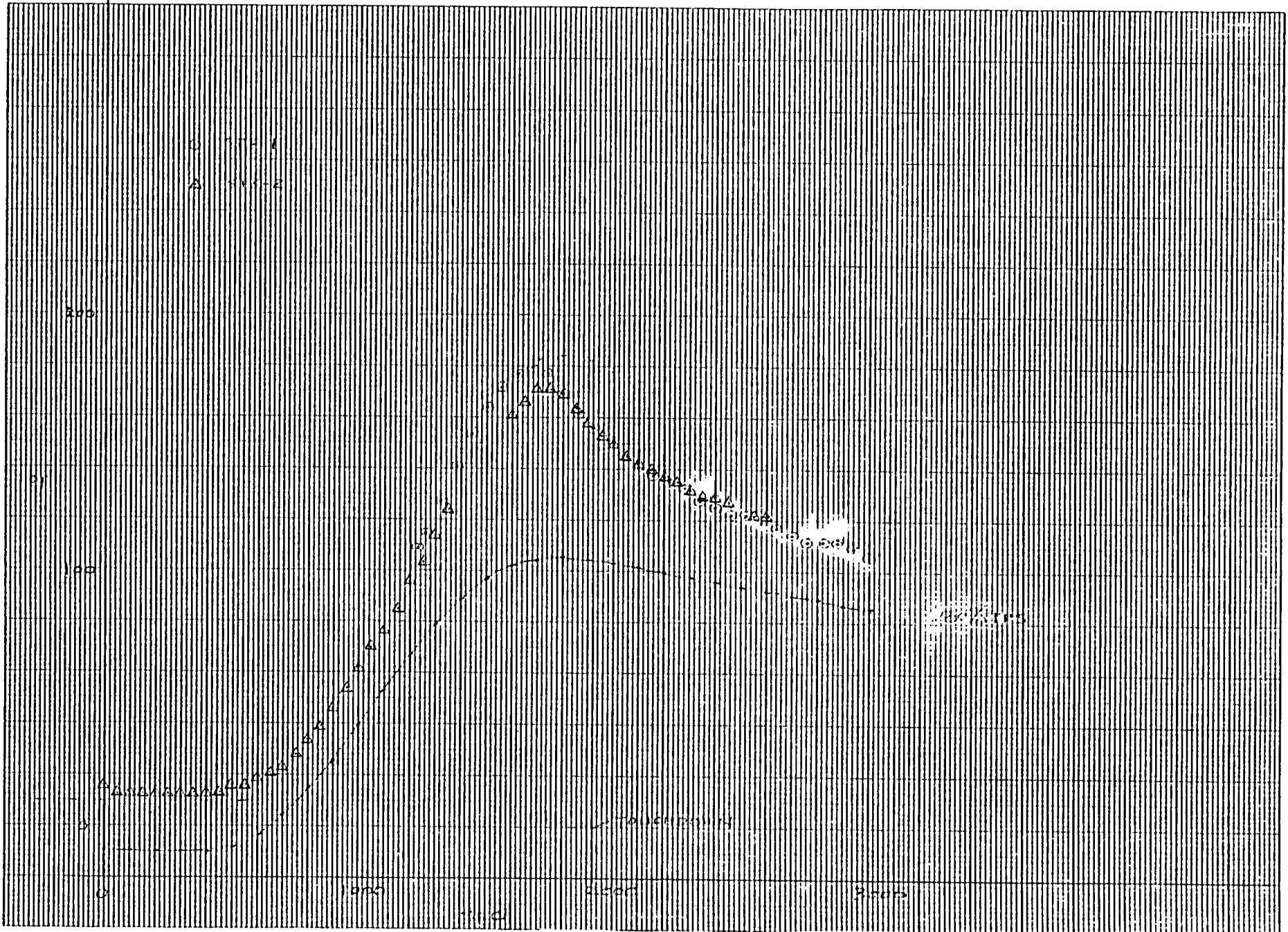


Figure 54 - Flight Temperatures Compared to Predictions - Wing

JL0C 480 (V09T9106) LWR

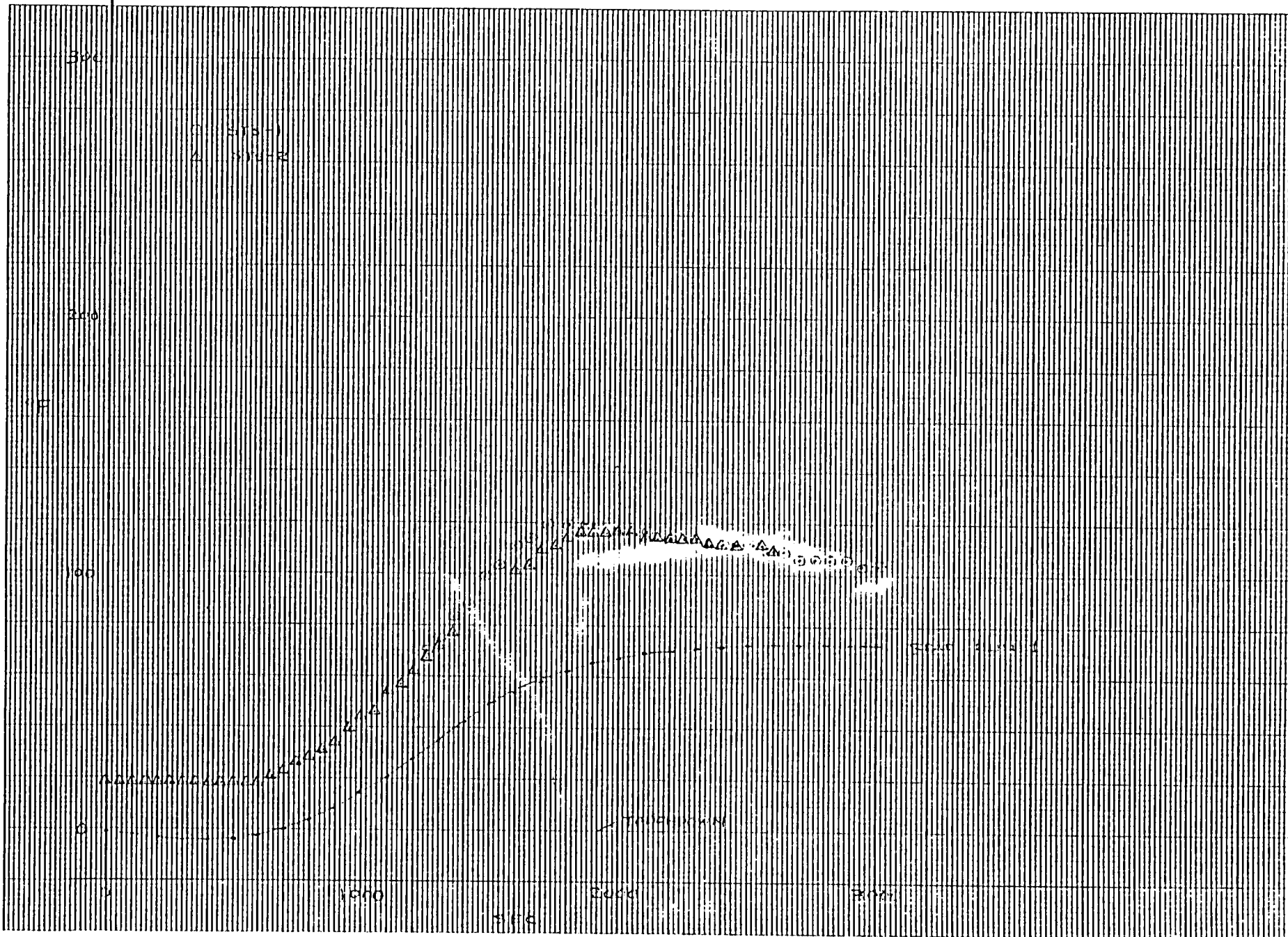


Figure 55 - Flight Temperatures Compared to Predictions - Wing

JL4C 691 (VO 9T9155) UPPER RAY 3 VO 1T9155 X 127.0. Y = 159.0

110

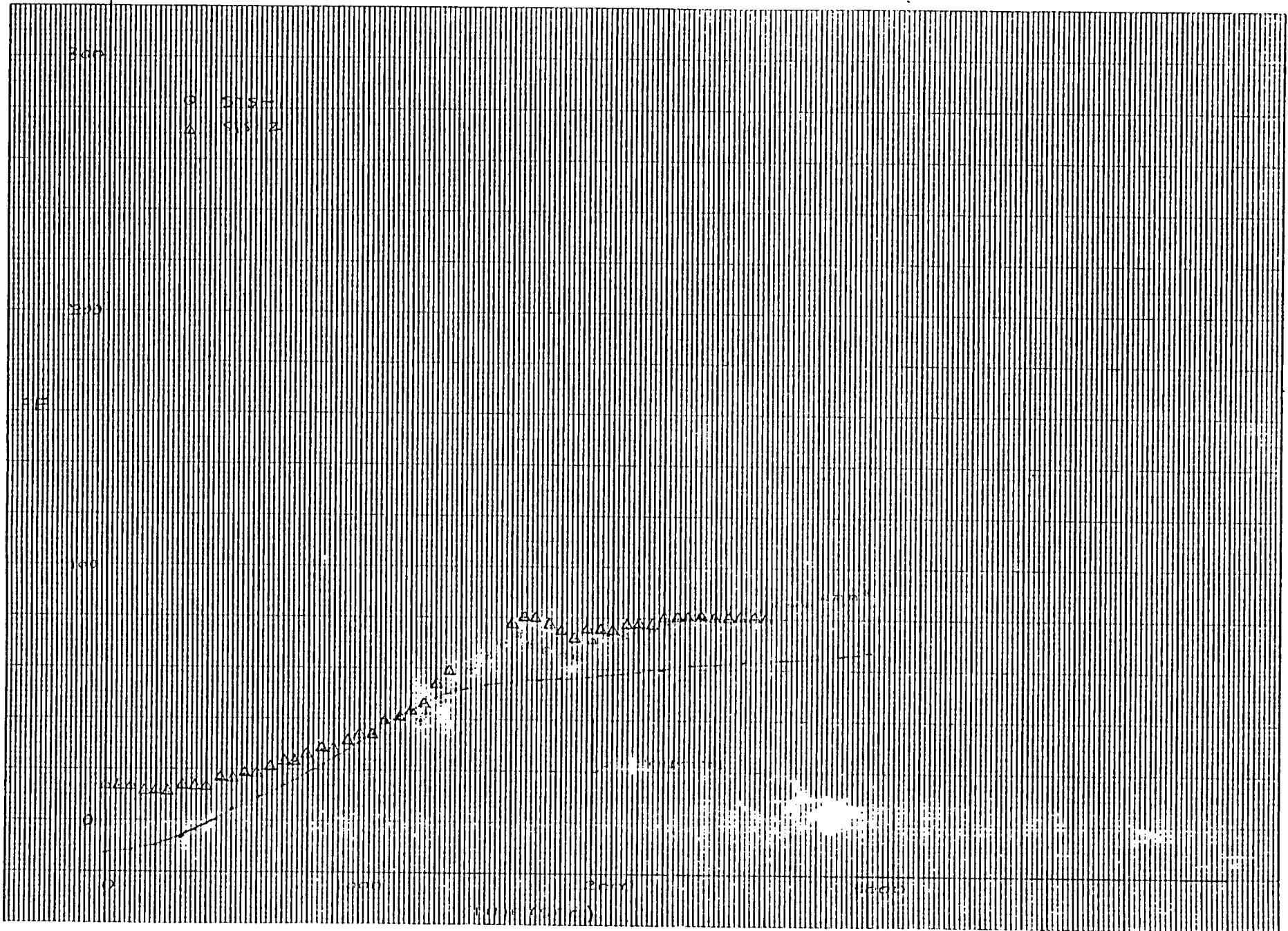


Figure 56 - Flight Temperatures Compared to Predictions - Wing

JL4C 611 (V09T 9159) UPRR B/Y 3

V09T 9159 10 10 1959 70-111.0

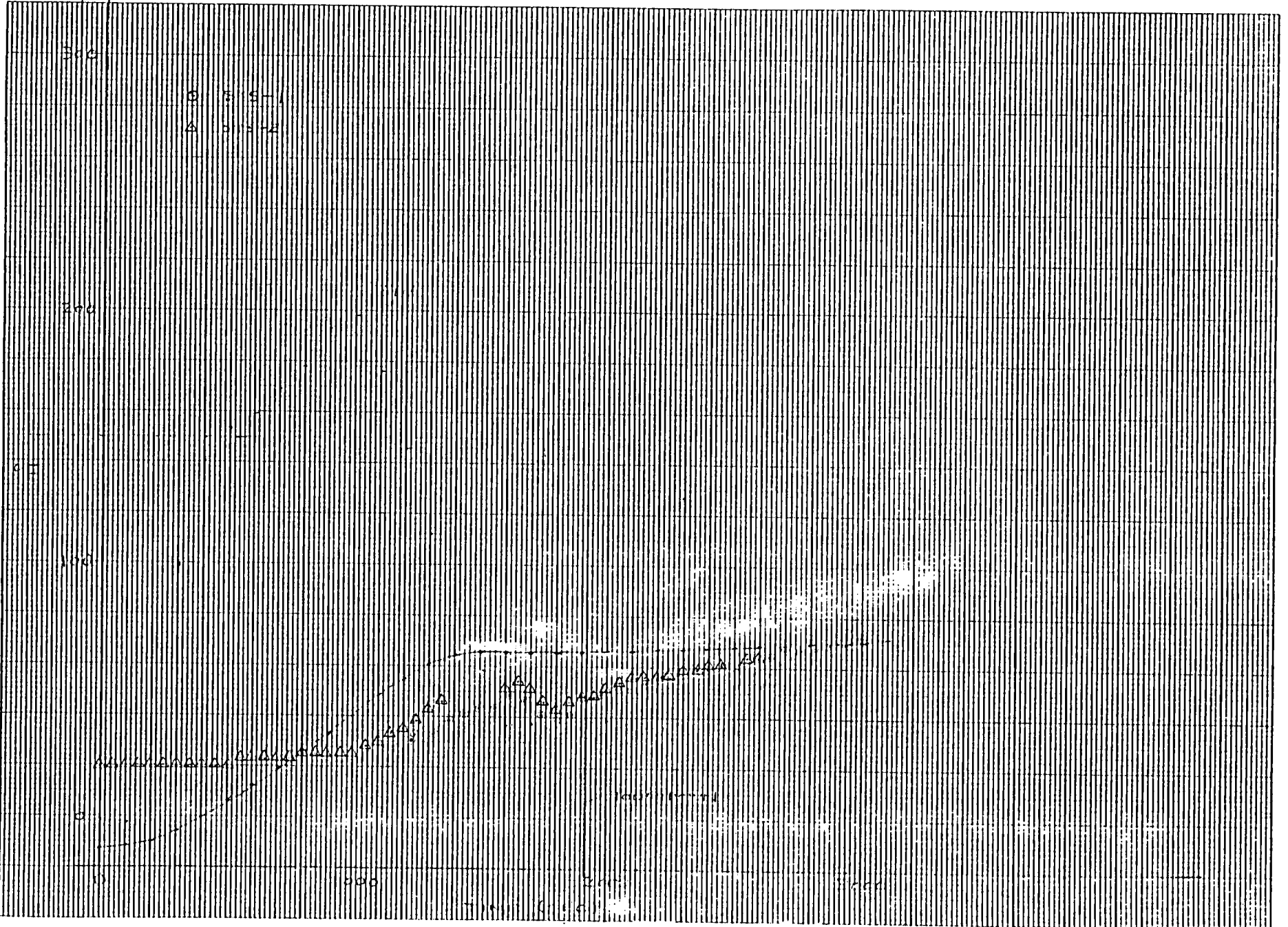


Figure 57 - Flight Temperatures Compared to Predictions - Wing

JLφC 679 (V09T9107) UPRR R45 3/4 V09T9107 X=1307.0. Y=-15.0.0

112

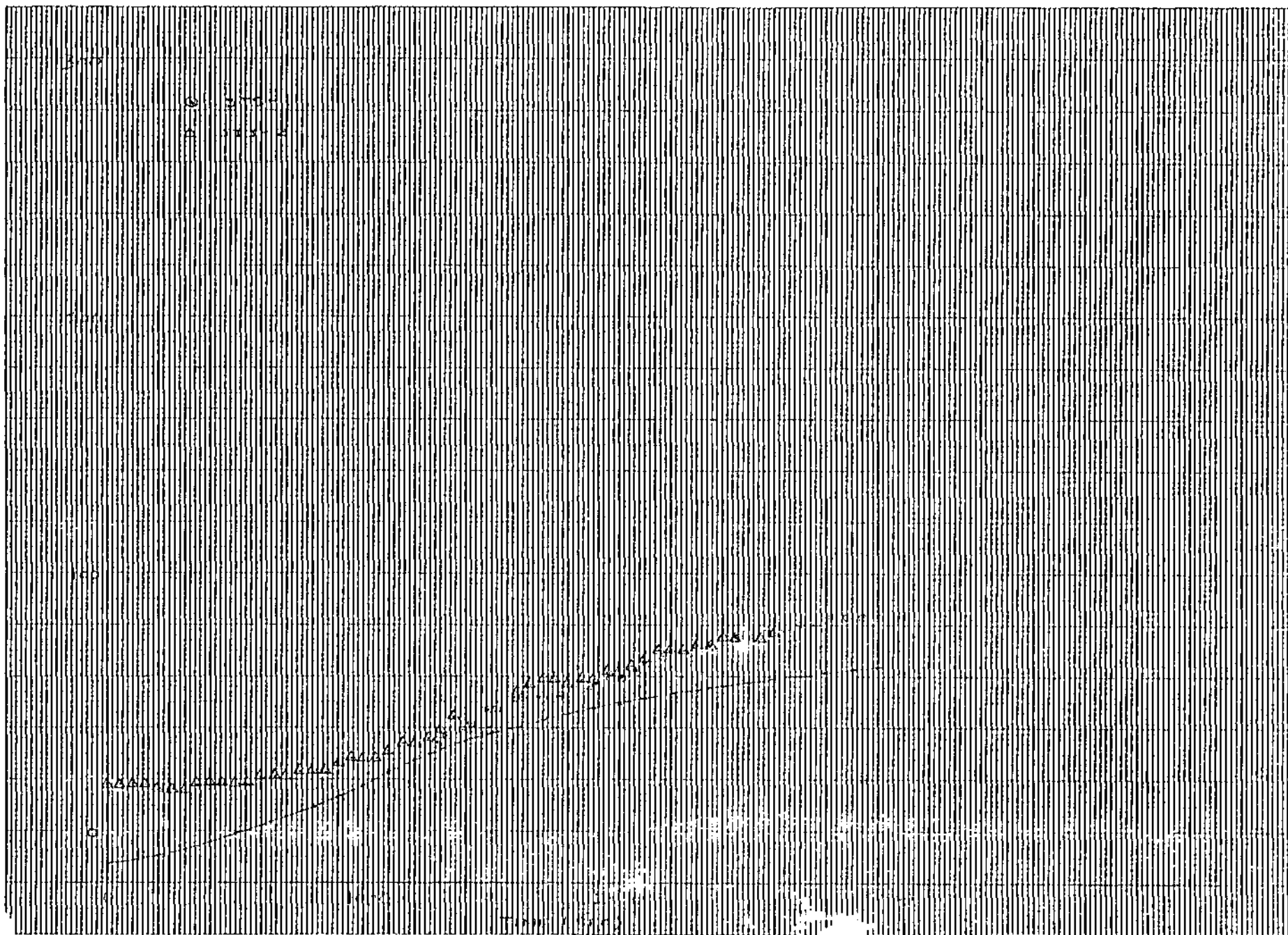


Figure 58 - Flight Temperatures Compared to Predictions - Wing

JLDC 1266, 1420 (V09T9157) GLOVE 11PRR

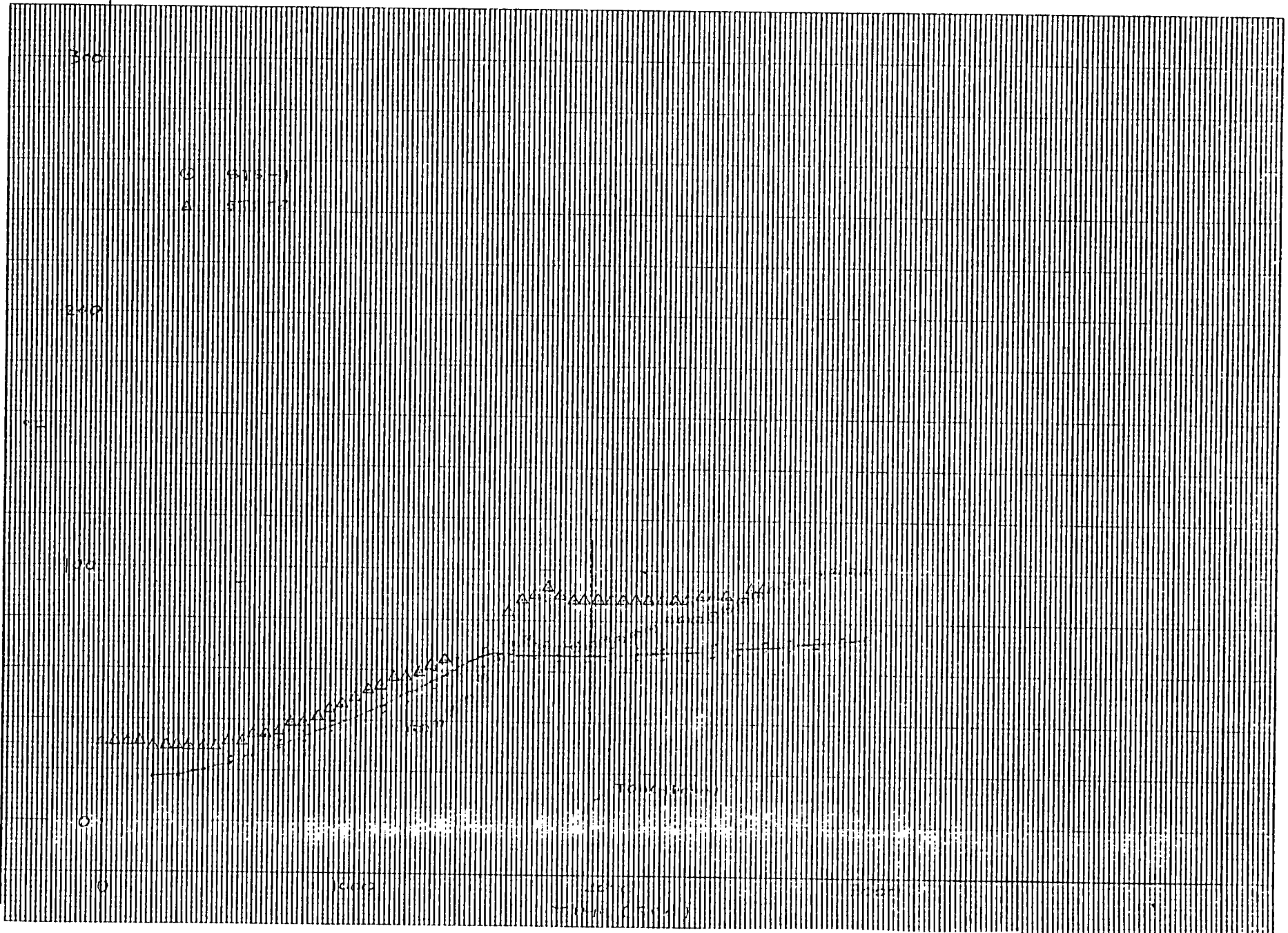


Figure 59 - Flight Temperatures Compared to Predictions - Wing

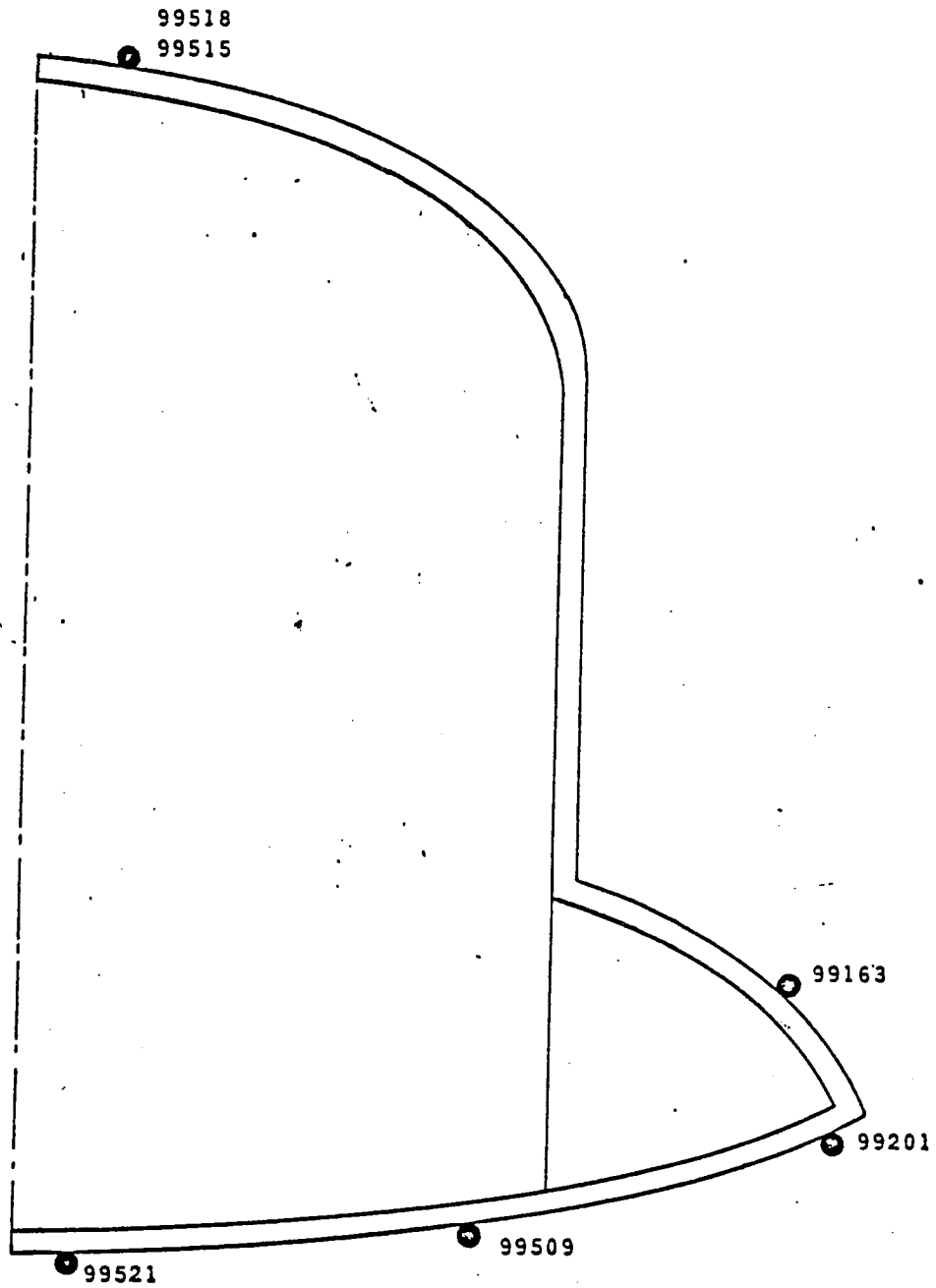


Figure 60 Locations of surface temperature measurements at FS 877.

V09T 9521

F 077 STS-1 Node 13

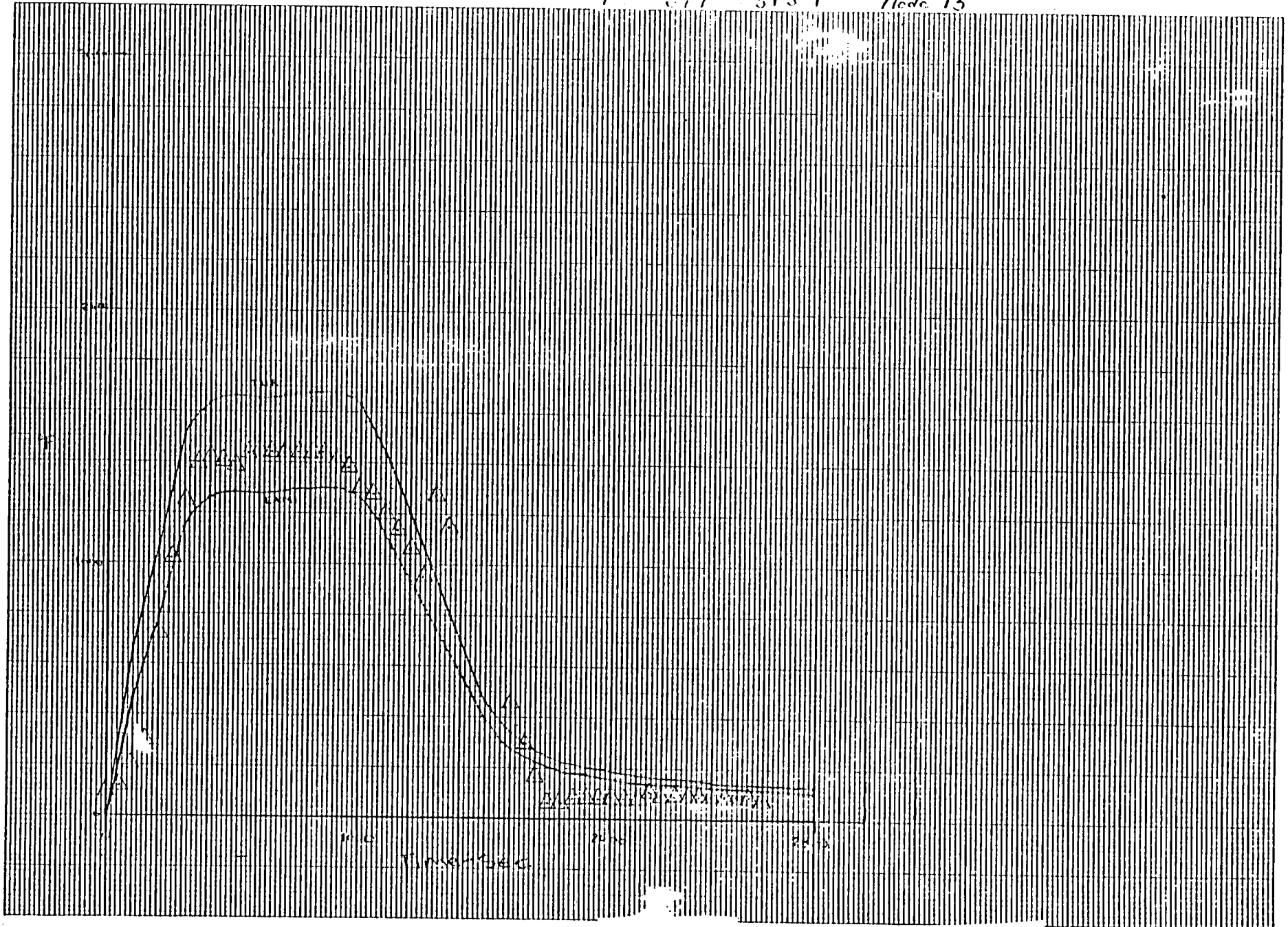


Figure 61 - Flight Temperatures Compared to Predictions - Fuselage

V09T9509

FSS 877 STS-1 Node 97

116

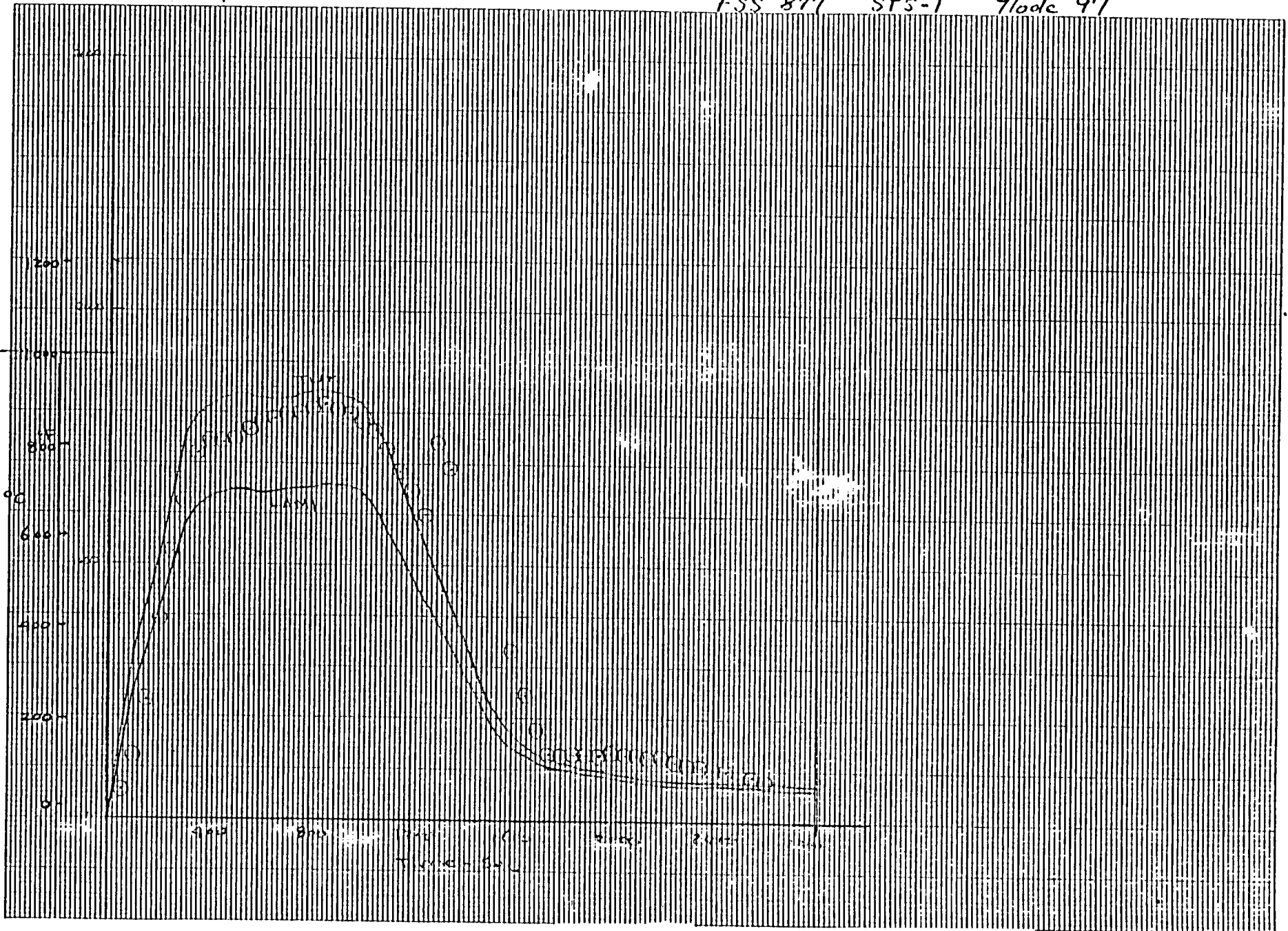


Figure 62 - Flight Temperatures Compared to Predictions - Fuselage

V09T9201

FSS 877

STS-1

Node 193

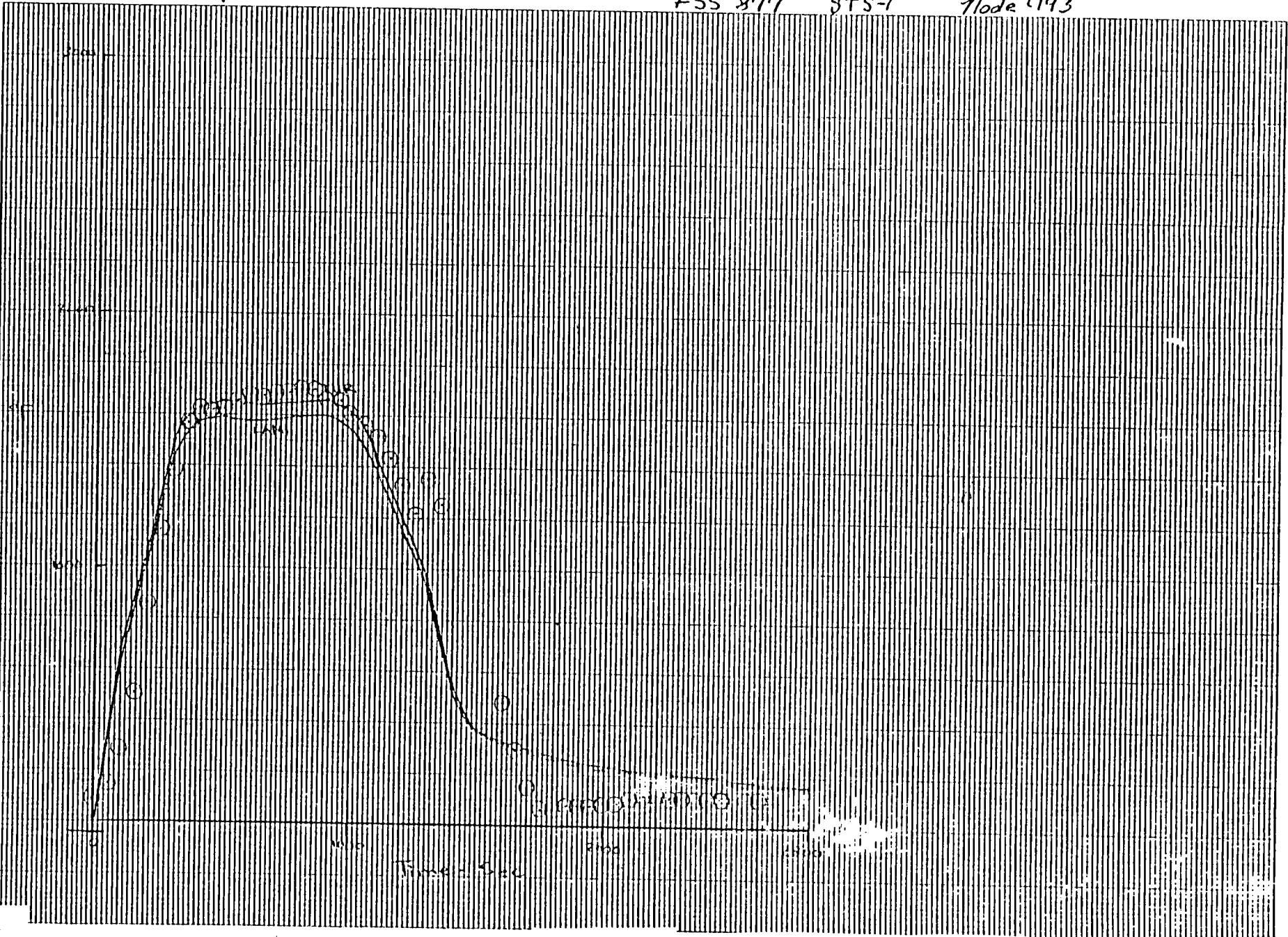


Figure 63 - Flight Temperatures Compared to Predictions - Fuselage

V09T9163

F55 R77

STG-1

Flights 263

118

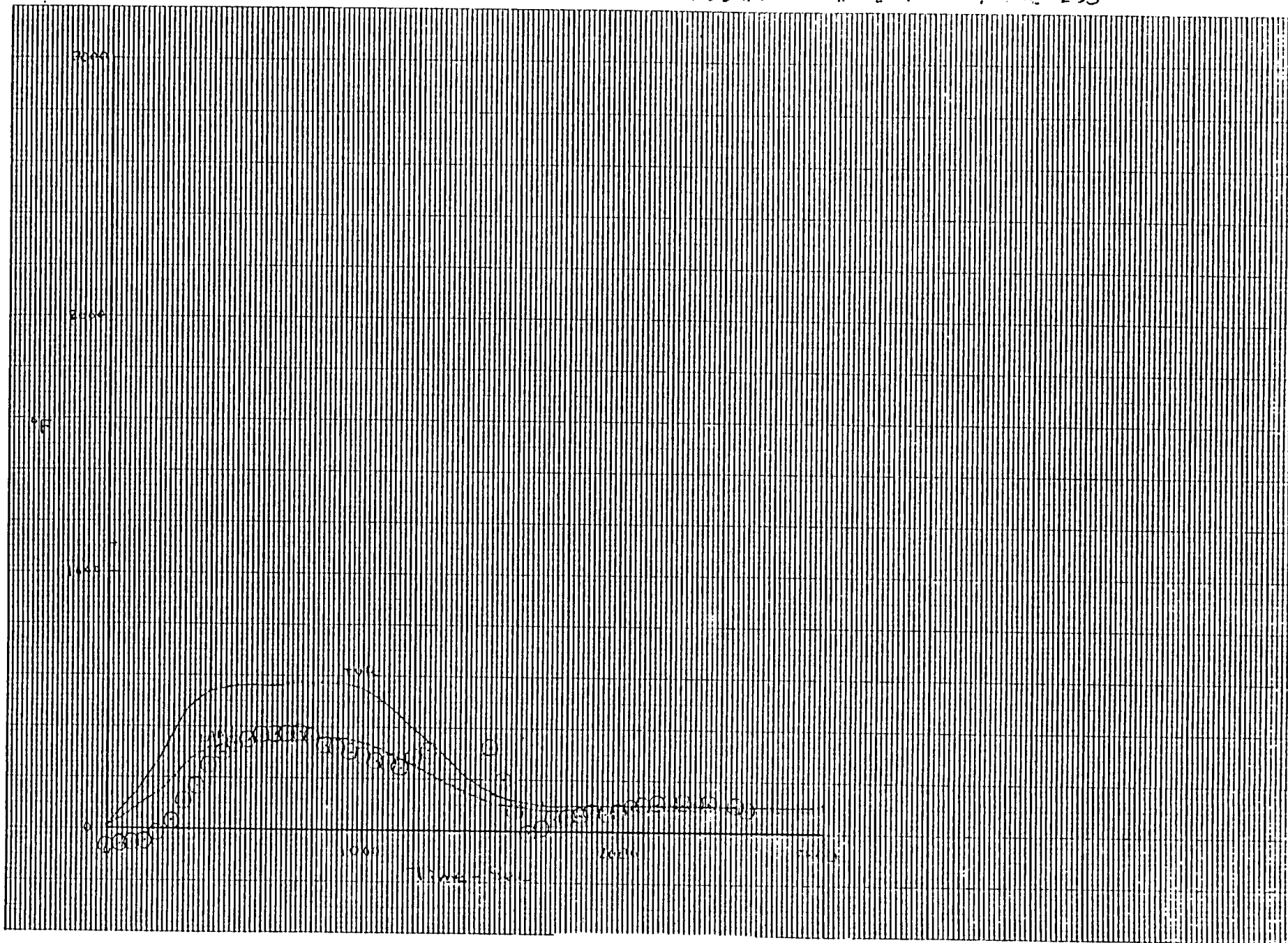


Figure 64 - Flight Temperatures Compared to Predictions - Fuselage

FS 877 JLOC 493 (V09T9518)
(V09T9515)

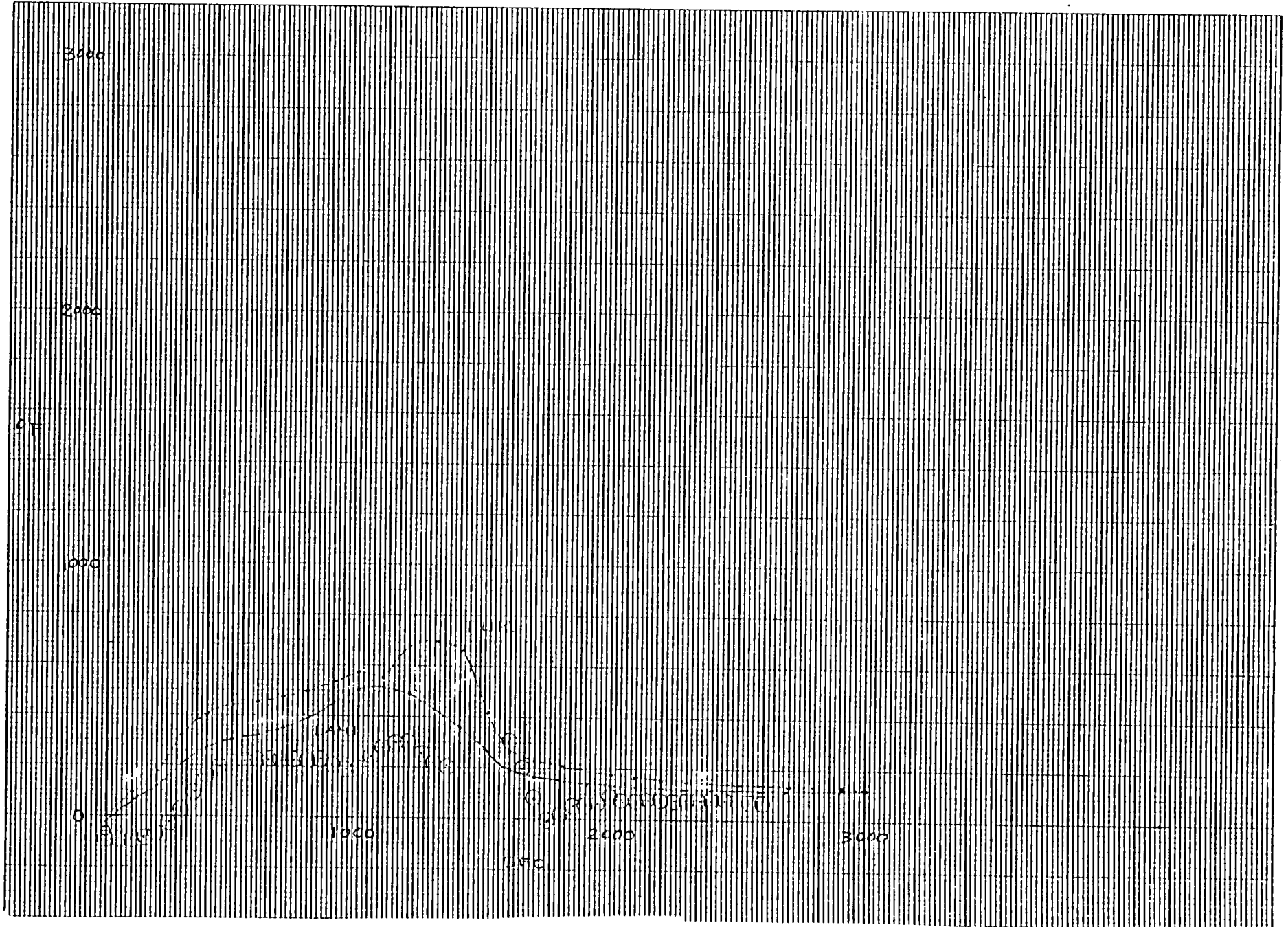


Figure 65 - Flight Temperatures Compared to Predictions - Fuselage

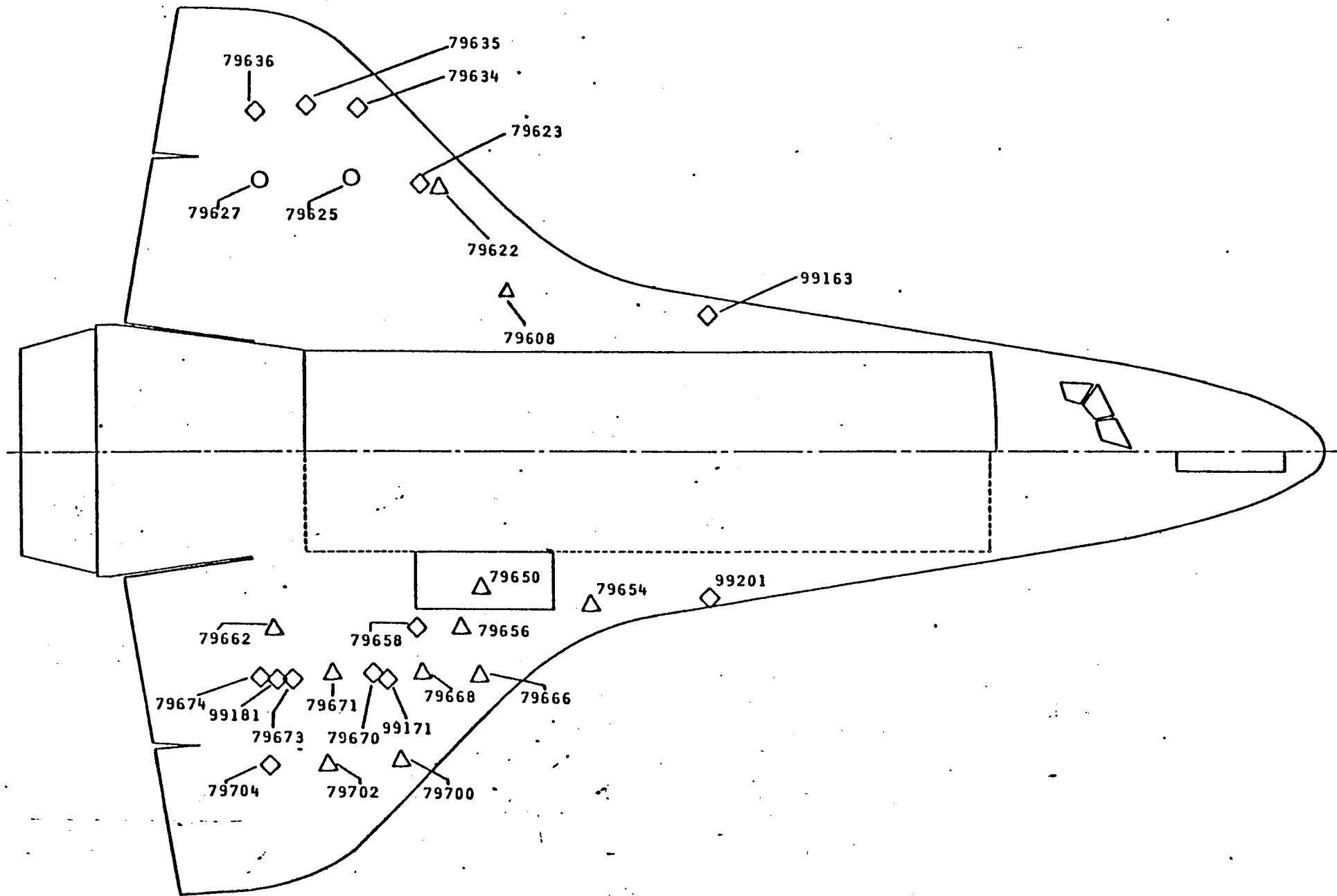


Figure 66 Locations of wing surface measurements

WS 134 TPS TC V09T9650 BAY 1 LWF JLOC 863 998

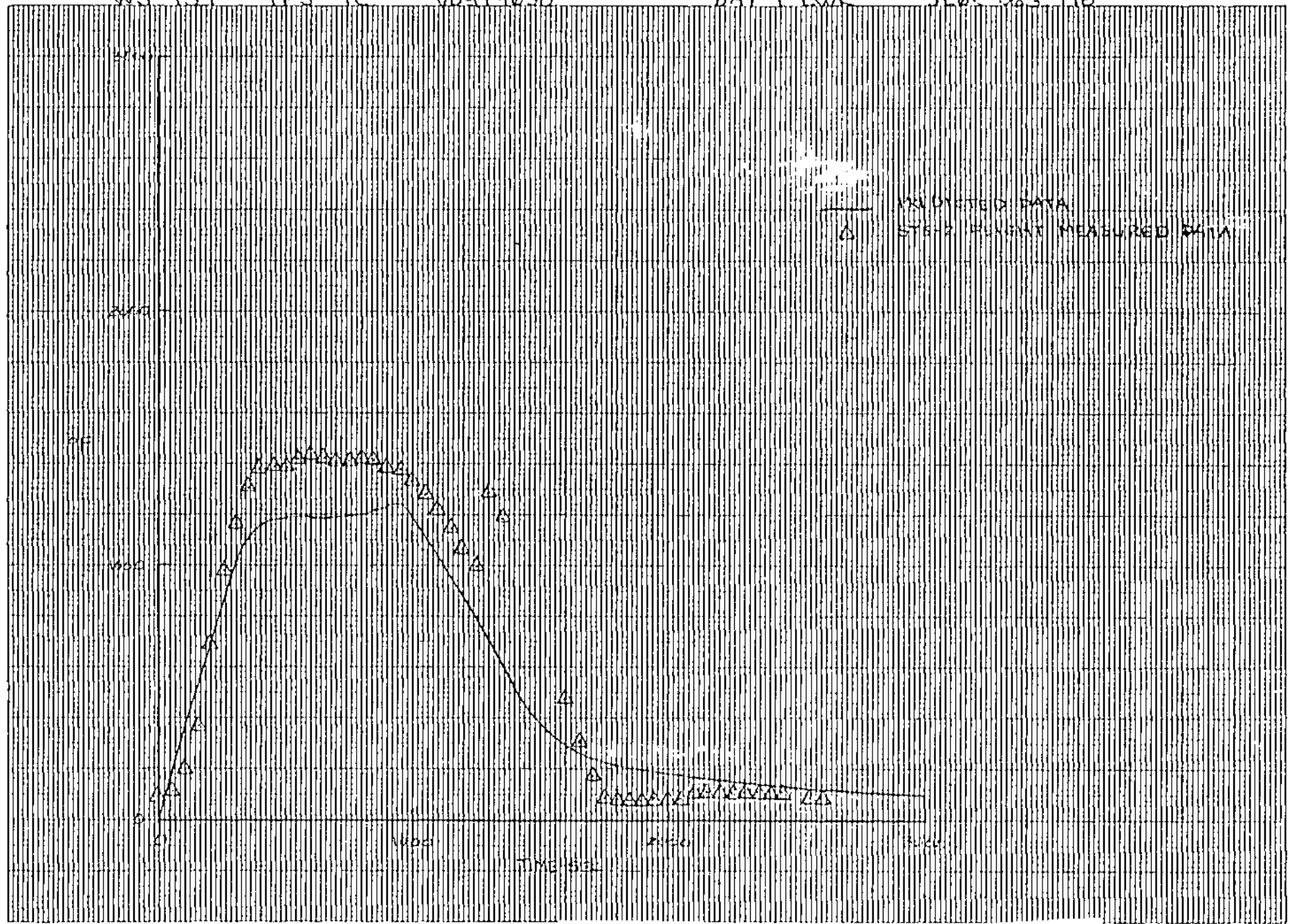


Figure 67 - Flight Temperatures Compared to Predictions - Wing Lower Surface

122

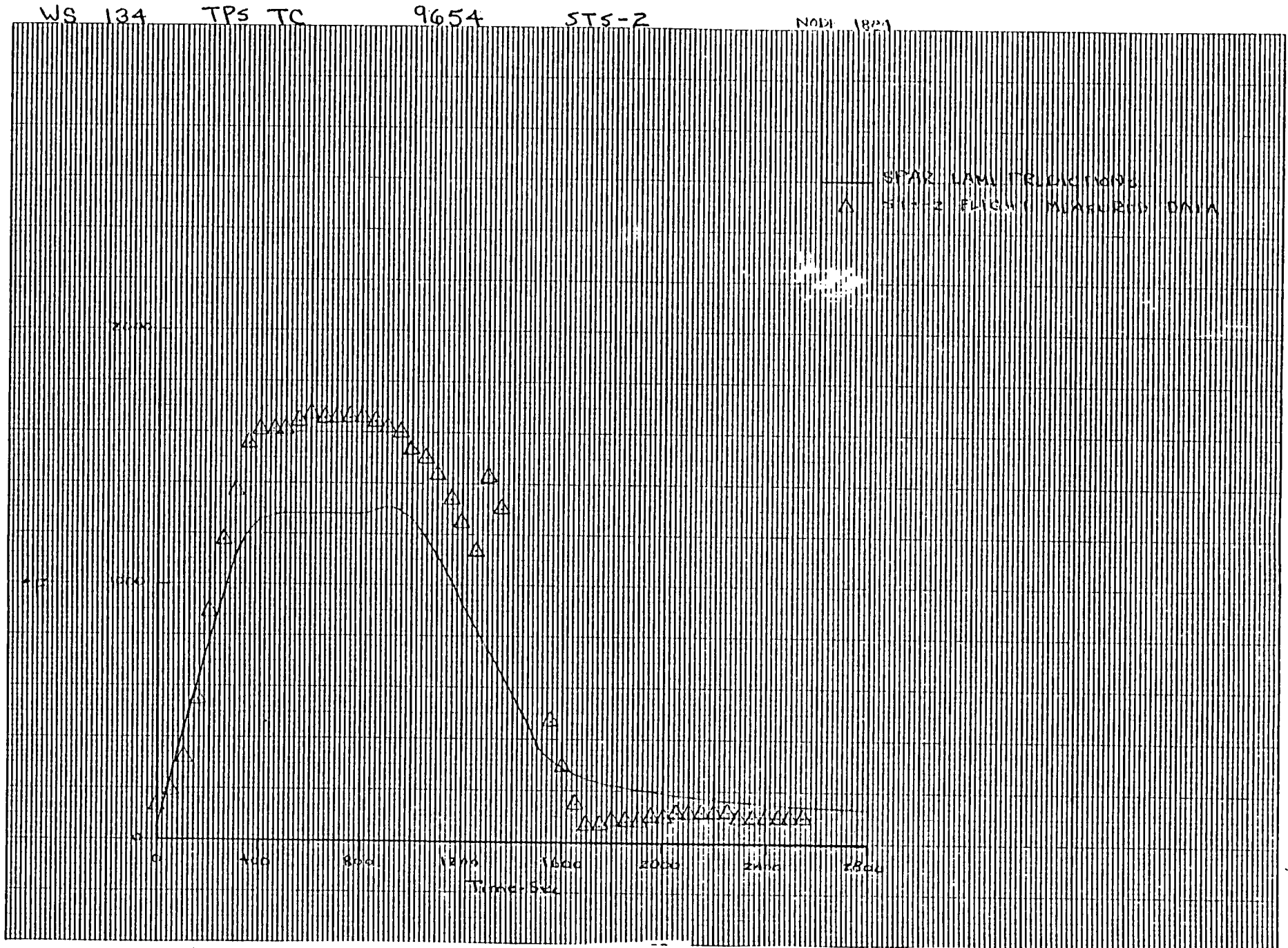


Figure 68 - Flight Temperatures Compared to Predictions - Wing Lower Surface

WS 134 TPS TC 9656 STS-2 NODE 1013

— STAR LAMINAR PREDICTIONS
 Δ STS-2 FLIGHT MEASURED DATA

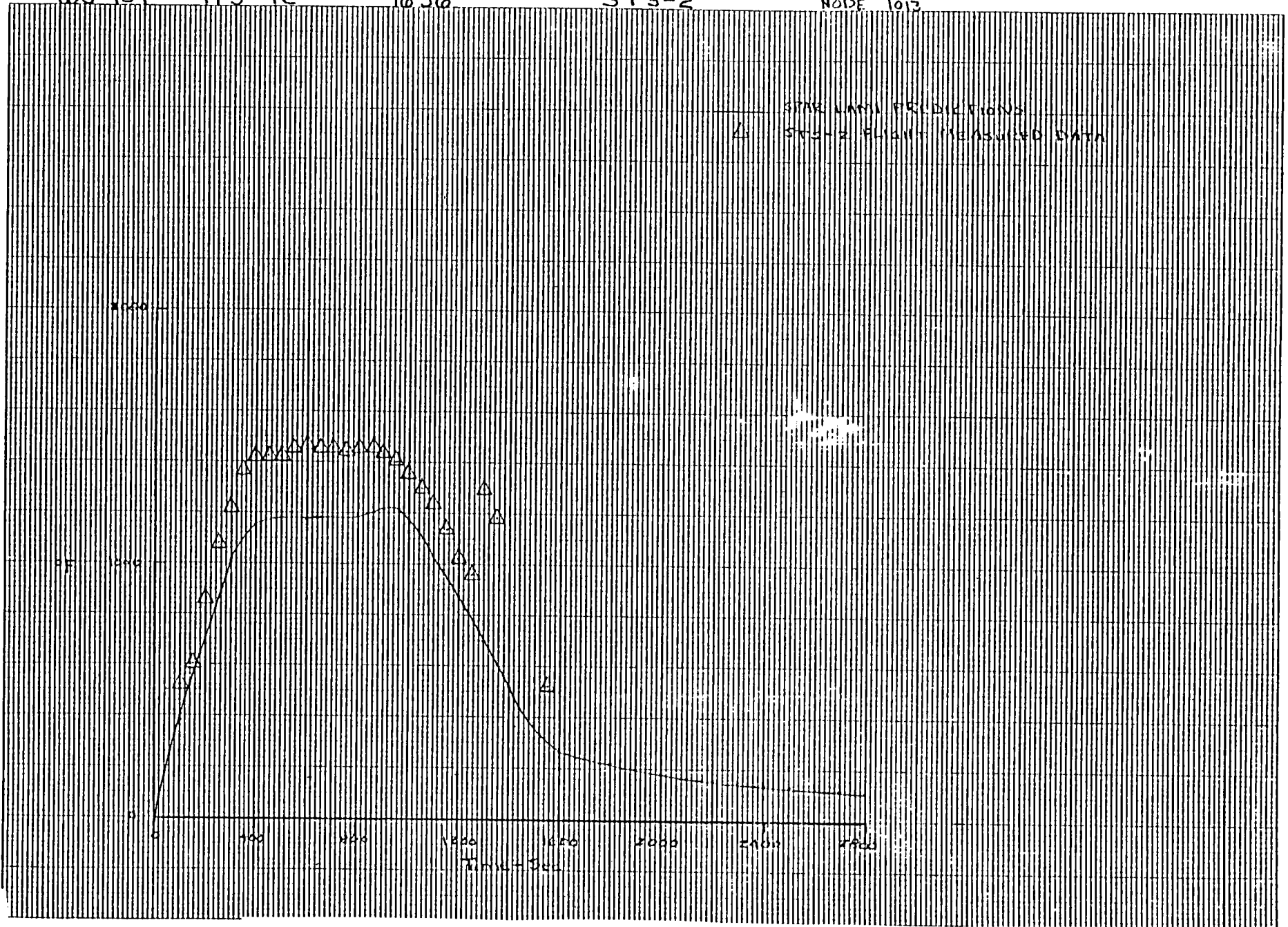


Figure 69 - Flight Temperatures Compared to Predictions - Wing Lower Surface

124

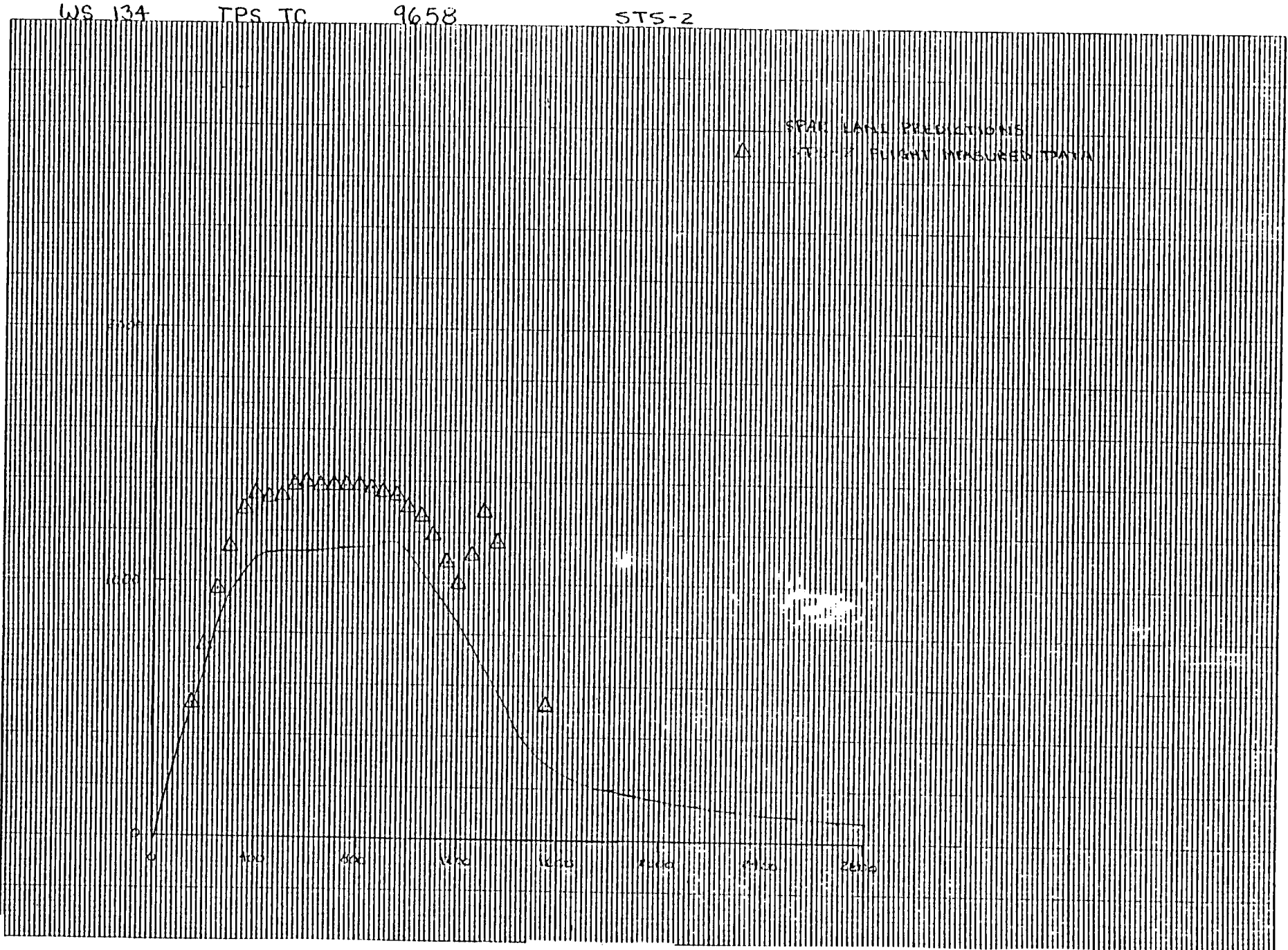


Figure 70 -. Flight Temperatures Compared to Predictions - Wing Lower Surface

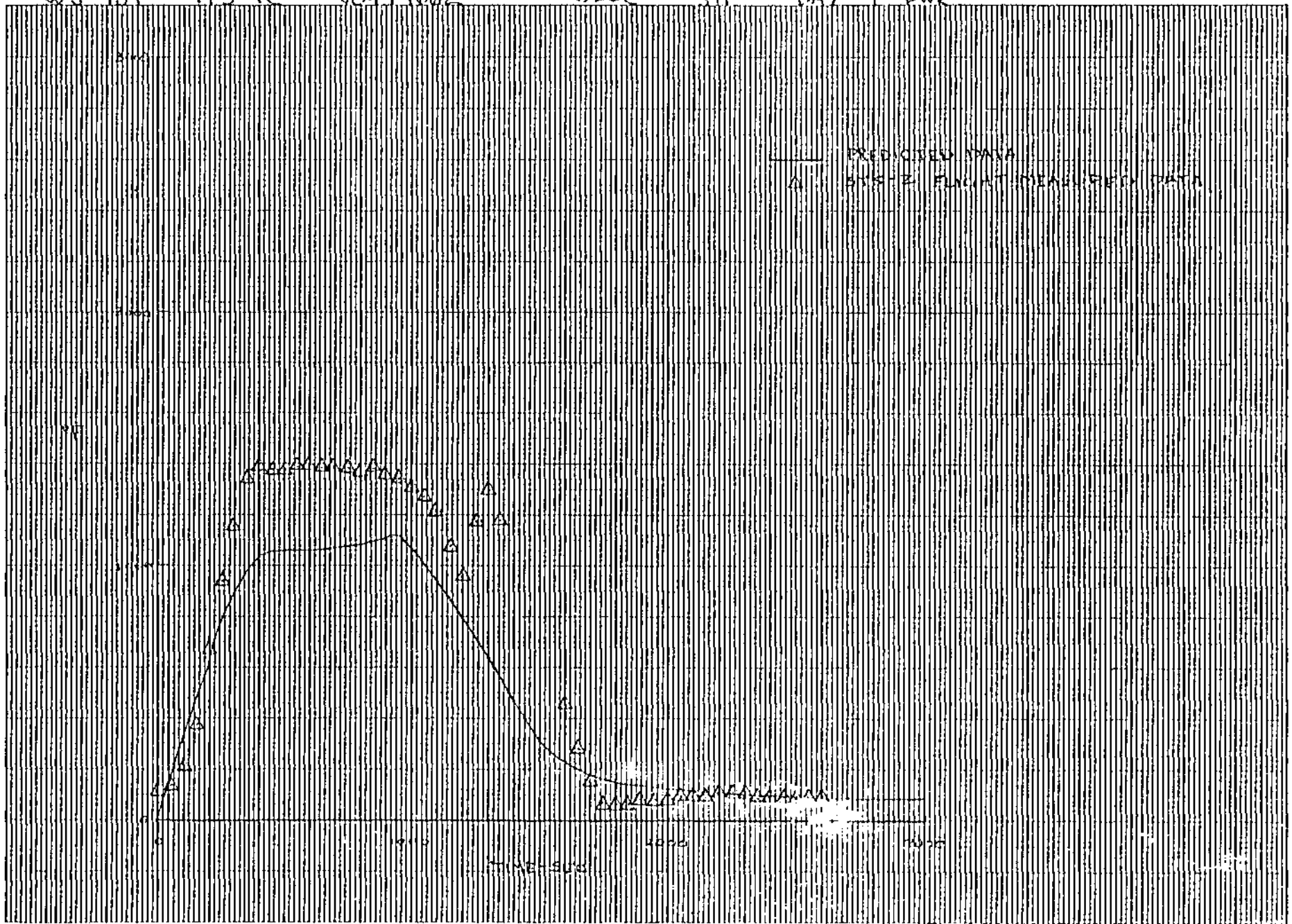


Figure 71 - Flight Temperatures Compared to Predictions - Wing Lower Surface

WS 134 TPS TC 9201 STS-2 UPR GLOVE

126

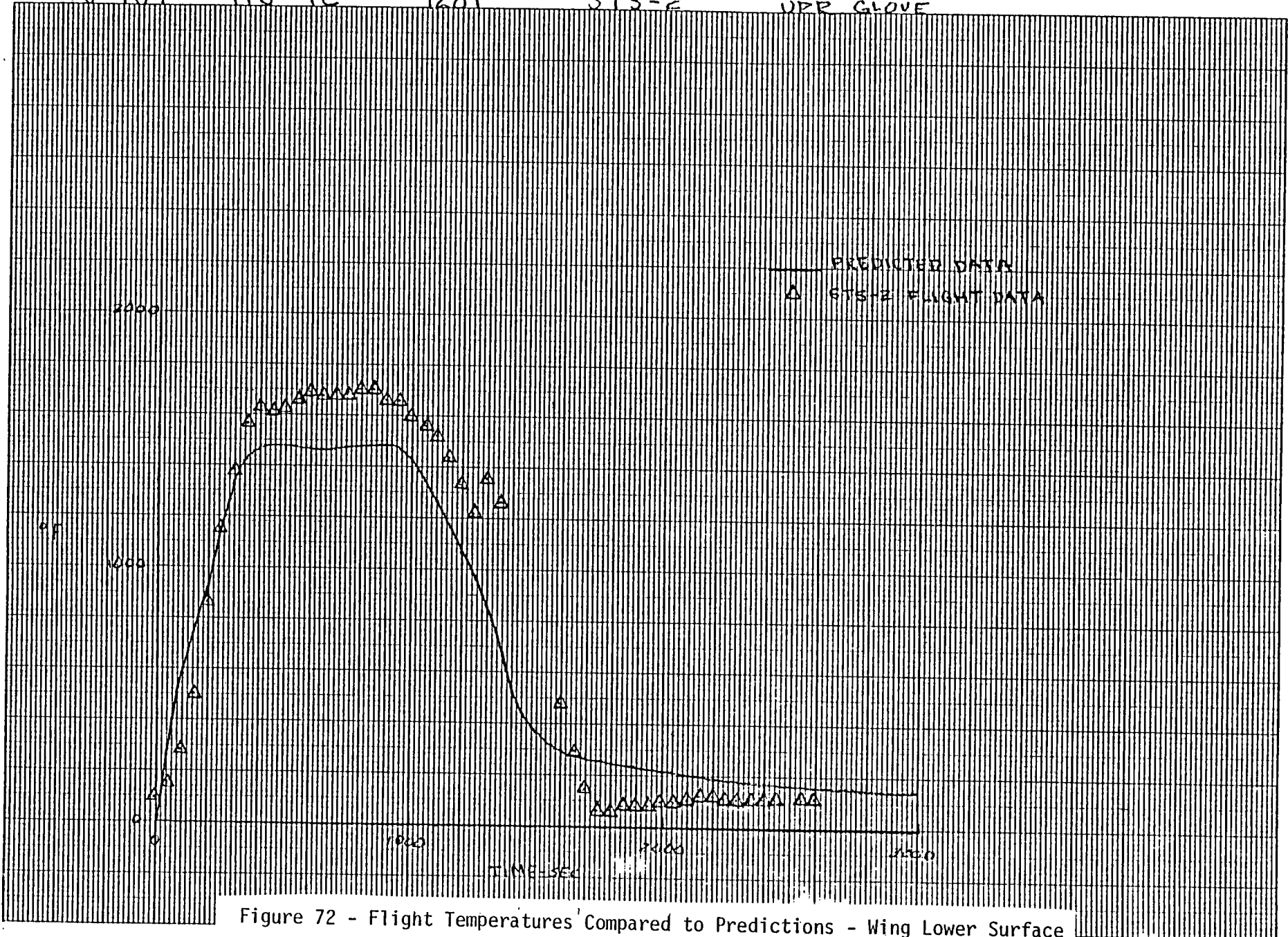


Figure 72 - Flight Temperatures Compared to Predictions - Wing Lower Surface

WS 134 TPS TC V07T⁹608 STS-2 NODE 1132

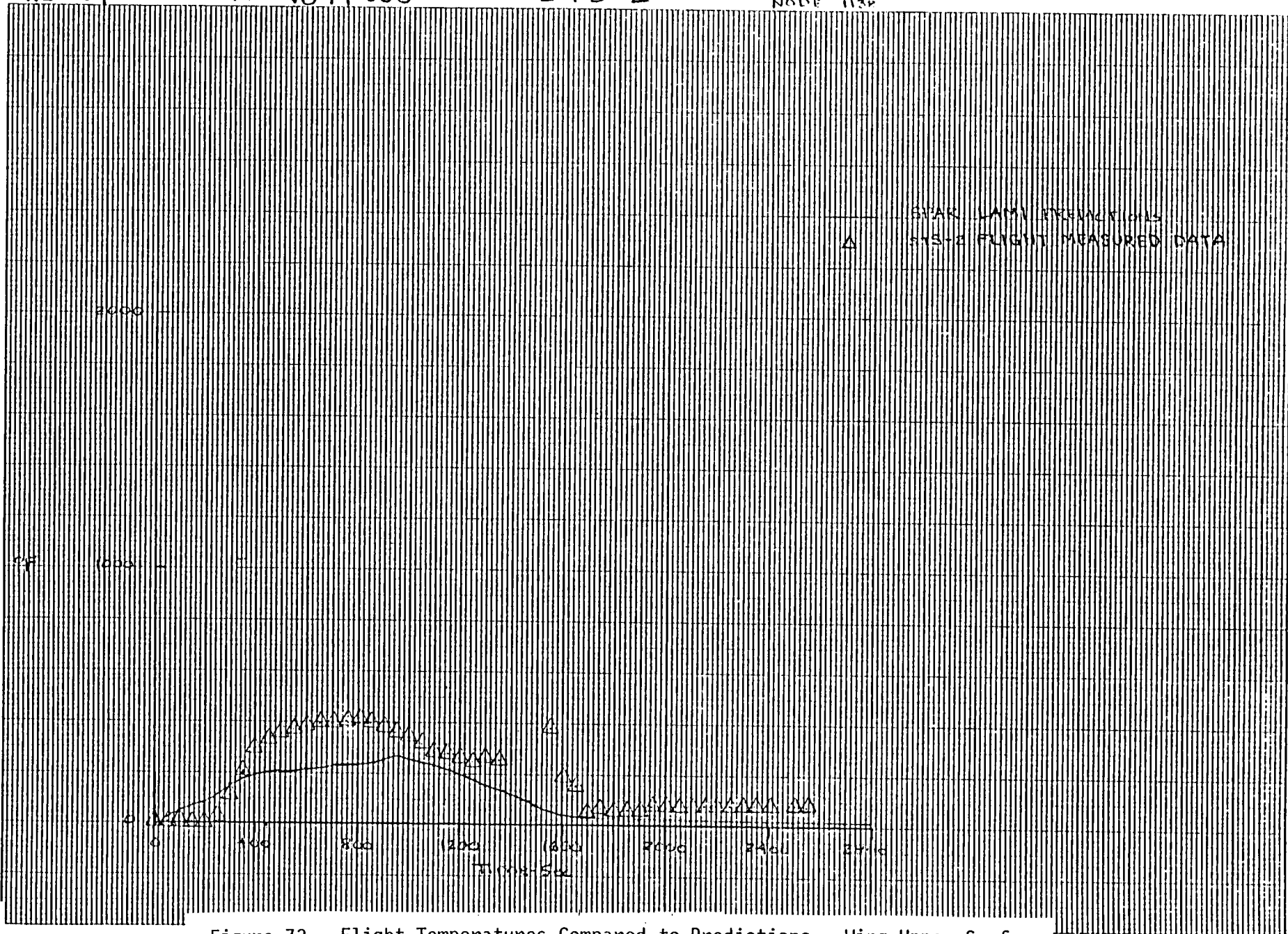


Figure 73 - Flight Temperatures Compared to Predictions - Wing Upper Surface

WS 134 TPS TC V09T9163 UPPER SURFACE J120 1412 1494

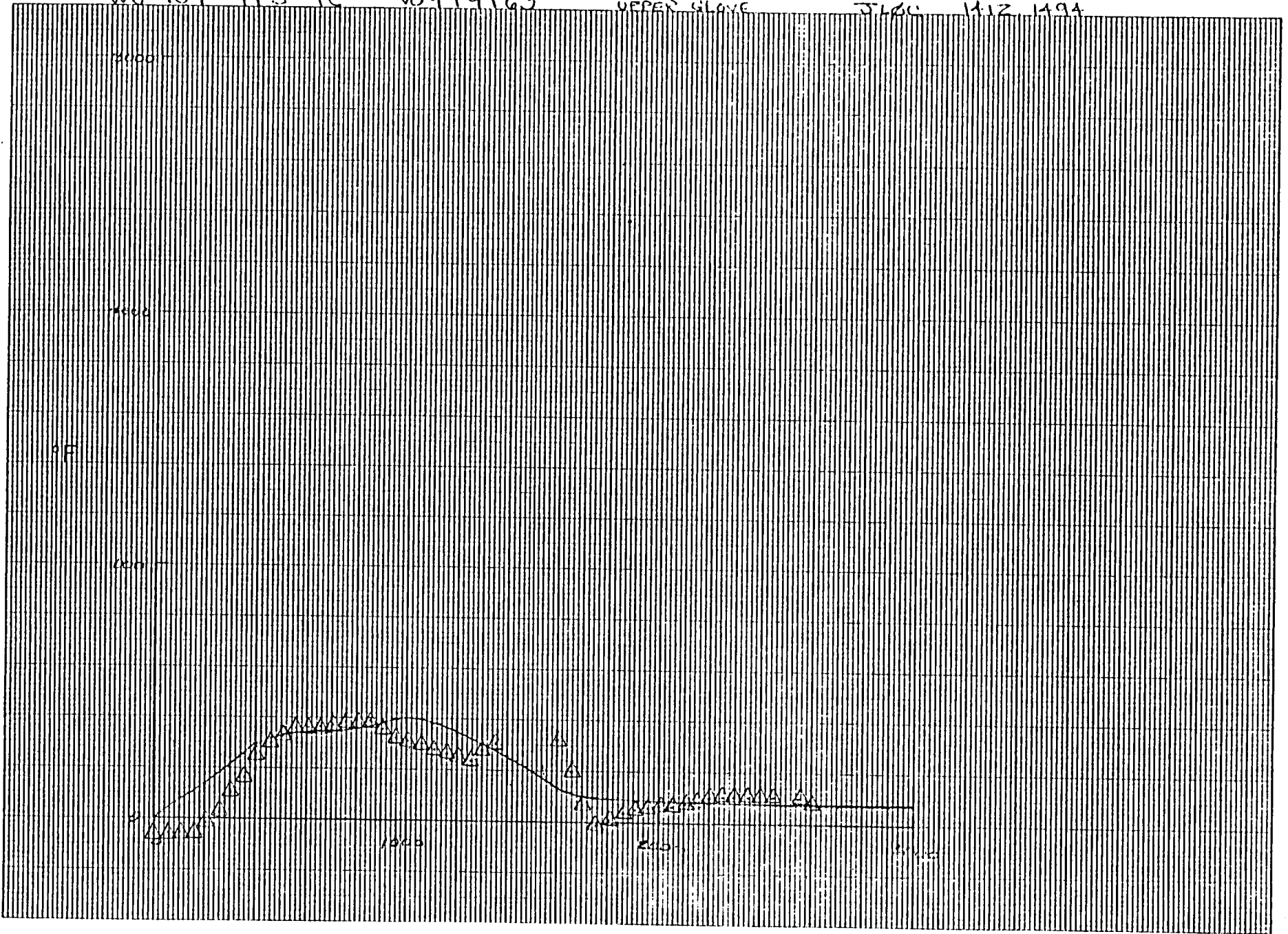


Figure 74 - Flight Temperatures Compared to Predictions - Wing Upper Surface

WS 240 715-1

JL4C 13 V07T 9666

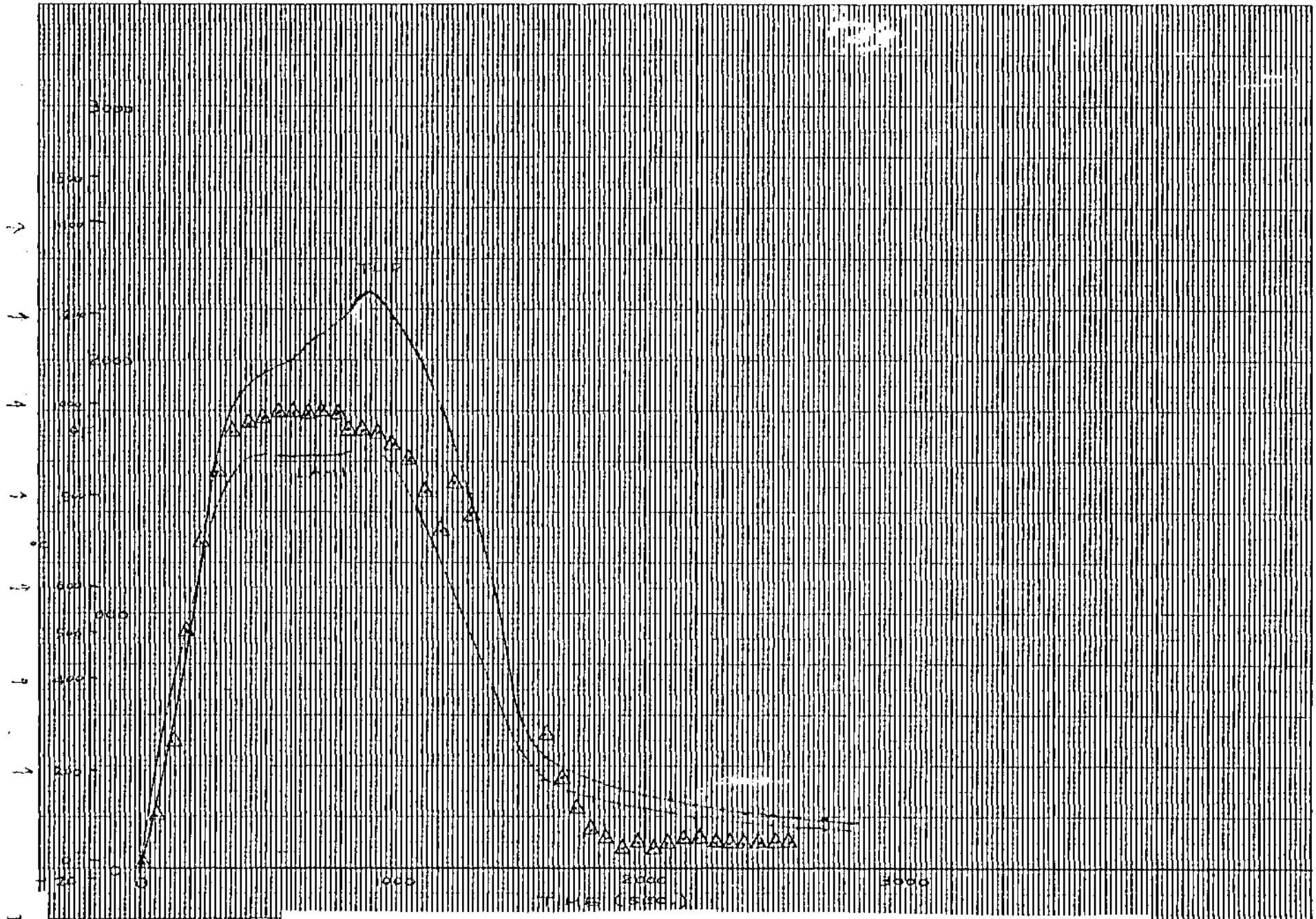


Figure 75 - Flight Temperatures Compared to Predictions - Wing Lower Surface

130

WS 240 JLOC 61 VOTT9668 BAY 1 LWR

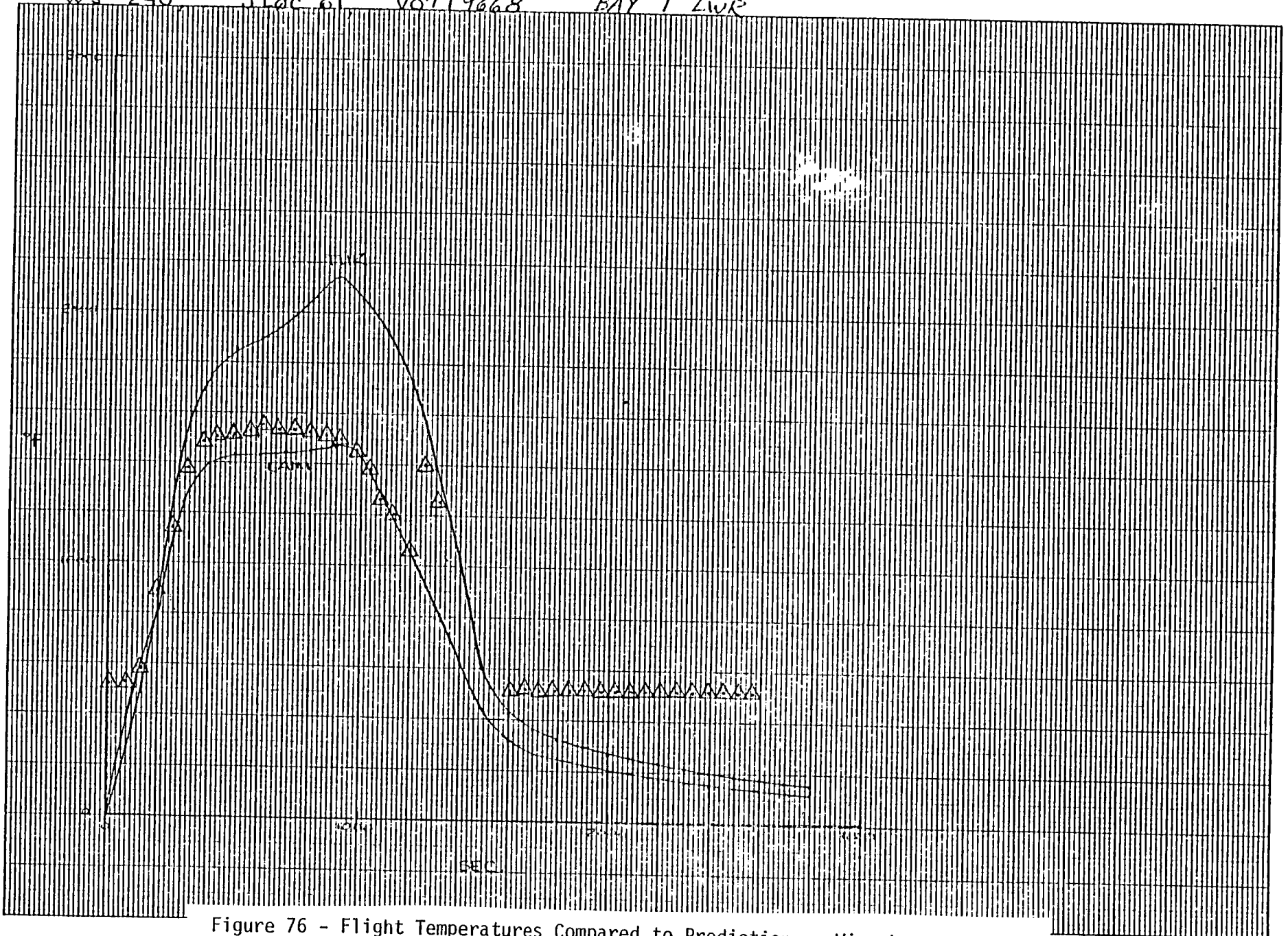


Figure 76 - Flight Temperatures Compared to Predictions - Wing Lower Surface

WS 240 STS-1

JL4C 109

V09T 9171

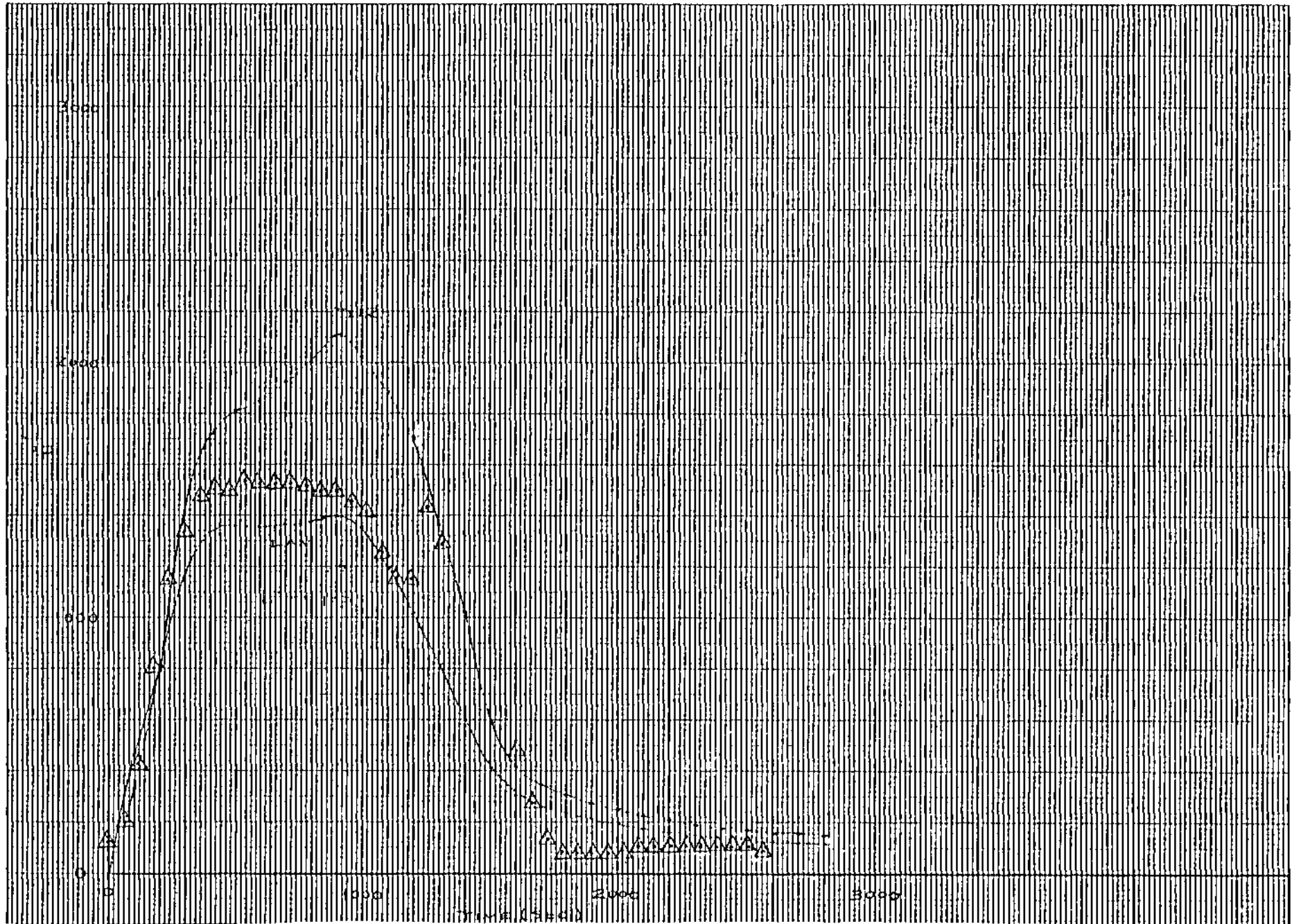


Figure 77 - Flight Temperatures Compared to Predictions - Wing Lower Surface

132

WS 240 JLOC 121 133 Y07T9670 BAY 2 LWR

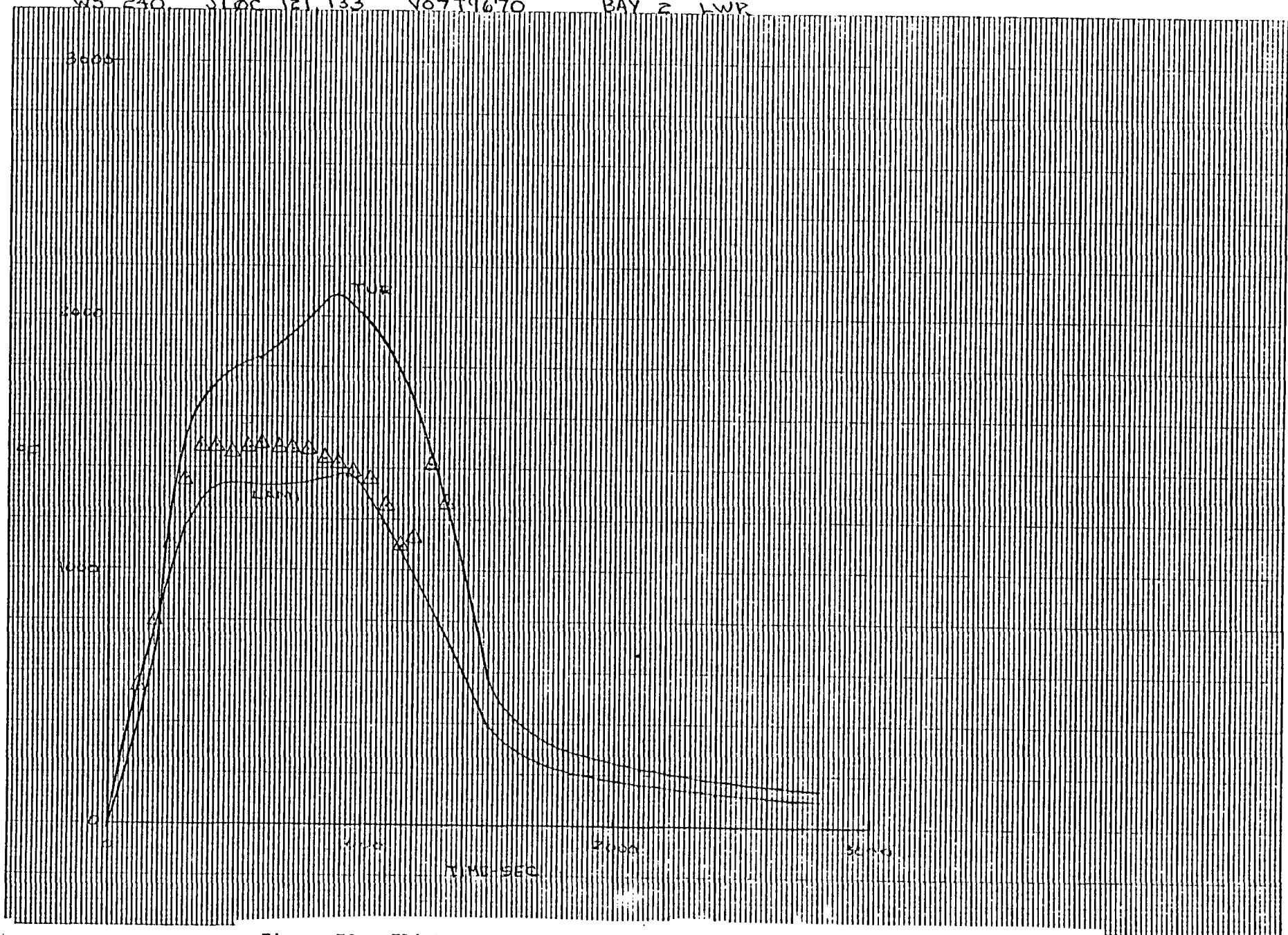


Figure 78 - Flight Temperatures Compared to Predictions - Wing Lower Surface

WS 240 JLOC 229 211 40719673 MAY 1 LWS



Figure 79 - Flight Temperatures Compared to Predictions - Wing Lower Surface

134

WS 240 JLOC 181 V07T9671

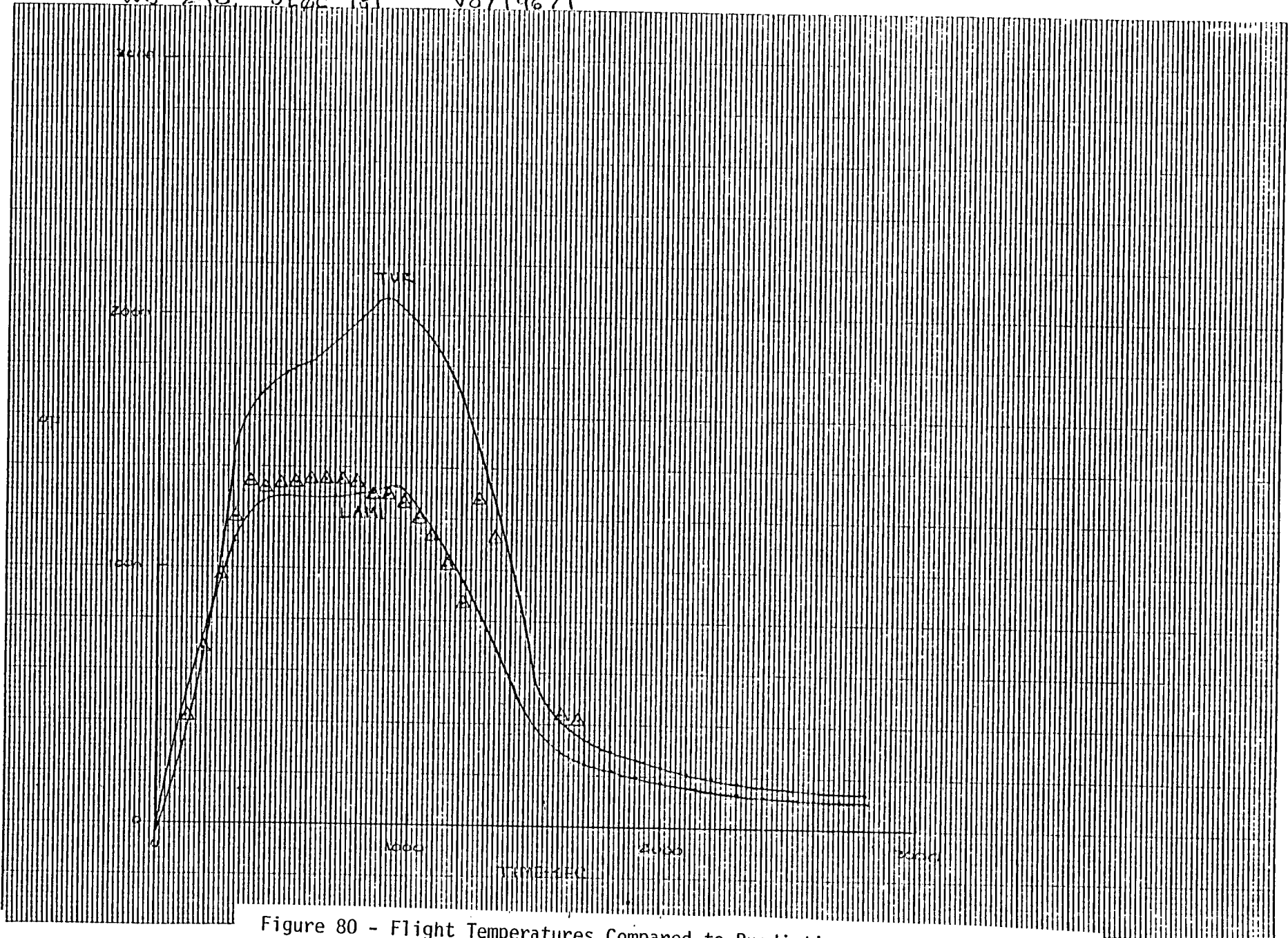


Figure 80 - Flight Temperatures Compared to Predictions - Wing Lower Surface

134

BAY 1 LWR

WS 240

STS-1 FSTS-2

JLDC 253

V09T9181

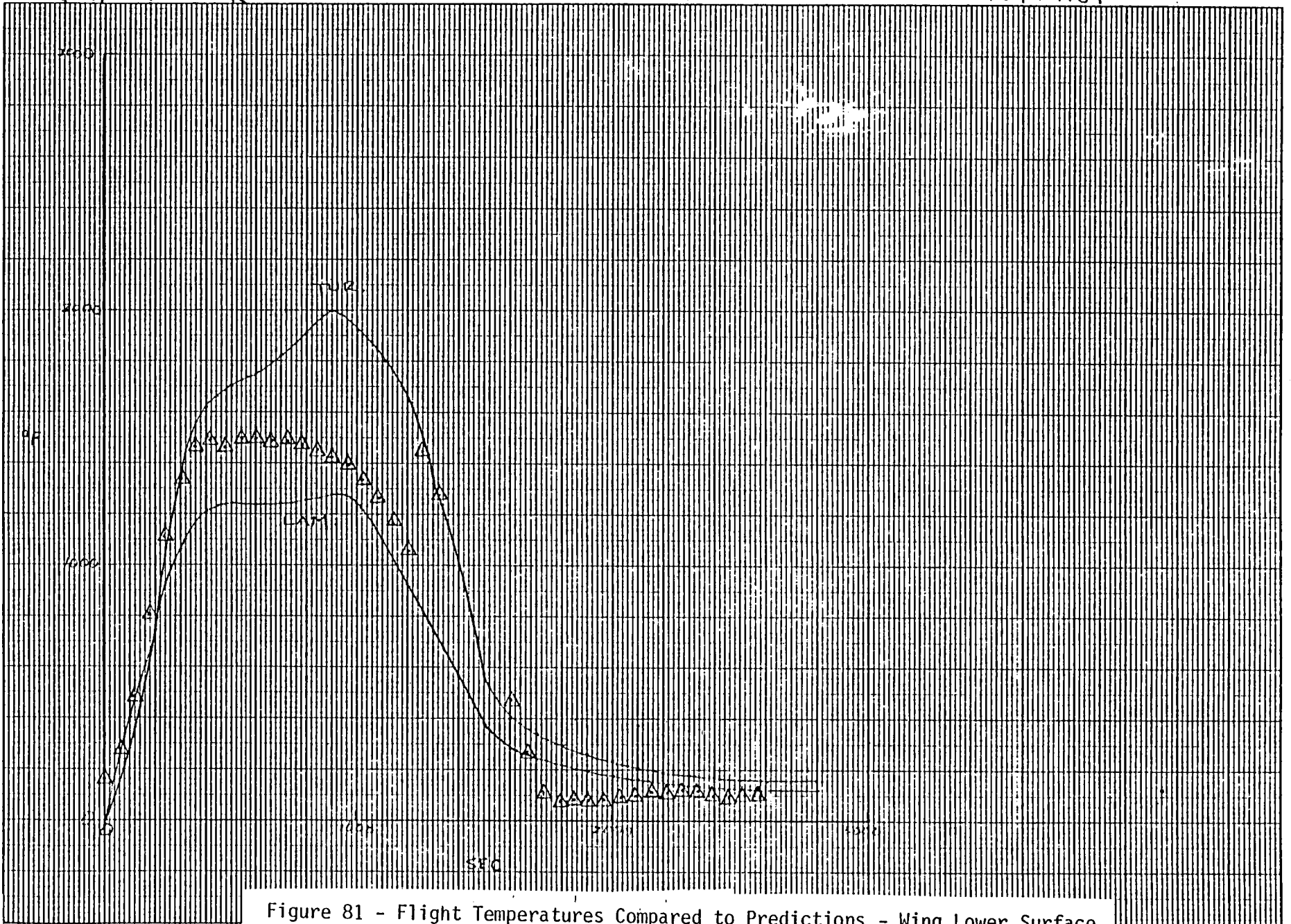


Figure 81 - Flight Temperatures Compared to Predictions - Wing Lower Surface

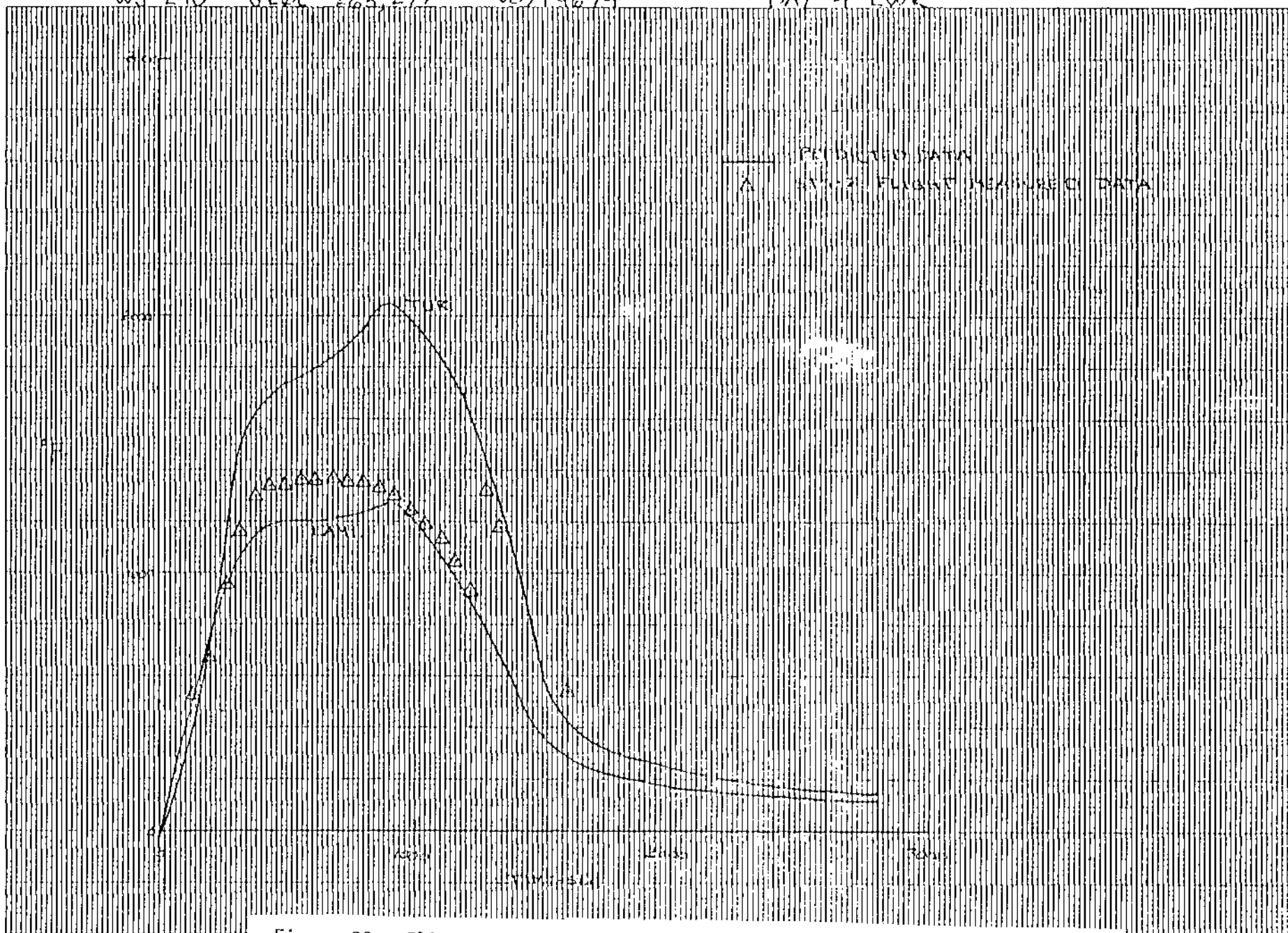


Figure 82 - Flight Temperatures Compared to Predictions - Wing Lower Surface

WS 240 JL0C 805 V09T9622 BAY 1 UPPER

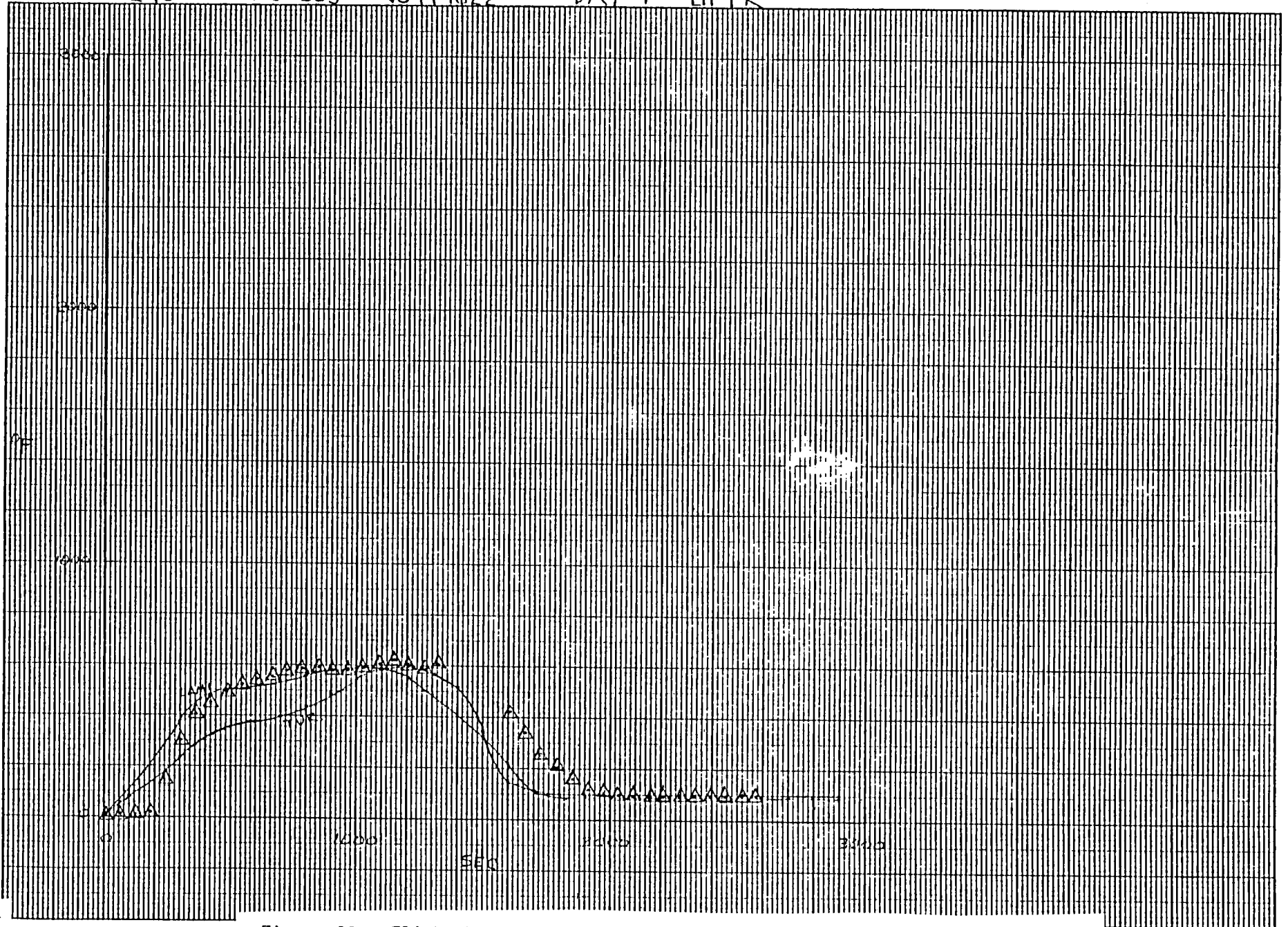


Figure 83 - Flight Temperatures Compared to Predictions - Wing Upper Surface

WS 240 JLOC 795 V09T9623 BAY 1 LIFT TPS SURFACE TEMPS

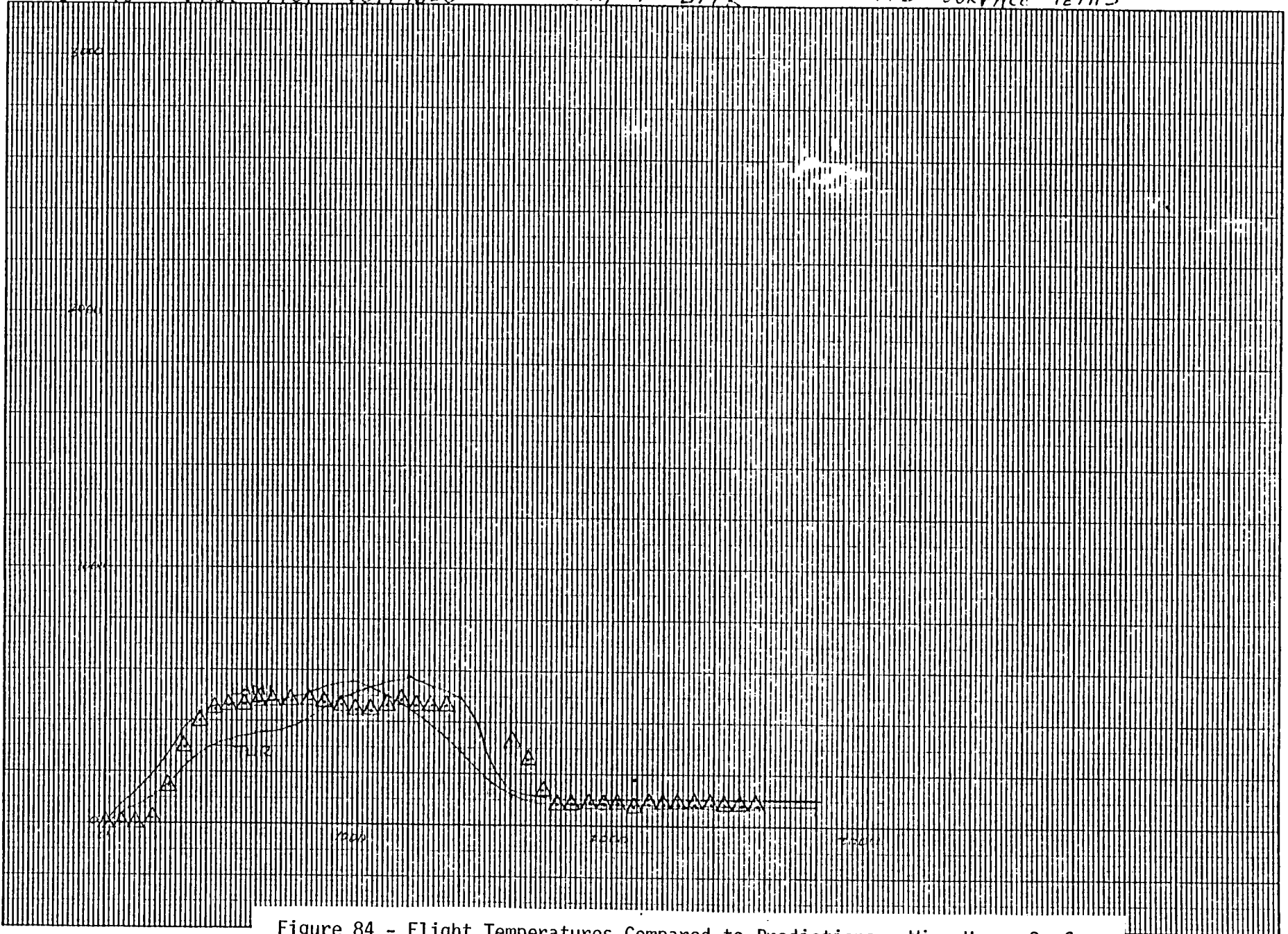


Figure 84 - Flight Temperatures Compared to Predictions - Wing Upper Surface

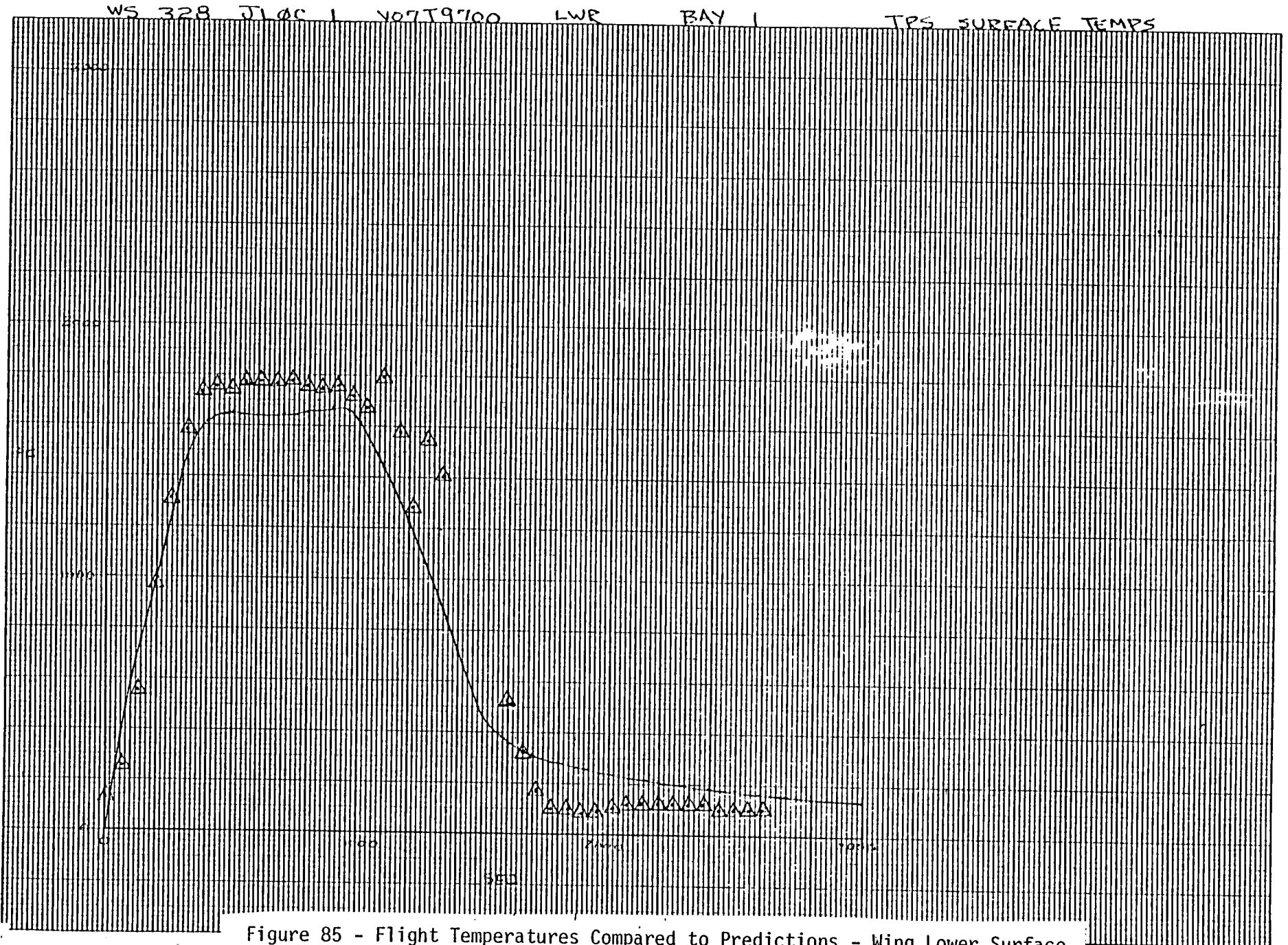


Figure 85 - Flight Temperatures Compared to Predictions - Wing Lower Surface

140

WS 328 JL0C 136 V07T9702 LWR BAY 2 TPS SURFACE TEMPS

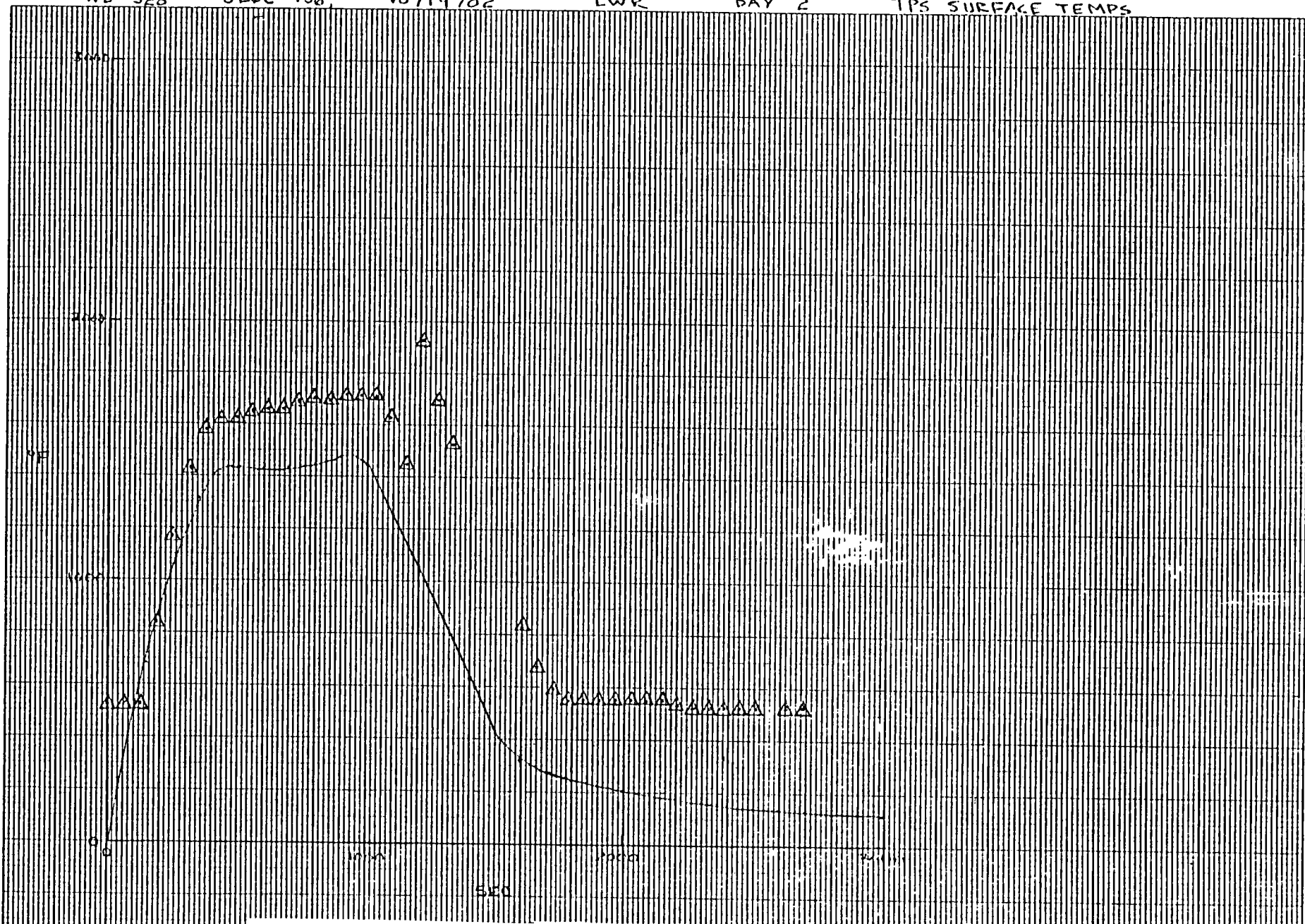


Figure 86 - Flight Temperatures Compared to Predictions - Wing Lower Surface

WS 328 JL0C 241 V04T9704 LWR BAY 3. TPS SURFACE TEMPS

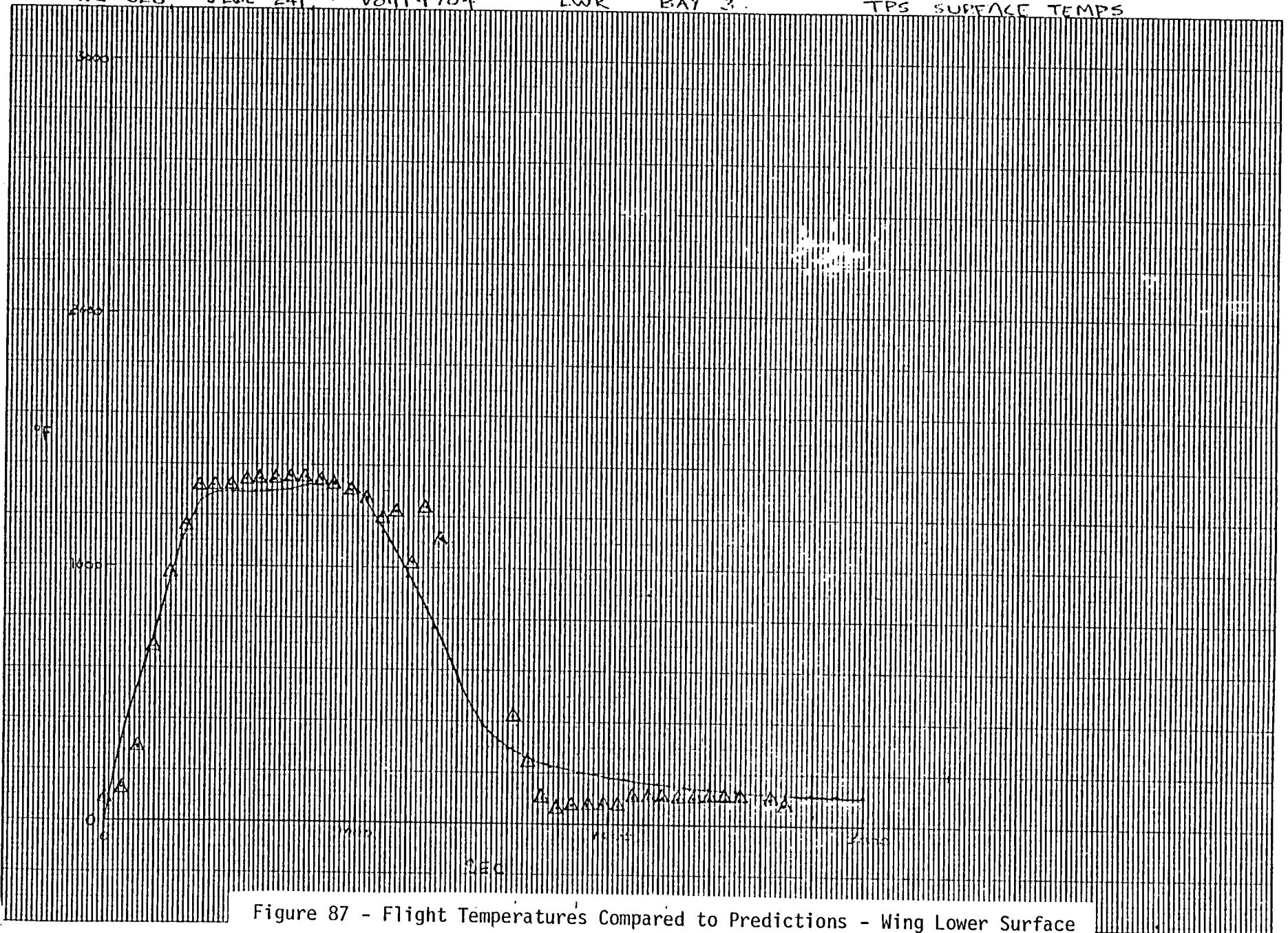


Figure 87 - Flight Temperatures Compared to Predictions - Wing Lower Surface

142

WS 328 JLOC 814 V07T9634 WPPR BAY 1 TPS SURFACE TEMPS

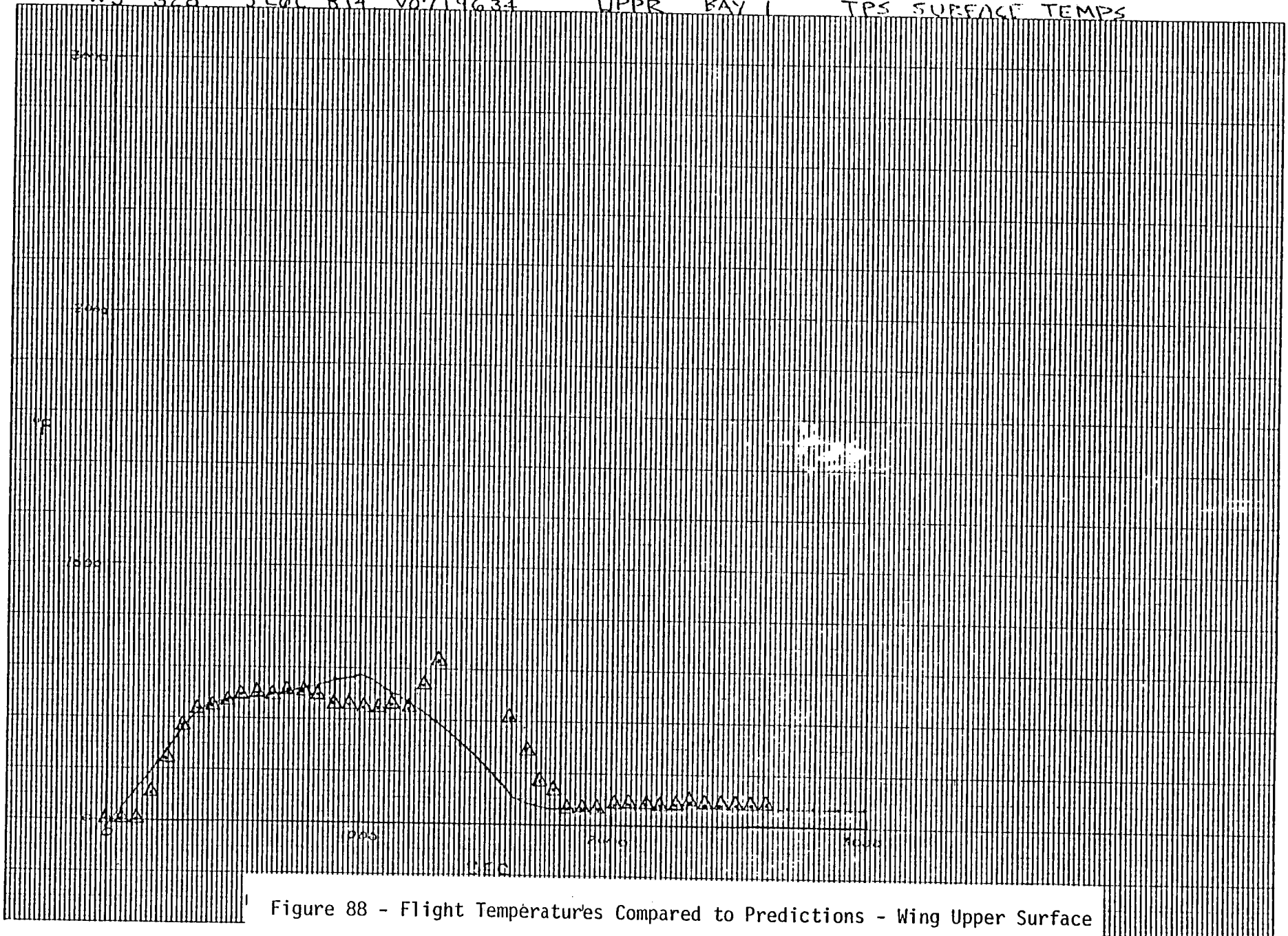


Figure 88 - Flight Temperatures Compared to Predictions - Wing Upper Surface

41

WS 328 J10C 772 V07T9635 UPPR BAY 2

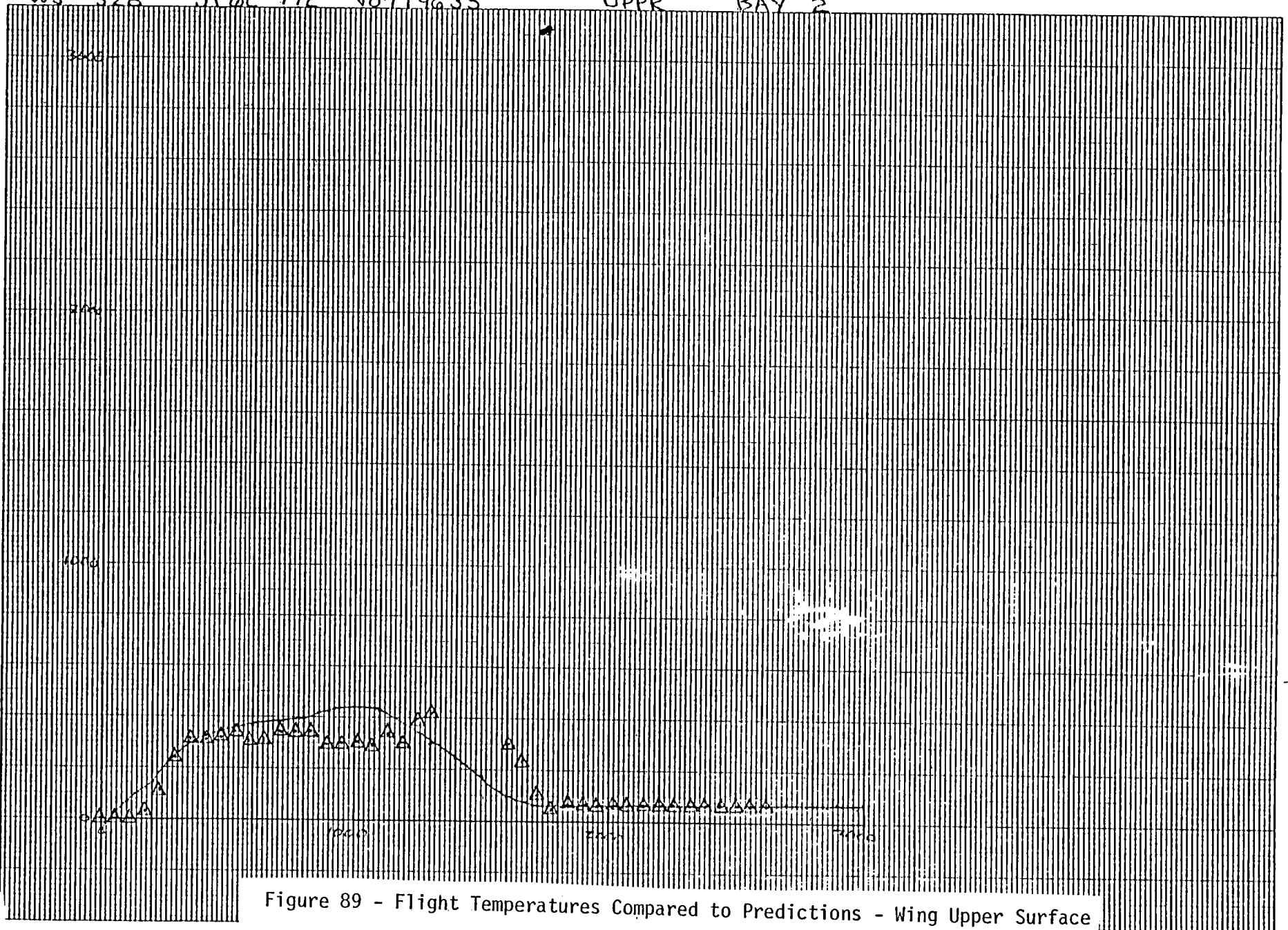


Figure 89 - Flight Temperatures Compared to Predictions - Wing Upper Surface

144

WS 328, JLOC 737, VOTT9636 UPPER BAY 3 TPS SURFACE TEMPS

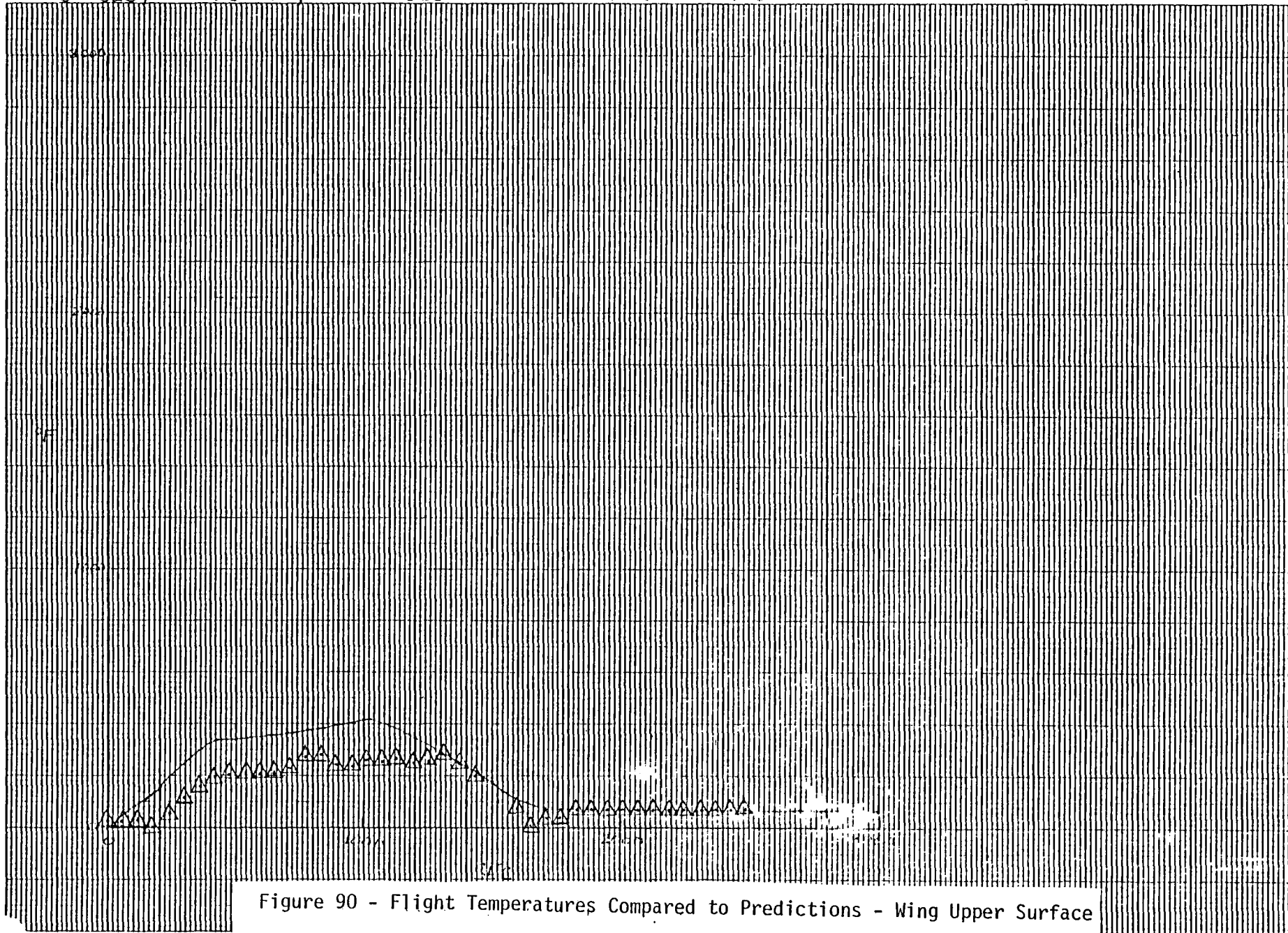



Figure 90 - Flight Temperatures Compared to Predictions - Wing Upper Surface

6

STAGNATION POINT TEMPERATURES
Wing Leading Edge 55 percent Sp. 11
one-dimensional analysis

1.  Leading edge thickness ≈ 0.25 in.

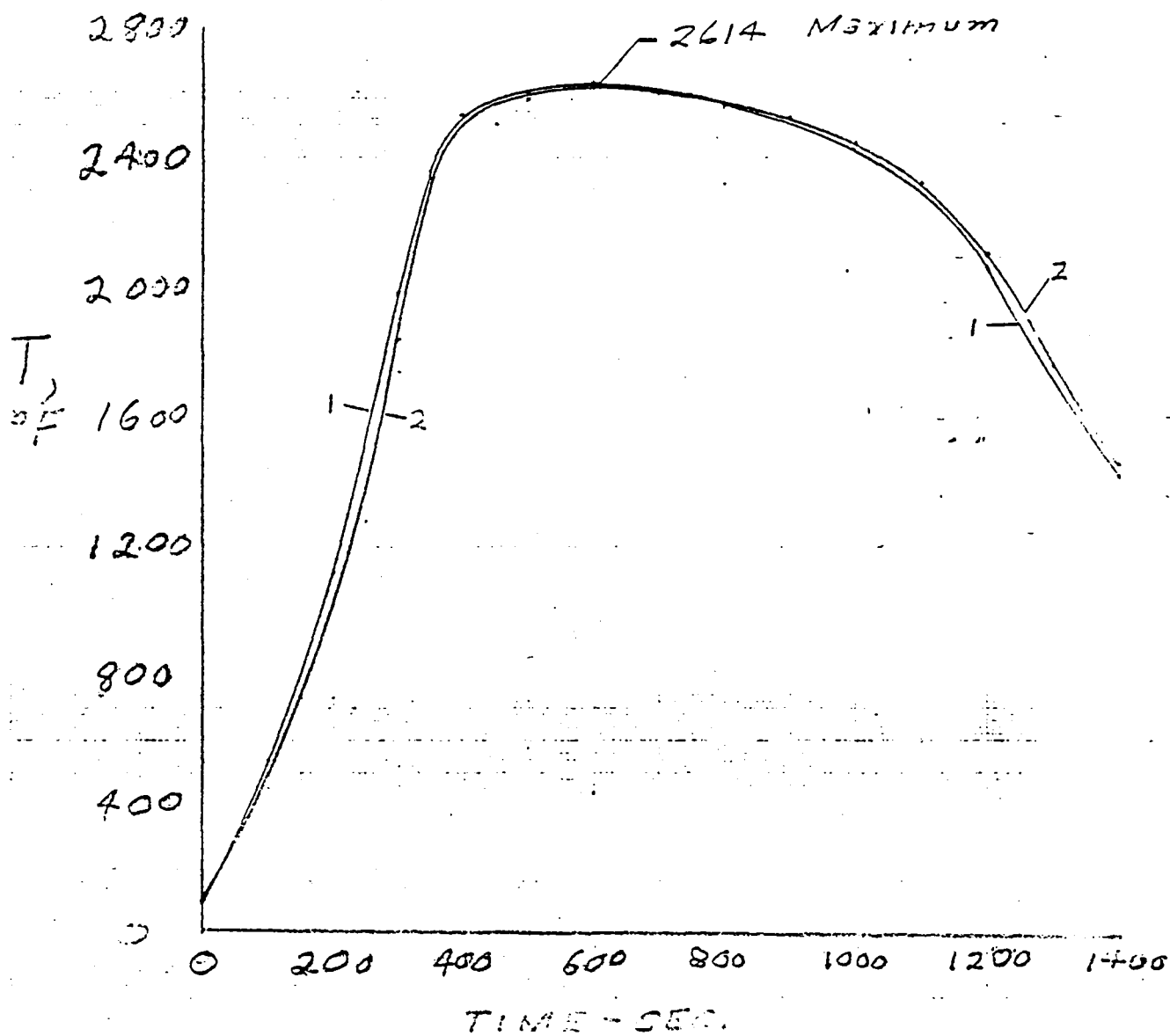


Figure 91

Concluding Remarks & Recommendations

A great deal has been learned about the stability and control derivatives from STS-1 and STS-2. The value of the ACIP package was shown on STS-1 for many of the maneuvers. The expected benefit of the PTI's is apparent in the superior stability and control maneuvers on STS-2. Questions still remain throughout the flight envelope, however most of these questions will be answered by continued emphasis on PTI maneuvers. The primary area that needs more study is below Mach 3. Even with the PTI's there is a great deal of uncertainty in the estimates in this region. With three controls operating in a high gain feedback system it is difficult to separate the individual effects of each of the controls. The problems of transonic flow, buffet, and wind shears will always be present, but past experience has shown that a concentrated effort in getting a large number of high quality maneuvers in a region will pay off with reliable estimates.

It does not seem appropriate to make any changes in the control system for the M=1-2 region until a better definition of the aerodynamic characteristics is obtained. The most reasonable approach that we see would be to turn off the yaw jets around M=2 and obtain PTI maneuvers with only the aileron and rudder active. From the data that we have analyzed, a neutrally damped oscillation would be present from M=2 to M=1 which would present no significant problem.

Dryden strongly recommends that there be a limiting minimum airspeed of ≈ 240 knots added to the autoland system to preclude the possibility of stretching a low energy case to the point of having insufficient airspeed to perform an adequate flare maneuver.

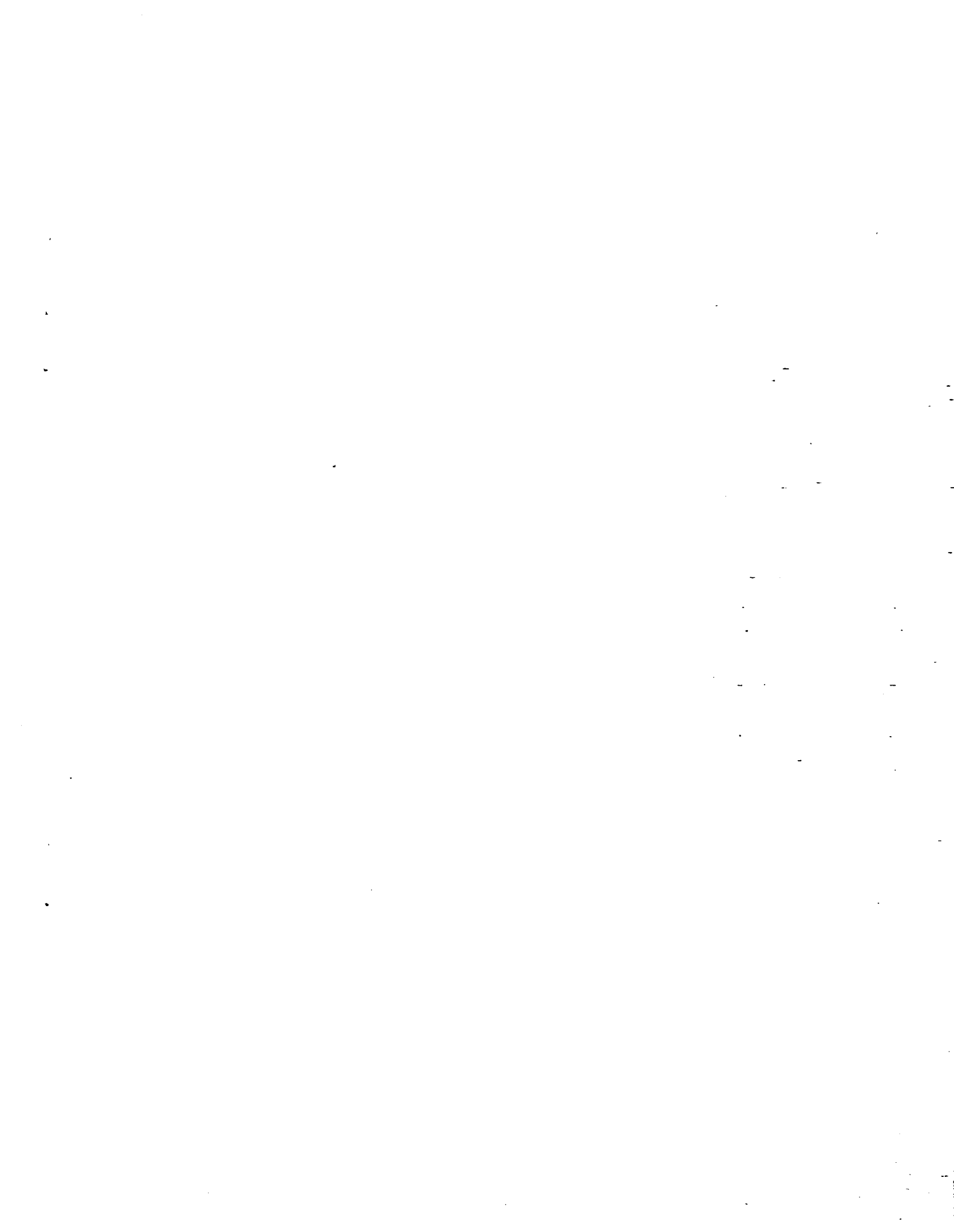
From the STS-2 data it is concluded that:

- a) The wing structural temperature measurements are generally repeatable and consistent with the trajectories.
- b) The Dryden predicted surface temperatures correlate well with the general shape of the measured surface temperature time histories.
- c) The measured wing lower surface temperatures were higher than predicted indicating that the Dryden predicted heating is too low, with progressively greater error as one moves inboard.
- d) The measured wing upper surface temperatures are in reasonable agreement with Dryden predictions.

On the basis of these comparisons, heating and heat transfer models will be adjusted (tuned) to improve the temperature prediction capability for future trajectories.

REFERENCES

1. Iliff, Kenneth W.; and Taylor, Lawrence W., Jr.: Determination of Stability Derivatives from Flight. Data Using a Newton-Raphson Minimization Technique. NASA TND-6579, 1972.
2. Maine, Richard E. and Iliff, Kenneth W.: MMLE-3, a General FORTRAN Program for Maximum Likelihood Parameter Estimation. NASA TP-1563, 1980.
3. Maine, Richard E.; and Iliff, Kenneth W.: Formulation and Implementation of Practical Algorithm for Parameter Estimation with Process and Measurement Noise. AIAA Paper 80-1603. August 1980.
4. Iliff, Kenneth W.; Maine, Richard E.; and Montgomery T.D.: Important Factors in the Maximum Likelihood Analysis of Flight Test Maneuvers. NASA TP-1459, 1979.
5. Iliff, Kenneth W.: Aircraft Identification Experience AGARD: LS-104, 1980.
6. Preliminary Analysis of STS-1 Entry Flight Data. NASA TM-81363, 1981.
7. Iliff, Kenneth W.; Maine, Richard E.; Cooke, Douglas R.: Selected Stability and Control Derivatives from the First Space Shuttle Entry. AIAA Paper 81-2451, November, 1981.



1. Report No. NASA TM-81371		2. Government Accession No.		3. Recipient's Catalog No.	
4. Title and Subtitle PRELIMINARY ANALYSIS OF STS-2 ENTRY FLIGHT DATA				5. Report Date	
				6. Performing Organization Code RTOP 989-10-00	
7. Author(s)				8. Performing Organization Report No.	
9. Performing Organization Name and Address NASA Ames Research Center Dryden Flight Research Facility P.O. Box 273 Edwards, California 93523				10. Work Unit No.	
				11. Contract or Grant No.	
12. Sponsoring Agency Name and Address National Aeronautics and Space Administration Washington, D.C. 20546				13. Type of Report and Period Covered Technical Memorandum	
				14. Sponsoring Agency Code	
15. Supplementary Notes					
16. Abstract <p>Dryden has completed a preliminary analysis of the data obtained during the entry of the STS-2 flight and a great deal has been learned about the stability and control derivatives from STS-1 and STS-2. Questions still remain throughout the flight envelope with the area below Mach 3 needing the most study. With three controls operating in a high gain feedback system, it is difficult to separate the individual effects of each of the controls. A reasonable approach to this problem might be to perform maneuvers in this area with the yaw jets turned off and just the aileron and rudder active.</p> <p>Analysis of the aerothermal data obtained shows that wing structural-temperature measurements are generally repeatable and consistent with the trajectories. The measured wing upper surface temperatures are in reasonable agreement with Dryden predictions but wing lower surface temperatures were higher than Dryden predictions. Heating and heat transfer models will be adjusted to improve the temperature prediction capability for future trajectories.</p>					
17. Key Words (Suggested by Author(s)) Orbiter Stability and control Performance Heating Derivative extraction			18. Distribution Statement Unclassified - Unlimited Subject category 18		
19. Security Classif. (of this report) Unclassified		20. Security Classif. (of this page) Unclassified		21. No. of Pages 154	22. Price* A08

*For sale by the National Technical Information Service, Springfield, Virginia 22161



LANGLEY RESEARCH CENTER



3 1176 00504 1885